

University of Southampton

Faculty of Engineering and Physical Sciences

Engineering

**Contributions to Secondary Control of Voltage and Reactive Power for Large-
area Islanded Microgrids with Power-Electronic-based Distributed Energy
Resources**

by

Yi Chyn Cassandra Wong

Thesis for the degree of Doctor of Philosophy

March 2022

University of Southampton

Abstract

Faculty of Engineering and Physical Sciences

Engineering

Thesis for the degree of Doctor of Philosophy

Contributions to Secondary Control of Voltage and Reactive Power for Large-area
Islanded Microgrids with Power-Electronic-based Distributed Energy Resources

by

Yi Chyn Cassandra Wong

Global concerns on natural resource depletion and environmental degradation have initiated the power grid evolution from one based on large-scale rotating generators to one with many small-scale distributed energy resources. Smart distribution microgrids can combine the advantages offered by the prevalence of power-electronic-interfaced distributed energy resources (DERs) into providing significant controllability and flexibility to end users through the embedded control system. However, the lack of large-scale, high-inertia rotating generators may lead to instability in the events of fast voltage and/or frequency deviation. For microgrids operating in the islanded mode, it is also crucial to govern the dynamics among the DERs whilst maintaining the grid voltage and frequency within the desired specification. Control system of microgrids typically appears in the form of hierarchical structure consisting of primary, secondary, and tertiary control layers, which are distinguished by control bandwidth and technical functionalities. Through the primary layer's decentralised droop control scheme, the active and reactive load powers can be shared autonomously among the DERs in an islanded microgrid. However, it is established that the reactive load power cannot be accurately shared through standard droop control alone. This is because of the voltage discrepancies at the points of DERs connection. Furthermore, it is also well established that voltage and frequency deviations are inevitable in droop mechanism.

This has motivated this research thesis to design, develop and implement novel secondary control strategies to improve the voltage regulation and reactive power sharing among the power-electronic-interfaced DERs for large-area droop-controlled islanded microgrids. Their performance is substantiated by a series of detailed and in-depth simulation studies and analyses. It is hoped that the work in this thesis can contribute to the evolution of conventional power grid towards future smart grid. A practical *DIGSILENT-PowerFactory-Python* co-simulation platform is established and exploited for control strategies verification. A variety of advanced droop control schemes targeting reactive power sharing improvement reported to date will be categorised and explained further in this thesis. An assessment is carried out on two groups of reactive power focused droop-based schemes, standard droop control with dispatch and virtual-output-impedance (VOI)-based droop control, to establish their merits and demerits. It is found that the latter, which is a relatively new technique made possible by the embedded control system of power-electronic-interfaced DERs, has controller gains to be tuned and that the resulted voltage deviation is slightly higher for the scheme with static-dynamic impedance components.

Owing to sparse communication requirement, distributed control structure is highly relevant to large-area microgrids as DERs and loads are sparsely connected across the network. Through the

previous assessment, it is found that the standard droop output voltages of all participating DERs converged upon proportional reactive power sharing through VOI-droop scheme. This has prompted its utilisation in distributed consensus control algorithm in conjunction VOI-droop scheme. To begin with, the state-of-the-art consensus VOI-droop control with reactive power is improved by nullifying the static component of virtual output impedance which, in turn, improves the voltage profile. The relationship between DER's reactive power output and virtual output resistance/reactance is established. An operating-point-dependent consensus control tuning guideline is also presented. It is found that virtual-output-reactance-based VOI-droop scheme results in faster correction and dynamic-only, single component (virtual output resistance/reactance) VOI variant is sufficient to realize proportional reactive power sharing with improved voltage profile. These findings, however, raise new research questions on why there is never a need to regulate both virtual output impedance components, and why the virtual output reactance leads to a faster correction dynamic.

Accordingly, a novel droop equivalent impedance concept is introduced as an attempt to answer the above questions. From the droop equivalent impedance equation, it is revealed that the reactance component has a more direct impact on reactive power, which explains the faster correction dynamic by the reactance-type control scheme. In addition, it is discovered that upon the convergence of droop equivalent reactance (resistance) through consensus control, the droop equivalent resistance (reactance) converges too. This hints that as far as reactive power sharing correction is concerned, there is never a need to simultaneously regulate both virtual impedance components. In due course, a novel droop-equivalent-reactance-based consensus adaptive VOI-droop control is developed. A systematic tuning guideline is introduced by first establishing the relationship between the droop equivalent reactance and the virtual output reactance. A well-tuned distributed controller with less cascaded *PI* controllers can certainly improve the practicality and robustness of the secondary control scheme while reducing the tuning effort especially in future large-area microgrids.

In the previous standard droop scheme and the reactive-power-focused improved variants of droop control schemes, it is concluded that network bus voltages will deviate due to intrinsic trade-off between DERs droop output voltage and reactive output power. Therefore, a computational-friendly, power-flow-embedded, centralised secondary optimal control strategy is subsequently designed to address the multi-objective control problem. In this thesis, secondary voltage regulation is categorised into those that regulate DER-buses and those that regulate load-buses. While voltage regulation at DER-buses is widely attempted, voltage regulation at load-buses is considerably challenging. This is due to the fact that information of load-buses (located remotely) is not directly available to the DER control system. However, not only does the voltage regulation in distributed islanded microgrids involves high number of DERs in a much shorter control timeframe, but classical power flow algorithms are also not directly applicable due to the inexistence of slack bus in droop-controlled islanded microgrids and the dependence of active/reactive powers on frequency/voltage droop. A non-iterative Decoupled Linearised Power Flow (DLPF), formerly proposed for large-scale power system planning and operation, is exploited as the linear approximation that fits well with the droop behaviour of islanded microgrids. In order to address the conflicting control objectives of voltage and reactive power regulation, standard droop control is preferred over the VOI-droop scheme as its aggregation with DLPF is rather straightforward. The centralised secondary optimal control strategy is proven capable of realising single (optimal reactive power sharing or single load-bus voltage regulation) and multi-objective (optimal reactive power sharing with single/multiple load-buses voltage regulation) controls. In addition, the effectiveness of the optimal control strategy in respecting the practical network constraints is successfully demonstrated.

Apart from the reliability issue, it is expected that the computational complexity of a centralised optimal control scheme will increase exponentially as the microgrid scales up. Therefore, a semi-distributed multi-objective secondary optimal control targeting very-large-area droop-controlled microgrids is relevant. It is proposed that the very-large-area microgrid's secondary control layer is first segregated into multiple sub-microgrid clusters. The intention is to segregate the

large-scale optimisation control problem into multiple sub-problems so that the computational burden can be distributed across multiple control entities. By embedding the consensus control concept into the design, a semi-distributed optimal control strategy is developed. The intra- and inter-cluster controls enable voltage and reactive power regulation within, respectively, each microgrid cluster and among multiple microgrid clusters. The viability of the semi-distributed control scheme is fully verified using MATLAB simulation. Through extensive simulation proofs, the effectiveness of the semi-distributed control strategy in collectively managing voltage and reactive power trade-off is fully demonstrated. The control scheme is expected to have a low risk of single-point failure while being highly scalable as the computational effort is distributed across multiple secondary controllers.

In this thesis, advanced secondary control strategies are designed and implemented for voltage regulation and/or reactive power sharing improvement among power-electronic-interfaced DERs in large-area droop-controlled islanded microgrids. All control strategies are fully verified via extensive theoretical derivation and simulation means. It is hope that the control schemes can benefit the development and motivate the adoption of future smart microgrids.

Table of Contents

| | |
|--|-------------|
| Table of Contents | i |
| List of Tables | v |
| List of Figures..... | vii |
| Research Thesis: Declaration of Authorship..... | xiii |
| Acknowledgements..... | xv |
| Definitions and Abbreviations | xvii |
| Chapter 1 Introduction..... | 19 |
| 1.1 Introduction | 19 |
| 1.2 Problem statement | 21 |
| 1.3 Research aim and objectives | 22 |
| 1.4 Research scope and contributions | 22 |
| 1.5 Outline of the thesis..... | 24 |
| Chapter 2 Literature Review | 27 |
| 2.1 Introduction | 27 |
| 2.2 Droop control | 27 |
| 2.3 Review of improved variants of droop control | 29 |
| 2.3.1 Decentralised schemes | 29 |
| 2.3.2 Centralised schemes | 32 |
| 2.3.3 Distributed schemes | 33 |
| 2.4 Review of secondary voltage regulation control..... | 35 |
| 2.4.1 Without reactive power sharing consideration..... | 35 |
| 2.4.2 With reactive power sharing consideration..... | 37 |
| 2.5 Summary | 40 |
| Chapter 3 Fundamental Concepts | 45 |
| 3.1 Introduction | 45 |
| 3.2 Dynamical modelling of voltage-controlled voltage source inverter-based DERs.. | 45 |
| 3.3 Distributed consensus algorithm | 50 |
| 3.4 Quadratic programming | 51 |

| | | |
|--|---|------------|
| 3.5 | Summary | 53 |
| Chapter 4 Droop-based Reactive Power Sharing Regulation – An assessment..... | | 55 |
| 4.1 | Introduction..... | 55 |
| 4.2 | Multi-bus radial islanded microgrid network configuration | 55 |
| 4.3 | Droop-based reactive power regulation schemes | 63 |
| 4.3.1 | Standard droop control..... | 64 |
| 4.3.2 | Virtual-output-impedance droop control through power-electronic-interfaced DERs | 65 |
| 4.4 | Assessment through the <i>DIGSILENT-PowerFactory-Python</i> co-simulation platform | 67 |
| 4.5 | Summary | 70 |
| Chapter 5 Consensus Virtual-Output-Impedance-based Droop Control Schemes for Accurate Reactive Power Sharing..... | | 73 |
| 5.1 | Introduction..... | 73 |
| 5.2 | Reactive power regulation through consensus-based virtual-output-impedance droop control | 73 |
| 5.2.1 | Consensus control design with reactive power | 76 |
| 5.2.2 | Simulation results | 81 |
| 5.3 | Reactive power regulation through a novel droop equivalent impedance-based consensus droop control..... | 88 |
| 5.3.1 | Novel droop equivalent impedance concept..... | 89 |
| 5.3.2 | Consensus control design with droop equivalent impedance | 91 |
| 5.3.3 | Simulation results | 93 |
| 5.4 | Summary | 98 |
| Chapter 6 Optimal Secondary Multi-Bus Voltage and Reactive Power Sharing Regulation..... | | 101 |
| 6.1 | Introduction..... | 101 |
| 6.2 | Modified decoupled linearised power flow | 101 |
| 6.3 | Centralised optimal control for large-area islanded microgrids | 106 |

| | | |
|---------------------|---|------------|
| 6.3.1 | The multi-bus islanded microgrid network | 106 |
| 6.3.2 | Estimation model with integral correction | 110 |
| 6.3.3 | Cost function with inequality constraints..... | 111 |
| 6.3.4 | Simulation results | 112 |
| 6.4 | Semi-distributed optimal control for intra- and inter-microgrids voltage and reactive power regulation..... | 119 |
| 6.4.1 | Clustering of multi-bus islanded microgrid network | 119 |
| 6.4.2 | Estimation model with integral correction | 120 |
| 6.4.3 | Cluster-oriented cost function | 122 |
| 6.4.4 | Simulation results | 124 |
| 6.5 | Summary | 134 |
| Chapter 7 | Conclusion..... | 137 |
| 7.1 | Conclusions | 137 |
| 7.2 | Recommendation for Future Work..... | 139 |
| Appendix A | <i>DIgSILENT-PowerFactory-Python</i> co-simulation platform configuration..... | 141 |
| Appendix B | Publications from the thesis..... | 145 |
| Bibliography | | 201 |

List of Tables

| | |
|--|-----|
| Table 2.1. Attributes of standard and advanced primary droop control schemes. | 42 |
| Table 2.2. Attributes of selected advanced secondary voltage regulation control schemes with improved reactive power sharing. | 43 |
| Table 4.1. Theoretical and simulated voltage profile of <i>IEEE-34 node test feeder</i> | 58 |
| Table 4.2. The modified <i>IEEE-34 node test feeder</i> -based islanded microgrid network parameters. | 63 |
| Table 4.3. Summary of the differences between dispatch-droop and VOI-droop reactive power sharing schemes. | 70 |
| Table 5.1. Common effective coupling gain κ_X for a range of operating points with scalar coupling $c = 0.2$ | 80 |
| Table 5.2. Common effective coupling gain κ_R for a range of operating points with scalar coupling $c = 0.2$ | 80 |
| Table 5.3. The modified <i>IEEE-34 node test feeder</i> -based islanded microgrid network parameters. | 82 |
| Table 5.4. Common effective coupling gain κ for a range of operating points with scalar coupling $c = 0.2$ | 92 |
| Table 6.1. Specifications of the islanded microgrid network and proposed centralised secondary optimal control. | 109 |
| Table 6.2. Steady state estimation error (absolute percentage) with/without integral-based correction control. | 111 |
| Table 6.3. Specifications of the islanded microgrid network and proposed semi-distributed secondary optimal control. | 125 |

List of Figures

| | |
|---|----|
| Fig. 1.1. Hierarchical control level of a microgrid (modified from Bidram and Davoudi (2012))... | 20 |
| Fig. 2.1. Single line diagram of a power-electronic-based DER connected to the microgrid load bus. | 28 |
| Fig. 2.2. Taxonomy of existing voltage regulation and reactive power control in the area of microgrids. | 44 |
| Fig. 3.1. (left) Clarke transformation and (right) Park transformation. | 46 |
| Fig. 3.2. Schematic diagram of the primary control of a standard droop-controlled DER. | 47 |
| Fig. 3.3. Primary control of a standard droop-controlled DER built in <i>DIGSILENT PowerFactory</i> | 49 |
| Fig. 4.1. An example of (a) overhead line configuration across bus 800-802 and (b) transformer setting between bus 888-890. | 56 |
| Fig. 4.2. <i>PV</i> curve plot of the <i>IEEE-34 node test feeder</i> base model. | 57 |
| Fig. 4.3. Percentage error of voltage magnitudes and angles of each bus for the <i>IEEE-34 node test feeder</i> base model. | 60 |
| Fig. 4.4. Single line diagram of the large-area islanded microgrid modified from the <i>IEEE-34 node test feeder</i> | 61 |
| Fig. 4.5. The modified <i>IEEE-34 node test feeder</i> -based islanded microgrid model in <i>DIGSILENT PowerFactory</i> | 62 |
| Fig. 4.6. Schematic diagram of the dispatch-droop-controlled DER with integral-based distributed secondary control. | 65 |
| Fig. 4.7. Schematic diagram of the VOI-droop-controlled DER with integral-based distributed secondary control. | 67 |
| Fig. 4.8. Default steady state with (left) dispatch-droop and (right) VOI-droop schemes: (top) DER's reactive output power; (middle) the corresponding droop output voltage references; and (bottom) DER-bus voltage magnitudes. | 68 |
| Fig. 4.9. Load step change with (left) dispatch-droop and (right) VOI-droop schemes: (top) DER's reactive output power; and (bottom) the corresponding DER-bus voltage magnitudes. Legend as in Fig. 4.8. | 69 |

List of Figures

| | |
|---|----|
| Fig. 4.10. DER disconnection with (left) dispatch-droop and (right) VOI-droop schemes: (top) DER's reactive output power; and (bottom) the DER-bus voltage magnitudes. Legend as in Fig. 4.8. | 69 |
| Fig. 4.11. Communication loss with (left) dispatch-droop and (right) VOI-droop schemes: (top) DER's reactive output power; and (bottom) the DER-bus voltage magnitudes. Legend as in Fig. 4.8. | 69 |
| Fig. 5.1. Schematic diagram of the adaptive virtual-output-reactance-droop controlled DER with secondary consensus-based reactive power sharing control. | 75 |
| Fig. 5.2. Single line diagram of a power-electronic-interfaced DER with virtual output impedance and a physical equivalent impedance as seen by the DER output towards the microgrid. | 76 |
| Fig. 5.3. The modified <i>IEEE-34 node test feeder</i> -based islanded microgrid with sparse communication links. | 81 |
| Fig. 5.4. Default steady state and load step change: DERs' reactive output power. | 83 |
| Fig. 5.5. Default steady state and load step change: DERs' virtual output impedance values. | 84 |
| Fig. 5.6. Default steady state and load step change: the corresponding DER-bus voltage magnitudes. | 84 |
| Fig. 5.7. Low-loading operating condition: DERs' reactive output power. | 85 |
| Fig. 5.8. Low-loading operating condition: DERs' virtual output impedance values. | 86 |
| Fig. 5.9. Plug-and-play of DER 2: DERs reactive output power. | 86 |
| Fig. 5.10. Plug-and-play of DER 2: DERs' virtual output impedance values. | 87 |
| Fig. 5.11. Plug-and-play of DER 2: the corresponding DER-bus voltage magnitudes. | 87 |
| Fig. 5.12. Communication time delay: DERs' reactive output power. | 88 |
| Fig. 5.13. Single line diagram of a power-electronic-interfaced DER with virtual output impedance and an output feeder impedance. | 89 |
| Fig. 5.14. Secondary control system instability caused by the attempt to converge the droop equivalent impedance through regulation of both virtual output resistance and reactive independently: DERs active/reactive output power. | 94 |

| | |
|--|-----|
| Fig. 5.15. Secondary control system instability caused by the attempt to converge the droop equivalent impedance through regulation of both virtual output resistance and reactive independently: DERs virtual output resistance/reactance..... | 94 |
| Fig. 5.16. Default steady state and load step change with fixed $\kappa = 0.103$: DERs' active and reactive output power; the corresponding droop output voltage references and DER-bus voltage magnitudes; and virtual output reactance values. | 95 |
| Fig. 5.17. Default steady state and load step change with fixed $\kappa = 0.3$: DERs reactive output power. | 96 |
| Fig. 5.18. Default steady state and load step change with adaptive κ : DERs' reactive output power and DER-bus voltage magnitudes..... | 96 |
| Fig. 5.19. DER 2 plug-and-play capability: DERs' reactive output power; the corresponding droop output voltage references; and the adaptive virtual output reactance generated..... | 97 |
| Fig. 5.20. DERs' reactive output power with communication time delay of (top) 0.6 s (mid) 1.4 s and (bottom) 1.8 s. | 98 |
| Fig. 6.1. Single-line diagram of the dispatch-droop-controlled islanded microgrid test network. . | 107 |
| Fig. 6.2. Detailed block diagram of a DER's primary control and the proposed centralised multi-objective secondary optimal control for islanded microgrid..... | 108 |
| Fig. 6.3. Optimal reactive power sharing control with and without integral-based corrective control: DERs reactive output power. | 111 |
| Fig. 6.4. Optimal reactive power sharing control: DERs active/reactive power, secondary droop dispatch input \mathbf{u} , DER droop voltage magnitudes and load-bus voltage magnitudes... | 113 |
| Fig. 6.5. Single load-bus voltage regulation control: DERs reactive output power, secondary droop dispatch input \mathbf{u} and load-bus voltage magnitudes. | 115 |
| Fig. 6.6. Optimal reactive power sharing and single load-bus voltage regulation control: DERs reactive output power and selected load-bus voltage magnitudes. | 116 |
| Fig. 6.7. Optimal reactive power sharing and prioritised multi-load-bus voltage regulation control: DERs reactive output power and selected load-bus voltage magnitudes..... | 117 |
| Fig. 6.8. Optimal reactive power sharing and multi-load-buses voltage regulation control: DERs reactive output power and selected load-bus voltage magnitudes. | 117 |
| Fig. 6.9. Constrained optimal reactive power sharing and multi-load-buses voltage regulation: DERs reactive output power and selected load-buses voltage magnitudes..... | 118 |

List of Figures

| | |
|--|-----|
| Fig. 6.10. Overall simulation platform of the semi-distributed optimal control within <i>MATLAB</i> .. | 125 |
| Fig. 6.11. Single line diagram of an islanded microgrid with detailed semi-distributed secondary control flowchart..... | 126 |
| Fig. 6.12. Optimal intra-cluster reactive power sharing control: DERs reactive output power, sub-microgrids reactive output power, load-bus voltage magnitudes and DER-bus voltage magnitudes..... | 127 |
| Fig. 6.13. Optimal intra- and inter-cluster reactive power sharing control without integral-based correction: DERs reactive output power, sub-microgrids reactive output power, load-bus voltage magnitudes and DER-bus voltage magnitudes. | 128 |
| Fig. 6.14. Optimal intra- and inter-cluster reactive power sharing control: DERs reactive output power, sub-microgrids reactive output power, load-bus voltage magnitudes and DER-bus voltage magnitudes. | 128 |
| Fig. 6.15. Single load-bus voltage regulation control at sub-microgrid <i>A</i> : DERs reactive output power, sub-microgrids reactive output power, load-bus voltage magnitudes and DER-bus voltage magnitudes. | 129 |
| Fig. 6.16. Single load-bus voltage regulation control at sub-microgrid <i>B</i> : DERs reactive output power, sub-microgrids reactive output power, load-bus voltage magnitudes and DER-bus voltage magnitudes. | 130 |
| Fig. 6.17. Simultaneous single load-bus voltage regulation control in two sub-microgrids: DERs reactive output power, sub-microgrids reactive output power, load-bus voltage magnitudes and DER-bus voltage magnitudes. | 130 |
| Fig. 6.18. Optimal intra- and inter-reactive power sharing and single load-bus voltage regulation control at sub-microgrid <i>A</i> : DERs reactive output power, sub-microgrids reactive output power, load- and DER-bus voltage magnitudes. | 131 |
| Fig. 6.19. Optimal intra- and inter-reactive power sharing and multi-load-bus voltage regulation control at sub-microgrid <i>A</i> : DERs reactive output power, sub-microgrids reactive output power, load- and DER-bus voltage magnitudes. | 132 |
| Fig. 6.20. Optimal intra- and inter-reactive power sharing and multi-load-bus voltage regulation control in sub-microgrid <i>B</i> : DERs reactive output power, sub-microgrids reactive output power, load- and DER-bus voltage magnitudes. | 132 |

| | |
|---|-----|
| Fig. 6.21. Optimal intra- and inter-reactive power sharing and inter-multi-load-bus voltage regulation control: DERs reactive output power, sub-microgrids reactive output power, load- and DER-bus voltage magnitudes..... | 133 |
| Fig. A.1. Illustration of the <i>DIgSILENT-PowerFactory-Python</i> co-simulation platform with detailed primary control of a standard droop-controlled DER. | 141 |
| Fig. A.2. External data measurement setup (a) basic data; (b) post-processing; (c) status; (d) external data link setup in <i>DIgSILENT PowerFactory</i> | 142 |
| Fig. A.3. (a) Pre-configured tags importing to <i>MatrikonOPC</i> ; (b) an alias group <i>PF</i> containing OPC tags; (c) uploading <i>PF</i> group OPC tags onto <i>MatrikonOPC</i> server; (d) parallel execution with <i>MatrikonOPC</i> | 143 |

Research Thesis: Declaration of Authorship

Print name:

Title of thesis: Contributions to Secondary Control of Voltage and Reactive Power for Large-area
Islanded Microgrids with Power-Electronic-based Distributed Energy Resources

I declare that this thesis and the work presented in it are my own and has been generated by me as the result of my own original research.

I confirm that:

1. This work was done wholly or mainly while in candidature for a research degree at this University;
2. Where any part of this thesis has previously been submitted for a degree or any other qualification at this University or any other institution, this has been clearly stated;
3. Where I have consulted the published work of others, this is always clearly attributed;
4. Where I have quoted from the work of others, the source is always given. With the exception of such quotations, this thesis is entirely my own work;
5. I have acknowledged all main sources of help;
6. Where the thesis is based on work done by myself jointly with others, I have made clear exactly what was done by others and what I have contributed myself;
7. Parts of this work have been published as:-

Wong, Y. C. C., Lim, C. S., Rotaru, M. D., Cruden, A. and Kong, X. (2018) 'Reactive power sharing study of an islanded microgrid in DIGSILENT PowerFactory', *International Conference on Renewable Energy Research and Applications*. Paris, France, 14–17 October. Paper No. 68.

Wong, Y. C. C., Lim, C. S., Cruden, A., Rotaru, M. D. and Ray, P. K. (2020) 'A consensus-based adaptive virtual output impedance control scheme for reactive power sharing in meshed microgrids', *IEEE International Conference on Power Electronics, Smart Grid and Renewable Energy*. Cochin, India, 2–4 January. Paper No. 323.

Wong, Y. C. C., Lim, C. S., Rotaru, M. D., Cruden, A. and Kong, X. (2020) 'Consensus virtual output impedance control based on the novel droop equivalent impedance concept for a multi-bus radial microgrid', *IEEE Transactions on Energy Conversion*, 35(2), pp. 1078–1087.

Wong, Y. C. C., Lim, C. S., Cruden, A., Rotaru, M. D. and Kong, X. (2021) 'Semi-distributed optimal secondary control based on decoupled linearized power flow for large-area

droop-controlled microgrids’, *International Conference on Green Energy, Computing and Sustainable Technology*. Sarawak, Malaysia, 7–9 July. Paper No. 1570727021.

Wong, Y. C. C., Lim, C. S., Cruden, A., Rotaru, M. D. and Ray, P. K. (2021) ‘A consensus-based adaptive virtual output impedance control scheme for reactive power sharing in radial microgrids’, *IEEE Transactions on Industry Applications*, 57(1), pp. 784–794.

Wong, Y. C. C., Lim, C. S., Goh, H. H., Cruden, A., Rotaru, M. D. and Kong, X. (2021) ‘An optimal secondary multi-bus voltage and reactive power sharing control based on non-iterative decoupled linearized power flow for islanded microgrids’, *IEEE Access*, 9, pp. 105242–105254.

Signature: Date:

Acknowledgements

Foremost, I would like to express my sincere gratitude to my supervisor, Assoc. Prof. Dr. Chee Shen Lim for his patience, motivation, and most importantly, his continuous support throughout my research time with University of Southampton, Malaysia Campus and UK Campus. His invaluable support and guidance helped me in all the time of research and writing of this thesis. Beyond all that, I thank him for the financial opportunities that he sought during the research duration.

Beside my supervisor, deepest gratitude to my co-supervisor, Prof. Andrew J. Cruden and external supervisors, Dr. Mihai D. Rotaru, Agency for Science, Technology, and Research (A*STAR), Singapore, and Dr. Xin Kong, Energy Research Institute at Nanyang Technological University (ERI@N), Singapore for their encouragement and insightful comments.

My acknowledgement is then extended to A*STAR, Singapore for the research attachment opportunity which broadened my research background and strengthen my software/simulation skills. Without the opportunity, this research work would not have been a smooth one.

I would also like to convey thanks to University of Southampton for providing financial support and technical support in simulation software.

Last but not least, I would like to express my love and gratitude to my beloved families for their understanding and endless love throughout the duration of my studies. My wonderful parents who have raised me to be the person I am today. My husband who accompanying me throughout my PhD period has given me great support and encouragement. My unborn baby boy who has made me stronger, better, and more fulfilled than I could ever imagined.

Definitions and Abbreviations

| | |
|-------------|--|
| $P-f$ | frequency-active-power |
| $P-V$ | voltage-active-power |
| $Q-V$ | voltage-reactive-power |
| $Q-f$ | frequency-reactive-power |
| $Q-\dot{V}$ | derivative-voltage-reactive-power |
| DER | Distributed Energy Resource |
| VSI | Voltage Source Inverter |
| PI | Proportional-Integral |
| ADMM | Alternating Direction Multiplier Method |
| PSO | Particle Swarm Optimisation |
| VOI | Virtual-Output-Impedance |
| MPC | Model Predictive Control |
| EOPF | Extended-Optimal Power Flow |
| SOCP | Second Order Cone Programming |
| QP | Quadratic Programming |
| OPC | Object linking and embedding for Process Control |
| IDLE | Integrated Development and Learning Environment |
| DLPF | Decoupled Linearised Power Flow |

Chapter 1 Introduction

1.1 Introduction

Motivated by the environmentally-conscious, economic and technological advancement, the existing electric grid infrastructure is evolving from a large-scale, centralised structure towards a relatively small-scale and distributed grid structure, which is known commonly as microgrid. A microgrid is a self-contained grid network which can facilitate the integration of distributed energy resources (DERs), i.e., conventional rotating generators, power-electronic-interfaced renewable energy resources and energy storage systems with interconnected loads. The microgrid's dual-operating modes, i.e., grid-connected and islanded modes, provide better energy security, resiliency, and reliability to the network users. Microgrids' dynamic is dominated by the high-inertia main grid when it is connected to the large electricity grid infrastructure. However, in the events of unscheduled disturbances or scheduled islanding, microgrids can be disconnected from the main grid to operate in the islanded mode. In this operating mode, the microgrid needs to self-govern the grid's voltage and frequency to ensure a stable operation. Regardless of which operating mode, the microgrid's control system is a prerequisite for a stable and economical operation. The control system typically appears in the form of a hierarchical structure consisting of primary, secondary, and tertiary control layers. The control layers are fundamentally segregated through the control bandwidth (or timescale) and are distinguished by their functionalities for different technical requirements. An example of the hierarchical structure is shown in Fig. 1.1.

Unlike the large-scale electric grid, microgrids are typically characterised by its low inertia property due to the prevalence of power-electronic-interfaced DERs in the network. Voltage source inverters (VSIs) are the most common power converter hardware that interfaces the emerging renewable energy resource into microgrids. One of the useful features enabled by the VSIs is the embedded control system that gives enormous flexibility and controllability to the power-electronic-based DERs and the microgrid system. For instance, some VSIs in a droop-controlled microgrids will be voltage-controlled to self-regulate the grid voltage and frequency; some other VSIs can be current-controlled to regulate the active and reactive output powers; during grid-connected mode, most VSIs are typically current(power)-controlled to supply the desired active and reactive output powers to the main grid. Although the power-electronic interface enhances the system controllability and dynamical performances, the lack of large-scale high-inertia rotating generators in the microgrids may lead to instability in the events of fast voltage and frequency deviation. The islanded mode is typically more susceptible to this risk. The microgrid control system is responsible to govern the dynamics among the DERs whilst maintaining the grid voltage and frequency within specification and regulating the power sharing among the DERs.

The recent research interest in voltage and reactive power regulation for islanded microgrids has been evidenced by various research literature. In the primary control, the decentralised droop control helps to autonomously share the active and reactive load power among the connected power-electronic-interfaced DERs whilst establishing the local voltage and frequency of the DERs. However, it is well established by now that droop mechanism alone may leads to significant voltage and frequency deviation and cannot ensure accurate sharing of reactive power supply among the DERs in the microgrids (Han *et al.*, 2016; Y. Han, Li, *et al.*, 2017). This motivated the research on various improved variants of droop control and advanced secondary control schemes for microgrids in recent years. For instance, virtual-output-impedance-based droop control which is used specifically for power-electronic-interfaced DERs, has been introduced by Guerrero *et al.* (2005, 2007), He *et al.* (2012), Mahmood, Michaelson and Jiang (2015a), Wang *et al.* (2015).

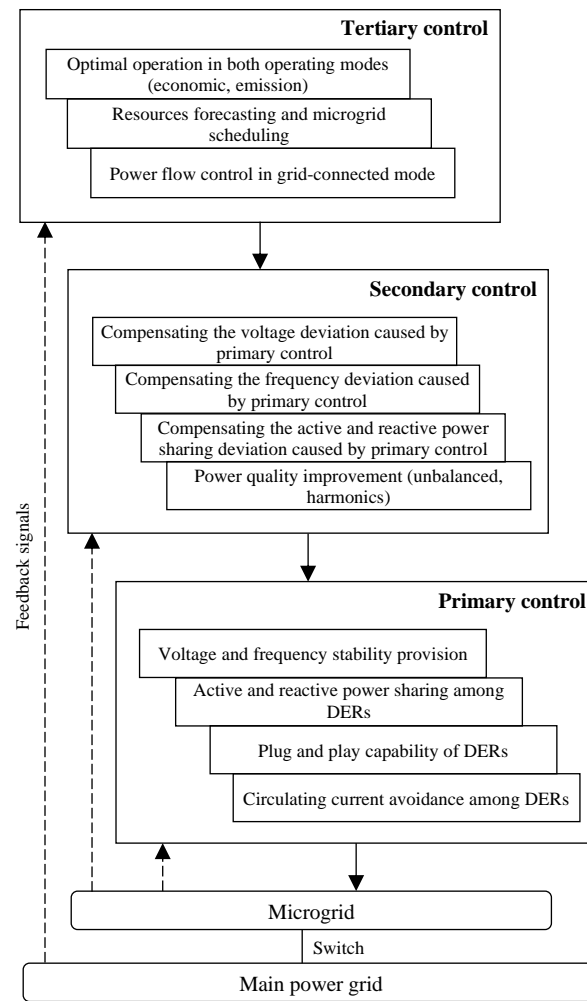


Fig. 1.1. Hierarchical control level of a microgrid (modified from Bidram and Davoudi (2012)).

In the early stage, secondary control is developed to provide voltage and frequency regulations. Recently, it also aids in improving the power sharing among the power-electronic-based DERs. The secondary control layer can be realised through centralised, distributed, or decentralised structure. With the centralised structure, all relevant information of the microgrid is required to be at the disposal of the central control system. A critical demerit of this system is the reliability risk posed by single point of failure, i.e., failure at a single point will lead to potential performance-derating or

even instability of the entire network. It is also known that redundant protection systems can help to address the said problem of single point of failure (Scroggins, n.d.; Farrar, 2018). As another alternative, the risk of single point of failure can also be mitigated through a decentralised or distributed structures. In the former, each DER will coordinate its own operation by requiring only the local information; in the latter, each DER will require neighbours' information, typically acquired through low-bandwidth distributed-graph communication channels, for the secondary control algorithm.

Advanced control algorithm, e.g., consensus control, quadratic programming etc. have been utilised for secondary voltage and reactive power regulation in recent research literature. In the view of the author, the secondary voltage control techniques can be categorised into the types of targeted buses: those that with directly connected power-electronic-based DERs (known as DER-buses hereinafter); and those that have no DERs (known as load-buses hereinafter). Voltage regulation at load-buses typically requires network model, and therefore power flow algorithm is relevant. However, the inexistence of slack bus in droop-controlled microgrids and the dependence of power on frequency/voltage droop means that the classical power flow is not directly applicable. The secondary voltage and reactive power sharing problem is fundamentally a multi-objective control problem, requiring the advanced optimal control algorithm to handle the intrinsic trade-offs.

Summarily, this work will design, develop, and realise advanced control techniques for the primary and secondary control of power-electronic-based DERs in large-area droop-controlled microgrids. Although large-area microgrids with sparsely connected DERs are common, secondary control of microgrids are often studied on small network. This motivates this PhD project to also build a realistic, large-area microgrid model for accurate algorithm verification. The aim and objectives of this thesis will be explained next followed by the research contributions of this PhD work. Lastly, an organised outline of the chapters of this thesis is provided.

1.2 Problem statement

Although the standard droop control allows DERs to autonomously distribute load demand in a decentralised manner, the significant voltage discrepancies at the points of interconnection of DERs will lead to inaccurate reactive power sharing among the DERs. Moreover, owing to the intrinsic trade-offs between frequency/voltage and active/reactive powers in droop actions, droop control inevitably results in voltage and frequency deviations. Voltage regulation is relatively challenging as bus voltages are local variables, involving high number of DERs and having a much shorter control timeframe than that in the classical power system. Classical nonlinear power flow algorithms that assume the existence of slack bus is also not directly applicable in islanded microgrids. These problems or limitations have formed the primary research questions in this thesis.

The overarching research goal is to contribute to the development of advanced secondary control strategies for future smart microgrids with prevalence of power-electronic-interfaced DERs.

1.3 Research aim and objectives

The aim of this research is to design, develop, and implement novel secondary control schemes to improve the voltage regulation and reactive power sharing among power-electronic-interfaced DERs, for large-area, droop-controlled microgrids. The aim of this research is met by completing the following objectives:

- i. To assess the working mechanism of standard droop control with dispatch commands and virtual-output-impedance-based droop control and to inform on their merits and demerits through a comprehensive comparison.
- ii. To improve the state-of-the-art consensus virtual-output-impedance-based droop control with reactive power sharing improvement and to also develop a distributed control tuning guideline for this emerging control technique.
- iii. To introduce a novel droop equivalent impedance concept that explains the underlying principle of virtual-output-impedance-based droop control schemes, and to develop a novel droop-based reactive power sharing scheme based on the concepts of droop equivalent impedance and distributed consensus control.
- iv. To design and develop a novel centralised secondary optimal control strategy with improved computational efficiency by exploiting linear power flow algorithm, and to address the conflicting control objectives of multiple load bus voltage and reactive power regulation in droop-controlled islanded microgrids.
- v. To design and develop a semi-distributed multi-objective control strategy for very-large-area droop-controlled islanded microgrids through the previously exploited consensus control and optimal concepts, and to address the problems of multi-bus voltage regulation and DERs' reactive power output sharing in the entire microgrid.

By achieving the objectives listed above, a substantial body of new knowledge has been produced. The research scope and contributions of this thesis are described in Section 1.4. The work presented in this thesis has resulted in a number of peer-reviewed journal and conference papers as appended to the thesis in Appendix B.

1.4 Research scope and contributions

The main contributions of this research work can be summarised as follows. The primary control of power-electronic-interfaced DERs consists of power controller, output voltage controller and inverter current controller; they are developed in the *DIgSILENT PowerFactory* through basic building blocks with the aim to accurately reflect the dynamics and interactions of the power-

electronic-based DERs in the islanded microgrids. In droop-controlled microgrids, the power-electronic-interfaced DERs are controlled through frequency-active power (P - f) and voltage-reactive power (Q - V) droop mechanisms. However, although accurate active power sharing is guaranteed, it is established that reactive power may be poorly shared among the power-electronic-interfaced DERs due to voltage discrepancies at their points of coupling with the network. Hence, the power control may be equipped with improved control algorithm.

A realistic *DIGSILENT-PowerFactory-Python* co-simulation platform is constructed in which the detailed microgrid networks and primary controls of the interconnected power-electronic-based DERs are modelled in *DIGSILENT PowerFactory* and is interfaced with the secondary controls developed in the *Python* environment. An interoperability standard for data exchange in industrial automation, *MatrikonOPC*, facilitates the data exchange (acquisition and transfer) between the clients, being *DIGSILENT PowerFactory* and *Python IDE*, through *ComLink* and *OpenOPC* interfaces, respectively. With the verified *DIGSILENT-PowerFactory-Python* co-simulation platform, the development and verification of novel control strategies are made possible as the specialist simulation packages (in different disciplines/domains) can collaborate more efficiently – becomes more relevant for large-area microgrid networks.

Disproportionate reactive power sharing problem in droop-controlled microgrids have been addressed with variants of improved droop control schemes. An assessment is carried out to review the two groups of reactive power focused droop-based schemes, i.e., standard droop control with dispatch commands and virtual-output-impedance-based droop control, through the *DIGSILENT-PowerFactory-Python* co-simulation platform. The power control of the power-electronic-interfaced DERs is equipped with the improved control schemes, e.g. with dispatch commands or virtual-output-impedance adjustment, both with distributed integral control having full-graph communication structure. The assessment is based on the reactive power sharing correction performance, the resulted voltage profile, and the parameters involved.

Upon establishing the understanding on the full-graph distributed control, the work progresses to developing a consensus-based adaptive virtual-output-impedance droop control, which is different from the previously reported virtual-output-impedance droop schemes in several aspects. First, the proposed control scheme utilises individual resistance/reactance component of the virtual-output-impedance as compared to the common ways of using both resistance and reactance components (which essentially means more controller gains to be tuned). Second, the commonly used *PI* controllers are avoided, and the approximate range of stable consensus control gain is successfully established, leading to a straightforward tuning task. Lastly, the proposed control scheme only uses the dynamical virtual impedance without the commonly used static component. In addition, the next-stage of the work proposes a novel concept of droop equivalent impedance, which provides a new alternative means to realise consensus-based reactive power sharing correction. It also helps to clarify the nature of each of the individual resistance and reactance components.

Upon establishing accurate reactive power sharing (single objective), the project progresses to multi-objective control problem. Apart from the reactive power sharing issue, it is well established that an islanded microgrid will suffer from voltage and frequency deviation (from nominal) due to the droop action. Since frequency in the islanded microgrids is a global variable, frequency regulation is relatively straightforward. Nevertheless, voltage regulation is relatively more challenging, especially in the applications where multiple bus voltages are to be regulated concurrently. This work develops a secondary optimal control scheme based on modified Decoupled Linearised Power Flow for addressing the intrinsic trade-off problem among multi-bus voltage regulation and reactive power sharing among DERs. Along with the adoption of quadratic programming, the compromise between voltage regulation at multiple buses and reactive power sharing among the power-electronic-based DERs can be optimised whilst addressing the relevant practical constraints. Lastly, this work extends the proposed optimal control scheme to one that is applicable for very-large-area microgrids. This is achieved by segregating the large-area microgrid network into multiple sub-microgrids. A semi-distributed secondary optimal control with cluster-oriented cost function is developed to address the problem of simultaneous intra- and inter- sub-microgrid voltage and reactive power regulation.

1.5 Outline of the thesis

This thesis is comprised of seven chapters including this introductory chapter. The following six chapters are organised as follows:

Chapter 2 presents a comprehensive literature review. First, the standard droop control of islanded microgrids is described. Then, a survey of improved variants of droop control in microgrid-themed studies, categorised into decentralised, centralised, and distributed schemes, is provided. This is followed by a thorough review of secondary voltage regulation control with and without reactive power sharing consideration.

Chapter 3 discusses the relevant fundamental concepts of this research work. The dynamical modelling of voltage-controlled voltage source inverter-interfaced DERs is detailed which includes standard droop-based power control, output voltage control and inverter current control. The fundamentals of consensus control algorithm and quadratic programming are then discussed.

Chapter 4 assesses the two groups of reactive power focused droop-based schemes, i.e., standard droop control with dispatch commands and virtual-output-impedance-based droop control through the *DigSILENT-PowerFactory-Python* co-simulation platform. An islanded microgrid modified from *IEEE-34 node test feeder* is analysed and modelled as the large-area islanded microgrid under study. The reactive power sharing correction mechanism of the standard droop control with dispatch commands and virtual-output-impedance-based droop control are analysed and a comparative study with distributed *PI* controllers is presented. Lastly, properties of both reactive power-focused droop-based schemes are summarised.

Chapter 5 presents consensus virtual-output-impedance-based droop control schemes in two approaches: one based on the conventional reactive power, and another one based on the novel droop equivalent impedance concept. The virtual-output-impedance technique is comprehensively analysed, and it will be revealed that the extensively used of both resistance and reactance components is redundant. It is shown that the proposed consensus-based virtual-output-impedance droop control can achieve the same reactive power sharing performance with the static component nullified. Furthermore, systematic guideline to approximate the range of stable consensus control gain is established, taking into account the consensus theorem and the dynamical relationship between virtual-output-reactance and reactive power.

Chapter 6 introduces a secondary optimal control which is developed to address the intrinsic trade-off between multi-bus voltage regulation and reactive power sharing in droop-controlled microgrids. Linear power flow algorithm has always been the preferred algorithm for large-area power system studies, and it will be shown to be relevant to load-bus voltage regulation here. The aggregation of standard droop control with dispatch commands with Decoupled Linearised Power Flow and the formulation of the constrained quadratic programming optimisation problem are discussed. It is shown that the secondary optimal control can account for the practical voltage and reactive power capacity constraints whilst realising not only single-objective control of optimal reactive power sharing or single bus voltage regulation, but also accomplishing multi-objective control of optimal multiple bus voltage regulation and reactive power sharing improvement with trade-offs. Lastly, a cluster-oriented, semi-distributed secondary control scheme that is capable of handling intra- and inter- sub-microgrid voltage and reactive power regulation, is developed and investigated.

Chapter 7 concludes this research thesis and emphasises the main findings of the developed secondary control strategies. Recommendation of future research work based on the developments of this research work is presented.

Appendix A describes the configuration of the *DIgSILENT-PowerFactory-Python* co-simulation platform used throughout this research work. The publications resulted from the work contained in this research thesis is listed in Appendix B.

Bibliography chapter provides a list of references used throughout the thesis.

Chapter 2 Literature Review

2.1 Introduction

This thesis emphasises on the design, development, and implementation of advanced primary and secondary control algorithms for large-area islanded microgrids with high penetration of power-electronic-based DERs. This chapter intends to provide a detailed literature review in the relevant subject areas and is organised as follows: Section 2.2 introduces the standard droop control and its inherent problems in islanded distribution microgrids. Section 2.3 surveys the improved variants of droop control that improves the power sharing among power-electronic-interfaced DERs. The power sharing improvement schemes are categorised based on the communication requirement into decentralised, centralised, and distributed architectures. Section 2.4 presents the secondary control strategies focusing on voltage regulation, with and without reactive power sharing consideration, in islanded microgrids. Finally, Section 2.5 summarises this chapter.

2.2 Droop control

In the last decade, the concept of grid-forming control has been actively studied in conjunction to smart distribution microgrid. The aim is to enhance system stability and resiliency of distribution microgrids with high penetration of power-electronic-based DERs. To date, numerous grid-forming techniques have been proposed e.g., iso-synchronous control, virtual synchronous machine, matching control, virtual oscillator control and droop control (Khan *et al.*, 2020). The operation principle of virtual synchronous machine control and matching control is about using the embedded control loops of the power converters to imitate the behaviour of synchronous machines. On the other hand, virtual oscillator techniques emulate the synchronising mechanism of non-linear Lienard-type oscillators. It is also worth noting that the oscillator-based techniques are only applicable for power-electronic-only microgrids (where all distributed energy resources are interfaced with the grid through power converters).

In general context, islanded distribution microgrids are either iso-synchronous- or droop-controlled to realise an autonomous operation where the DERs will self-regulate the grid voltage and/or frequency. An iso-synchronous-controlled microgrid responds to the changes in loading by letting the main/dominant DER (typically the one with the largest kVA rating) to maintain the power balance in the network. This network architecture poses the risk of single-point failure to the microgrid and is typically only suitable for small microgrid networks. Beyond the subject of grid-forming techniques, the focus is on improving the voltage and reactive power regulation. Therefore, droop control that is widely adopted in actual implementation, is most relevant. Some well acknowledged advantages include better stability and wider operating range as compared to the iso-

synchronous counterpart. Ideally, droop control allows multiple DERs to operate in tandem by distributing the load active and reactive powers in an autonomous manner which eliminates communication between DERs, while providing some provisions of voltage and frequency stability.

The standard frequency-active power (P - f) and voltage-reactive power (Q - V) droop control can be mathematically expressed as

$$\begin{aligned}\omega_i &= \omega_i^* - m_i P_i \\ V_i &= V_i^* - n_i Q_i\end{aligned}\quad (2.1)$$

where ω_i and V_i are the per-unit operating frequency and droop output voltage amplitude (typically normalised to network's phase peak voltage) of i^{th} DER whilst ω_i^* and V_i^* are the corresponding per-unit no-load frequency and voltage reference. P_i and Q_i are the per-unit active and reactive output powers (typically low-pass-filtered), normalised to a common base power. The per-unit droop coefficients, m_i and n_i are typically set based on the maximum allowable frequency and voltage deviations and per-unit DER rating. In general, the droop coefficients of a DER should be in inverse proportion to the kVA rating in order to share the load powers in proportion.

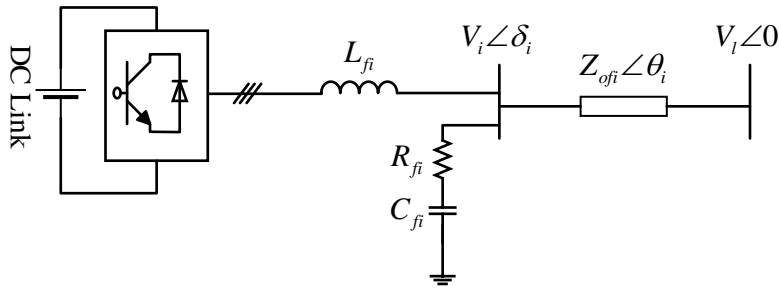


Fig. 2.1. Single line diagram of a power-electronic-based DER connected to the microgrid load bus.

Consider that a DER, equipped with a LC filter, connects to a network/load-bus through a complex feeder impedance $\mathbf{Z}_{ofi} = Z_{ofi} \angle \theta_i$, as depicted in Fig. 2.1, the active and reactive powers delivered by the DER to the load-bus can be calculated from

$$\begin{aligned}P_i &= \frac{V_l V_i}{Z_{ofi}} \cos(\theta_i - \delta_i) - \frac{V_l^2}{Z_{ofi}} \cos \theta_i \\ Q_i &= \frac{V_l V_i}{Z_{ofi}} \sin(\theta_i - \delta_i) - \frac{V_l^2}{Z_{ofi}} \sin \theta_i\end{aligned}\quad (2.2)$$

where V_l is the load-bus voltage magnitude, δ_i is the DER voltage angle with load-bus voltage angle being the reference angle. Under the assumption that the voltage angle is relatively small (i.e. $\sin \delta_i \approx \delta_i$ and $\cos \delta_i \approx 1$), the standard droop control is developed based on a typical assumption of having an inductive line dominated network, e.g. the transmission system. This means that X/R ratio is large (i.e., R is negligible, hence $\sin \theta_i = 1$ and $\cos \theta_i = 0$), which (2.2) can be reduced to

$$\begin{aligned}
P_{i,droop} &= \frac{V_l V_i}{Z_{ofi}} \delta_i \\
Q_{i,droop} &= \frac{V_l (V_i - V_l)}{Z_{ofi}}
\end{aligned} \tag{2.3}$$

However, this assumption is usually being challenged in microgrid networks owing to the non-trivial resistive impedance across the distribution lines (Yang *et al.*, 2016; Bidram *et al.*, 2017), causing the microgrids to suffer from cross-coupling of active and reactive powers (Li and Kao, 2009; Y. Han, Li, *et al.*, 2017).

In addition to that, as opposed to the frequency being a common variable which guarantees accurate active power sharing, the significant voltage discrepancies at the point of coupling of DERs leads to disproportionate reactive power sharing among DERs in droop-controlled islanded microgrids (Bidram and Davoudi, 2012).

2.3 Review of improved variants of droop control

A substantial body of works on reactive power sharing improvement in islanded microgrids have been reported to date. Here, they are grouped into decentralised, centralised, and distributed control schemes. In the decentralised structure, communication can be disregarded; in the latter two, the secondary control is enhanced through the use of low-bandwidth communication.

2.3.1 Decentralised schemes

Instead of the standard droop, voltage-active power P - V and frequency-reactive power Q - f droop scheme was adopted in the works by Engler and Soultanis (2008) and Bidram *et al.* (2017):

$$\begin{aligned}
V_i &= V_i^* - m_i P_i \\
\omega_i &= \omega_i^* + n_i Q_i
\end{aligned} \tag{2.4}$$

This scheme is known as inverse droop, aiming to accommodate microgrids with predominately resistive distribution lines. Although the inverse droop control offers improved control performance, the scheme is not suitable for microgrids without the property of highly resistive lines. Mohamed and El-Saadany (2008) reported on a modified droop control which exploits additional derivative terms with adaptive droop coefficients to provide damping to the power sharing oscillation among power-electronic-based DERs. The scheme delivers a classical PI -equivalent control dynamic with which the adaptive transient droop coefficients provide damping to the power sharing oscillations without compromising the voltage and frequency steady-state regulation performance (as dictated by the static droop coefficients). However, despite requiring the knowledge of the network parameters (for designing the adaptive transient droop coefficients), it can be deduced that the modified droop

control will not be able to guarantee accurate reactive power sharing the microgrid. This is because the added transient droop coefficients will not be able to compensate the steady-state voltage discrepancies at multiple points of coupling (i.e., points of connection of DERs to the microgrid).

A coupled droop control was proposed by Yao *et al.* (2011) and Qunais and Karimi-Ghartemani (2019) to address the active and reactive powers cross coupling due to complex feeder impedance. Although power sharing improvement is reported in parallel-connected microgrids, it can be deduced that the scheme cannot be generalised/extended to large-area microgrids with radial structure because there is no provision to account for the significant voltage discrepancies at the points of coupling of DERs.

Alternatively, Lee, Chu, and Cheng (2013) presented a derivative voltage-reactive power ($Q-\dot{V}$) droop control with dispatch command to address the reactive power sharing error in standard droop control. The dispatch command is locally computed from cascaded time-derivative voltage (\dot{V}) restoration control. While \dot{V} decays to zero in steady state, the dispatch command deviated from the desired value, leading to degradation of the power sharing performance. Accordingly, Zhou and Cheng (2019) proposed a modified \dot{V} restoration mechanism to address the said dispatch deviation. An additional modification term based on the first derivative of DER reactive output power is added to the restoration control to compensate the dispatch deviation. However, as reported in the literature, although accurate reactive power sharing can be achieved among DERs with equal kVA ratings in parallel-connected microgrids, reactive power sharing error is not fully eliminated among DERs within radial microgrids. Moreover, it is also deduced that since the modified \dot{V} restoration algorithm (Zhou and Cheng, 2019) does not account for the differences in kVA ratings, it will not be able to solve the problem of inaccurate reactive power sharing.

As mentioned, apart from the active/reactive powers cross coupling, the local DER voltage discrepancies due to mismatched feeder impedances is one of the reasons that cause disproportionate reactive power sharing. Consequently, a new family of control scheme made possible by the use power-electronic control in DERs emerged, and it is commonly known as virtual-output-impedance control scheme (Guerrero *et al.*, 2005, 2007). The virtual-output-impedance control exploits an additional degree of freedom enabled by the local voltage controllers in attempts to decouple the active and reactive powers and compensate the feeder impedance mismatch. For instance, He *et al.* (2013), and Altahir, Yan, and Liu (2017) adopted complex virtual output impedance into the standard droop control to realise accurate regulation of reactive power sharing among paralleled DERs. It is said that, with the physical feeder impedance and the desired equivalent impedance known *in prior*, the desired virtual output impedance can be determined. Similarly, Liu and Zhang (2017) and Wang, Liu and Zhang (2017) exploited the virtual-output-impedance method to compensate for the voltage drops across the mismatched feeder impedances, achieving improved reactive power sharing. The virtual resistance is adaptively tuned using the feeder impedance and load active/reactive power

values. The virtual inductive reactance is determined from the virtual resistance based on the actual X/R ratio of the physical feeder impedance. On the other hand, capacitive virtual-output-impedance technique was exploited by Xu *et al.* (2014) to compensate the reactive power sharing error. The virtual capacitance value is decided based on the reactive output power of local DER through proportional control. However, it is recognised that reactive power sharing error cannot be fully eliminated unless the controller gain is accurately tuned based on actual line impedance - which is usually not known in advanced and will deviate with the changes of network topology.

On the other hand, the emerging virtual-output-impedance scheme is reportedly exploited in conjunction with advanced droop variants. For instance, Zhong (2013) has exploited the virtual-output-impedance schemes, forcing the equivalent feeder impedance to be resistive, to justify the adoption of inverse $P-V$ and $Q-f$ droop control for proportional power sharing. As shown in the same work, the mismatch resulted in opposite regulation effect (i.e., for two of the DERs with kVA rating ratio of 2:1, the reactive power sharing was regulated to 1:2 ratio instead). An *et al.* (2018) proposed and investigated virtual-output-impedance scheme in a $Q-\dot{V}$ droop-controlled islanded microgrid where only virtual inductance is utilised. The virtual inductance is adaptively tuned based on the reactive power deviation from the desired setpoint. Different from the norm of compensating the output voltage drop through virtual output impedance, a standard droop control with dispatch command scheme is enhanced with a feeder voltage drop compensator in Zhang *et al.* (2019) to eliminate the effects of feeder impedance mismatch in parallel-connected microgrid. The compensation terms are determined candidly from the voltage difference between desired voltage magnitude and actual droop output voltage magnitude. Recently, advanced computational algorithm is gradually exploited in microgrid-themed application. An offline genetic algorithm-based virtual output impedance control is presented in Zhu *et al.*, (2015, 2016) for reactive power sharing improvement in islanded microgrids of radial structure. The decision factors for adaptive tuning of virtual resistance are optimised using the genetic algorithm with the help of reactive power sharing estimator while fixing the virtual inductive reactance constant. Not only does the approach requires microgrid's parameters at the estimation stage, but the genetic algorithm-based virtual-output-impedance control was only designed for power-electronic-based DERs with equal kVA ratings. Later, the estimator is further enhanced in Zhu *et al.* (2018) to account for DERs with different capacity ratings. While proportional reactive power sharing improvement is noticed, it is obvious that the decentralised approach remains to be heavily dependent on the microgrid network model. Similarly, Peng *et al.* (2019) reported on an algorithm-based reactive power sharing improvement control with constant virtual output impedance and improved coupled droop control. Offline particle swarm optimisation control is implemented to determine the coupled droop coefficients.

In some literature, virtual-output-impedance scheme is used specifically for reactive power sharing improvement of low-voltage islanded microgrids, e.g., Li and Kao (2009). In order to achieve active and reactive powers decoupling of a low voltage coupled-droop-controlled islanded microgrid,

static virtual output impedance is introduced to the low voltage microgrid with resistive line impedance to represent the network with a high X/R ratio. Meanwhile, an estimation is presented in which droop coefficient is estimated during the grid-connected mode based on the voltage drop across feeder impedance and is subsequently implemented in the islanded mode. Similarly, Chen *et al.* (2016) proposed a coupled droop control with resistive-capacitive virtual output impedance for parallel-connected DERs in a low-voltage microgrid. The complex virtual output impedance is designed to modify the equivalent impedance to not only improve reactive power sharing among the parallel-connected DERs but also provide damping to high-frequency resonances (due to the presence of a large amount of high-order physical filters at the output stages of DERs) in the network.

As summarised above, it can be established that most of the decentralised schemes are tailored for microgrids with parallel architecture. Their model-dependent nature causes the decentralised schemes to be less feasible for their adoption in large-area islanded microgrids with complex structure, e.g., radial-structured microgrids. In addition, due to the absence of communication, it is conjectured that the model-dependent decentralised schemes will be less robust for ever-changing loading and network topology (as a result of plug-and-play of DERs).

2.3.2 Centralised schemes

To overcome the drawbacks of decentralised virtual-output-impedance-based control schemes, as mentioned in Subsection 2.3.1, Mahmood, Michaelson and Jiang (2015a) designed and investigated on a centralised reactive power sharing improvement control that exploits adaptive virtual impedance values. Communication is utilised to facilitate the tuning of the virtual output impedance, through PI controller, based on the reactive power reference generated by the central controller. In the work by Mahmood, Michaelson and Jiang (2015a), the virtual resistance and inductive reactance are equally tuned although it is discovered by Zhu *et al.* (2015, 2016) that the reactive power regulation effect of virtual resistance and inductive reactance are in principle not equivalent. Likewise, a centralised adaptive virtual-output-impedance control scheme was reported by Hoang and Lee (2018) and Pham and Lee (2021). The virtual inductance in the control scheme proposed by Hoang and Lee (2018) is adaptively tuned through an integral controller that tracks the reactive power sharing error; the virtual X/R ratio is kept arbitrarily at 5 for setting the virtual resistance based on the virtual reactance. While in the work by Pham and Lee (2021), the virtual inductive reactance is adaptively tuned against reactive power sharing by the means of PI controllers with virtual resistance negatively tuned due to the counter effect. In another work by Liu *et al.* (2018), a centralised control is proposed to realise reactive power sharing improvement through impedance mismatch elimination for parallel-connected microgrids. The physical feeder impedance is estimated from the voltage at point of common coupling, available through communication link and DER output currents. Along with a desired equivalent impedance, the virtual output impedance can be calculated.

Apart from the virtual-output-impedance scheme, the standard droop control with dispatch is implemented in centralised structure for reactive power sharing improvement among DERs in islanded microgrids. For example, a centralised secondary control complemented Q - V droop control was reported by Micallef *et al.* (2012) and Shi *et al.* (2020), in which the no-load voltage reference is adaptively tuned through PI controllers to achieve accurate reactive power sharing. Instead of adjusting the no-load voltage reference through dispatch, Mahmood, Michaelson and Jiang (2015b) presented a centralised secondary control that adaptively tunes the Q - V droop coefficients by means of integration of reactive power sharing error at the central controller. It is exhibited that although the reactive power sharing accuracy is slightly affected in the event of communication interruption, the adaptive droop coefficient scheme is able to improve the reactive power sharing. On the other hand, Raju P. and Jain (2019) introduced a modified Q - \dot{V} droop control with dispatch command for reactive power sharing improvement. Communication device, i.e., phasor measurement unit is utilised to acquire the total active and reactive power generation and, along with the prescribed power sharing ratio, generate the dispatch commands.

On the other hand, power flow analysis is adopted in conjunction with various microgrid control studies in recent years. A centralised, particle swarm optimisation control with the modified nonlinear load flow was proposed by Elrayah, Sozer and Elbuluk (2014) to optimally determine the droop parameters, i.e., the no-load voltage reference and droop coefficients, for improved reactive power sharing. In each iteration, the particle swarm optimisation control solves for the reactive power sharing error minimisation cost function and subsequently, the load flow analysis determines the operating points with the computed droop parameters. Mueller and Kimball (2017) designed and investigated a quasi-Newton power flow algorithm operating in the synchronous reference frame. The representation in synchronous reference frame is standard to power-electronic-based DER primary control. The centralised control scheme determines the operating points by means of optimising the Q - V droop coefficients through solving the Jacobian of the power flow algorithm using the steepest descent iteration method.

Summarily, different from the decentralised approach, the centralised schemes adopting full-graph communication typically do not require network parameters *in prior*. However, the centralised control structure poses a reliability risk of single point of failure. Without an appropriate provision, the centralised control may also face with the limitation of accommodating network topology changes caused by the plug-and-play requirement.

2.3.3 Distributed schemes

Alternatively, distributed secondary control schemes eliminate the risk posed by single point of failure as individual secondary controls are spread out across the microgrid network with each controller communicating with its neighbouring DER(s). Consensus algorithm is a distributed control protocol that is widely adopted in microgrid-themed studies. In its fundamental form, it drives the

individual system's states to a common set of steady-state values. For instance, consensus algorithm with $Q-\dot{V}$ droop control is exploited in the work by Schiffer *et al.* (2014, 2016) for weighted reactive power sharing. The weighting coefficients can be designed based on any criteria from generation costs, fuel consumption to emission costs, upon which the DERs reactive output power are weighted in order to realise proportional sharing. The proposed approach tracks the local and neighbouring DERs reactive output power to generate the corresponding references for inner voltage control loop. Bidram, Davoudi and Lewis (2014), R. Han *et al.* (2017), Lu *et al.* (2018) and Shafiee *et al.* (2018) reported on a similar form of consensus-based secondary control that ensures proportional reactive power sharing for droop-controlled microgrids. While the no-load voltage reference is appropriately adjusted in the proposals by Bidram, Davoudi and Lewis (2014) and Lu *et al.* (2018), from the consensus error, the approach proposed by Shafiee *et al.* (2018) adaptively tunes the $Q-V$ droop coefficients. Instead of droop parameters adjustment, the consensus-based scheme with PI controller proposed by R. Han *et al.* (2017) reportedly adjusts the reference voltage of the inner voltage control loop in parallel to the standard droop power control. This is different from the usual form of cascaded control loops. Consequently, the primary control stability is therefore also dependent on the distributed controller gains, posing a difficulty in control stability analysis.

Distributed consensus algorithm is also exploited in conjunction with virtual-output-impedance scheme by Zhang *et al.* (2017) and Zhou *et al.* (2018). In the former work by Zhang *et al.* (2017), the reactive power mismatch of the local DER and its neighbours, as computed by the consensus algorithm, is fed to a PI controller to generate the virtual output impedance correction term. Subsequently, the virtual resistance and inductance are adaptively tuned by the proportional controller for reactive power sharing error elimination. The consensus-based reactive power regulation scheme presented by Zhou *et al.* (2018) adaptively tunes the dynamic component of the virtual output impedance based on the tracking of neighbouring reactive output powers. Apart from the proportional fundamental positive sequence reactive power sharing, the work also expands the concept to account for unbalanced and harmonic power regulation.

Another advanced distributed algorithm - alternating direction multipliers method (ADMM) - is developed and studied by Lu and Chu (2018) for $Q-\dot{V}$ droop-controlled DERs. The ADMM-based approach realises accurate reactive power sharing through adaptively tuned droop coefficients which, reportedly, has a faster convergence rate as compared to the first-order consensus algorithm. Alshammari and El-Refaie (2020) presented a distributed secondary control with full communication graph for a standard droop control with dispatch. A quadratic optimisation function is implemented in the distributed control of each DERs to generate the required reactive power dispatch, tracking the average reactive power reference. The same full-graph communication architecture is adopted by Lai *et al.* (2018) in a distributed control algorithm having PI controllers that adaptively adjust the droop control's no-load voltage reference. However, the use of full communication graph reduces the attractiveness of the distributed control owing to the full information exchange requirement.

2.4 Review of secondary voltage regulation control

Although the reactive power focused schemes significantly improve the accuracy of reactive power sharing among DERs, the voltage and frequency deviations due to droop control would inevitably require secondary control for an acceptable system-wide regulation. This is a more-relevant consideration for large area microgrids than the small-area counterparts. The secondary (steady-state) frequency regulation is relatively more straightforward as compared to the voltage counterpart as frequency is a global variable; this means that proportional active power sharing at steady state is always guaranteed. In contrast, bus voltages are essentially local variables. Therefore, droop-based reactive power sharing control poses a trade-off problem between voltage and reactive power output. Therefore, one of the main objectives of this thesis is to improve the secondary voltage control in conjunction with the primary reactive power sharing control. In what follows, the secondary voltage regulation literatures are reviewed. The literatures have been categorised into two groups: one focuses only on the voltage control; the other considers both voltage and reactive power sharing.

2.4.1 Without reactive power sharing consideration

Bidram *et al.* (2013), Guo *et al.* (2015), Cai *et al.* (2016) and Dehkordi, Sadati and Hamzeh (2017) implemented a similar form of distributed reference tracking secondary voltage control for droop-controlled microgrids. Feedback linearisation is exploited for dynamical model linearisation of the voltage(droop)-controlled power-electronic-based DERs to facilitate the consensus-based control. The individual no-load voltage reference (Bidram *et al.*, 2013; Dehkordi, Sadati and Hamzeh, 2017) or voltage correction term (Guo *et al.*, 2015; Cai *et al.*, 2016) is dispatched by the corresponding secondary consensus control by means of eliminating the local and neighbouring bus-voltage disagreement. If accessible, the control scheme can also converge the voltage references in leader DERs. Similarly, Y. Han, Shen, *et al.*, (2017) reported on a *PI*-based distributed secondary voltage control in which the voltage correction is adjusted to compensate the voltage deviation caused by the DER's primary droop control. On a different note, a centralised secondary voltage control for single load-bus voltage regulation (through a *PI* controller) was studied by Aprilia *et al.* (2019). The work exploited a modified backward forward sweep power flow to determine the voltage magnitude of remote buses. The dispatch is generated such that the load-bus voltage magnitude is to be tracked to nominal, and is proportionally shared among DERs. Meanwhile, in the work by and Imran, Wang and Flaih (2019), the no-load voltage references of *dq*-voltage droop control are adjusted through individual *PI* controllers for single load-bus voltage restoration.

Aside from the aforementioned single load-bus voltage regulation, voltage control at multiple load-buses is also reported in literature. A similar form of single-objective voltage regulation scheme for islanded microgrids was proposed and studied in several works by Falahi, Butler-Purry and

Ehsani (2013), Zhang *et al.* (2015), Bayat *et al.* (2016), Sheng *et al.* (2016), Lou *et al.* (2017), Deckmyn *et al.* (2018) and Chen and Guo (2019). The voltage restoration proposed by Falahi, Butler-Purry and Ehsani (2013) is achieved through centralised model predictive control through the adjustment of no-load voltage reference of a non-inverter-based DER (which operates in the iso-synchronous mode). A simplified model is used to establish the optimisation control algorithm that exploits the surplus reactive power capacity for minimising the total voltage deviation of the load-buses. However, it was acknowledged by the work that, unless preceded by an accurate model simplification, the approach is by default not suitable for large-area microgrids.

Different from load-bus, voltage control at DER-bus utilised the directly available local information of the power-electronic-interfaced DER. Distributed consensus-based model predictive control was proposed by Guo, Li and Zheng (2017) and Lou *et al.* (2017, 2018) for secondary voltage regulation at DER-buses. Lou *et al.* (2017) proposed a reference tracking consensus-based model predictive control in which the discrete-time secondary control is supplemented with a predictive term. Droop correction is designed such that, given the global reference and the information of its immediate neighbours, the DER voltages can try to converge to a common value. However, this control design reduces the “distributed nature” of the distributed control algorithm where it is always assumed that only selected DERs (usually a small number) has access to the global reference. The control strategy is extended by Guo, Li and Zheng (2017) and Lou *et al.* (2018) to account for the nonlinear dynamical nature of power-electronic-interfaced DERs. The non-linearity is linearised through feedback linearisation method. With the partially-linearised model, the consensus-based receding horizon optimisation attempts to eliminate local-neighbouring DER voltage error and, if directly communicating to the leader DER, to converge it to a predefined reference value. Chen and Guo (2019) designed and investigated a first-order consensus-based voltage regulation control that tracks its immediate neighbours and the reference, if accessible. Differently, La Bella *et al.* (2017) presented a centralised model predictive control for voltage regulation of an inversely-droop-controlled islanded microgrid. The predictive control scheme enables an optimal output power coordination of dispatchable rotating generators and intermittent DERs (with power profiles prediction) through optimal adjustment of the no-load voltage references of the non-intermittent DERs (note: these DERs use inverse droop instead of the standard droop scheme). The proposed approach works at a low bandwidth of one-minute sampling rate, over fifteen-minute prediction horizon. Following the receding horizon principle, the controller implements the first entry of the computed control variable, and the process is repeated at the next time instant.

Other than the consensus control, advanced control algorithm is recently exploited in conjunction with secondary voltage control of islanded microgrids. In the secondary control scheme proposed by Zhang *et al.* (2015), the control problem of reactive power support of power-electronic-interfaced DERs and demand response resources is casted as a distributed dual decomposition problem to minimise network losses with the voltage regulation represented as equality constraint.

Generic nonlinear power flow is utilised, and the optimisation problem is solved by adopting convex semi-definite programming relaxation. In another work by Bayat *et al.* (2016), particle swarm optimisation is utilised for coordinating DERs and demand responses of the islanded microgrid while regulating the load-bus voltages to within the admissible limits. The Jacobian of power flow is modified (by adding an additional state variable) to accommodate the frequency deviation caused by the absence of slack bus. A similar reactive power scheduling of DERs and switching devices (e.g., under-load tap changer and shunt capacitors) realising secondary voltage regulation was proposed and investigated by Sheng *et al.* (2016) in offline mode (one-day ahead planning). Trust region sequential quadratic programming method and branch and bound technique are exploited to solve the optimisation control problem of active power loss and number of switching operation minimisation. The inequality constraint feature is exploited for maintaining the grid voltages to within the allowable tolerance. Instead of reactive power support, the secondary control scheme proposed by Deckmyn *et al.* (2018) attempts to maintain bus voltages to within the allowable margin through active power coordination of DERs operating under inverse droop control.

Based on the literature review, it is established clearly that classical power flow algorithms, e.g., Gauss Seidel, Newton Raphson, etc are normally not applicable directly for microgrids. This is due to two reasons: the inexistence of slack bus in islanded microgrids and the dependence of active/reactive powers on frequency/voltage due to the primary droop control. Various microgrid-themed power flow algorithms have been proposed in the past decade (Abdelaziz *et al.*, 2013; Mumtaz *et al.*, 2016; Allam, Hamad and Kazerani, 2018; Ren and Zhang, 2018; Cai and Khatib, 2019; Jamalzadeh and Hong, 2019; Pompodakis, Kryonidis and Alexiadis, 2020). In recent few years, power flow algorithms embedded multi-load-bus voltage control scheme has emerged as a research subject. For example, Agundis-Tinajero *et al.* (2019) implemented an extended-optimal-power-flow-based secondary central control for droop-controlled islanded microgrids. The secondary optimal control is designed for microgrid efficiency improvement and voltage regulation through reactive power management with compliance of generation unit capacities constraint. The mismatches between generic power flow and droop equations are used to solve for the no-load voltage references and droop coefficients, through *fmincon* optimisation solver in MATLAB.

2.4.2 With reactive power sharing consideration

In order to improve the power sharing accuracy while achieving average voltage regulation at DER-buses for islanded microgrids with predominantly resistive lines, Golsorkhi, Hill and Karshenas (2018) and Golsorkhi *et al.* (2019) introduced the communication-based voltage-current ($V-I$) droop control with dispatch in the primary control. The problem of proportional power sharing among DERs is represented as a current sharing control problem. The voltage correction term is computed from the consensus control, attempting to eliminate the local-neighbouring per-unit current magnitude disagreement. On top of that, an integral control is used to regulate the estimated average

voltage across DER-buses to nominal by means of d -axis voltage correction term. On the other hand, Hoang and Lee (2019) reported an integral-based, centralised secondary control for average voltage regulation across DER-buses and proportional reactive power sharing among power-electronic-based DERs in islanded microgrids. Dynamic component of virtual inductance is adaptively tuned by means of an integral controller to eliminate the reactive power sharing errors with a predefined static virtual inductance (while the virtual resistance is empirically adjusted to maintain a fixed X/R ratio of five). In addition, the common voltage correction dispatch restored the DER-bus voltages without compromising the power sharing accuracy. A distributed PI -based control scheme was proposed by Shafiee, Guerrero and Vasquez (2014) and Lai *et al.* (2018). The controller realises average DER voltage regulation and reactive power sharing improvement through droop's no-load voltage reference adjustment. However, since full/complete communication graph is required to compute the desired average voltage using all DER-bus voltages, the "distributed control" nature of the control algorithm has diminished. On the other hand, Gu *et al.* (2017) presented an estimator-based decentralised secondary control. The nonlinear estimator, embedded in each power-electronic-interfaced DER, determines the average DER voltage independently using the local DER voltage value and locally estimated neighbouring DERs' average voltage value, assuming that network/line parameters are known in advanced. After estimation, the decentralised PI controller tracks the predefined voltage reference through dispatch. However, owing to the reliance of network model, its extension to large-area microgrids with complex structure is conjectured to be difficult.

In another group of works by Nasirian *et al.* (2016), Zhang *et al.* (2017), , Lu *et al.* (2018), Shafiee *et al.* (2018) and M. Shi *et al.* (2020), a new type of secondary voltage consensus control techniques based on the use of estimator were proposed. Apart from the non-droop-based power control in the control scheme proposed by Nasirian *et al.* (2016)), all other control schemes use consensus-based reactive droop power control. Broadly speaking, each estimator approximates the average voltage magnitude of local DER-bus by making use of the local and estimated averaged voltage of the neighbours. Then, the estimated average voltage is fed into a PI controller which then generates control references for the inner voltage control loop (Nasirian *et al.*, 2016), as the dispatch term (Shafiee *et al.*, 2018; M. Shi *et al.*, 2020), or as the no-load voltage reference adjustment term (Zhang *et al.*, 2017; Lu *et al.*, 2018). In these works, the reactive power sharing improvement and the average DERs voltage restoration (some maintain DER-bus voltages to within the acceptable margin) are achieved through the consensus control, maintaining a fully distributed algorithm. Another variant of estimator-based secondary control was proposed by Lai *et al.* (2019) for multiple microgrid clusters. The distributed secondary control is grouped into intra-cluster (i.e., control among DERs within a microgrid cluster) and inter-cluster schemes (i.e., control among multiple clusters). The intra-cluster DERs are categorised into leaders and followers, where the leaders are responsible for information exchange within its own cluster and in facilitating the communication with neighbouring clusters. The inter-cluster control exploited the consensus control mechanism to eliminate the differences between the local and neighbouring (estimated) voltage, and the reactive

power sharing errors among clusters. If required, the consensus control can also converge the voltage to predefined nominal value by generating the desired voltage and reactive power references, which then propagated to the follower DERs (in the intra-cluster control) for no-load voltage reference adjustment.

A distributed model predictive control is proposed by Gómez *et al.* (2020) to optimise a multi-objective quadratic cost function. The control aim is to regulate the average frequency/voltage and to reach consensus on the DERs' active/reactive power. The predictive approach reportedly demonstrated a superior reactive power sharing performance than the widely reported distributed *PI*-based control, even with the presence of communication delay.

While average voltage control can be realised either through the single-input single-output *PI* controller or estimator-based consensus control based on average voltage generation/estimation, the voltage control at multiple DER-buses makes use of the live information (i.e., DER-bus voltage magnitude which is locally available). In the work by Elrayyah, Sozer and Elbuluk (2014), the primary droop control is modified with coupled voltage correction term based on the active power. It is proposed that with the correction gain designed in the proportion of P - f droop coefficients, the voltages at DER-buses can be regulated equally with the improved reactive power sharing through particle swarm optimisation remains unaffected. Consensus-based secondary control for multiple DER voltage regulation is reported in Bidram, Davoudi and Lewis (2014), R. Han *et al.* (2017) and Xu and Sun (2018). Different from the dispatch-based reactive power sharing scheme in Bidram, Davoudi and Lewis (2014), and R. Han *et al.* (2017), Xu and Sun (2018) adaptively tuned the virtual resistance and inductance based on the consensus reactive power sharing error. However, the reactive power sharing accuracy may be compromised with the adoption of coupled control gain to dispatch no-load voltage reference for reactive power sharing improvement and multi-DER voltages regulation (Bidram, Davoudi and Lewis, 2014). In R. Han *et al.* (2017), the voltage control is presented as containment-based scheme to regulate DER voltages within tolerance range. The DER voltages are directly adjusted from local-neighbouring and reference tracking in which the reference can either be the lower/upper voltage boundaries. Similarly, a distributed *PI*-based secondary control is reported in Han *et al.* (2016) to directly regulate the DER voltages to a common reference in an islanded microgrid exploiting a virtual-output-impedance scheme for reactive power sharing improvement. However, the primary control stability will become dependent on the secondary control gain (Han *et al.*, 2016; R. Han *et al.*, 2017).

Different from the aforementioned consensus control where the secondary control effort (i.e., voltage regulation and reactive power sharing improvement) is evenly divided among the power-electronic-interfaced DERs, Simpson-Porco *et al.* (2015) and Liu *et al.* (2020) report on a tuneable consensus-based secondary control to address the conflicting objectives of multi-DER-buses voltage regulation and reactive power sharing. It is proposed that a leader DER is tuned for voltage regulation while the remaining follower DERs are controlled for reactive power sharing improvement. By this

way, the leader DER voltage can be regulated and the follower DER voltages will track the leader DER while accurate reactive power sharing among all DERs can be simultaneously achieved.

Different from DER-buses, voltage regulation at load-buses is relatively complicated as information is not directly available at the power-electronic-based DER. In several works by Bidram, Davoudi and Lewis (2014), Wu, Shen and Iravani (2018) and Wu *et al.* (2020), voltage regulation at single load-bus is enabled by means of *PI* controller which determines the voltage reference. Subsequently, the corresponding voltage reference is tracked in the consensus control to regulate the DER voltages through the adjustment of no-load voltage references. As expected, this form of hierarchical control design enables single load-bus voltage regulation while achieving an accurate reactive power sharing. Afshar *et al.* (2019) implemented a neural-network-based centralised control for accurate power sharing and load voltage restoration, replacing the primary droop-based power control. The control problem is formulated considering parallel-connected DERs sharing a common load-bus and nominal load voltage. With the desired power sharing, the power-electronic-based DER voltages magnitude and phase angle references are computed using the neural-network-based secondary control for the inner voltage and current control. Similarly, a *PI* controller is utilised in another work by Zhang *et al.* (2019) to regulate the DER voltages, eliminating the undesired single load-bus voltage deviation. However, owing to the direct control of load-bus voltage without considering the overall network characteristic/dynamic, the system equilibrium and primary control stability consequently become heavily dependent on the secondary control parameters.

While the single load-bus voltage regulation is typically enabled through the single-input single-output *PI* controller, voltage regulation at multiple load-buses generally exploits power flow analysis. In the work by Yang *et al.* (2016), a centralised secondary optimal control for multiple load-bus voltage regulation and reactive power sharing improvement is developed and investigated. The multi-objective control problem is formulated in the form of quadratic function, through exploiting the iterative-based classical Newton Raphson power flow algorithm. Primal dual interior point method is adopted to solve the constrained optimisation problem. The optimal output adaptively tunes the no-load voltage references of the droop function adopted in the DERs. Similarly, Ouyang, Xia and Zou (2018) formulated a quadratic programming control problem based on the Jacobian of generic power flow equations. The multi-objective control problem is solved for the desired no-load frequency/voltage references, which will in turn regulate the frequency, voltage, and active/reactive powers of the DERs.

2.5 Summary

This chapter has provided a detailed literature review in the relevant subject areas. First, the standard droop control is introduced and its inherent shortcoming in microgrid application is analysed. This is followed by a comprehensive review of the droop-based control schemes focusing

on reactive power correction, with and without the utilisation of communication. Attributes of the standard and advanced droop control schemes are outlined in Table 2.1. Then, secondary voltage regulation with and without the consideration of reactive power sharing issue are summarised. The surveyed control schemes have been further sub-categorised into control schemes targeting DER-bus and load-bus voltage regulation. Attributes of selected secondary control schemes with improved reactive power sharing are highlighted in Table 2.2. All the reviewed works in the area of voltage regulation and reactive power sharing control in microgrids are tabulated in Fig. 2.2.

Based on the provided surveys, the following points are established:

- In the early stage of research (2005-2013), majority of the research works focused on solving the reactive power sharing issue of microgrids. Summarily, the unequal/disproportionate reactive power sharing issue is a result of voltage discrepancies at the points of couplings of the DERs with the microgrid network at different nodes. In about the same period, the interest on virtual-output-impedance-based droop control had emerged and gained increasing attention. This relatively new (as compared to the dispatch-based droop control technique) primary control technique is mainly being used in conjunction with power-electronic-based DERs whereas the dispatch-based technique can be used in all kinds of DERs, both power-electronic and rotating machine types. Also, despite the significant amount of works on the dispatch-based droop control and the virtual-output-impedance-based droop control, there is no clear evidence on the merits and demerits of these two variants of droop control schemes. Hence, Chapter 4 of this thesis will present an assessment of the two groups of reactive power focused droop-based schemes through a *DIGSILENT-PowerFactory-Python* co-simulation platform.
- Although decentralised control schemes rule out communication requirement from the outset, the model-dependent nature limits its implementation to microgrid with ever-changing loading and/or network topology. While centralised control technique is able to accommodate the loading changes due to the adoption of communication, the central controller imposes the risk of single point failure. In addition, the rigid centralised structure may also face with the limitation of accommodating network topology changes. Distributed control structure serves as an alternative that single point of failure risk is obviated due to the spread of controls across microgrid network. Moreover, due to the sparse communication requirement, distributed control can accommodate changes in either loading or network topology which aligns with the plug-and-play feature of microgrids. Furthermore, distributed control is highly relevant to large-area microgrids in which DERs/loads are sparsely connected across the network. Chapter 5 of this thesis will present two distributed secondary control schemes in conjunction with the virtual-output-impedance-based droop control, which realise proportional reactive power sharing for large-area islanded microgrids.

- In recent few years (2016-2019), various secondary, multi-objective optimal controls of voltage and reactive power have been implemented in conjunction with microgrids of different sizes. However, as far as large-area microgrid is concerned, there have been very limited attempts to date. The main obstacle is on the needs of an efficient power flow algorithm that can provide accurate near-real-time information, enabling the secondary control of remote-buses' operating points. Thus, Chapter 6 of this thesis will provide two novel optimal control solutions that fulfils the multi-objective control while having a relatively more efficient algorithm than the existing works.

Table 2.1. Attributes of standard and advanced primary droop control schemes.

| Control schemes | Attributes |
|--------------------------|---|
| Standard droop control | <ul style="list-style-type: none"> • Simple implementation • Only appropriate for highly inductive line • Results in voltage and frequency deviation |
| Inverse droop control | <ul style="list-style-type: none"> • Simple implementation • Tailored for highly resistive line |
| Adaptive droop control | <ul style="list-style-type: none"> • Simple implementation • Improved reactive power sharing accuracy • Results in voltage and frequency deviation |
| Coupled droop control | <ul style="list-style-type: none"> • Complicated implementation • Address the effect of active and reactive power coupling |
| Virtual output impedance | <ul style="list-style-type: none"> • Simple implementation • Compensate for feeder impedance mismatch • May require network parameters • Results in further voltage deviation |

Table 2.2. Attributes of selected advanced secondary voltage regulation control schemes with improved reactive power sharing.

| Secondary control schemes | Attributes |
|--|---|
| (Nasirian <i>et al.</i> , 2016; Lu <i>et al.</i> , 2018; Shafiee <i>et al.</i> , 2018; Lai <i>et al.</i> , 2019; M. Shi <i>et al.</i> , 2020) | <ul style="list-style-type: none"> • Consensus control with estimator • Multi-DER bus voltage regulation • Multiple microgrid clusters (Lai <i>et al.</i>, 2019) • No clear tuning rule to ensure stability |
| (Gómez <i>et al.</i> , 2020) | <ul style="list-style-type: none"> • Distributed MPC • Superior reactive power sharing performance • Multi-DER bus voltage regulation • Frequency regulation • Operational constraints considered |
| (Bidram, Davoudi and Lewis, 2014; Simpson-Porco <i>et al.</i> , 2015; R. Han <i>et al.</i> , 2017; Xu and Sun, 2018; Liu <i>et al.</i> , 2020) | <ul style="list-style-type: none"> • Consensus control (tuneable consensus control in Simpson-Porco <i>et al.</i> (2015) and Liu <i>et al.</i> (2020)) • Multi-DER bus voltage regulation (containment-based in R. Han <i>et al.</i> (2017)) • Consider voltage margin (R. Han <i>et al.</i>, 2017) • Coupled control gain may compromise reactive power sharing accuracy |
| (Bidram, Davoudi and Lewis, 2014; Wu, Shen and Iravani, 2018; Wu <i>et al.</i> , 2020) | <ul style="list-style-type: none"> • Consensus control with <i>PI</i> • Single load bus voltage regulation • No clear tuning rule to ensure stability |
| (Afshar <i>et al.</i> , 2019) | <ul style="list-style-type: none"> • Neural-network-based centralised control • Single load bus voltage regulation • Prone to single-point failure • Control system equilibrium and primary control stability heavily dependent on secondary control parameters |
| (Yang <i>et al.</i> , 2016; Ouyang, Xia and Zou, 2018) | <ul style="list-style-type: none"> • Centralised optimal control • Multi-load bus voltage regulation • Operational constraints considered • Prone to single-point failure • Exploited iterative-based power flow equations • Computationally intensive |

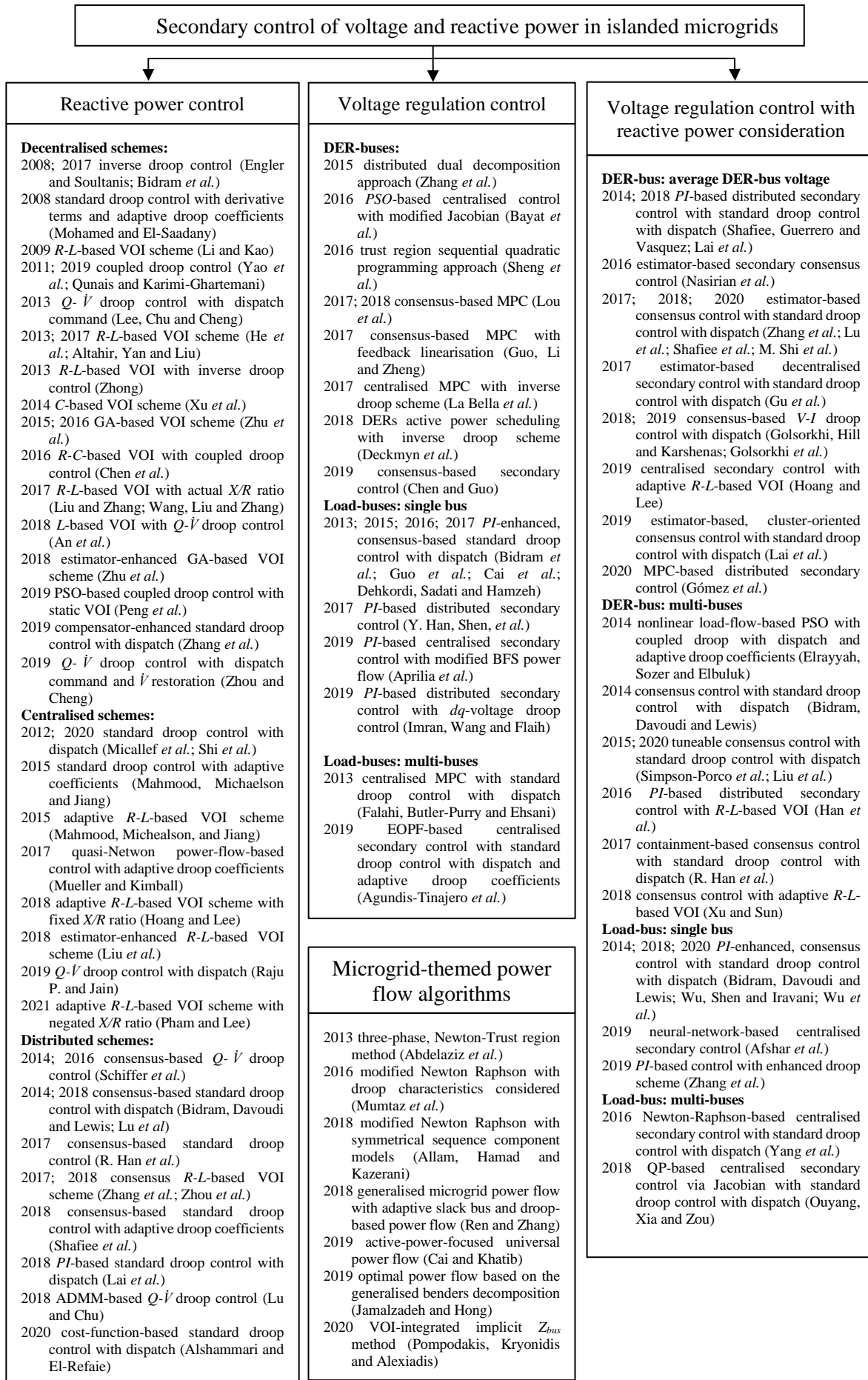


Fig. 2.2. Taxonomy of existing voltage regulation and reactive power control in the area of microgrids.

Chapter 3 Fundamental Concepts

3.1 Introduction

This chapter discusses the fundamental concepts used in this thesis and is organised as follows: Section 3.2 introduces the alpha-beta, direct-quadrature transformations, and dynamical model of droop-controlled power-electronic-interfaced DERs. Section 3.3 describes the algebraic graph theory and discusses the consensus algorithm for first-order discrete-time systems. Section 3.4 reviews the fundamental principles of quadratic programming. Finally, Section 3.5 summarises this chapter.

3.2 Dynamical modelling of voltage-controlled voltage source inverter-based DERs

The alpha-beta transformation (also referred to as “Clarke transformation”) represents the transformation that converts the time-domain three-phase (abc) current and voltage quantities to a space vector, which is expressed in the stationary, two-axis ($\alpha\beta$) reference frame. The transformation matrix is given by

$$\begin{bmatrix} \alpha \\ \beta \end{bmatrix} = k \begin{bmatrix} 1 & -\frac{1}{2} & -\frac{1}{2} \\ 0 & \frac{\sqrt{3}}{2} & -\frac{\sqrt{3}}{2} \end{bmatrix} \begin{bmatrix} a \\ b \\ c \end{bmatrix} \quad (3.1)$$

where $k = \frac{2}{3}$ for an amplitude-invariant transformation and $k = \sqrt{\frac{2}{3}}$ for a power-invariant transformation. Through the alpha-beta transformation, the real and imaginary components can be identified, in which the real part of the space vector is equal to the instantaneous value of the α -axis components and the imaginary part is equal to that of the β -axis, as depicted in Fig. 3.1(left).

The direct-quadrature transformation (also referred to as “Park transformation”) is used to realise the transformation of the stationary-axis space vector into a rotating synchronous (dq) reference frame. The transformation matrix is given by

$$\begin{bmatrix} d \\ q \end{bmatrix} = \begin{bmatrix} \cos \theta & \sin \theta \\ -\sin \theta & \cos \theta \end{bmatrix} \begin{bmatrix} \alpha \\ \beta \end{bmatrix} \quad (3.2)$$

where θ is the angle between the stationary α -axis and the d -axis (real-axis) of the synchronous reference frame, as illustrated in Fig. 3.1(right).

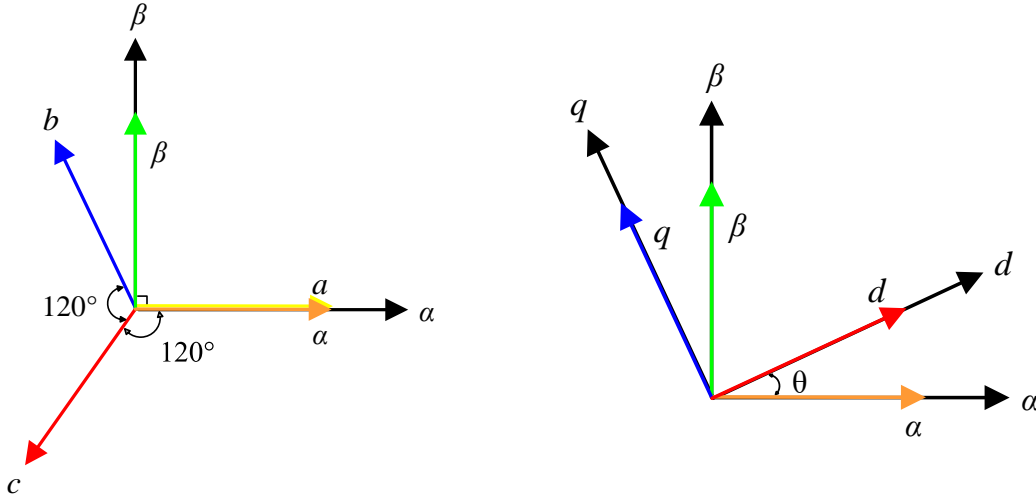


Fig. 3.1. (left) Clarke transformation and (right) Park transformation.

Power-electronic-interfaced DERs are expected to be prevalent in future microgrids. They are the main physical layer to integrate the emerging renewable energy resources e.g., photovoltaic systems, wind turbines and fuel cells, into the grids. An accurate power-electronic-based DER model that is suitable for analysing the integration of large amount of DER units into islanded microgrids is crucial to enable an accurate investigation of the behaviour of large-area microgrids in conjunction with the developed hierarchical control techniques in this thesis. Since this work focuses on islanded microgrids, droop(voltage)-controlled DERs are relevant. The modelling of droop-controlled power-electronic-based DERs is presented next.

The primary control of a droop-controlled DER includes a droop-based power control, an output voltage control, and an inverter current control, as depicted in Fig. 3.2 (modified from the figures by Bidram *et al.* (2017)). With all the local control loops operating in the synchronous reference frame, the direct (d) and quadrature (q) notations will be used throughout the modelling of the primary control layer.

In the power control loop, the synchronous reference frame is made aligned to the d -axis component of the droop output voltage vector \mathbf{v}_{odi}^d . Therefore, the voltage components can be expressed as

$$\begin{aligned} v_{odi}^d &= V_i \\ &= V_i^* - n_i Q_i \\ v_{oqi}^d &= 0 \end{aligned} \quad (3.3)$$

where $\mathbf{v}_{oi}^d = v_{odi}^d + jv_{oqi}^d$, v_{odi}^d and v_{oqi}^d is the d - and q -axis components of the droop voltage reference, normalised to the phase peak voltage. The synchronous reference frame's angular position is obtainable from the standard P - f droop in (2.1) after synchronisation of the corresponding DER with the microgrid. The active and reactive output powers with low-pass filtering and amplitude-invariant

transformation can be calculated as

$$\begin{aligned}\tau_c \frac{dP_i}{dt} + P_i &= \frac{3}{2} (v_{odi} i_{odi} + v_{oqi} i_{oqi}) \\ \tau_c \frac{dQ_i}{dt} + Q_i &= \frac{3}{2} (v_{oqi} i_{odi} - v_{odi} i_{oqi})\end{aligned}\quad (3.4)$$

The output voltage control loop is summarised as

$$\begin{aligned}
v_{odi,err} &= v_{odi}^d - v_{odi} \\
v_{oqi,err} &= v_{oqi}^d - v_{oqi} \\
i_{fdi}^* &= K_{vi}^P v_{odi,err} + K_{vi}^I \int u_{odi,err} dt + i_{odi} - \omega_b C_{fi} v_{oqi} \\
i_{fqj}^* &= K_{vi}^P v_{oqi,err} + K_{vi}^I \int u_{oqi,err} dt + i_{oqi} + \omega_b C_{fi} v_{odi}
\end{aligned} \tag{3.5}$$

where i_{fdi}^* and i_{fqd}^* are the inverter current reference components, ω_b is the nominal angular frequency, C_{fi} is the capacitive filter of i^{th} DER, and K_{vi}^P and K_{vi}^I are the output voltage control's PI control gains.

The computed inverter current reference components are then propagated to the inverter current control loop, summarised as

$$\begin{aligned} i_{fdi,err} &= i_{fdi}^* - i_{fdi} \\ i_{fqd,err} &= i_{fqd}^* - i_{fqd} \\ v_{cdi}^* &= K_{ci}^P i_{fdi,err} + K_{ci}^I \int i_{fdi,err} dt - \omega_b L_{fi} i_{fqd} \\ v_{cqf}^* &= K_{ci}^P i_{fqd,err} + K_{ci}^I \int i_{fqd,err} dt + \omega_b L_{fi} i_{fdi} \end{aligned} \quad (3.6)$$

where v_{cdi}^* and v_{cqf}^* are the converter voltage reference components, L_{fi} is the inductive filter of i^{th} DER, and K_{ci}^P and K_{ci}^I are the inverter current PI control gains.

An overview of the primary control of a standard droop-controlled DER implemented in *DigSILENT PowerFactory* (i.e. described in Appendix A) is depicted in Fig. 3.3. The *PowerFactory* measurement block, i.e. *voltage/current measurement device* which operates in stationary reference frame by default, is used to obtain the required measurements, e.g. output voltage/current and inverter current. The signals are then sampled through the *sample and hold* module at a clock signal before rotationally transformed into synchronous reference frame and feed-forwarded for primary control.

In this thesis, since the focus is on the advancement of the droop control and the secondary control strategies, the primary output voltage and inverter current controller gains are tuned empirically. The basic tuning principle is to ensure that the control bandwidth is sufficiently decoupled, assuming that the voltage control dynamic is much faster than the droop-based power control dynamic. The innermost current control loop is tuned first with the assumption of a constant inverter current reference components, typically being the control output of voltage control loop. Then, the voltage control is tuned in a similar way, by assuming a constant voltage reference (i.e., normally being the output of droop-based power control loop). It is worth noting here that tuning of the primary voltage and current control loops can be achieved through analytical means. One example is through the state-space small-signal model of a power-electronic-based DER, presented by Pogaku, Prodanović and Green (2007).

A conference paper, i.e. (Wong *et al.*, 2018) is produced to report on the power-electronic-interfaced DER model implemented in *DigSILENT PowerFactory* simulation package. It is justified that the model is able to reflect the controller's dynamics onto the islanded microgrid and the subsequent research work can then be made possible.

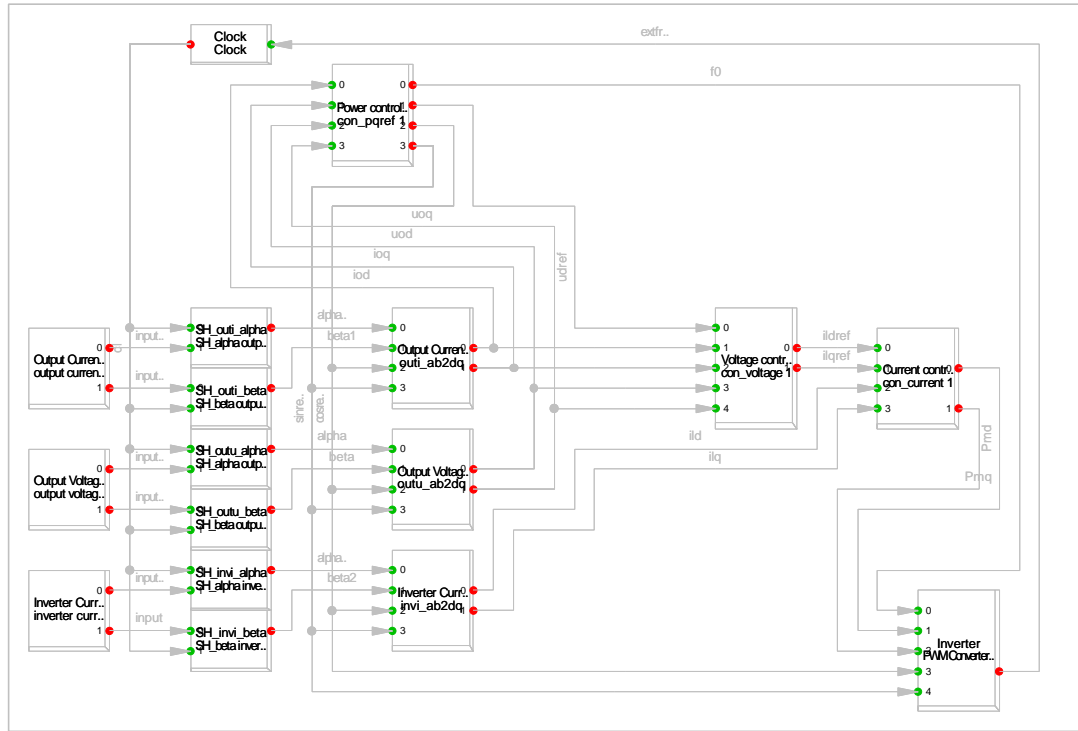


Fig. 3.3. Primary control of a standard droop-controlled DER built in *DIGSILENT PowerFactory*.

The prevalence of power-electronic-interfaced DERs in distribution microgrids may result in significant voltage and frequency deviations due to low rotating inertial energy. It is assumed that the droop (voltage) controlled DERs considered in this thesis are connected to an ideal, dispatchable source, e.g., fuel cell and battery unit. The “ideal” source assumption is justified through two aspects: first, since secondary control has a very short control time frames (in seconds), the “ideal” or unlimited capacity assumption is justifiable if the DC-bus energy storage is sufficiently large; second, in a stable secondary control where the voltage/frequency references are well within the practical ranges, the “ideal” voltage and power rating assumption is acceptable. However, if the controller would become unstable for a sustained period (e.g., longer than few seconds), the “ideal” assumption will affect the accuracy of the simulation result. However, this situation (of attempting to bring any unstable system back to stability) is seldom considered in this area of research as the overarching aim of primary/secondary control research is to completely avoid control instability.

The DER inverters are of grid-forming type, which provides a provision to actively regulate the network frequency and voltage profile through the output frequency and voltages of inverter output frequency and droop output voltages in a microgrid with a large number of power-electronic-interfaced inverters. For current-controlled DERs, the inverters are normally configured in the closed-loop power control mode where the input-output powers of the inverters are controlled to given references (from the tertiary control layer). For simplification, these (generating) loads can be considered as “negative” loads in the microgrid. Since this is beyond the scope of the thesis, current-controlled DERs are not considered hereafter.

Every physical DER has a finite power and capacity ratings. The finite power rating will appear as the maximum power exchange that a DER can make with the microgrid. In terms of control design, it appears as the non-linear limits or constraints that are normally not considered by linear control design. Chapter 5 focuses on linear consensus control design and hence will not take this into account. Chapter 6 does indirectly consider the power/capacity rating in the form of constraints in the optimal control. It is also worth highlighting that the power fluctuation due to resource intermittency and state of charge fluctuation due to unmodelled phenomena at energy storages (which are commonly considered in tertiary control but rarely in secondary control) are not considered in this thesis.

3.3 Distributed consensus algorithm

In a distributed cooperative system, the control protocol must respect the prescribed distributed graph theory. That is, the individual unit control is dependent only on the information of the local unit and those from its neighbours as defined by the designed communication graph (detailed next).

The communication network of a microgrid can be modelled as a graph with edges corresponding to the allowed information flow between DERs, denoted as nodes. The graph is generally expressed as $G = (V_G, E_G, A_G)$ with a set of N nodes $V_G = \{v_1, v_2, \dots, v_N\}$, a set of edges $E_G \subset V_G \times V_G$ and an adjacency matrix $A_G = [a_{ij}] \in \mathbb{R}^{N \times N}$. The edges of the graph denote the communication links between DERs and each edge $(v_j, v_i) \in E_G$ represents the flow of information from node j to node i . The number of edges having information flowing into v_i is denoted as in-degree while the number of edges having information flowing out of v_i is denoted as out-degree. The graph is termed to be undirected if $(v_j, v_i) \Rightarrow (v_i, v_j) \in E_G$; otherwise, it is termed as directed graph or digraph. Associated with a weight a_{ij} of edge (v_j, v_i) , $a_{ij} > 0$ if there is an edge from node j to node i ; otherwise, $a_{ij} = 0$. Node j is called a neighbour of node i if $(v_j, v_i) \in E_G$ and the set of neighbours of node i is denoted as $N_i = \{v_j : (v_j, v_i) \in E_G\}$. The in-degree matrix is defined as $D = \text{diag}\{d_i\} \in \mathbb{R}^{N \times N}$ with the weighted in-degree of node v_i , d_i is equivalent to the i^{th} row sum of adjacency matrix A_G (i.e., $d_i = \sum_{j \in N_i} a_{ij}$). The Laplacian matrix of the graph is defined as $L_G = D - A_G$ which is used to analyse the properties of a distributed graph topology. A digraph is said to have a spanning tree if there is a root node with a directed path to all the other nodes and every other node has in-degree equal to one except the root node. A graph may have multiple spanning trees.

Consensus control algorithm is fundamentally a distributed control protocol that attempts to drive the selected states to a consensus value at steady state: $x_i = x_j, \forall i, j$. Considering that all N nodes in graph G have a first-order discrete-time dynamics, the consensus equations can be given by

$$\begin{aligned} x_i(k+1) &= x_i(k) + \delta_i(k) \\ \delta_i(k) &= -c \sum_{j \in N_i} a_{ij} [x_i(k) - x_j(k)] \end{aligned} \quad (3.7)$$

where c is the consensus control coupling gain, and x_i and δ_i denote the state variable and control input of node i . The global dynamics of the consensus control can be expressed in compact matrix form as

$$\begin{aligned}\mathbf{x}(k+1) &= (\mathbf{I} - c\mathbf{L}_G)\mathbf{x}(k) \\ &= \mathbf{P}\mathbf{x}(k)\end{aligned}\tag{3.8}$$

where $\mathbf{x} = [x_1 \ x_2 \ \dots \ x_N]^T \in \mathbb{R}^N$. It is established that consensus is guaranteed if the control coupling gain satisfies (Stanoev and Smilkov, 2013)

$$c < \frac{1}{d_{\max}}\tag{3.9}$$

i.e., a sufficient condition for the Perron matrix \mathbf{P} to have all eigenvalues within the unit circle where $d_{\max} = \max(\mathbf{D})$.

However, since information is exchanged among nodes through communication link, time delays from information transmission may need to be considered, depending on the focus of the analysis. Let τ denotes the time delay in information communicated between two nodes, the consensus control protocol in (3.7) can be re-expressed as

$$\begin{aligned}x_i(k+1) &= x_i(k) + \delta_i(k) \\ \delta_i(k) &= -c \sum_{j \in N_i} a_{ij} [x_i(k-\tau) - x_j(k-\tau)]\end{aligned}\tag{3.10}$$

Provided that the communication graph is time-invariant, undirected and connected, the time-delayed consensus control is said to be globally asymptotically stable if and only if (Olfati-Saber and Murray, 2004; Olfati-Saber, Fax and Murray, 2007; Zhang *et al.*, 2017; Zhou *et al.*, 2018)

$$0 < \tau < \frac{1}{2\lambda_{\max}c}\tag{3.11}$$

where λ_{\max} is the maximum eigenvalue of the communication graph's Laplacian matrix \mathbf{L}_G .

Although consensus control is widely exploited in secondary control of microgrids, it is crucial to highlight here that consensus control typically does not solve for optimality. This is one of the motivations to advance the developed consensus control technique (Chapter 5) into one that solves for optimality (Chapter 6).

3.4 Quadratic programming

Quadratic programming is a tool to solve an optimisation problem with quadratic objective function. Consider a discrete-time linear system of

$$\mathbf{y}(k+1) = \mathbf{A}\mathbf{x}(k) + \mathbf{B}\mathbf{u}(k) \quad (3.12)$$

where \mathbf{u} , \mathbf{x} and \mathbf{y} are the input, state and output variable vectors. Suppose that a tracking control objective with integral action (i.e., to get offset free tracking) is assumed, which gives

$$J = (\mathbf{y}^*(k+1) - \mathbf{y}(k+1))^T \mathbf{W} (\mathbf{y}^*(k+1) - \mathbf{y}(k+1)) + \Delta \mathbf{u}^T(k) \mathbf{R} \Delta \mathbf{u}(k) \quad (3.13)$$

where \mathbf{y}^* is the output reference vector, and weighting factor \mathbf{W} and penalty factor \mathbf{R} are symmetric matrices. Accordingly, the system (3.12) can be augmented with $\mathbf{u}(k) = \mathbf{u}(k-1) + \Delta \mathbf{u}(k)$ and the cost function (3.13) can be formulated into a quadratic programming problem, expressed in the form of

$$\begin{aligned} \text{minimise } J &= \frac{1}{2} \Delta \mathbf{u}^T(k) \mathbf{H} \Delta \mathbf{u}(k) + \mathbf{h}^T \Delta \mathbf{u}(k) \\ \text{subject to } \mathbf{A}_{ieq} \Delta \mathbf{u}(k) &\leq \mathbf{b}_{ieq} \\ \mathbf{A}_{eq} \Delta \mathbf{u}(k) &= \mathbf{b}_{eq} \end{aligned} \quad (3.14)$$

where \mathbf{H} and \mathbf{h} are the corresponding system matrices while matrix-vector couples $(\mathbf{A}_{ieq}, \mathbf{b}_{ieq})$ and $(\mathbf{A}_{eq}, \mathbf{b}_{eq})$ define, respectively, the inequality and equality constraints.

There are several frequently encountered operational constraints in the optimisation control problem. First, the constraint imposed on the input vector incremental variable and amplitude, followed by the output constraints (supposing that the output \mathbf{y} has a practical limit) is given as

$$\begin{aligned} \Delta \mathbf{u}_{\min} &\leq \Delta \mathbf{u}(k) \leq \Delta \mathbf{u}_{\max} \\ \mathbf{u}_{\min} &\leq \mathbf{u}(k) \leq \mathbf{u}_{\max} \\ \mathbf{y}_{\min} &\leq \mathbf{y}(k) \leq \mathbf{y}_{\max} \end{aligned} \quad (3.15)$$

In order to fit the constraints into quadratic programming formulation, the constraints are required to be decomposed into lower and upper limits (Wang, 2009), such that

$$\begin{bmatrix} -\mathbf{I} \\ \mathbf{I} \end{bmatrix} \Delta \mathbf{u}(k) \leq \begin{bmatrix} -\Delta \mathbf{u}_{\min} \\ \Delta \mathbf{u}_{\max} \end{bmatrix} \quad (3.16 \text{ a})$$

$$\begin{bmatrix} -\mathbf{I} \\ \mathbf{I} \end{bmatrix} \mathbf{u}(k) \leq \begin{bmatrix} -\mathbf{u}_{\min} \\ \mathbf{u}_{\max} \end{bmatrix} \quad (3.16 \text{ b})$$

$$\begin{bmatrix} -\mathbf{I} \\ \mathbf{I} \end{bmatrix} \mathbf{y}(k) \leq \begin{bmatrix} -\mathbf{y}_{\min} \\ \mathbf{y}_{\max} \end{bmatrix} \quad (3.16 \text{ c})$$

Recall from (3.14) that the constraints are to be expressed in term of input vector $\Delta \mathbf{u}$. Thus, we can re-express (3.16 b) and (3.16 c) as

$$\begin{bmatrix} -\mathbf{I} \\ \mathbf{I} \end{bmatrix} \Delta \mathbf{u}(k) \leq \begin{bmatrix} -\mathbf{u}_{\min} + \mathbf{u}(k-1) \\ \mathbf{u}_{\max} - \mathbf{u}(k-1) \end{bmatrix} \quad (3.17 \text{ a})$$

$$\begin{bmatrix} -\mathbf{B} \\ \mathbf{B} \end{bmatrix} \Delta \mathbf{u}(k) \leq \begin{bmatrix} -\mathbf{y}_{\min} \\ \mathbf{y}_{\max} \end{bmatrix} - \begin{bmatrix} -\mathbf{A} \\ \mathbf{A} \end{bmatrix} \mathbf{x}(k) - \begin{bmatrix} -\mathbf{B} \\ \mathbf{B} \end{bmatrix} \mathbf{u}(k-1) \quad (3.17 \text{ b})$$

Then, the inequality constraints can be expressed in the compact form as

$$\mathbf{A}_{ieq} = \begin{bmatrix} -\mathbf{I} \\ \mathbf{I} \\ -\mathbf{I} \\ \mathbf{I} \\ -\mathbf{B} \\ \mathbf{B} \end{bmatrix} ; \quad \mathbf{b}_{ieq} = \begin{bmatrix} -\Delta \mathbf{u}_{\min} \\ \Delta \mathbf{u}_{\max} \\ -\mathbf{u}_{\min} + \mathbf{u}(k-1) \\ \mathbf{u}_{\max} - \mathbf{u}(k-1) \\ -\mathbf{y}_{\min} + \mathbf{Ax}(k) + \mathbf{Bu}(k-1) \\ \mathbf{y}_{\max} - \mathbf{Ax}(k) - \mathbf{Bu}(k-1) \end{bmatrix} \quad (3.18)$$

To solve the quadratic programming problem, there are established solvers readily available, e.g. *ECOS/Gurobi/MOSEK/OSQP* in *qpsolvers* module, *quadprog* and *CVXOPT* in *Python*. As reported in Caron (2021), though the *ECOS* and *OSQP* are superior than *CVXOPT* in terms of computation performance in both dense and sparse problems, *ECOS* is actually a second order cone programming (SOCP) solver. Therefore, *CVXOPT* numerical solver is adopted in this research work; having its own matrix type which is convenient during the control problem matrix-vector representation.

3.5 Summary

This chapter has discussed briefly on the background knowledge for the subsequent chapters of this thesis. Alpha-beta and direct-quadrature transformations of three-phase AC quantities are discussed, followed by the modelling of droop-controlled primary control in the synchronous reference frame. Simplification of the modelled grid-forming DER and the corresponding limitations are discussed. Next, the fundamentals of consensus control algorithm that is widely adopted in microgrid application were presented, followed by the introduction of constrained quadratic programming.

One of the challenges faced when investigating the performance of power electronic-based advanced primary/secondary control schemes for large-area microgrids is the accuracy of simulation. Often times, power electronic devices' primary control layer are heavily simplified to e.g. open-loop first-order system (Falahi, Butler-Purpy and Ehsani, 2013), disregarding the closed-loop control and the internal/physical limits. In order to better justify the power-electronic-interfaced DERs model and co-simulation platform developed (in Appendix A), a reactive power focused assessment on droop-based schemes, in conjunction with a realistically large-area islanded microgrid network, will be examined in the next chapter.

Chapter 4 Droop-based Reactive Power Sharing Regulation – An assessment

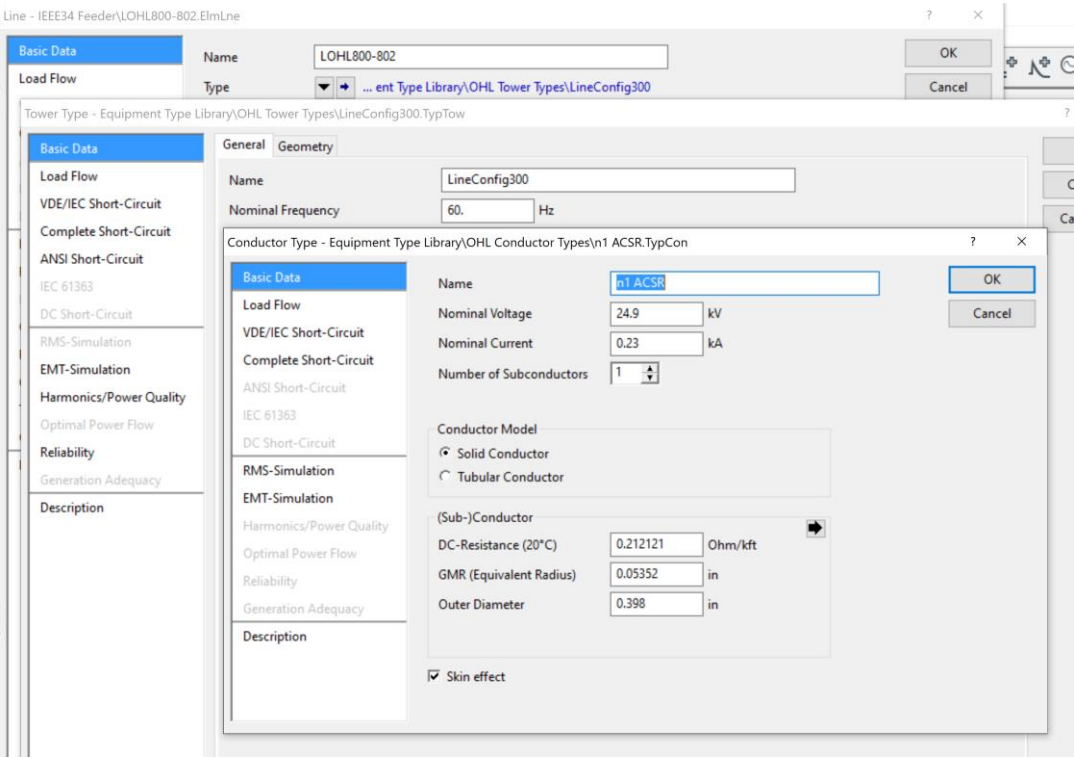
4.1 Introduction

The assumption of purely inductive or purely resistive network lines does not apply to large-area distribution microgrids. As established in Chapter 2, two groups of reactive power sharing controls, i.e., standard droop control with dispatch (known as dispatch-droop hereinafter), and virtual-output-impedance-based droop control (known as VOI-droop hereinafter), are relevant and are the focus of this thesis. This chapter is dedicated to investigating and assessing the reactive power sharing mechanisms of dispatch-droop and VOI-droop control techniques for an islanded microgrid. The two droop-based control schemes are fundamentally different in their correction mechanism – one based entirely on the availability of communication (among the peers, or from the central control) and the other one exploited the new possibility of having a modified primary control loop in power-electronic-based distributed energy resources. The microgrid network that is utilised for this assessment is detailed in Section 4.2. Section 4.3 explains and analyses the fundamental working principle of dispatch-droop and VOI-droop control schemes. Section 4.4 illustrates the assessment through the *DIGSILENT-PowerFactory-Python* co-simulation platform. Section 4.5 summarises the chapter.

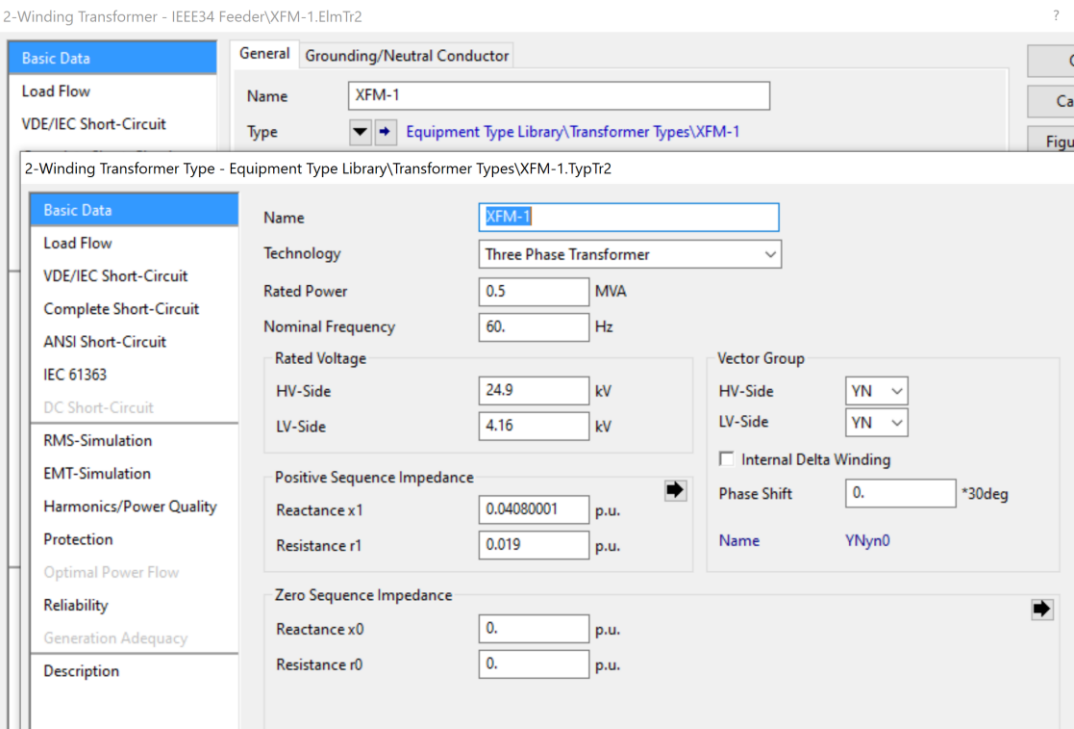
4.2 Multi-bus radial islanded microgrid network configuration

Through an extensive literature study, *IEEE-34 node test feeder* is identified as a sufficiently large distribution network that is suitable for this research work. It is an actual network located in Arizona, with a nominal voltage of 24.9 kV and a short 4.16 kV lateral, with a total load of 1.769 MW and 1.044 MVar. The test feeder has been developed as a part of the preliminary work:

- *IEEE-34 node test feeder* base model is first modelled in *DIGSILENT PowerFactory*. The distributed loads type includes constant power loads, constant impedance loads, and constant current loads that are arbitrarily distributed across the lines with the loads capped as documented. The overhead lines are modelled through geometrical parameters data published in Kersting (2001) and line length (as tabulated in (IEEE Power and Energy Society, 2010)). For instance, the overhead line across bus 800 to bus 802 has a configuration of 300 which, by referring to Kersting (2001), is a three-phase, four-wire overhead line. The line configuration is of aluminium conductor steel reinforced type with a size of # 1/0 (see Table 3 of Kersting (2001) for the geometrical parameters). Correspondingly, the conductor data is embedded into the overhead lines in *DIGSILENT PowerFactory*; the summary of the



(a)



(b)

Fig. 4.1. An example of (a) overhead line configuration across bus 800-802 and (b) transformer setting between bus 888-890.

conductor data is shown in Fig. 4.1(a). The conductor's resistance at 50°C tabulated is used as the resistance at 20°C in *PowerFactory*. The transformer between bus 888-890 (see Fig. 4.1(b)) and

voltage regulators are modelled based on the X/R settings as provided in (IEEE Power and Energy Society, 2010) whilst the shunt capacitors are modelled based on their rated reactive power.

- Unbalanced load flow analysis (i.e. Newton-Raphson approach by default in *PowerFactory*) is simulated onto the unbalanced *IEEE-34 node test feeder* base model. This is to compare the built network voltage profile with the benchmark provided by IEEE Power and Energy Society (2010). The voltage profile of an exemplar load flow calculation that converged after three iterations is tabulated in Table 4.1, together with the percentage error of the voltage profile. The base model built in *DIGSILENT PowerFactory* depicts a maximum voltage magnitude and angle deviation of, respectively 0.9381% at bus 890 and 15.45% (i.e., angle difference of 0.36°) at bus 822 (as illustrated in Fig. 4.3). The acceptable small error justifies the accuracy of the built-model against the published *IEEE-34 node test feeder*.
- Typically, active power-voltage (*PV*) curve analysis is vital for analysing the voltage stability of power systems. The analysis informs on the critical node of voltage instability by increasing the load demand until load flow analysis no longer converges. Subsequently, *PV* curve analysis is performed on the base model (see Fig. 4.2 for the *PV* curve plot) to identify the critical buses of the distribution network for DERs connection, i.e. lateral 852-890 and 862-840 as reported also by Aslanzadeh and Jamali (2007) and Owuor, Munda and Jimoh(2011). In addition, the grid-connection at bus 800 and voltage regulator at bus 814-850 are replaced with DERs connection.

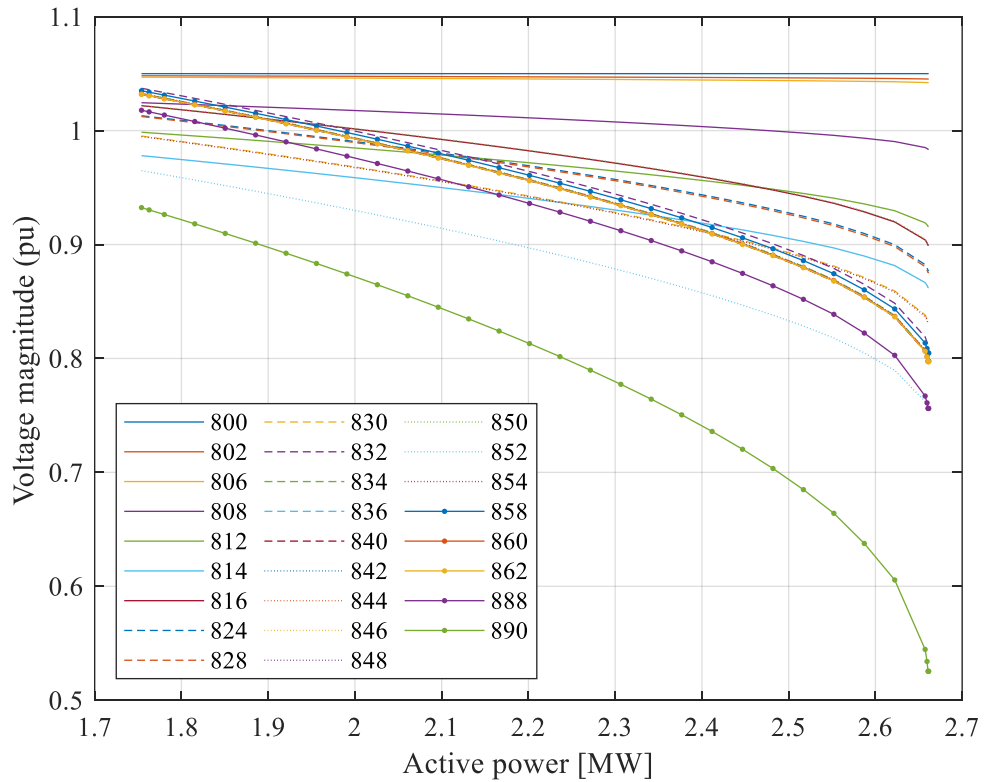


Fig. 4.2. *PV* curve plot of the *IEEE-34 node test feeder* base model.

Table 4.1. Theoretical and simulated voltage profile of IEEE-34 node test feeder.

| Node | Phase A | | | | Phase B | | | | Phase C | | | |
|------|--------------|----------------|--------------|----------------|--------------|----------------|--------------|----------------|--------------|----------------|--------------|----------------|
| | Theoretical | | Simulated | | Theoretical | | Simulated | | Theoretical | | Simulated | |
| | Mag. (pu) | Ang. (deg.) | Mag. (pu) | Ang. (deg.) | Mag. (pu) | Ang. (deg.) | Mag. (pu) | Ang. (deg.) | Mag. (pu) | Ang. (deg.) | Mag. (pu) | Ang. (deg.) |
| 800 | 1.0500 | 0.00 | 1.0500 | 0.00 | 1.0500 | -120.00 | 1.0500 | -120.00 | 1.0500 | 120.00 | 1.0500 | 120.00 |
| 802 | 1.0475 | -0.05 | 1.0475 | -0.05 | 1.0484 | -120.07 | 1.0484 | -120.06 | 1.0484 | 119.95 | 1.0485 | 119.94 |
| 806 | 1.0457 | -0.08 | 1.0458 | -0.08 | 1.0474 | -120.11 | 1.0474 | -120.10 | 1.0474 | 119.92 | 1.0475 | 119.91 |
| 808 | 1.0136 | -0.75 | 1.0141 | -0.72 | 1.0296 | -120.95 | 1.0290 | -120.84 | 1.0289 | 119.30 | 1.0298 | 119.21 |
| 810 | | | | | 1.0294 | -120.95 | 1.0288 | -120.83 | | | | |
| 812 | 0.9763 | -1.57 | 0.9772 | -1.49 | 1.0100 | -121.92 | 1.0083 | -121.69 | 1.0069 | 118.59 | 1.0092 | 118.38 |
| 814 | 0.9467 | -2.26 | 0.9478 | -2.13 | 0.9945 | -122.70 | 0.9920 | -122.38 | 0.9893 | 118.01 | 0.9928 | 117.72 |
| 850 | 1.0176 | -2.26 | 1.0179 | -2.12 | 1.0255 | -122.70 | 1.0232 | -122.40 | 1.0203 | 118.01 | 1.0240 | 117.74 |
| 816 | 1.0172 | -2.26 | 1.0175 | -2.13 | 1.0253 | -122.71 | 1.0229 | -122.41 | 1.0200 | 118.01 | 1.0237 | 117.73 |
| 818 | 1.0163 | -2.27 | 1.0167 | -2.13 | | | | | | | | |
| 820 | 0.9926 | -2.32 | 0.9975 | -2.00 | | | | | | | | |
| 822 | 0.9895 | -2.33 | 0.9941 | -1.97 | | | | | | | | |
| 824 | 1.0082 | -2.37 | 1.0078 | -2.27 | 1.0158 | -122.94 | 1.0142 | -122.62 | 1.0116 | 117.76 | 1.0154 | 117.52 |
| 826 | | | | | 1.0156 | -122.94 | 1.0141 | -122.62 | | | | |
| 828 | 1.0074 | -2.38 | 1.0070 | -2.28 | 1.0151 | -122.95 | 1.0136 | -122.64 | 1.0109 | 117.75 | 1.0147 | 117.50 |
| 830 | 0.9894 | -2.63 | 0.9877 | -2.58 | 0.9982 | -123.39 | 0.9978 | -123.07 | 0.9938 | 117.25 | 0.9983 | 117.07 |

| | | | | | | | | | | | | |
|-----|--------|-------|--------|-------|--------|---------|--------|---------|--------|--------|--------|--------|
| 854 | 0.9890 | -2.64 | 0.9872 | -2.59 | 0.9978 | -123.40 | 0.9974 | -123.08 | 0.9934 | 117.24 | 0.9979 | 117.06 |
| 852 | 0.9581 | -3.11 | 0.9534 | -3.12 | 0.9680 | -124.18 | 0.9698 | -123.85 | 0.9637 | 116.33 | 0.9689 | 116.28 |
| 832 | 1.0359 | -3.11 | 1.0308 | -3.12 | 1.0345 | -124.18 | 1.0364 | -123.85 | 1.0360 | 116.33 | 1.0416 | 116.28 |
| 858 | 1.0336 | -3.17 | 1.0283 | -3.19 | 1.0322 | -124.28 | 1.0342 | -123.94 | 1.0338 | 116.22 | 1.0393 | 116.17 |
| 834 | 1.0309 | -3.24 | 1.0255 | -3.27 | 1.0295 | -124.39 | 1.0317 | -124.04 | 1.0313 | 116.09 | 1.0368 | 116.05 |
| 842 | 1.0309 | -3.25 | 1.0255 | -3.28 | 1.0294 | -124.39 | 1.0316 | -124.02 | 1.0313 | 116.09 | 1.0367 | 116.04 |
| 844 | 1.0307 | -3.27 | 1.0252 | -3.30 | 1.0291 | -124.42 | 1.0313 | -124.06 | 1.0311 | 116.06 | 1.0365 | 116.02 |
| 846 | 1.0309 | -3.32 | 1.0253 | -3.33 | 1.0291 | -124.46 | 1.0312 | -124.09 | 1.0313 | 116.01 | 1.0366 | 115.99 |
| 848 | 1.0310 | -3.32 | 1.0254 | -3.34 | 1.0291 | -124.47 | 1.0312 | -124.10 | 1.0314 | 116.00 | 1.0366 | 115.98 |
| 860 | 1.0305 | -3.24 | 1.0251 | -3.26 | 1.0291 | -124.39 | 1.0321 | -124.03 | 1.0310 | 116.09 | 1.0364 | 116.05 |
| 836 | 1.0303 | -3.23 | 1.0249 | -3.26 | 1.0287 | -124.39 | 1.0309 | -124.03 | 1.0308 | 116.09 | 1.0362 | 116.05 |
| 840 | 1.0303 | -3.23 | 1.0248 | -3.26 | 1.0287 | -124.39 | 1.0309 | -124.03 | 1.0308 | 116.09 | 1.0362 | 116.05 |
| 862 | 1.0303 | -3.23 | 1.0249 | -3.26 | 1.0287 | -124.39 | 1.0309 | -124.03 | 1.0308 | 116.09 | 1.0362 | 116.05 |
| 838 | | | | | 1.0285 | -124.39 | 1.0308 | -124.03 | | | | |
| 864 | 1.0336 | -3.17 | 1.0283 | -3.19 | | | | | | | | |
| 888 | 0.9996 | -4.64 | 0.9946 | -4.65 | 0.9983 | -125.73 | 1.0003 | -125.40 | 1.0000 | 114.82 | 1.0054 | 114.76 |
| 890 | 0.9167 | -5.19 | 0.9081 | -5.05 | 0.9235 | -126.78 | 0.9272 | -126.24 | 0.9177 | 113.98 | 0.9261 | 113.84 |
| 856 | | | | | 0.9977 | -123.41 | 0.9973 | -123.09 | | | | |

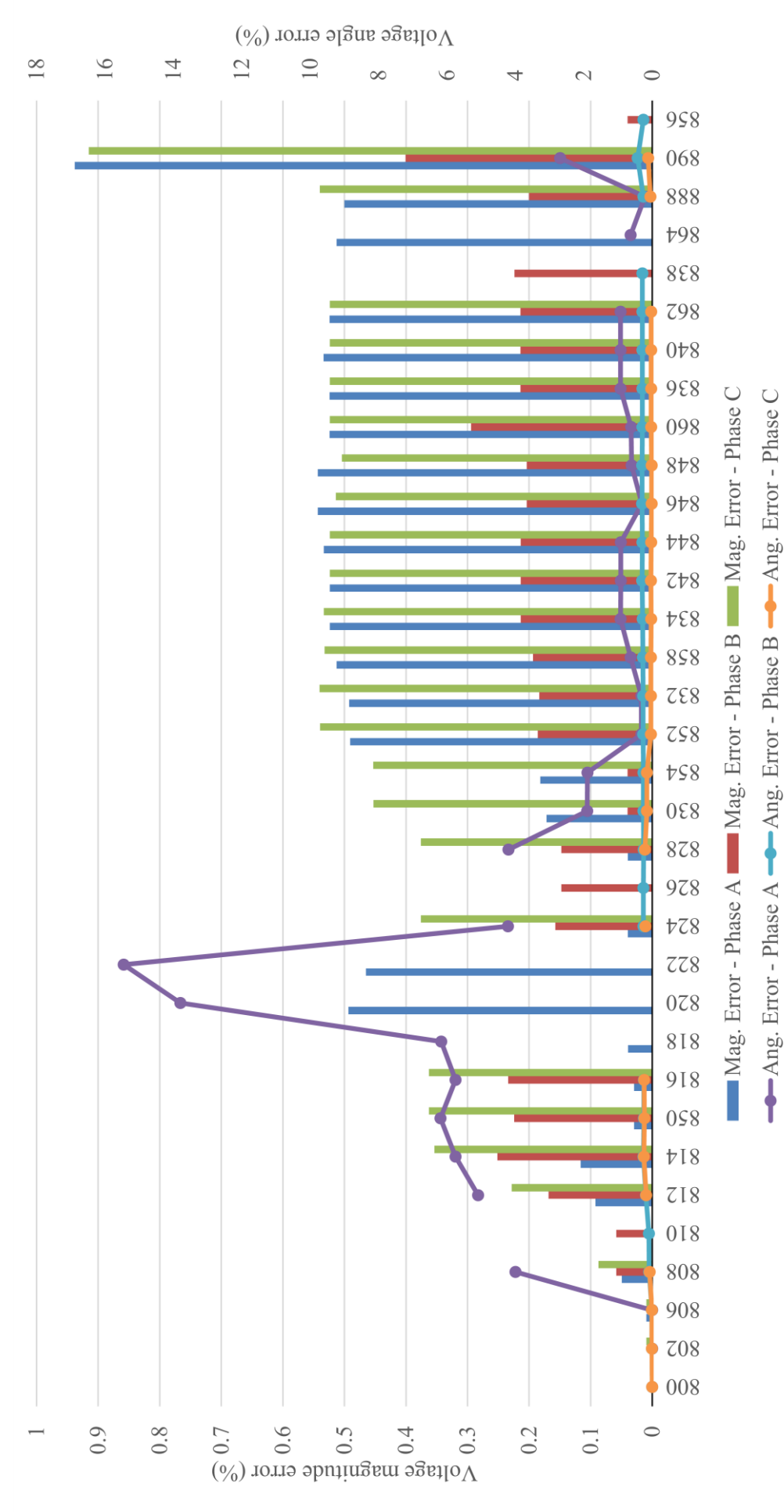


Fig. 4.3. Percentage error of voltage magnitudes and angles of each bus for the IEEE-34 node test feeder base model.

After validating the base model of the distribution network and identifying the DERs point of connections, power-electronic-interfaced DERs are connected to the network and the entire distribution microgrid is disconnected from the main grid. This forms an islanded microgrid, which is known as the modified *IEEE-34 node test feeder*-based microgrid, as shown in Fig. 4.4 and Fig. 4.5. In subsequent simulation studies, all power-electronic-based DER models are assumed to have an ideal, constant DC source. Basic parameters of the DERs and the islanded microgrid network are tabulated in Table 4.2, and some features are highlighted here:

- i. Power-electronic-based DERs of different power ratings are connected to the islanded microgrid through Y-Y, 400V/24.9kV transformer (4.16kV for the short 888-890 lateral).
- ii. Shunt capacitors of the default *IEEE-34 node test feeder* (at bus 844 and 848) are retained in the islanded microgrid network, and they are of a total rating of 0.75MVar.
- iii. LC filter with resistive damping is used as the switching harmonic filter for the power-electronic-based DERs.
- iv. Primary control sampling frequency F_{s1} is 10kHz with secondary control sampling frequency $F_{s2} = 1\text{Hz}$.

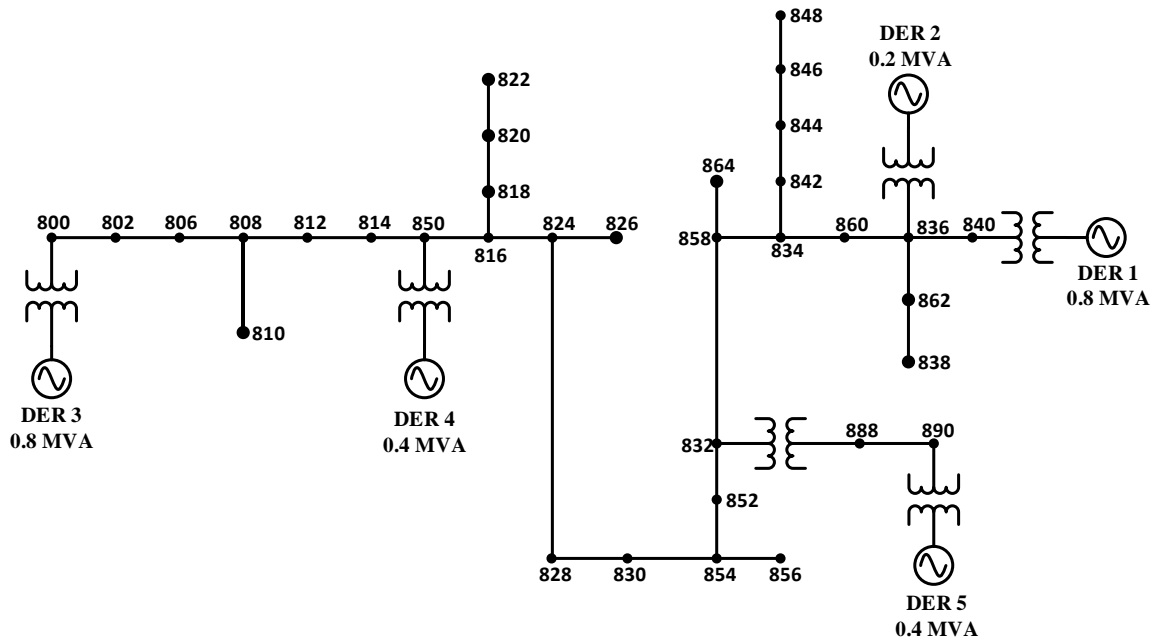


Fig. 4.4. Single line diagram of the large-area islanded microgrid modified from the *IEEE-34 node test feeder*.

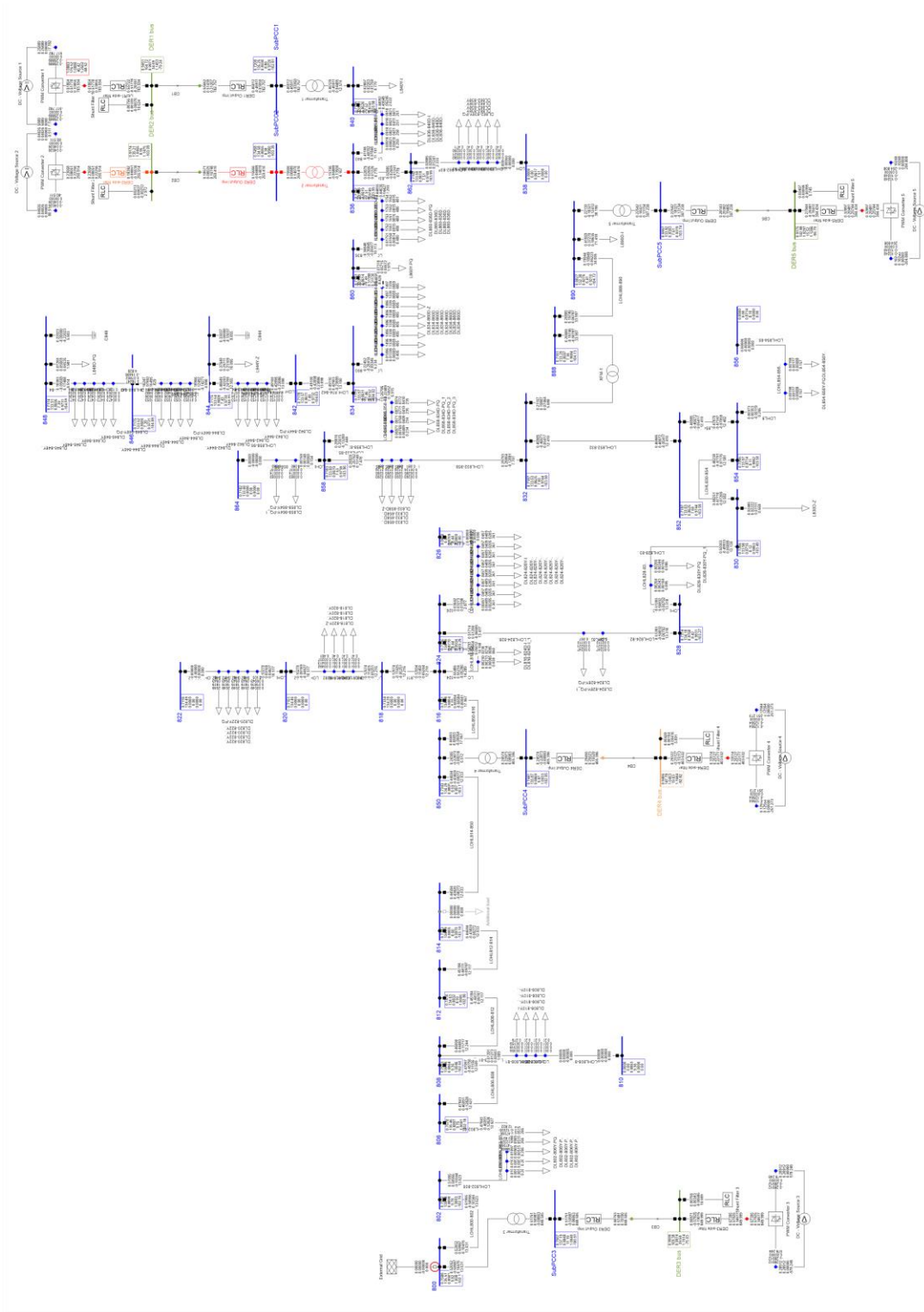


Fig. 4.5. The modified IEEE-34 node test feeder-based islanded microgrid model in *DiGSILENT PowerFactory*.

As already discussed in Section 2.2, droop coefficients in standard droop control are typically being inversely proportional to the kVA ratings, with the aim to result in accurate sharing of the load powers through droop actions. Since the active/reactive power values are normalised to DERs respective kVA ratings, this would mean that, for DERs with different power ratings, reactive power (Q) is proportionally shared among DERs when the ratio of absolute reactive power follows the ratio of their kVA ratings. Under this condition, the normalised active or reactive power values will essentially be equal. Consequently, the droop coefficients m and n are common among the DERs.

Table 4.2. The modified *IEEE-34 node test feeder*-based islanded microgrid network parameters.

| Parameter | Value | Parameter | Value | |
|----------------------------|---------------|---|--------------------------------------|-------------------------|
| Network freq. | 60Hz | P - f droop coeff. m (pu) | 0.0625 | |
| Nominal voltage | 24.9/4.16kV | No-load freq. ω^* (pu) | 1.02 | |
| DC voltage | 1kV | Q - V droop coeff. n (pu) | 0.075 | |
| Sw. freq. F_{sl} | 10kHz | No-load voltage V^* (pu) | 1.02 | |
| DER ratings: | | Power-electronic-based DERs: | | |
| Apparent power (pf) | | Filter impedances L-RC | | |
| DER 1 | 0.8 MVA (0.8) | \mathbf{Z}_{f1} | 0.1905mH, 10 Ω , 1200 μ F | |
| DER 2 | 0.2 MVA (0.8) | \mathbf{Z}_{f2} | 0.7620mH, 10 Ω , 300 μ F | |
| DER 3 | 0.8 MVA (0.8) | \mathbf{Z}_{f3} | 0.1905mH, 10 Ω , 1200 μ F | |
| DER 4 | 0.4 MVA (0.8) | \mathbf{Z}_{f4} | 0.3810mH, 10 Ω , 600 μ F | |
| DER 5 | 0.4 MVA (0.8) | \mathbf{Z}_{f5} | 0.3810mH, 10 Ω , 600 μ F | |
| DER primary control | | Power-electronic-based DERs: | | |
| | | Output feeder impedances | | |
| Power control | τ_c | 0.2 | \mathbf{Z}_{of1} | 0.03 Ω , 0.35mH |
| Voltage control | K_v^P | 1.23 | \mathbf{Z}_{of2} | 0.056 Ω , 0.35mH |
| | K_v^I | 4.67 | \mathbf{Z}_{of3} | 0.03 Ω , 0.35mH |
| Current control | K_c^P | 0.27 | \mathbf{Z}_{of4} | 0.043 Ω , 0.35mH |
| | K_c^I | 1.61 | \mathbf{Z}_{of5} | 0.043 Ω , 0.35mH |

4.3 Droop-based reactive power regulation schemes

As established in Chapter 2, the unequal or non-proportional, reactive power sharing in islanded microgrids is a consequence of voltage discrepancies at the points of connection/coupling of the DERs at different nodes in the network. What follows examines two particular groups of droop control schemes focusing on reactive power improvement: dispatch-droop and VOI-droop schemes.

4.3.1 Standard droop control

First, as explained earlier, the necessary condition to achieve accurate/proportional reactive power sharing among the DERs in an islanded microgrid can be expressed on per-unit basis (i.e. normalised to respective kVA ratings) as

$$\lim_{t \rightarrow \infty} [Q_1(t) = Q_2(t) = \dots = Q_N(t)] \quad (4.1)$$

To improve the reactive power sharing, the dispatch-droop scheme introduces dispatch command to the standard Q - V droop. As a result, the dispatch-droop for i^{th} DER can be expressed as

$$V_i = V_i^* - n_i (Q_i - Q_{i,dis}) \quad (4.2)$$

where $Q_{i,dis}$ is the reactive power dispatch command. Fundamentally, one can easily establish that the dispatch command works by adjusting the effective no-load reference, which in turn alters the droop voltage reference of DER such that reactive power output can be adjusted.

The schematic diagram of a dispatch-droop-controlled DER is depicted in Fig. 4.6, consisting of the dispatch-droop power control, standard output voltage control and inverter current control as detailed in Chapter 3.

Next, a distributed secondary control with a full-graph communication structure (for simplicity) is adopted to define the dispatch command for the above-mentioned droop control. Each DER is embedded with an individual integrator, resulting in a so-called integrator-based reactive power sharing correction scheme. For i^{th} DER, the scheme essentially computes the individual dispatch command $Q_{i,dis}$ using the first-order, backward-Euler discretised integral equation:

$$Q_{i,dis}(k) = Q_{i,dis}(k-1) + T_s K_{iQ,DD} [Q_i^*(k) - Q_i(k)] \quad (4.3)$$

where T_s and $K_{iQ,DD}$ are the secondary control sampling time constant and dispatch-droop integral control gain. The i^{th} DER's reactive power reference Q_i^* , in pu, can be calculated based on the DERs' per-unit reactive output power and respective kVA rating, as

$$Q_i^*(k) = \frac{\sum_{i=1}^N Q_i(k) S_i}{\sum_{i=1}^N S_i} \quad (4.4)$$

Similar to the majority of the existing works available in literature (Zhang *et al.*, 2017; Hoang and Lee, 2018; Lai *et al.*, 2018; C. Shi *et al.*, 2020; Pham and Lee, 2021), this assessment sets the integral control gain $K_{iQ,DD}$ through empirical tuning.

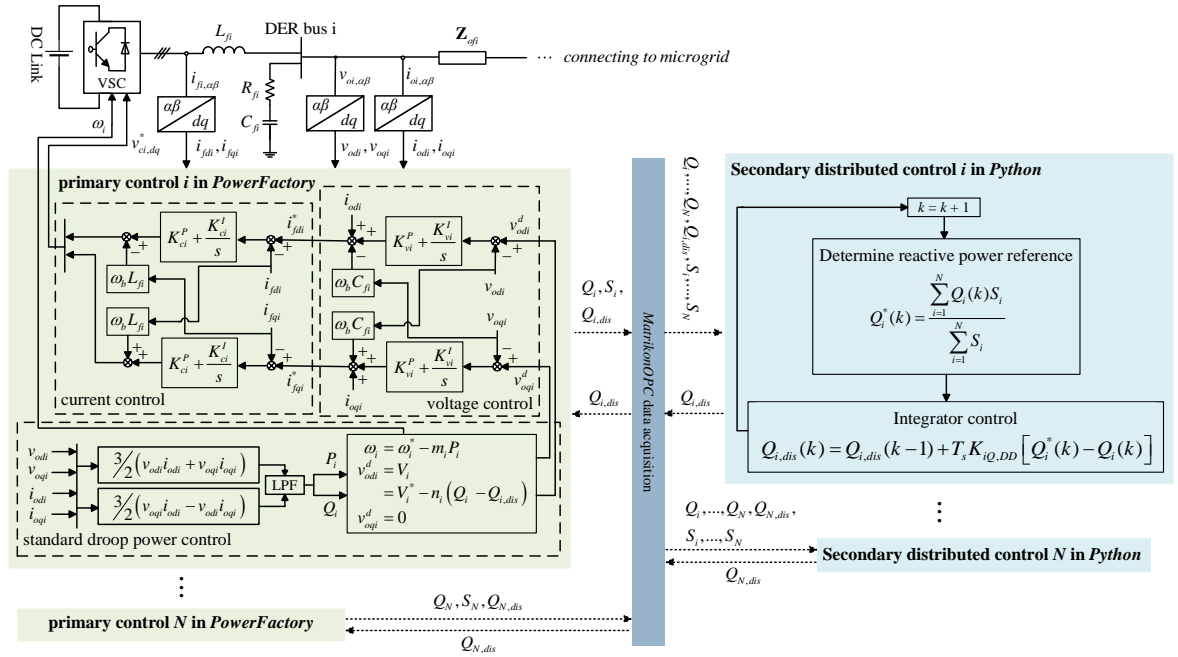


Fig. 4.6. Schematic diagram of the dispatch-droop-controlled DER with integral-based distributed secondary control.

4.3.2 Virtual-output-impedance droop control through power-electronic-interfaced DERs

The schematic diagram of a VOI-droop-controlled DER is depicted in Fig. 4.7. It consists of droop power control, output voltage control and inverter current control loops, which have already been detailed in Chapter 3, and a virtual output impedance control block. The VOI-droop control works by modifying the effective droop output voltage from the standard droop control through virtual voltage drop across the virtual output impedance. This can be expressed mathematically as

$$\begin{aligned} v_{odi}^* &= v_{odi}^d - v_{vdi} \\ v_{oqi}^* &= -v_{vqi} \end{aligned} \quad (4.5)$$

where v_{odi}^* and v_{oqi}^* are the output voltage references (to the subsequent output voltage control) after virtual output impedance control and v_{vdi} and v_{vqi} are the virtual voltage drop. The (electrical) steady-state virtual voltage drops (i.e. \bar{v}_{vdi} and \bar{v}_{vqi} , with the assumption that $d/dt = 0$) are calculated as

$$\begin{aligned} \bar{v}_{vdi} &= R_{vi} i_{odi} - \omega_b L_{vi} i_{oqi} \\ \bar{v}_{vqi} &= R_{vi} i_{oqi} + \omega_b L_{vi} i_{odi} \end{aligned} \quad (4.6)$$

where R_{vi} and L_{vi} are the virtual resistance and inductance. Then, the output voltage control loop can be expressed as

$$\begin{aligned}
v_{odi,err} &= v_{odi}^d - \bar{v}_{vdi} - v_{odi} \\
v_{oqi,err} &= -\bar{v}_{vqi} - v_{oqi} \\
i_{fdi}^* &= K_{vi}^P v_{odi,err} + K_{vi}^I \int v_{odi,err} dt + i_{odi} - \omega_b C_{fi} v_{oqi} \\
i_{fq i}^* &= K_{vi}^P v_{oqi,err} + K_{vi}^I \int v_{oqi,err} dt + i_{oqi} + \omega_b C_{fi} v_{odi}
\end{aligned} \tag{4.7}$$

Previous literature review had summarised the variation of virtual output impedances (He *et al.*, 2013; Xu *et al.*, 2014; Mahmood, Michaelson and Jiang, 2015a; Zhu *et al.*, 2015, 2016; Chen *et al.*, 2016; Altahir, Yan and Liu, 2017). This assessment will only consider the virtual output inductive reactance $X_{vi} = \omega_b L_{vi}$. A commonly used approach of using static and dynamic components is adopted here:

$$X_{vi}(k) = X_{vi,static} + X_{vi,dyn}(k) \tag{4.8}$$

where subscript *static* and *dyn* denote, respectively, the static and dynamic components. As described in Subsection 2.3.1, the static component is mainly implemented to introduce a high X/R ratio, attempting to validate the assumption of pure inductive line used in standard droop control.

Suppose that a VOI-droop-controlled DER is connected to an islanded microgrid through a complex output feeder impedance $\mathbf{Z}_{ofi} = R_{ofi} + jX_{ofi}$, the DER's reactive output power to the microgrid is defined as

$$Q_i = \frac{V_l (v_{odi}^d \cos \delta_i - V_l) (X_{ofi} + X_{vi}) - V_l v_{odi}^d \sin \delta_i R_{ofi}}{R_{ofi}^2 + (X_{ofi} + X_{vi})^2} \tag{4.9}$$

where V_l is the microgrid bus voltage where DER is connected to, v_{odi}^d is the droop voltage amplitude before VOI control, and δ_i is the angle difference between the two voltage phasors. By assuming that the angle difference δ_i is very small and that the feeder resistance R_{ofi} is negligible as compared to the reactance counterpart, the derivative of Q_i with respect to X_{vi} can be simplified to become

$$\frac{\partial Q_i}{\partial X_{vi}} = -\frac{V_l (v_{odi}^d - V_l)}{(X_{ofi} + X_{vi})^2} \tag{4.10}$$

A negative dynamic of Q_i with respect to the change of X_{vi} is noted from the result in (4.10). Therefore, the dynamic component of the VOI-droop integrator control should be regulated based on the negated (negative sign) reactive power error, given as

$$L_{vi,dyn}(k) = L_{vi,dyn}(k-1) - T_s K_{iQ,VOI} [Q_i^*(k) - Q_i(k)] \tag{4.11}$$

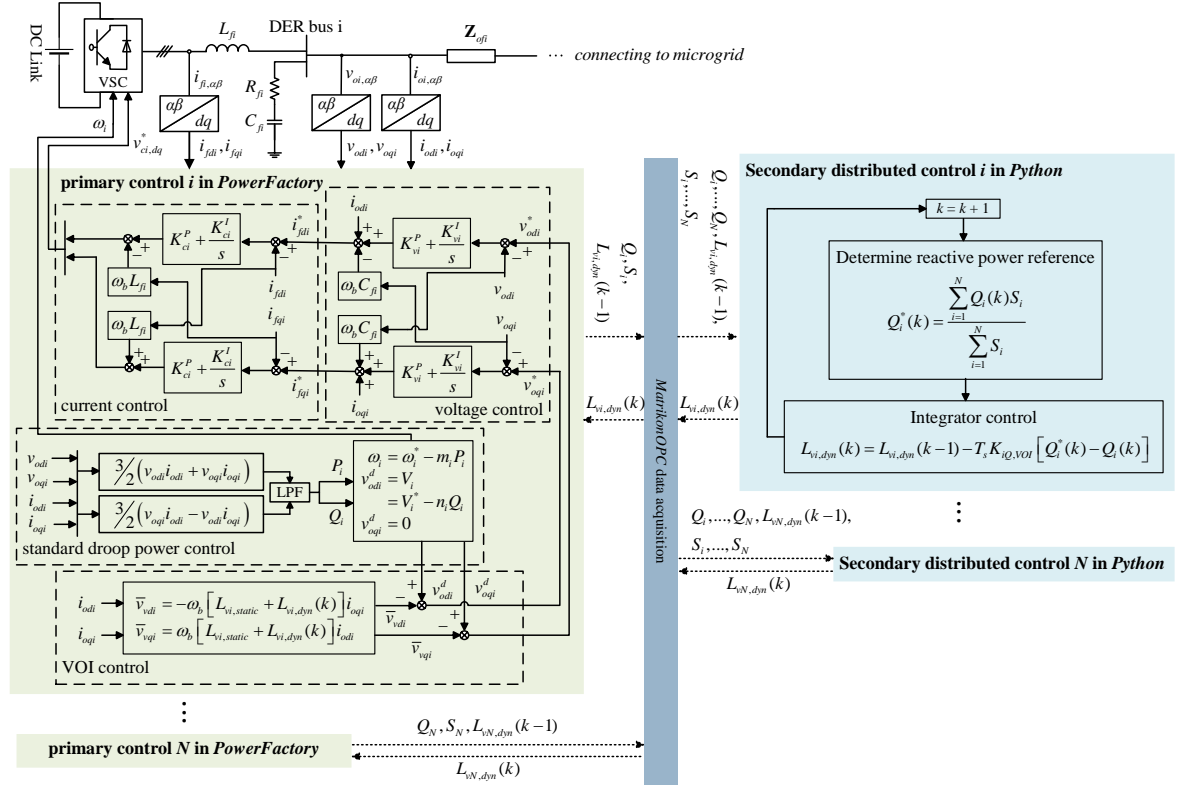


Fig. 4.7. Schematic diagram of the VOI-droop-controlled DER with integral-based distributed secondary control.

(4.11) is essentially the VOI-droop's counterpart of the dispatch-droop's integral update equation (4.3), and they are opposite in sign. Similarly, this assessment relies on empirical tuning to obtain a suitable $K_{IQ,VOI}$ control gain for VOI-droop reactive power sharing scheme.

4.4 Assessment through the *DIGSILENT-PowerFactory-Python* co-simulation platform

This reactive power sharing schemes (i.e., dispatch-droop and VOI-droop control techniques) assessment is carried out on the islanded microgrid model modified from the *IEEE-34 node test feeder* detailed in Section 4.2, through the *DIGSILENT-PowerFactory-Python* co-simulation platform introduced in Appendix A. The objective of this assessment is twofold: (i) to identify the merits and demerits of the two variants of droop control; (ii) to examine the usability of the established co-simulation platform. Different scenarios are considered in this assessment: default steady state, step load change, DER disconnection, and communication loss.

In the steady state case, a total of 1.769 MW and 1.044 MVar passive loads are by default present in the islanded microgrid distribution network. It can be observed from Fig. 4.8 that reactive load power is not proportionately shared among the power-electronic-based DERs when DERs are initially droop controlled without the initiation of reactive power sharing scheme and that some DERs are even absorbing reactive power from the microgrid. The dispatch-droop and VOI-droop reactive

power sharing schemes are activated at $t = 5$ s. With $K_{iQ,DD}$ arbitrary tuned at 1.78, it is shown clearly in Fig. 4.8 that reactive power is now proportionally shared among the DERs with the implementation of dispatch-droop scheme and achieved a 2% band settling time at about 7 s. On the other hand, the VOI-droop control gain $K_{iQ,VOI}$ is empirically tuned such that the VOI-droop scheme achieves a settling time close to that of the dispatch-droop scheme, at about 9 s (i.e. minimum possible before instability occurs). It is revealed also in Fig. 4.8 that the VOI-droop scheme achieves proportional reactive power sharing by regulating the droop output voltage v_{odi}^d of all participating power-electronic-interfaced DERs to be the same. The static-dynamic VOI-droop scheme adopted in this assessment achieves proportional reactive power sharing at the expense of lowering the voltage profile as depicted in Fig. 4.8, due to the static component. In contrast, the dispatch-droop scheme realises the same accurate reactive power sharing without affecting the voltage profile significantly.

For the load step change scenario, an additional passive load of $0.15 + j0.32$ MVA is connected to the islanded microgrid at bus 814 at $t = 10$ s with the secondary reactive power control initially activated. It is clearly demonstrated in Fig. 4.9 that upon load up-stepping, the bus voltage profile of the VOI-droop scheme significantly deviates as compared to the dispatch-droop scheme while both schemes are equivalent in terms of reactive power sharing performance. This hints about a potential demerit of VOI-droop scheme in causing sustained low voltage in the microgrid, more so in the event of near-full/full loading.

The dynamic performance of the secondary reactive power sharing controls considering DER disconnection is explored next. Again, the islanded microgrid is operated under default loading condition with secondary control initially activated. A circuit breaker is opened to disconnect DER 2 from the distribution microgrid at $t = 10$ s. As observed in Fig. 4.10, proportional power sharing is retained by the remaining participating DERs in both schemes with the corresponding voltage profiles at the DER-buses depicted.

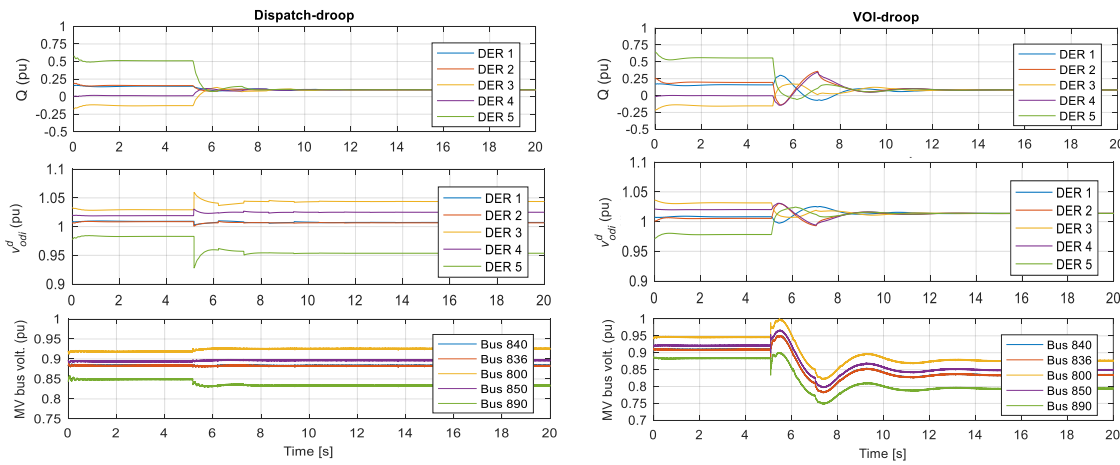


Fig. 4.8. Default steady state with (left) dispatch-droop and (right) VOI-droop schemes: (top) DER's reactive output power; (middle) the corresponding droop output voltage references; and (bottom) DER-bus voltage magnitudes.

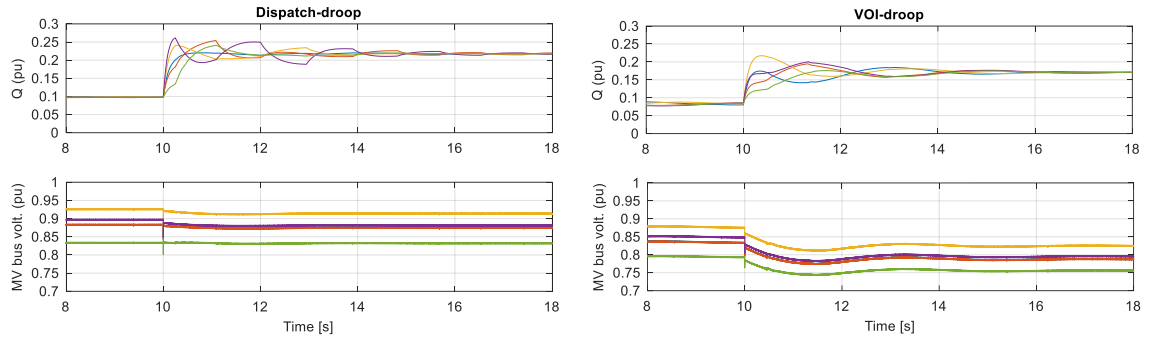


Fig. 4.9. Load step change with (left) dispatch-droop and (right) VOI-droop schemes: (top) DER's reactive output power; and (bottom) the corresponding DER-bus voltage magnitudes. Legend as in Fig. 4.8.

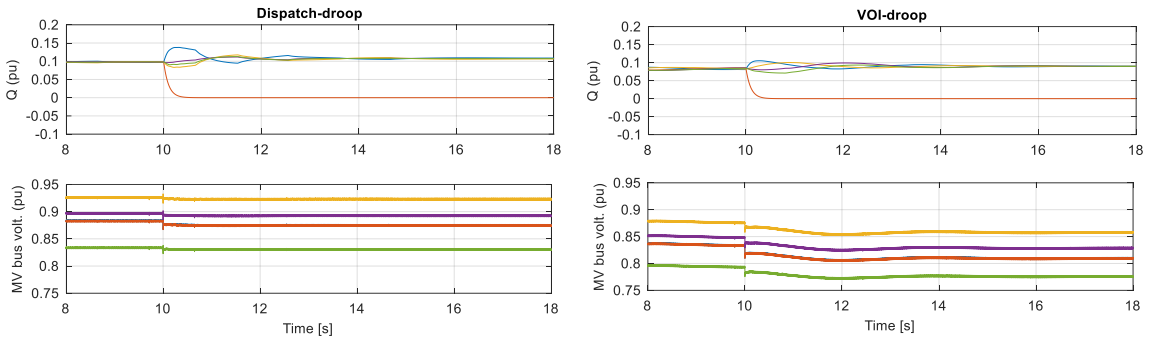


Fig. 4.10. DER disconnection with (left) dispatch-droop and (right) VOI-droop schemes: (top) DER's reactive output power; and (bottom) the DER-bus voltage magnitudes. Legend as in Fig. 4.8.

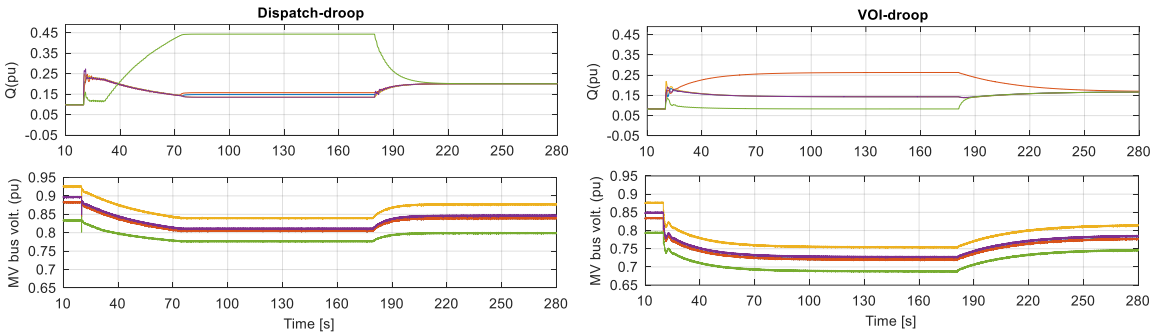


Fig. 4.11. Communication loss with (left) dispatch-droop and (right) VOI-droop schemes: (top) DER's reactive output power; and (bottom) the DER-bus voltage magnitudes. Legend as in Fig. 4.8.

Finally, the robustness of the reactive power sharing control schemes against communication loss is examined. Communication in and out of DER 5 is intentionally lost at $t = 15$ s and consequently, the secondary control of DER 5 retains the last communicated information of the remaining DERs while the remaining DERs also hold on to the last communicated information of DER 5. A step change of load (i.e., of 0.15 MW and 0.32 MVar additional loading) is implemented to bus 814 at $t = 20$ s to assess the power sharing performance under communication disruption. It is shown in Fig. 4.11 that the steady state accurate reactive power sharing that has been achieved prior is affected upon load changes during the communication disruption. For secondary dispatch-droop

scheme, reactive output power of DER 5 has saturated to about 0.47 pu while the remaining DERs are affected marginally. As observed, reactive power is proportionately shared among DER 1-4 until reactive output power of DER 5 saturates at about $t = 75$ s, after which the power sharing accuracy is slightly compromised. As for the VOI-droop scheme, apart from DER 5, the smallest kVA rating DER 2 is also significantly affected by the communication loss. Upon communication restoration at $t = 180$ s, proportional reactive power sharing is restored in both secondary controls. The corresponding DER-bus voltage profiles are as depicted in Fig. 4.11. It can be clearly observed that the bus voltages, particularly for VOI-droop scheme, have dropped significantly, in a range of 0.67 – 0.82 pu.

4.5 Summary

This chapter presents the analytical design and assessment of dispatch-droop and VOI-droop for distributed secondary reactive power sharing controls. The assessment is studied in conjunction with a realistically large-area islanded microgrid through the *DigSILENT-PowerFactory-Python* co-simulation platform. It is demonstrated that the co-simulation platform successfully enables the assessment by facilitating concurrent simulation of different domains. It is also confirmed that proportional reactive power sharing is realisable in both droop-based schemes regardless of load variations and topology changes. The differences between the two schemes are summarised in Table 4.3. It is worth highlighting two of the main comparative features: first, in terms of the number of control gain, VOI-droop scheme is slightly disadvantaged as there is an additional static component to be tuned (note: the problem would be aggravated further by the large number of DERs); and second, the static-dynamic variant of VOI-droop tend to suffer from larger voltage deviations.

Table 4.3. Summary of the differences between dispatch-droop and VOI-droop reactive power sharing schemes.

| Feature | Dispatch-droop | VOI-droop |
|---|---|--|
| Number of control gains | One | Two |
| Power correction transient | Integral gain dependent | Integral gain and static virtual-output-impedance dependent, higher overshoots |
| Voltage deviation | Mixture of positive and negative deviations; larger at higher loading | Only negative deviations; larger at higher loading |
| Susceptibility to communication loss (in terms of number of DERs) | Affected less | Affected more |

Therefore, to improve the reactive power sharing accuracy and voltage deviation aspects of the VOI-droop scheme, the next chapter will introduce two improved schemes with distributed consensus control. Another important observation from this assessment is that, through a uniform area-wide droop control setting and upon reactive power sharing improvement through VOI-droop scheme, the droop output voltage would eventually converge. This observation provides the theoretical basis in developing a novel VOI-based distributed consensus droop control scheme, presented next.

Chapter 5 Consensus Virtual-Output-Impedance-based Droop Control Schemes for Accurate Reactive Power Sharing

5.1 Introduction

Incorporating advanced consensus control algorithm, this chapter proposes and investigates two VOI-droop schemes with sparse-graph communication structures. This is a form of distributed control strategy. Section 5.2 presents the first control scheme - consensus-based VOI-droop control scheme - that improves the reactive output power sharing among DERs. In addition, a systematic tuning guideline is also introduced. The dynamical-virtual-impedance-based droop control scheme is simulated on the modified *IEEE34 node test feeder*-based islanded microgrid (as detailed in Section 4.2) and the resulted performance is benchmarked against a recent VOI-droop control scheme by Zhang *et al.* (2017), which is referred to as “dual-impedance consensus control” hereinafter. On the other hand, Section 5.3 presents the second control scheme of this chapter, i.e., secondary consensus-based VOI-droop scheme based on a novel droop equivalent impedance concept. The choice of using only one of the two impedance components (i.e., virtual resistance or reactance) of a generic VOI-droop scheme is analysed in detail in conjunction with the proposed droop equivalent impedance concept. The viability and performance of the droop-equivalent-impedance-based consensus VOI-droop control are verified through the modified *IEEE-34 node test feeder*-based microgrid. Finally, Section 5.4 summarises this chapter.

5.2 Reactive power regulation through consensus-based virtual-output-impedance droop control

The literature survey in Chapter 2 has established that static-only virtual-output-impedance scheme will not be able to solve the inaccurate reactive power sharing in non-parallel-connected microgrids. To overcome this problem, VOI-droop controls consisting of static and dynamic components have been extensively introduced and investigated to date. In this section, a new variant of VOI-droop control scheme is proposed. It is different from the existing variations in several aspects and the novel features are highlighted below:

- i. Instead of adopting both virtual resistance and reactance static-dynamic components, only the dynamic component of individual virtual resistance/reactance (i.e., the static components are nullified) is utilised. Hypothetically, despite the simplification, the control scheme should be able to achieve a similar reactive power sharing performance.

- ii. Implementation of distributed consensus control with discrete integral feature can remove the need for having *PI* controller (which is normally cascaded at the outer loop of the DER's primary control). This is expected to ease the control gain tuning process and is relevant for large-scale integration of DERs in future microgrids.
- iii. The work also approximates the range of consensus control gain that can ensure stable distributed control. This is achieved through developing a systematic, operating-point-dependent tuning guideline.

The full schematic diagram of the proposed adaptive VOI-droop-controlled DERs is illustrated in Fig. 5.1. The schematic diagram also annotates the secondary control layer, in the form of consensus-based reactive power correction control, and the primary control layer, which consists of the standard droop-based power control, the adaptive virtual-output-reactance control, the output voltage control, and the inverter current control. The basic control structure of the standard droop power control and the inverter current control have been detailed in Chapter 3, but with a main difference in the virtual output impedance - it consists of the dynamic component alone (being $\omega_b L_{vi} = X_{vi} = X_{vi,dyn}$) without the static part. The corresponding steady-state virtual voltage drops are expressed as

$$\begin{aligned}\bar{v}_{vdi} &= -\omega_b L_{vi} i_{oqi} \\ \bar{v}_{vqi} &= \omega_b L_{vi} i_{odi}\end{aligned}\tag{5.1}$$

The full output voltage control equations have been given in (4.7).

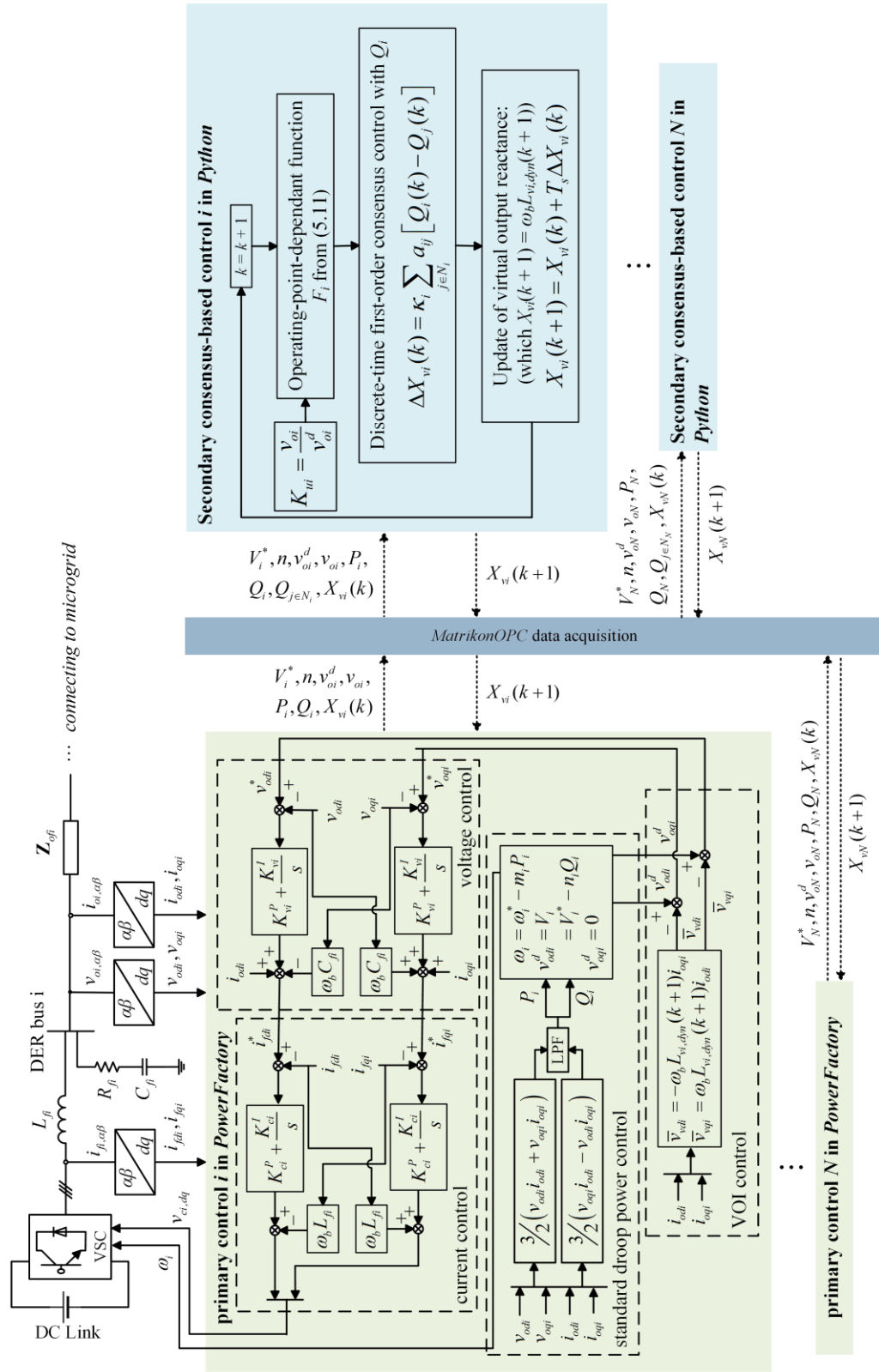


Fig. 5.1. Schematic diagram of the adaptive virtual-output-reactance-droop controlled DER with secondary consensus-based reactive power sharing control.

5.2.1 Consensus control design with reactive power

A linear first-order consensus control protocol for the secondary reactive power improvement can be written as:

$$\dot{Q}_i = -c_i \sum_{j \in N_i} a_{ij} [Q_i - Q_j] \quad (5.2)$$

It is worth highlighting that the per-unit reactive output power Q_i cannot be directly manipulated under droop control. Instead, it will be regulated through virtual output reactance X_{vi} - which is selected as the control input for the consensus control. However, owing to the nonlinearity of VOI-droop reactive power sharing scheme, it is proposed here that the correlation between reactive output power Q_i and virtual output reactance X_{vi} is first to be found, as detailed in what follows.

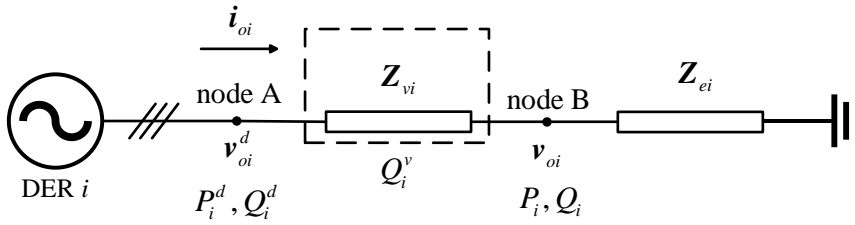


Fig. 5.2. Single line diagram of a power-electronic-interfaced DER with virtual output impedance and a physical equivalent impedance as seen by the DER output towards the microgrid.

The single line diagram of a VOI-droop-controlled DER along with the corresponding virtual output impedance $Z_{vi} = jX_{vi}$ and the physical equivalent impedance $Z_{ei} = R_{ei} + jX_{ei}$ is depicted graphically in Fig. 5.2. The physical equivalent impedance Z_{ei} as seen from i^{th} DER output can be calculated using

$$\begin{aligned} R_{ei} &= \frac{3v_{oi}^2 P_i}{P_i^2 + Q_i^2} \\ X_{ei} &= \frac{3v_{oi}^2 Q_i}{P_i^2 + Q_i^2} \end{aligned} \quad (5.3)$$

where v_{oi} is the normalised output voltage magnitude with $\mathbf{v}_{oi} = v_{odi} + jv_{oqi}$. The reactive output power before virtual output impedance and the virtual reactive power across the virtual output reactance can be expressed as

$$\begin{aligned} Q_i^d &= \frac{3v_{oi}^{d2} (X_{vi} + X_{ei})}{R_{ei}^2 + (X_{vi} + X_{ei})^2} \\ Q_i^v &= \frac{3i_{oi}^2 X_{vi}^2}{X_{vi}} \end{aligned} \quad (5.4)$$

where output current magnitude i_{oi} (being $\mathbf{i}_{oi} = i_{odi} + j\mathbf{i}_{oqi}$) can be expressed as

$$i_{oi}^2 = \frac{v_{oi}^{d2}}{R_{ei}^2 + (X_{vi} + X_{ei})^2} \quad (5.5)$$

Correspondingly, the X_v -based VOI-droop controlled DER's reactive output power can be obtained by manipulating (5.4) and (5.5) further:

$$Q_i = Q_i^d - Q_i^v = \frac{3v_{oi}^{d2}X_{ei}}{R_{ei}^2 + (X_{vi} + X_{ei})^2} \quad (5.6)$$

Substitute (5.3) into (5.6) gives the virtual output reactance as

$$X_{vi} = \sqrt{\frac{9v_{oi}^{d2}v_{oi}^2Q_i}{Q_i(P_i^2 + Q_i^2)} - \left(\frac{3v_{oi}^2P_i}{P_i^2 + Q_i^2}\right)^2} - \frac{3v_{oi}^2Q_i}{P_i^2 + Q_i^2} \quad (5.7)$$

In order to simplify the expression to improve its usability for subsequent tuning purpose, an operating-point-dependent voltage factor K_{ui} , being the ratio of output voltage magnitude v_{oi} to droop voltage magnitude v_{oi}^d , is introduced:

$$K_{ui} = \frac{v_{oi}}{v_{oi}^d} \quad (5.8)$$

Consequently, the virtual output reactance in (5.7) can be re-expressed in terms of standard droop control as in (3.3), the newly introduced voltage factor K_{ui} , the output active power (P_i), and the output reactive power (Q_i) as

$$X_{vi} = \sqrt{\frac{9K_{ui}^2(V_i^* - nQ_i)^4Q_i}{Q_i(P_i^2 + Q_i^2)} - \left(\frac{3K_{ui}^2(V_i^* - nQ_i)^2P_i}{P_i^2 + Q_i^2}\right)^2} - \frac{3K_{ui}^2(V_i^* - nQ_i)^2Q_i}{P_i^2 + Q_i^2} \quad (5.9)$$

Two realistic/practical assumptions with respect to the changes of X_{vi} are made here, in an attempt to obtain an approximate linear relation between Q_i and X_{vi} : first, the voltage factor K_{ui} is assumed relatively constant with respect to the change of X_{vi} (as in any practical grid); second, the active output power P_i remains relatively unchanged due to the change of X_{vi} (being an inherent characteristic of droop control). On the basis that K_{ui} and P_i do not change significantly during reactive power correction (due to X_{vi} adjustment), and since V_i^* and n are constants, the linear dynamical relationship between Q_i and X_{vi} can be approximated to

$$\dot{X}_{vi} = F_i(V_i^*, n, K_{ui}, P_{oi}, Q_{oi})\dot{Q}_i \quad (5.10)$$

where F_i is a function of standard droop parameters V_i^* and n , and operating point terms K_{ui} , P_{oi} and Q_{oi} given as

$$F_i = -\frac{9}{\sqrt{\frac{9K_{ui}^2(V_i^* - nQ_{oi})^4}{P_{oi}^2 + Q_{oi}^2} - \frac{9K_{ui}^4 P_{oi}^2 (V_i^* - nQ_{oi})^4}{(P_{oi}^2 + Q_{oi}^2)^2}}} \left[\frac{K_{ui}^2 Q_{oi} (V_i^* - nQ_{oi})^4}{(P_{oi}^2 + Q_{oi}^2)^2} \right. \\ - \frac{2K_{ui}^4 P_{oi}^2 Q_{oi} (V_i^* - nQ_{oi})^4}{(P_{oi}^2 + Q_{oi}^2)^3} + \frac{2K_{ui}^2 (V_i^{*2} n - 3V_i^{*2} n^2 Q_{oi} + 3V_i^* n^3 Q_{oi}^2 - n^4 Q_{oi}^3)}{P_{oi}^2 + Q_{oi}^2} \\ \left. - \frac{2K_{ui}^4 P_{oi}^2 (V_i^{*2} n - 3V_i^{*2} n^2 Q_{oi} + 3V_i^* n^3 Q_{oi}^2 - n^4 Q_{oi}^3)}{(P_{oi}^2 + Q_{oi}^2)^2} \right] + \frac{6K_{ui}^2 Q_{oi}^2 (V_i^* - nQ_{oi})^2}{(P_{oi}^2 + Q_{oi}^2)^2} \\ - \frac{3K_{ui}^2 (V_i^{*2} - 4V_i^* nQ_{oi} + 3n^2 Q_{oi}^2)}{P_{oi}^2 + Q_{oi}^2} \quad (5.11)$$

By substituting (5.10) to (5.2) and upon forward-Euler discretisation, the consensus-based adaptive virtual-output-reactance control with reactive power can be re-expressed as

$$\Delta X_{vi}(k) = \kappa_{Xi} \sum_{j \in N_i} a_{ij} [Q_i(k) - Q_j(k)] \quad (5.12)$$

where the effective coupling gain $\kappa_{Xi} = -c_i F_i(V_i^*, n, K_{ui}, P_{oi}, Q_{oi})$. Finally, the virtual output reactance can be updated from

$$X_{vi}(k+1) = X_{vi}(k) + T_s \Delta X_{vi}(k) \quad (5.13)$$

Next, adaptive virtual-output-resistance-based control is considered by configuring the virtual output impedance as a pure resistive term (i.e., $\mathbf{Z}_{vi} = R_{vi}$). The R_v -based VOI-droop controlled DER's reactive output power can be expressed as

$$Q_i = \frac{3V_{oi}^{d2} X_{ei}}{(R_{ei} + R_{vi})^2 + X_{ei}^2} \quad (5.14)$$

with $Q_i^v = 0$ as $X_{vi} = 0$. By manipulating (3.3), (5.3), (5.8) and (5.14), the virtual output resistance can be given by

$$R_{vi} = \sqrt{\frac{9K_{ui}^2 (V_i^* - nQ_i)^4}{(P_i^2 + Q_i^2)} - \left(3K_{ui}^2 \frac{(V_i^* - nQ_i)^2 Q_i}{P_i^2 + Q_i^2} \right)^2} - 3K_{ui}^2 \frac{(V_i^* - nQ_i)^2 P_i}{P_i^2 + Q_i^2} \quad (5.15)$$

By adopting the same assumptions of non-changing steady-state active output power P_i and voltage factor K_{ui} , the relationship between R_{vi} and Q_i (i.e., the counterpart of (5.10)) can be approximated to a linear, operating-point-dependent function:

$$\dot{R}_{vi} = G_i (V_i^*, n, K_{ui}, P_{oi}, Q_{oi}) \dot{Q}_i \quad (5.16)$$

where

$$\begin{aligned} G_i = & -\frac{9}{\sqrt{\frac{9K_{ui}^2(V_i^* - nQ_{oi})^4}{P_{oi}^2 + Q_{oi}^2} - \frac{9K_{ui}^4Q_{oi}^2(V_i^* - nQ_{oi})^4}{(P_{oi}^2 + Q_{oi}^2)^2}}} \left[\frac{K_{ui}^2Q_{oi}(V_i^* - nQ_{oi})^4}{(P_{oi}^2 + Q_{oi}^2)^2} \right. \\ & + \frac{2K_{ui}^2n(V_i^* - nQ_{oi})^3}{P_{oi}^2 + Q_{oi}^2} - \frac{2K_{ui}^4Q_{oi}^2n(V_i^* - nQ_{oi})^3 - K_{ui}^4Q_{oi}(V_i^* - nQ_{oi})^4}{(P_{oi}^2 + Q_{oi}^2)^2} \\ & \left. - \frac{2K_{ui}^4Q_{oi}^3(V_i^* - nQ_{oi})^4}{(P_{oi}^2 + Q_{oi}^2)^3} \right] + \frac{6K_{ui}^2P_{oi}Q_{oi}(V_i^* - nQ_{oi})^2}{(P_{oi}^2 + Q_{oi}^2)^2} + \frac{6K_{ui}^2P_{oi}n(V_i^* - nQ_{oi})}{P_{oi}^2 + Q_{oi}^2} \end{aligned} \quad (5.17)$$

Finally, the consensus-based adaptive virtual-output-resistance control with reactive power can be re-expressed as

$$\begin{aligned} \Delta R_{vi}(k) &= \kappa_{Ri} \sum_{j \in N_i} a_{ij} [Q_i(k) - Q_j(k)] \\ R_{vi}(k+1) &= R_{vi}(k) + T_s \Delta R_{vi}(k) \end{aligned} \quad (5.18)$$

where $\kappa_{Ri} = -c_i G_i(V_i^*, n, K_{ui}, P_{oi}, Q_{oi})$.

As discussed in Chapter 3, consensus control algorithm stability is guaranteed if condition (3.9) is met. However, as revealed in (5.12) and (5.18), the effective coupling gain κ_{Xi}/κ_{Ri} for a given scalar coupling gain c is essentially operating-point-dependent. There are two possible ways of setting the effective coupling gain, provided that scalar coupling gain complies to (3.9):

- i. calculate individual F_i or G_i for each DER on the fly and individual κ_{Xi} or κ_{Ri} is updated accordingly, or
- ii. compute the smallest F_{min} or G_{min} for a given range of practical operating points and subsequently, set the effective coupling gain that is made common to all participating DERs.

The subsequent analysis considers only the second approach as it is expected to deliver a more reliable control as it avoids the real-time adjustment of the gain (which, if poorly tuned, would affect the overall closed-loop stability). The possible effective coupling gain κ_X and κ_R values for a given range of operating points of different P_o and Q_o with a rated power factor of 0.8 are tabulated in Table

5.1 and Table 5.2. The calculation assumes that v_{oi} is kept constant at 0.9 pu and the load power factor of 0.8, minimum. Note that the grey-shaded column represents a power factor less than 0.8 and hence, no calculation is carried out with regards to the common effective coupling gain. The tabulations clearly show that κ changes significantly, particularly towards the low loading region. Hence, it is recommended that the static common effective coupling gain κ should be fixed at high loading operating point to ensure control system stability for most operating conditions. It is also acknowledged here that such a selection would entail a slow control dynamic at low loading condition. However, since non-proportional power sharing is naturally not a concern at low-load region, hence, it is still sensible to adopt the common effective coupling gain κ suggested earlier.

Table 5.1. Common effective coupling gain κ_X for a range of operating points with scalar coupling $c = 0.2$.

| Q_o (% of Q_{rated}) | K_u | P_o (% of P_{rated}) | | | | | | |
|---------------------------|-------|----------------------------|-------|------|------|------|------|------|
| | | Note: $S_{rated} = 1.0$ pu | | | | | | |
| | | 5 | 10 | 30 | 50 | 70 | 90 | 95 |
| 5 | 0.884 | 54.52 | 32.89 | 6.86 | 2.77 | 1.48 | 0.93 | 0.84 |
| 10 | 0.887 | | 13.49 | 5.06 | 2.35 | 1.33 | 0.86 | 0.78 |
| 30 | 0.894 | | | 1.43 | 1.05 | 0.76 | 0.57 | 0.53 |
| 50 | 0.902 | | | | 0.49 | 0.41 | 0.34 | 0.33 |
| 70 | 0.915 | | | | | 0.23 | 0.21 | 0.20 |
| 90 | 0.919 | | | | | | 0.13 | 0.13 |
| 95 | 0.921 | | | | | | | 0.12 |

Table 5.2. Common effective coupling gain κ_R for a range of operating points with scalar coupling $c = 0.2$.

| Q_o (% of Q_{rated}) | K_u | P_o (% of P_{rated}) | | | | | | |
|---------------------------|-------|----------------------------|-------|-------|-------|-------|-------|-------|
| | | Note: $S_{rated} = 1.0$ pu | | | | | | |
| | | 5 | 10 | 30 | 50 | 70 | 90 | 95 |
| 5 | 0.884 | 3.285 | 0.534 | 0.055 | 0.027 | 0.018 | 0.014 | 0.013 |
| 10 | 0.887 | | 0.850 | 0.069 | 0.030 | 0.019 | 0.014 | 0.013 |
| 30 | 0.894 | | | 0.106 | 0.038 | 0.021 | 0.015 | 0.014 |
| 50 | 0.902 | | | | 0.041 | 0.022 | 0.015 | 0.014 |
| 70 | 0.915 | | | | | 0.022 | 0.015 | 0.013 |
| 90 | 0.919 | | | | | | 0.014 | 0.012 |
| 95 | 0.921 | | | | | | | 0.012 |

With regards to communication delay, which is a concern in any distributed control system, the consensus-based reactive power sharing problem can be represented in the form of (3.10), expressible as

$$\begin{aligned}\Delta X_{vi}(k) &= \kappa_X \sum_{j \in N_i} a_{ij} [Q_i(k-\tau) - Q_j(k-\tau)] \\ \Delta R_{vi}(k) &= \kappa_R \sum_{j \in N_i} a_{ij} [Q_i(k-\tau) - Q_j(k-\tau)]\end{aligned}\tag{5.14}$$

As far as control stability is concerned, the delayed control system would be asymptotically stable if and only if condition (3.11) is met.

5.2.2 Simulation results

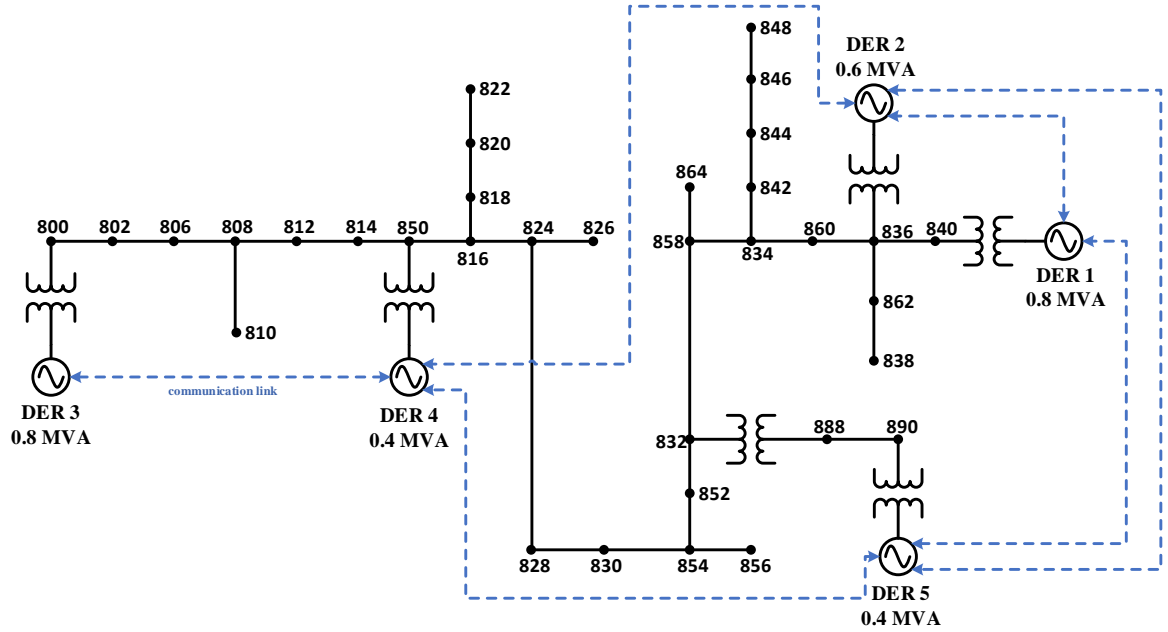


Fig. 5.3. The modified *IEEE-34 node test feeder*-based islanded microgrid with sparse communication links.

The modified *IEEE-34 node test feeder*-based islanded microgrid with five VOI-droop controlled DERs, as illustrated in Fig. 5.3, is utilised for the secondary control performance evaluation through the *DIGSILENT-PowerFactory-Python* co-simulation platform. The Laplacian matrix of the sparse communication graph (blue dotted lines) as shown in Fig. 5.3 is given as

$$L_G = \begin{bmatrix} 2 & -1 & 0 & 0 & -1 \\ -1 & 3 & 0 & -1 & -1 \\ 0 & 0 & 1 & -1 & 0 \\ 0 & -1 & -1 & 3 & -1 \\ -1 & -1 & 0 & -1 & 3 \end{bmatrix}$$

where c is scaled to 0.2 ((3.9) with $d_{max} = 3$), as per Table 5.1 and Table 5.2. The basic parameters of the islanded microgrid and VOI-droop-based DERs are as tabulated in Table 5.3. Differences in these parameters as compared to those in Section 4.2 are: the kVA rating of DER 2 is increased from 0.2

MVA to 0.6 MVA; and the filter impedances are adjusted to have a resonance frequency of approximately one-tenth of the switching frequency.

Four test scenarios have been conducted: default steady state, load stepping, plug-and-play DER and communication time delay. The performance of the consensus-based control with reactive power is benchmarked against the recently reported dual-impedance consensus control by Zhang *et al.* (2017). The dual-impedance consensus control adopts static and dynamic components of both virtual resistance and reactance in the VOI-droop scheme. Features of the dual-impedance consensus control used for benchmarking are highlighted below:

- i. The secondary consensus-based VOI-droop control is assisted with cascaded *PI* controls.
- ii. Virtual output resistance and inductance with both static and dynamic components of the virtual output impedance are considered in the reactive power sharing control.
- iii. The dynamic consensus-based voltage control presented in Zhang *et al.* (2017) is not implemented in this study that focuses on the reactive power sharing problem.

Table 5.3. The modified *IEEE-34 node test feeder*-based islanded microgrid network parameters.

| Parameter | Value | Parameter | Value |
|----------------------------|---------------|--|--|
| Network freq. | 60Hz | <i>P</i> - <i>f</i> droop coeff. <i>m</i> (pu) | 0.0625 |
| Nominal voltage | 24.9/4.16kV | No-load freq. ω^* (pu) | 1.02 |
| DC voltage | 1kV | <i>Q</i> - <i>V</i> droop coeff. <i>n</i> (pu) | 0.075 |
| Sw. freq. F_{sl} | 10kHz | No-load voltage V^* (pu) | 1.02 |
| DER ratings: | | Power-electronic-based DERs: | |
| Apparent power (pf) | | Filter impedances <i>L-RC</i> | |
| DER 1 | 0.8 MVA (0.8) | \mathbf{Z}_{f1} | 0.1905mH, 10 Ω , 132.96 μ F |
| DER 2 | 0.6 MVA (0.8) | \mathbf{Z}_{f2} | 0.2540mH, 10 Ω , 88.64 μ F |
| DER 3 | 0.8 MVA (0.8) | \mathbf{Z}_{f3} | 0.1905mH, 10 Ω , 132.96 μ F |
| DER 4 | 0.4 MVA (0.8) | \mathbf{Z}_{f4} | 0.3810mH, 10 Ω , 66.48 μ F |
| DER 5 | 0.4 MVA (0.8) | \mathbf{Z}_{f5} | 0.3810mH, 10 Ω , 66.48 μ F |
| DER primary control | | Power-electronic-based DERs: | |
| | | Output feeder impedances | |
| Power control | τ_c 0.2 | \mathbf{Z}_{of1} | 0.03 Ω , 0.35mH |
| Voltage control | K_v^P 1.23 | \mathbf{Z}_{of2} | 0.056 Ω , 0.35mH |
| | K_v^I 4.67 | \mathbf{Z}_{of3} | 0.03 Ω , 0.35mH |
| Current control | K_c^P 0.27 | \mathbf{Z}_{of4} | 0.043 Ω , 0.35mH |
| | K_c^I 1.61 | \mathbf{Z}_{of5} | 0.043 Ω , 0.35mH |

In the default steady state with load change, the islanded microgrid is initially loaded at $1.52 + j1.27$ MVA with DERs initially controlled through standard droop scheme without reactive power sharing control. It is clearly shown in Fig. 5.4 that prior to $t = 5$ s, the reactive power is not proportionately shared among the DERs. The consensus-based VOI-droop control with reactive power sharing improvement is activated at $t = 5$ s and the common effective coupling gain κ is set for high-loading operating points, i.e. 0.12 for X_v -based and 0.012 for R_v -based schemes. On the other hand, the controller gains of the dual-impedance consensus control are arbitrarily tuned in such a way that a similar settling time as the X_v -based scheme is obtained. The dual-impedance control gains are summarised here: scalar coupling gain $C_Q = 4$, PI control gains $D_P = 0.03$ and $D_I = 1.2$, virtual inductance proportional gain $K_{Q_L} = 0.15$, virtual resistance proportional gain $K_{Q_R} = 0.02$, $R_{v,static} = 0.05 \Omega$ and $L_{v,static} = 0.5$ mH (refer to Zhang *et al.* (2017) for more information on the control schemes and definitions). Upon activation of the reactive power sharing control, the reactive load power can be shared proportionally among the DERs as depicted in Fig. 5.4. The corresponding VOI values for all three consensus controls are as shown in Fig. 5.5 which in the adaptive X_v - or R_v -based control without static components, the X_v or R_v values can either be positive or negative, whereas the dual-impedance scheme's X_v and R_v are confined to positive value only. At $t = 180$ s, an additional load is connected to bus 814, resulting in a total load demand of $1.75 + j1.66$ MVA. Fig. 5.4 also shows that the control schemes continue to realise proportional reactive power sharing regardless of load changing. However, as seen in Fig. 5.6, the dual-impedance consensus control has resulted in larger bus voltage deviations as compared to those in the proposed control schemes. This can be explained

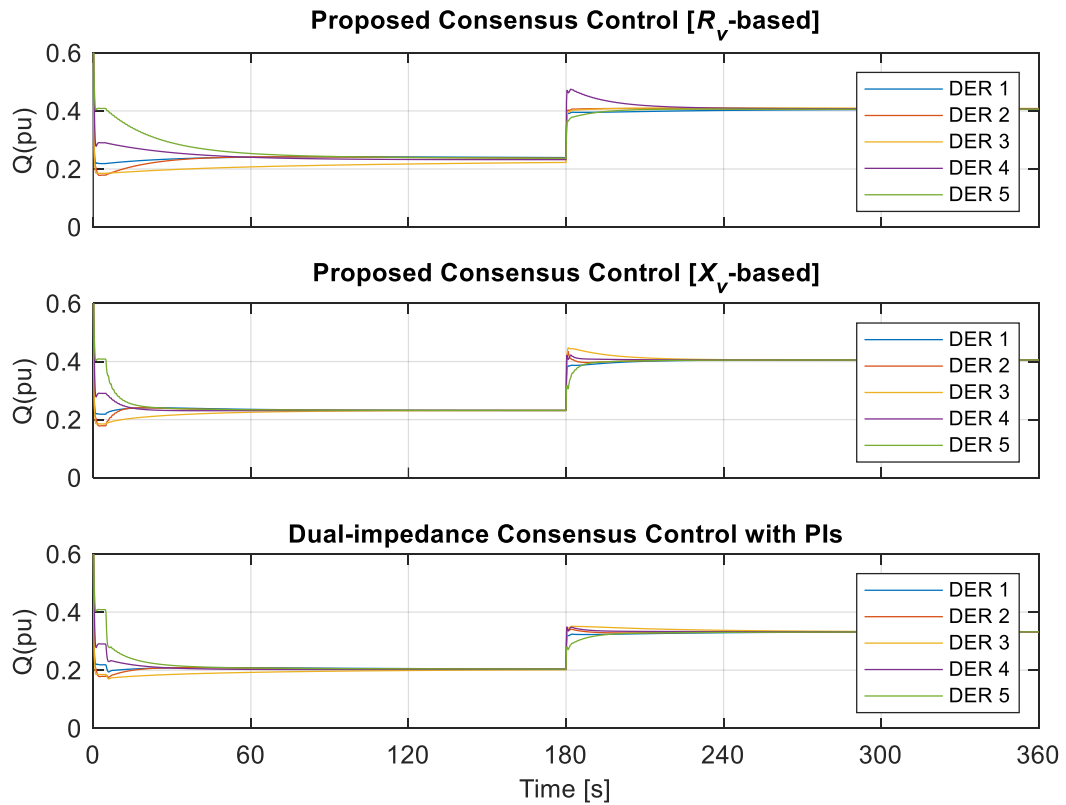


Fig. 5.4. Default steady state and load step change: DERs' reactive output power.

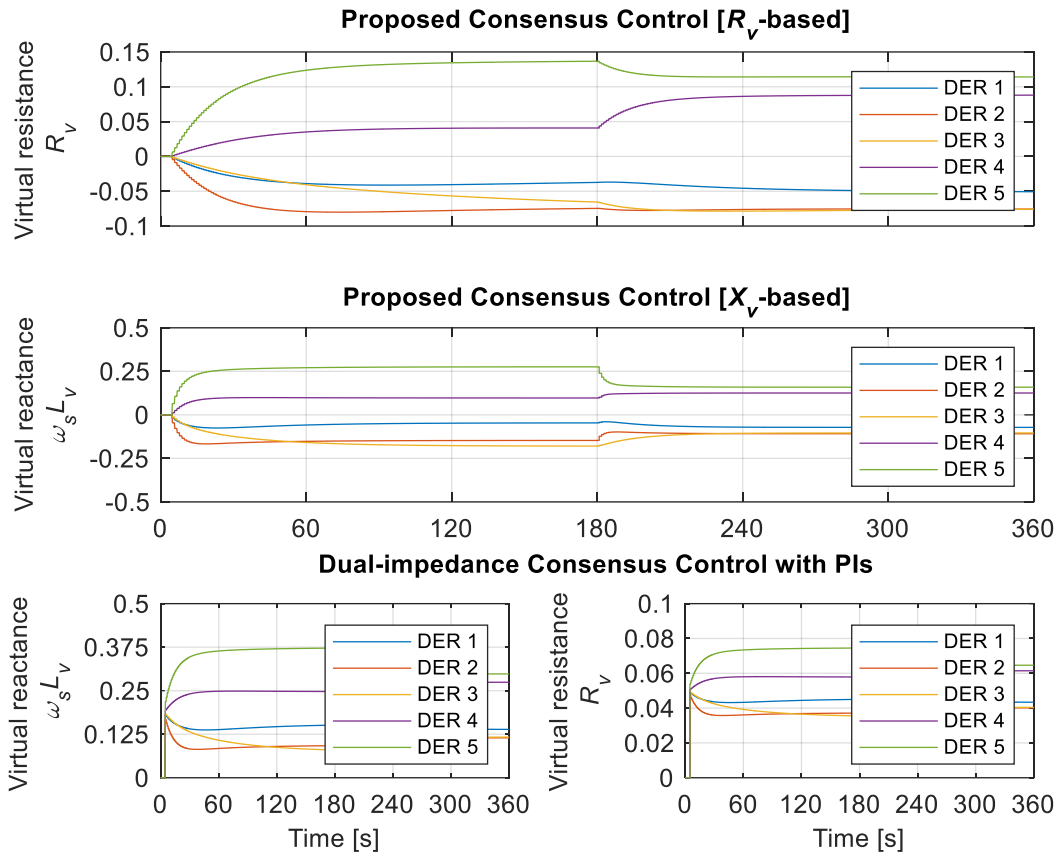


Fig. 5.5. Default steady state and load step change: DERs' virtual output impedance values.

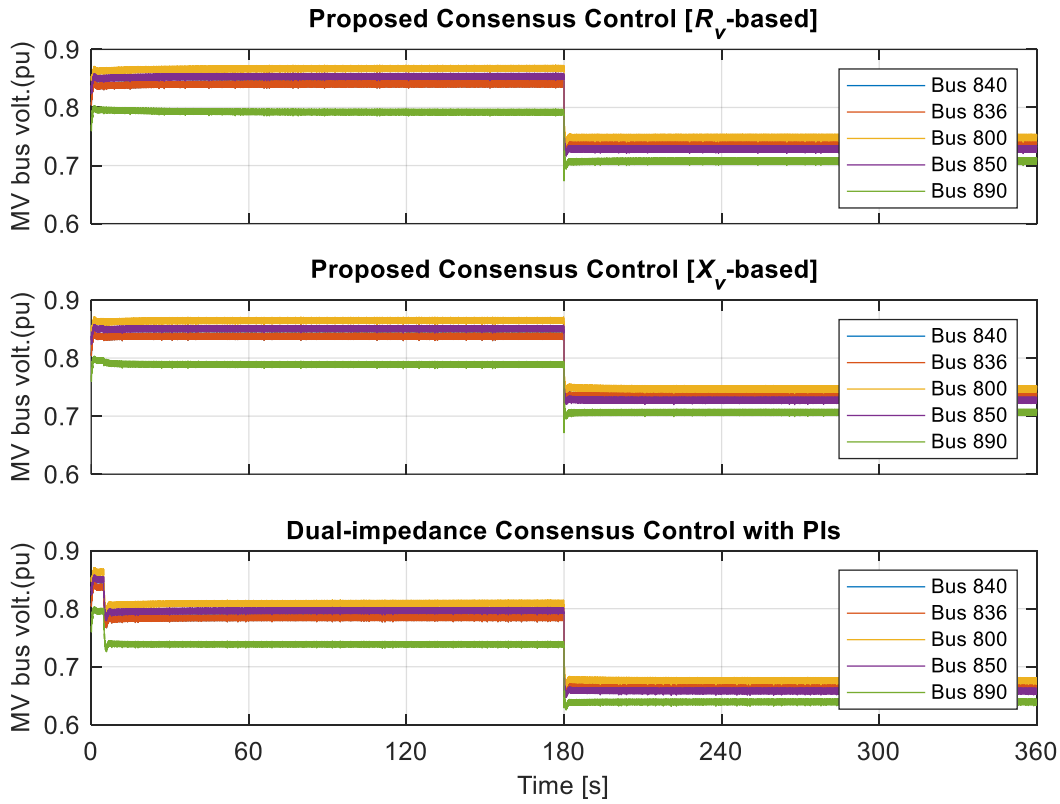


Fig. 5.6. Default steady state and load step change: the corresponding DER-bus voltage magnitudes.

by the non-zero static impedance components. On the other hand, it can be clearly seen in Fig. 5.4 that the adaptive R_v -based scheme achieves proportional reactive power sharing at a much slower pace than that of the X_v -based scheme given that both κ_X and κ_R have been chosen at the same high loading operating point. This hints that, as compared to the X_v -based control counterpart, R_v -based control is in a way inferior in reactive power sharing improvement of islanded microgrid with line impedances of moderate X/R ratio. Therefore, although both adaptive R_v - and X_v -based control results in the same voltage profile (as shown in Fig. 5.6), X_v -based control is preferred as it results in a faster control dynamic.

In order to justify the validity of the developed coupling gain tuning guideline, the islanded microgrid is lightly loaded at $0.246 + j0.036$ MVA. The proposed consensus-based VOI-droop control for reactive power sharing improvement is activated at $t = 5$ s with the common effective coupling gain κ set at low-loading operating point, i.e., 13.49 for X_v -based and 0.85 for R_v -based schemes. Similarly, Fig. 5.7 shows that both proposed control schemes are able to realise proportional reactive power sharing with the corresponding VOI values as depicted in Fig. 5.8. It can be clearly seen in Fig. 5.7 that, the adaptive R_v -based scheme results in a slower reactive power sharing improvement dynamic as compared to the X_v -based counterpart, provided that both κ_X and κ_R are tuned at the same low loading operating point. Hence, the subsequent scenarios will focus on the adaptive X_v -based control scheme as it is expected to result in a quick correction.

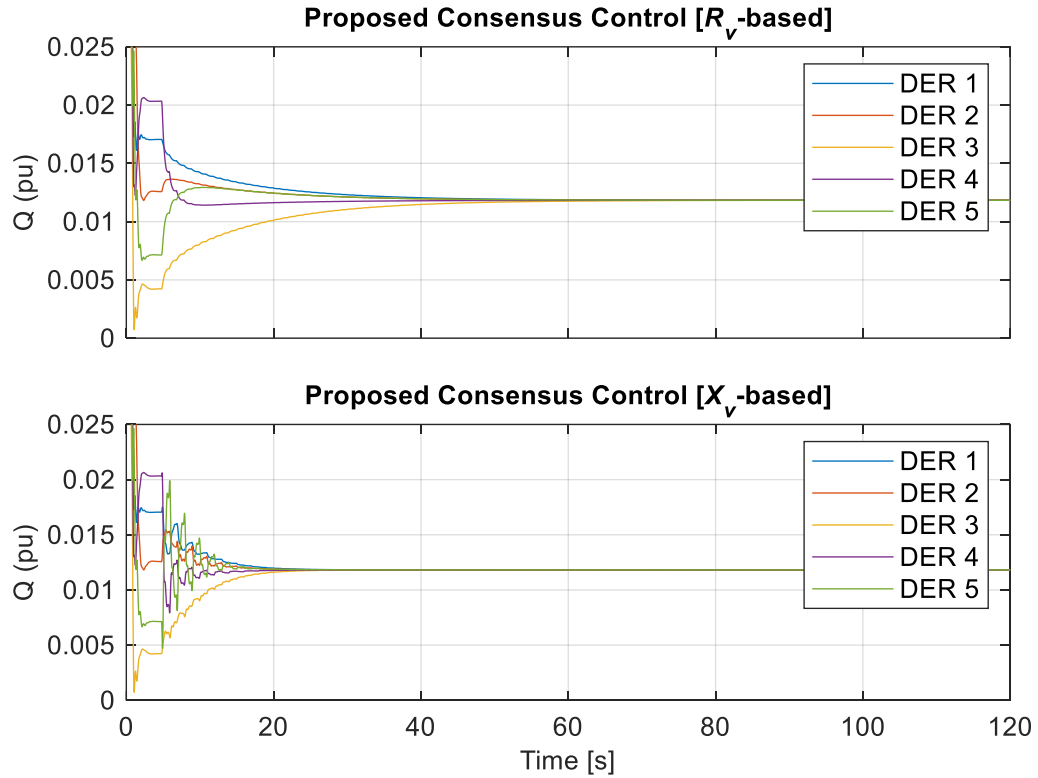


Fig. 5.7. Low-loading operating condition: DERs' reactive output power.

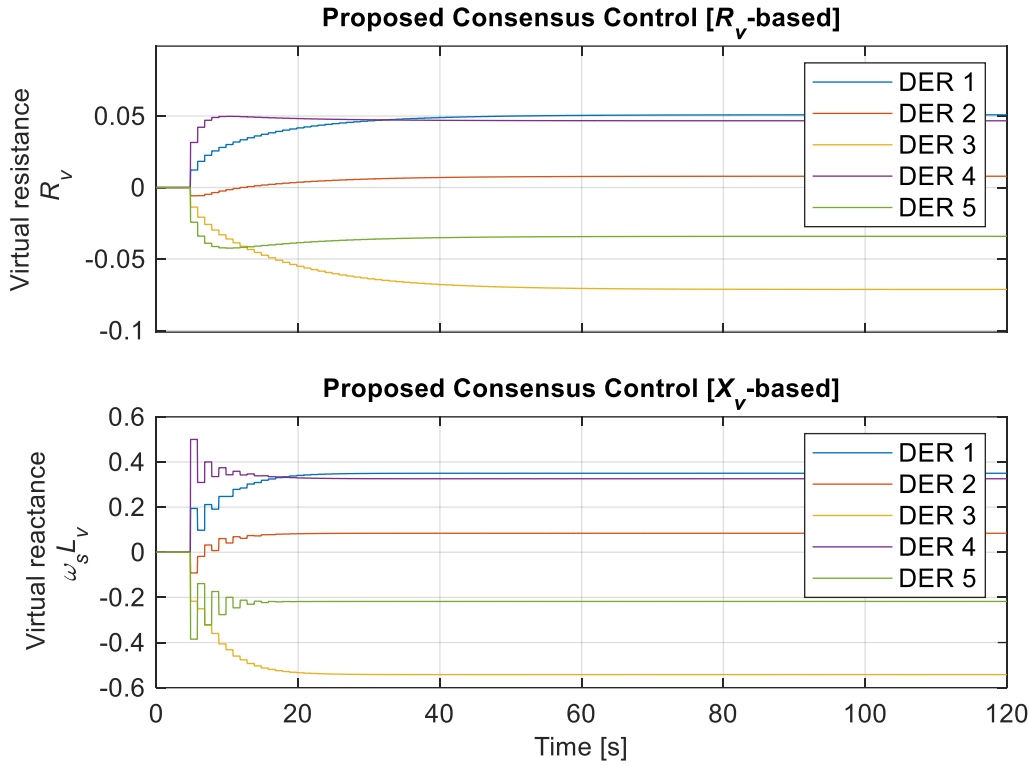


Fig. 5.8. Low-loading operating condition: DERs' virtual output impedance values.

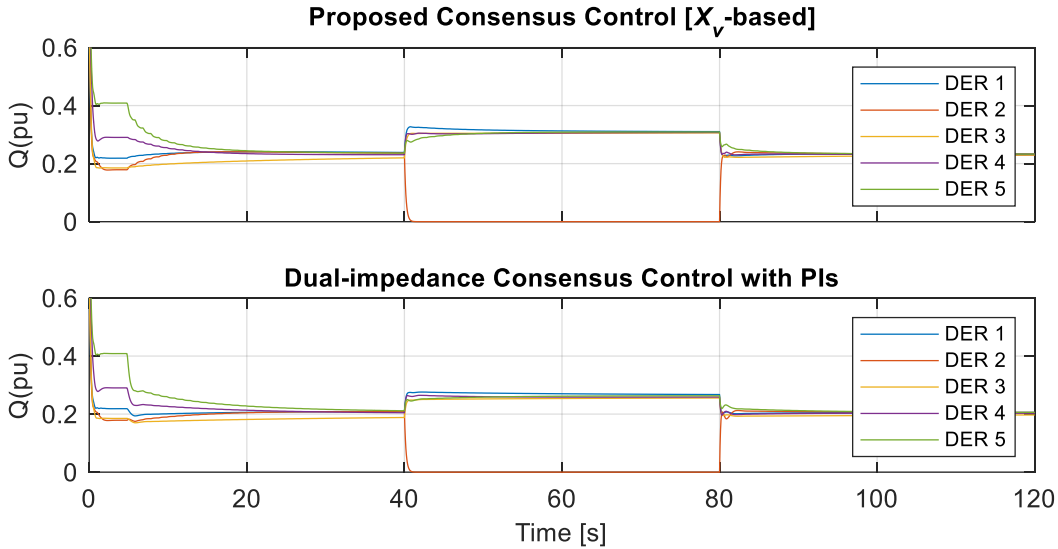


Fig. 5.9. Plug-and-play of DER 2: DERs reactive output power.

Next, the performance of the adaptive X_v -based consensus control considering the plug-and-play feature of an islanded microgrid is investigated. The islanded microgrid is operated under the default steady state loading with reactive power sharing improvement controls activated after $t = 5$ s. At $t = 40$ s, DER 2 (arbitrarily chosen) is disconnected from the islanded microgrid. This means that the communication of DER 2 to and from neighbours are lost. As shown in Fig. 5.9, proportional reactive power sharing is retained in both adaptive X_v -based and dual-impedance consensus controls regardless of the change in network topology. Upon disconnecting DER 2, the remaining DERs are required to deliver more reactive power to meet the load demand, which is accompanied with

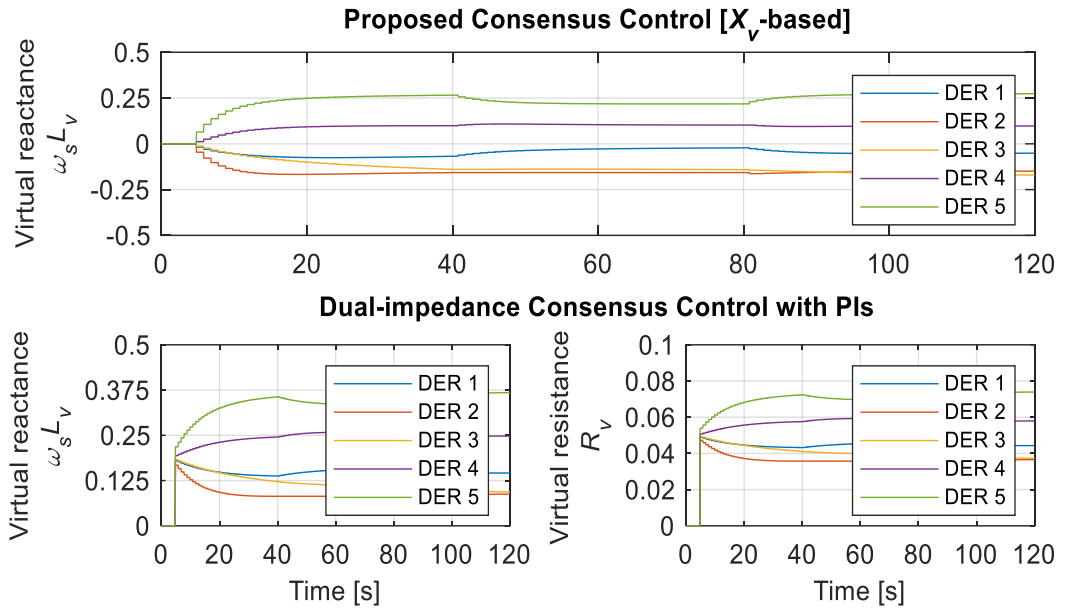


Fig. 5.10. Plug-and-play of DER 2: DERs' virtual output impedance values.

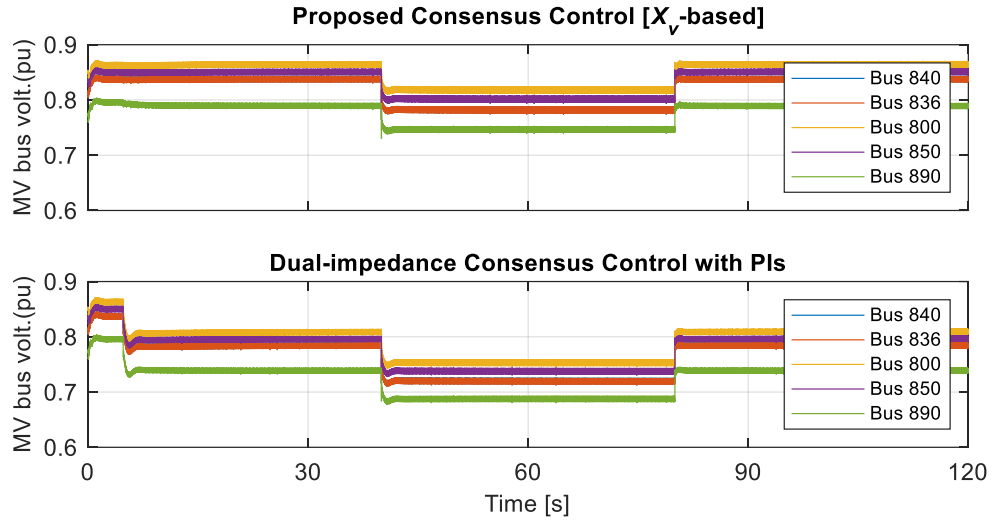


Fig. 5.11. Plug-and-play of DER 2: the corresponding DER-bus voltage magnitudes.

lowering of voltage profile. It can be clearly seen in Fig. 5.10 that, during the disconnection, the VOI values of DER 2 prior to disconnection is kept constant to ensure stability. Subsequently, upon reconnecting DER 2 at $t = 80$ s, the voltage profile is elevated without any noticeable compromise of the reactive power sharing accuracy. Once again, the dual-impedance consensus control exhibits larger bus voltage deviations as shown in Fig. 5.11.

Lastly, the robustness of the adaptive X_v -based consensus control against communication time delays is examined. Based on the Laplacian matrix of the communication graph and the developed consensus control algorithm, the maximum allowable time delay is $\tau_{max} = 1.75$ s as conditioned in (3.11) with $\lambda_{max} = 4.48$ and $c = 0.2$. Correspondingly, time delays of 1.4 s and 1.8 s are tested with the islanded microgrid loaded under the default condition. It is shown clearly in Fig. 5.12 that the developed consensus control remains stable for $\tau = 1.4$ s (with the secondary control activated at $t =$

5 s) but becoming unstable for $\tau = 1.8$ s. It is important to highlight that the adaptive X_v -based consensus control only complies with the time delay limit defined in (3.11) provided that the effective coupling gain κ is tuned according to (5.10). This essentially proves that the tuning gain analysis in Subsection 5.2.1 can indeed improve the practicality of the VOI-based consensus control.

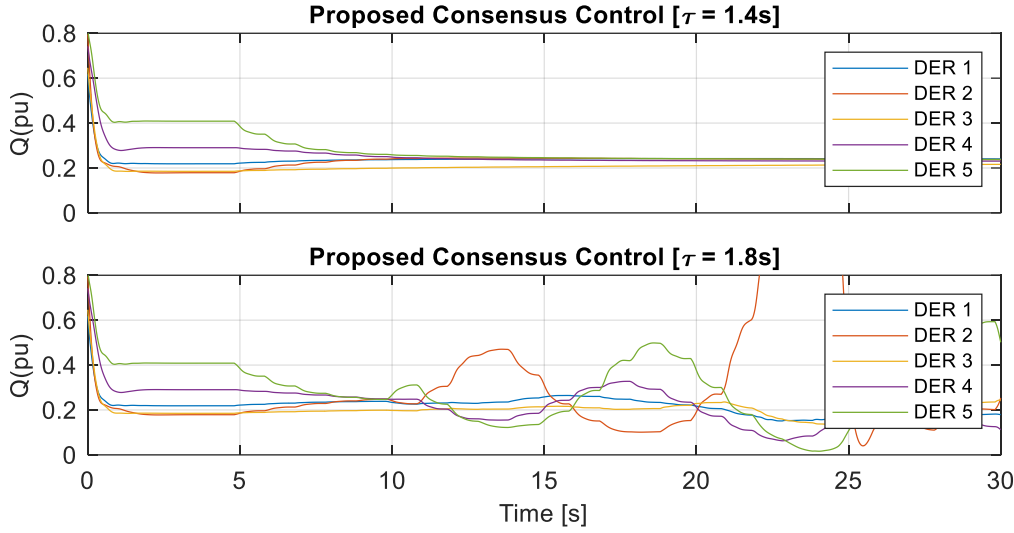


Fig. 5.12. Communication time delay: DERs' reactive output power.

5.3 Reactive power regulation through a novel droop equivalent impedance-based consensus droop control

In the previous study, it is revealed that virtual resistance or reactance alone is sufficient to ensure an accurate sharing of reactive power in a radial-structured islanded microgrid. In what follows, a novel droop equivalent impedance concept is introduced for consensus VOI-droop-based reactive power sharing control of islanded microgrids. The analysis provides a theoretical basis on why there is never a need to have both virtual resistance and reactance component in the VOI-droop scheme, but instead, only either one of them is sufficient for reactive power sharing improvement. In addition, the novel droop equivalent impedance-based consensus control adopts a single integral action without needing any *PI* control, simplifying the gain tuning process of the secondary control. Similarly, a tuning guideline that determines the approximate range of stable coupling gain for this consensus control scheme, will be presented.

5.3.1 Novel droop equivalent impedance concept

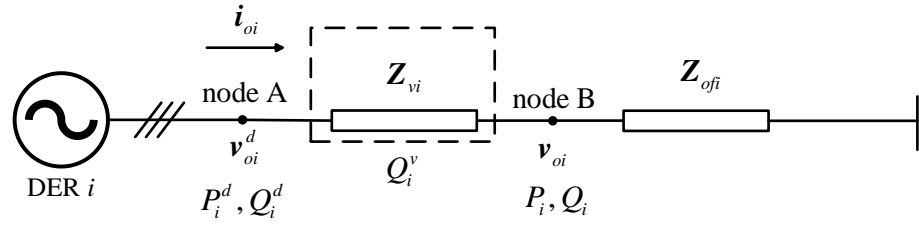


Fig. 5.13. Single line diagram of a power-electronic-interfaced DER with virtual output impedance and an output feeder impedance.

A single line diagram that consists of the virtual output impedance $Z_{vi} = R_{vi} + jX_{vi}$ and the physical output feeder impedance $Z_{ofi} = R_{ofi} + jX_{ofi}$, is shown in Fig. 5.13. Since the voltage vector at node A is synchronised to the droop angular position, i.e. $v_{oqi}^d = 0$, the phase voltage amplitude can be obtained directly from the d -axis component, which is in turn equal to the droop output voltage as reflected in (3.3). The novel concept of droop equivalent impedance $Z_{ei}^d = R_{ei}^d + jX_{ei}^d$ is introduced by first defining the droop equivalent impedance quantity:

$$Z_{ei}^d = \frac{3v_{odi}^{d2}}{S_i^*} = \frac{3v_{odi}^{d2}}{P_i - jQ_i} \quad (5.15)$$

where $S_i = P_i + jQ_i$ is the fundamental apparent power at node B and v_{odi}^d is the droop output voltage magnitude at node A. Note that this droop equivalent impedance is different from the commonly known physical equivalent impedance Z_{ei} defined in (5.3).

The basic droop control mechanism adopted in the consensus-based control schemes of this thesis is that all DERs should adopt the same droop profile (as already explained in Section 4.2). Initially, upon steady state (before reactive power correction by the consensus control action), it is known that the active load power will be accurately shared among DERs as the operating frequency is a global variable. This can be written mathematically as

$$\lim_{t \rightarrow \infty} [P_1(t) = P_2(t) = \dots = P_N(t)] \quad (5.16)$$

in pu (normalised to DER respective kVA rating). On the other hand, upon successful correction by the consensus-based VOI-droop control scheme, the following conditions are expected:

- i. The reactive load power, in pu (normalised to DER respective kVA rating), will be proportionately shared as

$$\lim_{t \rightarrow \infty} [Q_1(t) = Q_2(t) = \dots = Q_N(t)] \quad (5.17)$$

- ii. The droop output voltage magnitude for all participating power-electronic-interfaced DERs will converge to a common value (as concluded in Section 4.4), giving

$$\lim_{t \rightarrow \infty} [v_{od1}^d(t) = v_{od2}^d(t) = \dots = v_{odN}^d(t)] \quad (5.18)$$

In the droop control schemes reported by He *et al.* (2013), Altahir, Yan, and Liu (2017), Liu and Zhang (2017) and Wang, Liu and Zhang (2017), the concept of converging the DER's equivalent impedance of $\mathbf{Z}_{vi} + \mathbf{Z}_{ofi}$ (refer to Fig. 5.13) to a common value to realise proportional reactive power sharing has been proposed and investigated. However, it is deduced that the approach is not applicable to multi-bus radial microgrid as it requires a common point of coupling. In what follows, the novel droop equivalent impedance concept aiming to address this limitation will be explained.

Based on the steady-state conditions in (5.16) – (5.18), it can be realised from (5.15) that the droop equivalent impedances of all DERs must also converge to a common value upon achieving proportional active and reactive power sharing:

$$\lim_{t \rightarrow \infty} [\mathbf{Z}_{e1}^d(t) = \mathbf{Z}_{e2}^d(t) = \dots = \mathbf{Z}_{eN}^d(t)] \quad (5.19)$$

One useful observation from (5.19) is that if the virtual output impedance \mathbf{Z}_{vi} can be regulated in such a way that the droop equivalent impedance \mathbf{Z}_{ei}^d converges, then proportionate reactive power sharing can be realised. On this basis, a linear, first-order consensus control of the following form is proposed:

$$\dot{\mathbf{Z}}_{ei}^d = -c_i \sum_{j \in N_i} a_{ij} [\mathbf{Z}_{ei}^d - \mathbf{Z}_{ej}^d] \quad (5.20)$$

Based on (5.20), upon correction, the droop equivalent impedance \mathbf{Z}_{ei}^d will converge to a consensus value. Further manipulation of (5.20) reveals that it can be simplified further. This is analysed in what follows by first expanding (5.15) as

$$\mathbf{R}_{ei}^d + j\mathbf{X}_{ei}^d = \left(\frac{3v_{odi}^{d2} P_i}{P_i^2 + Q_i^2} \right) + j \left(\frac{3v_{odi}^{d2} Q_i}{P_i^2 + Q_i^2} \right) \quad (5.21)$$

Based on conditions (5.16), (5.18) and (5.21), it can be deduced that

- i. If the droop equivalent reactance X_{ei}^d of all DERs were to converge to a common (consensus) value, proportional reactive power sharing, i.e. condition (5.17), will be achieved. Consequently, the droop equivalent resistance R_{ei}^d will also be equalised.
- ii. Vice versa, if the droop equivalent resistance R_{ei}^d of all DERs were to converge to a common value, proportional reactive power sharing will be achieved. Consequently, the droop equivalent reactance X_{ei}^d will also be equalised.

In essence, this shows that as far as reactive power sharing is concerned, there is never a need to regulate both components of droop equivalent impedance. In fact, any attempt to regulate both together would be an ill-posed problem and may result in control instability if the control gains (e.g., consensus gain) are not tuned appropriately. This observation also agrees with some existing VOI-droop works with the features of: regulating R_v with fixed X_v (Zhu *et al.*, 2015, 2016, 2018); fixing X_v/R_v ratio from outset (Mahmood, Michaelson and Jiang, 2015a; Zhang *et al.*, 2017; Hoang and Lee, 2018). It is worth noting that although there are individual virtual resistance and reactance control loops in Zhang *et al.* (2017), the two virtual impedance components are inherently coupled since their integral loop is common, which leads to an approximately fixed X_v/R_v ratio.

5.3.2 Consensus control design with droop equivalent impedance

Based on the previous finding, it is proposed here that only the droop equivalent reactance is regulated for reactive power sharing improvement control (i.e. droop equivalent resistance neglected). Hence, (5.20) can be simplified to

$$\dot{X}_{ei}^d = -c_i \sum_{j \in N_i} a_{ij} [X_{ei}^d - X_{ej}^d] \quad (5.22)$$

It is worth acknowledging here that the droop equivalent resistance R_{ei}^d may also be exploited as the consensus error, however, it can be deduced from (5.21) that droop equivalent reactance X_{ei}^d has a “more direct” impact on reactive power adjustment and hence would logically be a better choice.

Similar to the analysis in Subsection 5.2.1, it can be established that (5.22) is still not suitable for control implementation as there is no direct mean to control the droop equivalent reactance X_{ei}^d for achieving proportional reactive power sharing but only the virtual output reactance X_{vi} is directly controllable. Hence, the relationship between droop equivalent reactance and virtual output reactance is analysed next. With the assumption that active output power P_i does not change significantly during reactive power sharing improvement control, the dynamical relationship between X_{ei}^d and Q_i can be approximated from (3.3) and (5.21) to a linear, operating-point-dependent relationship, expressed as

$$\dot{X}_{ei}^d = H_i (V_i^*, n, P_{oi}, Q_{oi}) \dot{Q}_i \quad (5.23)$$

where

$$H_i = \frac{3V_i^{*2} P_{oi}^2 - 3V_i^{*2} Q_{oi}^2 - 12V_i^* n P_{oi}^2 Q_{oi} + 9n^2 P_{oi}^2 Q_{oi}^2 + 3n^2 Q_{oi}^4}{(P_{oi}^2 + Q_{oi}^2)^2} \quad (5.24)$$

Correspondingly, the approximated linear relationship between the time derivative of X_{vi} and X_{ei}^d can be obtained from (5.10) and (5.23), as

$$\dot{X}_{vi} = J_i(V_i^*, n, K_{ui}, P_{oi}, Q_{oi}) \dot{X}_{ei}^d \quad (5.25)$$

where $J_i = F_i/H_i$. By substituting (5.25) into (5.22), the consensus-based VOI-droop scheme that utilises the droop equivalent impedance can be re-expressed as

$$\dot{X}_{vi} = -\kappa_i \sum_{j \in N_i} a_{ij} [X_{ei}^d - X_{ej}^d] \quad (5.26)$$

where $\kappa_i = c_i J_i(V_i^*, n, K_{ui}, P_{oi}, Q_{oi})$.

Upon first-order discretisation, the virtual output reactance can be obtained from

$$\begin{aligned} X_{vi}(k+1) &= X_{vi}(k) + T_s \Delta X_{vi}(k) \\ \Delta X_{vi}(k) &= -\kappa_i \sum_{j \in N_i} a_{ij} [X_{ei}^d(k) - X_{ej}^d(k)] \end{aligned} \quad (5.27)$$

Considering delay in communication among the distributed controllers, the droop-equivalent-impedance-based consensus control with communication delay can be written as

$$\Delta X_{vi}(k) = -\kappa_i \sum_{j \in N_i} a_{ij} [X_{ei}^d(k - \tau) - X_{ej}^d(k - \tau)] \quad (5.28)$$

A tuning approach that is similar to the one presented in Section 5.2 is used in what follows. It considers the smallest value of J_{min} for a given range of operating points and subsequently, use cJ_{min} as the effective coupling gain κ common to all participating DERs. The possible κ gains for a given range of practical operating points that are of different P_o and Q_o with a rated power factor of 0.8 is summarised in Table 5.4. The calculation assumes a constant output voltage v_{oi} of 0.9 and a minimum load power factor of 0.8 (note: in Table 5.4, the grey-shaded columns are those load power factors below 0.8). Based on the analysis, it is recommended that the common effective coupling gain κ should be chosen at low loadings, e.g. one with 10% P_{rated} and 5% Q_{rated} .

Table 5.4. Common effective coupling gain κ for a range of operating points with scalar coupling $c = 0.2$

| Q_o (% of Q_{rated}) | K_u | P_o (% of P_{rated}) | | | | Note: $S_{rated} = 1.0$ pu | | |
|---------------------------|-------|---------------------------|-------|-------|-------|----------------------------|-------|-------|
| | | 5 | 10 | 30 | 50 | 70 | 90 | 95 |
| 5 | 0.884 | 0.159 | 0.103 | 0.134 | 0.146 | 0.152 | 0.156 | 0.151 |
| 10 | 0.887 | | 0.161 | 0.115 | 0.131 | 0.141 | 0.148 | 0.149 |
| 30 | 0.894 | | | 0.167 | 0.105 | 0.111 | 0.120 | 0.122 |
| 50 | 0.902 | | | | 0.174 | 0.110 | 0.107 | 0.107 |
| 70 | 0.915 | | | | | 0.181 | 0.116 | 0.112 |
| 90 | 0.919 | | | | | | 0.188 | 0.158 |
| 95 | 0.921 | | | | | | | 0.189 |

5.3.3 Simulation results

The droop-equivalent-impedance-based consensus control is tested on the modified *IEEE-34 node test feeder*-based islanded microgrid (which has been detailed in Section 4.2) along with the *DigSILENT-PowerFactory-Python* co-simulation platform. The network/DERs parameters are as tabulated in Table 5.3 but with a different set of output feeder impedances: $\mathbf{Z}_{of1} = 0.03\Omega, 0.35\text{mH}$; $\mathbf{Z}_{of2} = 0.06\Omega, 0.35\text{mH}$; $\mathbf{Z}_{of3} = 0.05\Omega, 0.40\text{mH}$; $\mathbf{Z}_{of4} = 0.03\Omega, 0.30\text{mH}$; $\mathbf{Z}_{of5} = 0.04\Omega, 0.35\text{mH}$. As described in Subsection 5.3.2, Fig. 5.14 provides evidence showing that the control system will become unstable if one attempt to converge, through consensus control, the DERs' droop equivalent impedance by independently regulating both virtual output resistance and reactance. The corresponding virtual output resistance and reactance values are as shown in Fig. 5.15. Next, four test scenarios are investigated: default steady state, load stepping, plug-and-play DER and communication time delay.

In the default steady state case with static load and load step change (i.e., after $t = 25$ s), the islanded microgrid is initially loaded at $1.52 + j1.27$ MVA. Before $t = 10$ s, the power-electronic-interfaced DERs are droop-controlled without VOI-droop-based reactive power sharing control and it can be established from Fig. 5.16 that the active load power is indeed always proportionately shared, but not the reactive power. At $t = 10$ s, the droop-equivalent-impedance-based secondary consensus control is activated. Based on the established tuning guideline, the effective coupling gain is made common to all participating DERs κ and is tuned to 0.103, as tabulated in Table 5.4. It is shown clearly that the load reactive power is now proportionally shared among the DERs. The corresponding virtual output reactance profiles in Fig. 5.16 show that the virtual reactance can take both positive and negative values. Traces in Fig. 5.16 show that upon activating the VOI-droop reactive power sharing scheme, the droop output voltages v_{od}^d converge at steady state. Subsequently, an additional load is connected to bus 814 at $t = 25$ s which the total load demand of the islanded microgrid is increased to $1.75 + j1.66$ MVA. It is shown that the consensus control responds accordingly without noticeable large transients but the DER-bus voltage profile have been lowered due to the load up-stepping. Fig. 5.17 depicts that control instability occurs when κ is tuned to 0.3 (i.e. fulfilling the consensus theorem (3.9)), neglecting the dynamical relationship between virtual output reactance X_{vi} and droop equivalent impedance X_{ei}^d in the consensus algorithm. This validates the analysis in Subsection 5.3.2. On the other hand, the performance of an adaptively tuned consensus control coupling gain (i.e., with local κ_i gain defined individually by the local operating points) is shown in Fig. 5.18. A stable and underdamped performance is noted. However, as mentioned earlier, in order to ensure a stable consensus control, it is more practical to tune κ to the smallest value. This is done for the following test scenarios.

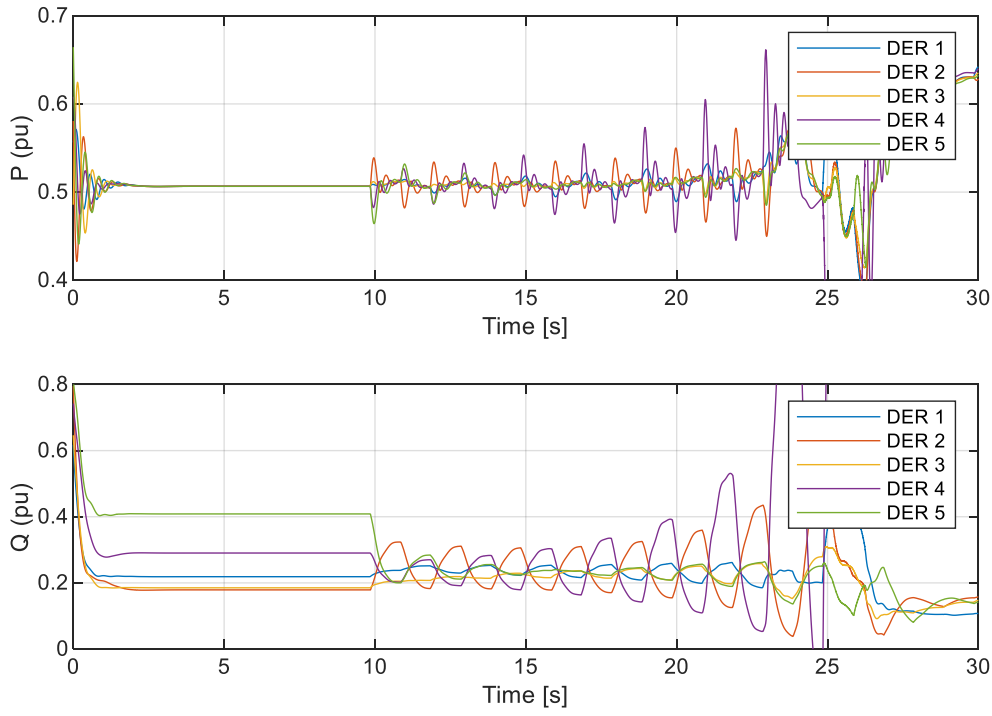


Fig. 5.14. Secondary control system instability is caused by the attempt to converge the droop equivalent impedance through regulation of both virtual output resistance and reactive independently: DERs active/reactive output power.

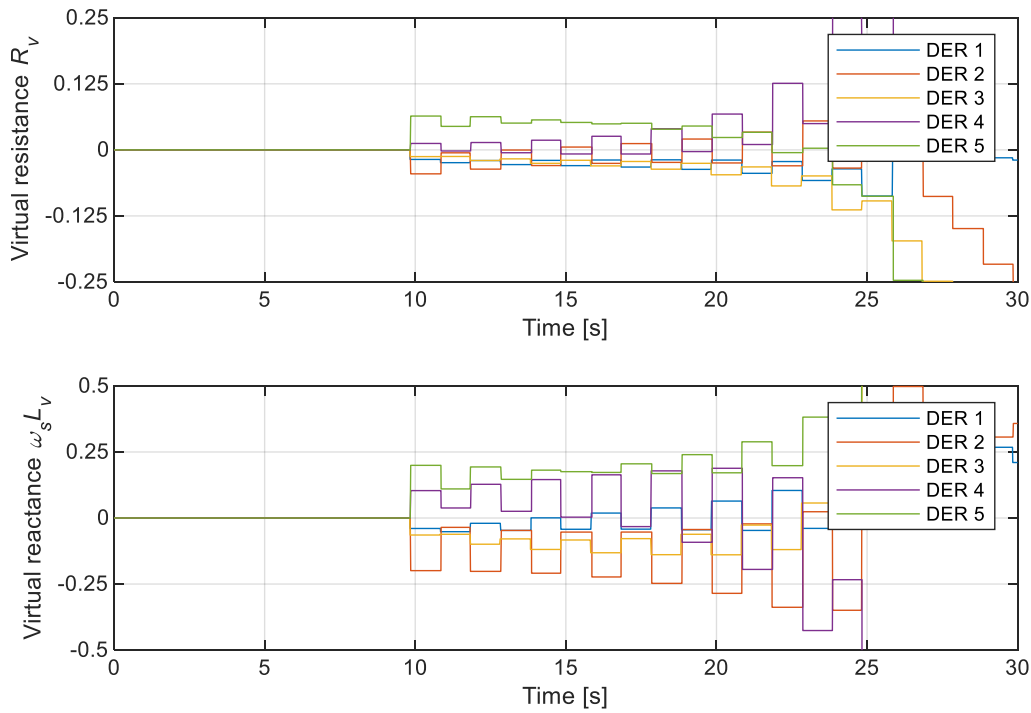


Fig. 5.15. Secondary control system instability is caused by the attempt to converge the droop equivalent impedance through regulation of both virtual output resistance and reactive independently: DERs virtual output resistance/reactance.

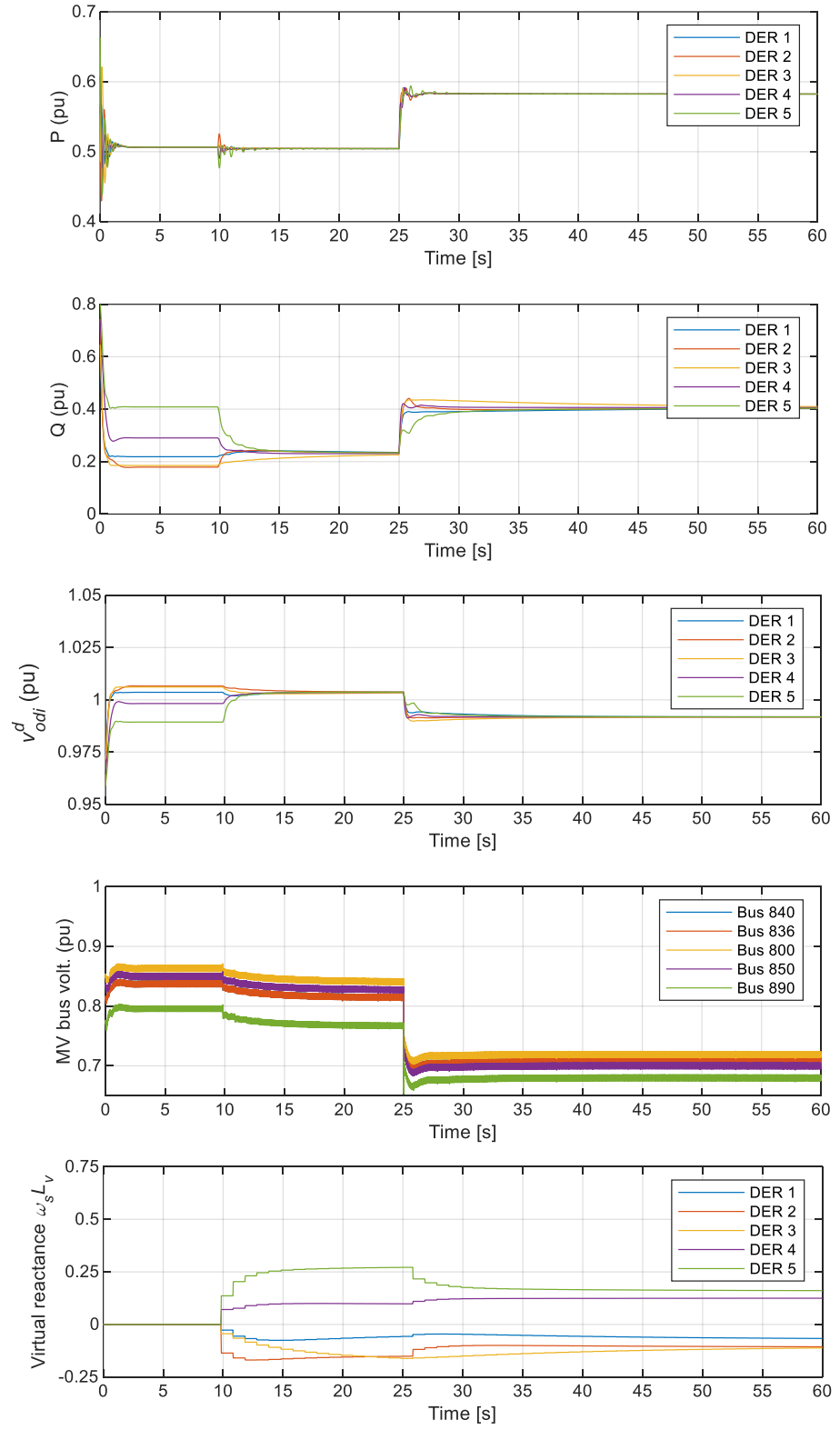


Fig. 5.16. Default steady state and load step change with fixed $\kappa = 0.103$: DERs' active and reactive output power; the corresponding droop output voltage references and DER-bus voltage magnitudes; and virtual output reactance values.

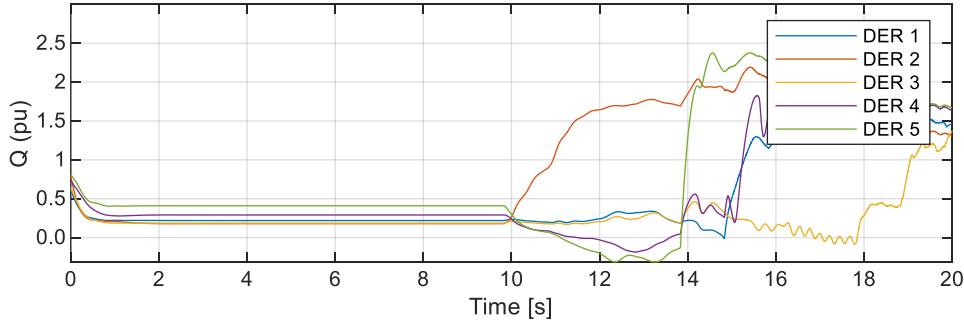


Fig. 5.17. Default steady state and load step change with fixed $\kappa = 0.3$: DERs reactive output power.

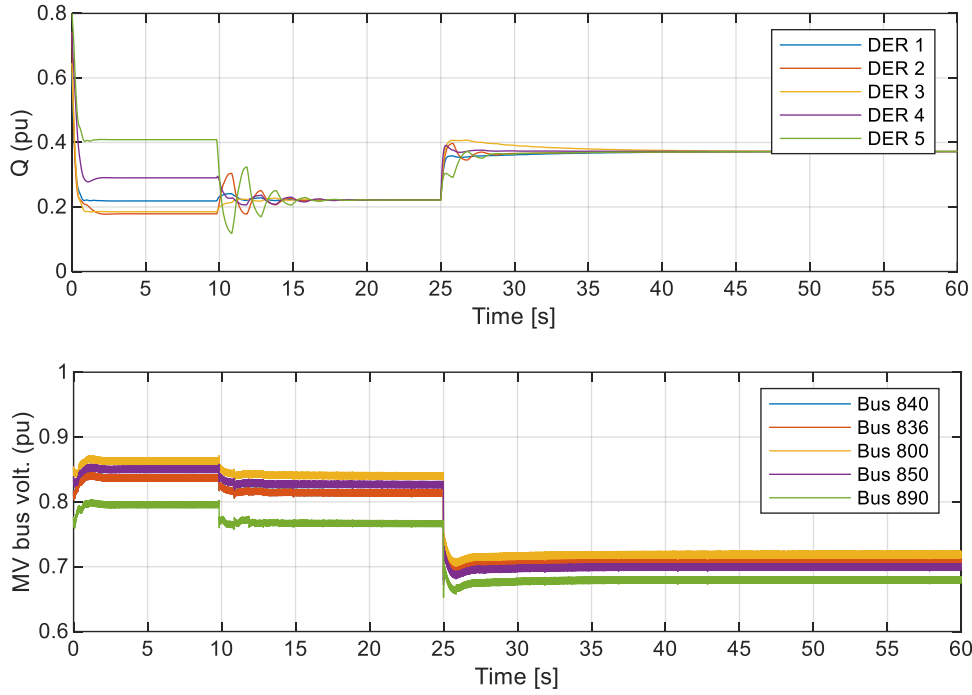


Fig. 5.18. Default steady state and load step change with adaptive κ : DERs' reactive output power and DER-bus voltage magnitudes.

Next, the dynamic performance of the VOI-droop consensus control with droop equivalent impedance considering the plug-and-play feature of a microgrid is studied. The islanded microgrid is operated under default loading condition with the proposed control scheme activated from the outset. DER 2 is disconnected from the islanded microgrid at $t = 20$ s and reconnected back to the microgrid at $t = 40$ s. As depicted in Fig. 5.19, proportional reactive power sharing is retained by the remaining DERs. It can be clearly seen that the reactive output powers of the remaining DERs increase to accommodate the default load reactive power demand. Correspondingly, the increase in DERs' reactive output power is associated with droop output voltage decrement due to droop action. With the reconnection of DER 2 at $t = 40$ s, the reactive load power is almost instantaneously re-distributed among the power-electronic-interfaced DERs with slight overshoots.

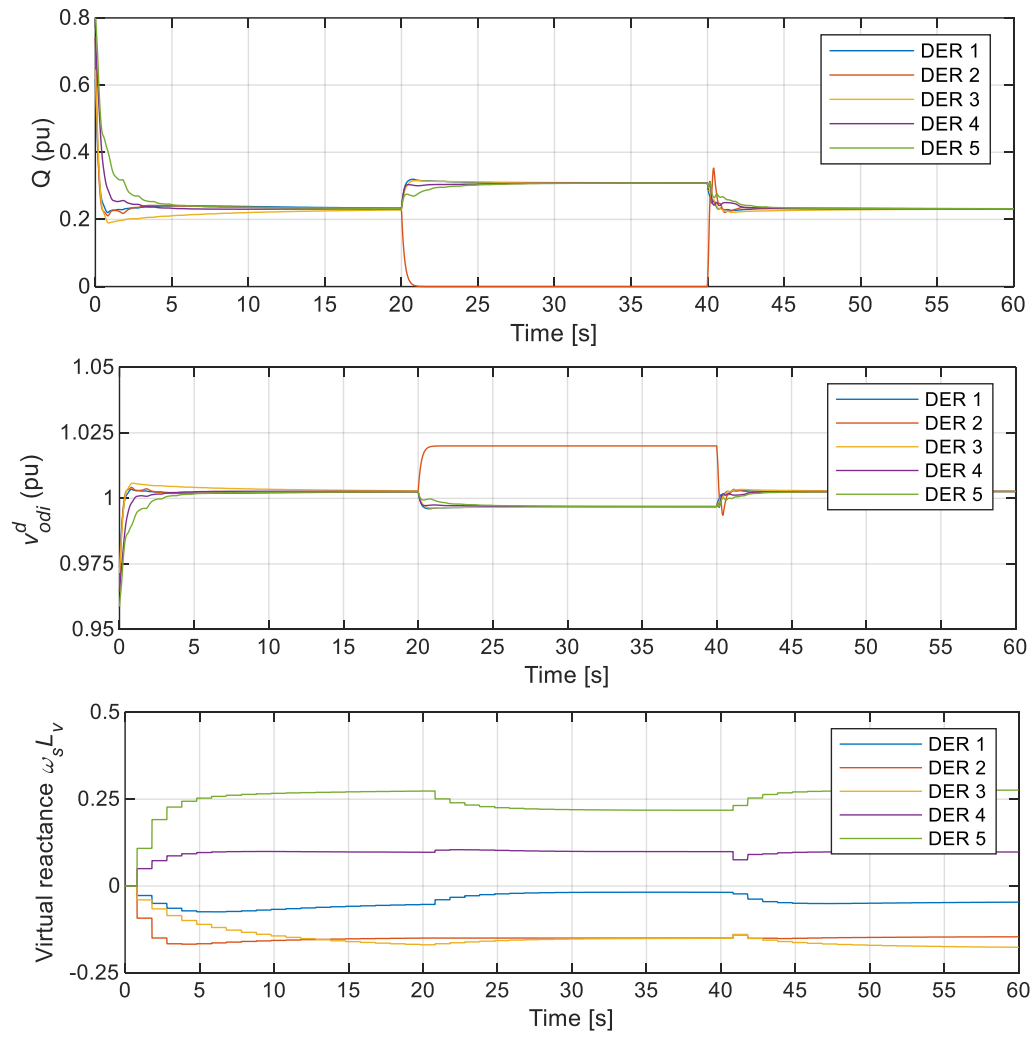


Fig. 5.19. DER 2 plug-and-play capability: DERs' reactive output power; the corresponding droop output voltage references; and the adaptive virtual output reactance generated.

The robustness of the secondary distributed control against communication link delay is examined in what follows. Based on the consensus theorem detailed in Chapter 3 and (5.28), the maximum allowable time delay is $\tau_{max} = 1.75$ s (i.e. with the maximum eigenvalue of $\lambda_{max} = 4.48$ and the scalar coupling gain $c = 0.2$). In this case study, the time delay τ is set to be 0.6, 1.4 and 1.8 s, respectively. Fig. 5.20 shows the corresponding reactive output power of DERs after activating the consensus control at $t = 10$ s. It can be clearly seen that proportional reactive power sharing is achieved for the case of $\tau = 0.6$ s ($\ll \tau_{max}$). For the case of $\tau = 1.4$ s, power oscillation can be seen before reaching the final steady state. However, upon time delay $\tau = 1.8$ s ($> \tau_{max}$), the secondary controller destabilises the islanded microgrid. This essentially verifies the communication delay discussion described in Chapter 3.

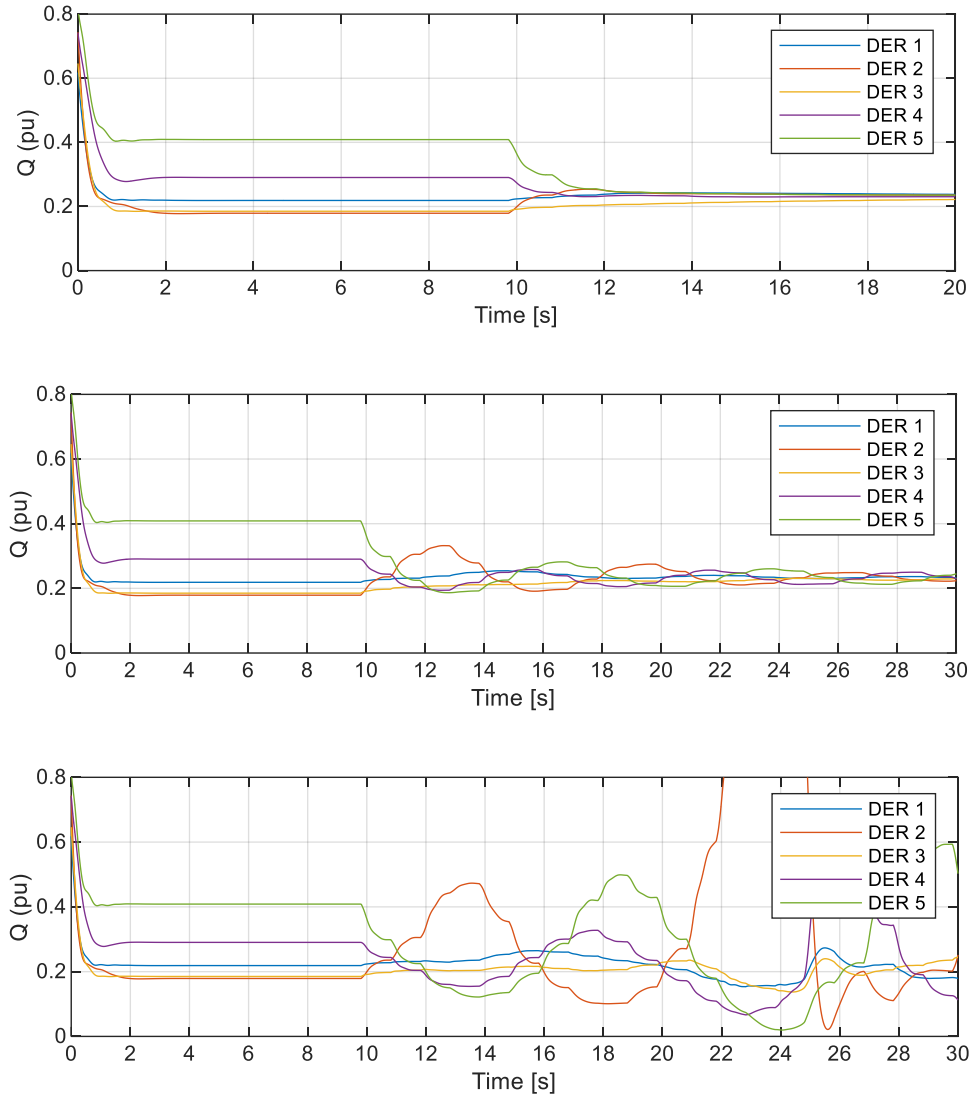


Fig. 5.20. DERs' reactive output power with communication time delay of (top) 0.6 s (mid) 1.4 s and (bottom) 1.8 s.

5.4 Summary

This chapter presents two consensus-based adaptive VOI-droop secondary controls for realising accurate reactive power sharing in an islanded, multi-bus radial microgrid. The exploitation of consensus algorithm only requires a sparse communication network to realise a fully distributed control strategy.

Instead of the widely adopted dual-impedance consensus control, Section 5.2 presents the first consensus-based VOI-droop control scheme that only exploits either, reactance or resistance components, of the dynamic virtual output impedances without the commonly used static component. The study confirms that dynamic component alone is sufficient to achieve an accurate sharing of reactive power. The relationship between the virtual output reactance/resistance and reactive power is analysed. The analysis confirms that an effective coupling gain is a dominant factor in ensuring a

stable, network-wide consensus control scheme. Moreover, it is also shown that the virtual-reactance-based scheme has a faster reactive power sharing correction dynamic.

In Section 5.3, a novel droop-equivalent-reactance-based consensus adaptive VOI-droop control scheme is proposed. The principle behind the single-virtual-impedance component VOI-droop scheme (i.e. with either virtual output reactance or virtual output resistance) is explained through the new concept of droop equivalent impedance. It is revealed that upon the convergence of the droop equivalent reactance (resistance) through the regulation of virtual output reactance (resistance), the droop equivalent resistance (reactance) will naturally be synchronised. Moreover, the relationship between the virtual output reactance and droop equivalent reactance is analysed in detail. Consequently, a consensus gain tuning guideline for the novel distributed consensus control scheme is developed. Its effectiveness has been verified against the case of communication delay – a common practical characteristic.

Both distributed consensus control schemes have avoided the use of static VOI component and the local *PI* controller (in each DER) which have been used extensively in literature. This simplification helps to improve the practicality of the consensus control schemes for microgrids as the number of DERs in future distribution networks (microgrids) is expected to be of a very high order (hundreds to tens of thousands); if the consensus stability issue is not addressed from the outset, it will pose a stability risk to the microgrids. The proposed systematic tuning approach with linearisation at practical operating points can ease the secondary control tuning process, contributing to large-scale integration of DERs in future microgrids. It is shown that a poorly designed coupling gain will destabilise the consensus control scheme – being a subject rarely discussed in the literature to date. This aspect is improved by this PhD work through the establishment of a systematic yet simple tuning guideline.

The research works in this chapter have been published in a conference paper, i.e. (Wong, Lim, Cruden, *et al.*, 2020) and two journal papers (Wong, Lim, Rotaru, *et al.*, 2020; Wong, Lim, A. Cruden, *et al.*, 2021).

The secondary control schemes developed thus far is of single objective reactive power sharing improvement, while in fact, there is an inherent trade-off between voltage regulation and reactive power sharing in the droop mechanism. In addition, while voltage regulation at DER buses is extensively attempted in literature, the same cannot be said for load buses. Therefore, advanced multi-objective secondary optimal control strategy is essential in addressing the conflicting control objectives of multiple load bus voltages and reactive power regulation. This provides the basis for Chapter 6.

Chapter 6 Optimal Secondary Multi-Bus Voltage and Reactive Power Sharing Regulation

6.1 Introduction

In this chapter, two novel secondary optimal control strategies addressing the conflicting control objectives of multiple bus voltages and reactive power regulation will be proposed and investigated. It is worth highlighting that the earlier part of this thesis has categorised the microgrid's secondary voltage regulation techniques into two groups: those that regulate DER-buses and those that regulate load-buses. Voltage regulation of DER-buses only needs to make use of information from the local buses to which the power-electronic-interfaced DER are connected, whereas voltage regulation at load-buses will usually require the power flow algorithm, as summarised in Chapter 2.

Hereafter, a centralised secondary optimal control scheme and a semi-distributed secondary optimal control scheme will be introduced and investigated. Section 6.2 details the aggregation of droop control with Decoupled Linearised Power Flow (DLPF) algorithm. This power flow algorithm is used in both of the optimal control schemes. Section 6.3 introduces the centralised optimal control scheme together with the problem formulation exploiting the use of constrained quadratic programming. The islanded microgrid network utilised for performance investigation will also be described. Section 6.4 first proposes a method to segregate large-area microgrids into sub-microgrid clusters in the secondary control layer. Then, the centralised control scheme in Section 6.3 is extended to becoming a semi-distributed optimal control scheme, which can simultaneously regulate intra- and inter-microgrid voltages and reactive powers. Lastly, Section 6.5 summarises the chapter.

6.2 Modified decoupled linearised power flow

Consider a power system network with M buses, the corresponding nodal network equation is given as

$$\begin{bmatrix} \tilde{I}_1 \\ \vdots \\ \tilde{I}_i \\ \vdots \\ \tilde{I}_M \end{bmatrix} = \begin{bmatrix} \tilde{Y}_{11} & \cdots & \tilde{Y}_{1i} & \cdots & \tilde{Y}_{1M} \\ \vdots & \ddots & \vdots & \ddots & \vdots \\ \tilde{Y}_{i1} & \cdots & \tilde{Y}_{ii} & \cdots & \tilde{Y}_{iM} \\ \vdots & \ddots & \vdots & \ddots & \vdots \\ \tilde{Y}_{M1} & \cdots & \tilde{Y}_{Mi} & \cdots & \tilde{Y}_{MM} \end{bmatrix} \begin{bmatrix} \tilde{V}_1 \\ \vdots \\ \tilde{V}_i \\ \vdots \\ \tilde{V}_M \end{bmatrix} \text{ or } \tilde{\mathbf{I}} = \tilde{\mathbf{Y}}\tilde{\mathbf{V}} \quad (6.1)$$

where the subscript i represents the bus number, and V_i and I_i are the voltage and current injection at i^{th} bus. Matrix \mathbf{Y} denotes the nodal admittance matrix with its element $Y_{ij} \in \mathbf{Y}$ obtainable from

$$\tilde{Y}_{ij} = \begin{cases} \tilde{y}_{i0} + \sum_{\substack{k=1 \\ k \neq i}}^M \tilde{y}_{ik} & \text{if } i = j \\ -\tilde{y}_{ij} & \text{otherwise} \end{cases} \quad (6.2)$$

where y_{i0} is the shunt admittance and y_{ij} is the admittance between bus i and bus j which $y_{ij} = g_{ij} + jb_{ij}$, with g and b being the conductance and susceptance, is the reciprocal of the corresponding complex line impedance z_{ij} , i.e. $= r_{ij} + jx_{ij}$, with r and x being the resistance and reactance. In essence, any off-diagonal element Y_{ij} is non-zero if and only if there is a branch linking bus i and j . If there are l branches in an M bus system then \mathbf{Y} would have M^2 elements, of which $(2l+M)$ elements are non-zero.

The current injection at i^{th} bus can be extracted from (6.1) as

$$\tilde{I}_i = \tilde{Y}_{ii}\tilde{V}_i + \sum_{\substack{j=1 \\ j \neq i}}^M \tilde{Y}_{ij}\tilde{V}_j \quad (6.3)$$

where the general form of the complex voltage and admittance can be written as $\tilde{V}_i = V_i \angle \delta_i$ and $\tilde{Y}_{ij} = Y_{ij} \angle \theta_{ij}$. Correspondingly, the apparent power injected at i^{th} bus can be expressed as

$$\begin{aligned} \tilde{S}_i &= P_i + jQ_i = \tilde{V}_i \tilde{I}_i^* \\ &= V_i^2 Y_{ii} e^{-j\theta_{ii}} + V_i \sum_{\substack{j=1 \\ j \neq i}}^M V_j Y_{ij} e^{j(\delta_i - \delta_j - \theta_{ij})} \end{aligned} \quad (6.4)$$

where the active and reactive power injected at i^{th} bus can be extracted from (6.4) as

$$\begin{aligned} P_i &= V_i^2 Y_{ii} \cos \theta_{ii} + \sum_{\substack{j=1 \\ j \neq i}}^M V_i V_j Y_{ij} \cos(\delta_i - \delta_j - \theta_{ij}) \\ &= V_i^2 G_{ii} + \sum_{\substack{j=1 \\ j \neq i}}^M V_i V_j \left[B_{ij} \sin(\delta_i - \delta_j) + G_{ij} \cos(\delta_i - \delta_j) \right] \end{aligned} \quad (6.5)$$

$$\begin{aligned} Q_i &= -V_i^2 Y_{ii} \sin \theta_{ii} + \sum_{\substack{j=1 \\ j \neq i}}^M V_i V_j Y_{ij} \sin(\delta_i - \delta_j - \theta_{ij}) \\ &= -V_i^2 B_{ii} + \sum_{\substack{j=1 \\ j \neq i}}^M V_i V_j \left[G_{ij} \sin(\delta_i - \delta_j) - B_{ij} \cos(\delta_i - \delta_j) \right] \end{aligned} \quad (6.6)$$

where $Y_{ij} = G_{ij} + jB_{ij}$.

The active and reactive power injection at each bus is essentially a nonlinear function of the system voltages. Classical iterative techniques such as Gauss Seidel and Newton Raphson methods are commonly used to solve the nonlinear power flow equations. It is widely acknowledged that nonlinear power flow will suffer from slow convergence. The state-of-the-art solution to this problem is to use DC power flow algorithm, which is essentially an alternative that approximates the linearity between active power and phase angle based on the assumption of constant bus voltages, requiring

the omission of reactive power injection characteristic. Moreover, classical power flow algorithms are usually not directly applicable to droop-controlled islanded microgrids due to two basic reasons: the inexistence of slack bus in islanded microgrids and the dependence of active/reactive powers on frequency/voltage due to primary droop control action.

Decoupled Linearised Power Flow, originally proposed by Yang *et al.* (2017) for large-scale power system planning and operation (e.g. contingency analyses and reliability assessments), is used here in conjunction with the proposed optimal control schemes. The adopted linear approximation that decouples the voltage magnitude and the phase angles fit well with the droop behaviour of islanded microgrids:

- i. the bus voltage magnitudes can be approximated at 1.0 pu, i.e. $V_i \approx V_j \approx 1.0$ for microgrids embedded with secondary voltage restoration control; and
- ii. for most practical scenarios, the absolute angle difference across distribution lines between two adjacent buses rarely exceed $\pi/9$ rad (i.e. 20°), which results in $\cos(\delta_i - \delta_j) \approx 1$ and $\sin(\delta_i - \delta_j) \approx \delta_i - \delta_j$.

On this basis, and together with (6.2), the general power flow equations (6.5) and (6.6) can be manipulated further to obtain the basic power flow equations of DLFPF:

$$\begin{aligned}
 P_i &= V_i^2 G_{ii} + \sum_{j=1, j \neq i}^M V_i V_j \left[B_{ij} \sin(\delta_i - \delta_j) + G_{ij} \cos(\delta_i - \delta_j) \right] \\
 &= V_i^2 G_{ii} + \sum_{j=1, j \neq i}^M V_i V_j G_{ij} + \sum_{j=1, j \neq i}^M V_i V_j B_{ij} \delta_i - \sum_{j=1, j \neq i}^M V_i V_j B_{ij} \delta_j \\
 &= V_i^2 \left(g_{i0} + \sum_{j=1, j \neq i}^M g_{ij} \right) + V_i \sum_{j=1, j \neq i}^M V_j (-g_{ij}) + V_i \delta_i \sum_{j=1, j \neq i}^M V_j (-b_{ij}) - V_i \sum_{j=1, j \neq i}^M V_j (-b_{ij}) \delta_j \quad (6.7) \\
 &= V_i \left(g_{i0} + \sum_{j=1, j \neq i}^M g_{ij} \right) + \sum_{j=1, j \neq i}^M V_j (-g_{ij}) - \left[\delta_i \sum_{j=1, j \neq i}^M b_{ij} + \sum_{j=1, j \neq i}^M (-b_{ij}) \delta_j \right] \\
 &= \sum_{j=1}^M G_{ij} V_j - \sum_{j=1}^M B'_{ij} \delta_j
 \end{aligned}$$

$$\begin{aligned}
 Q_i &= -V_i^2 B_{ii} + \sum_{j=1, j \neq i}^M V_i V_j \left[G_{ij} \sin(\delta_i - \delta_j) - B_{ij} \cos(\delta_i - \delta_j) \right] \\
 &= -V_i^2 B_{ii} + \sum_{j=1, j \neq i}^M V_i V_j G_{ij} \delta_i - \sum_{j=1, j \neq i}^M V_i V_j G_{ij} \delta_j - \sum_{j=1, j \neq i}^M V_i V_j B_{ij} \\
 &= -V_i^2 \left(b_{i0} + \sum_{j=1, j \neq i}^M b_{ij} \right) - V_i \sum_{j=1, j \neq i}^M V_j (-b_{ij}) + V_i \delta_i \sum_{j=1, j \neq i}^M V_j (-g_{ij}) - V_i \sum_{j=1, j \neq i}^M V_j (-g_{ij}) \delta_j \quad (6.8) \\
 &= -V_i \left(b_{i0} + \sum_{j=1, j \neq i}^M b_{ij} \right) - \sum_{j=1, j \neq i}^M V_j (-b_{ij}) - \left[\delta_i \sum_{j=1, j \neq i}^M g_{ij} + \sum_{j=1, j \neq i}^M (-g_{ij}) \delta_j \right] \\
 &= -\sum_{j=1}^M B_{ij} V_j - \sum_{j=1}^M G'_{ij} \delta_j
 \end{aligned}$$

or in compact matrix form,

$$\begin{bmatrix} \mathbf{P} \\ \mathbf{Q} \end{bmatrix} = \begin{bmatrix} -\mathbf{B}' & \mathbf{G} \\ -\mathbf{G}' & -\mathbf{B} \end{bmatrix} \begin{bmatrix} \boldsymbol{\delta} \\ \mathbf{V} \end{bmatrix} \quad (6.9)$$

where \mathbf{G} and \mathbf{B} (i.e. $G_{ij} \in \mathbf{G}$ and $B_{ij} \in \mathbf{B}$) are the real and imaginary components of the admittance matrix, and \mathbf{G}' and \mathbf{B}' (i.e. $G'_{ij} \in \mathbf{G}'$ and $B'_{ij} \in \mathbf{B}'$) are the corresponding matrices without the shunt element.

Next, this work proposes that the characteristic of droop control with dispatch be embedded into DLPF in the manner described in what follows. In an islanded microgrid, $\boldsymbol{\delta}$ and \mathbf{V} , respectively, consist of two sub-vectors that correspond to the load- and DER-buses. The types of buses are denoted with subscript L and G respectively in what follows. In order to enable voltage and reactive power regulations in a droop-controlled islanded microgrid with N DERs, dispatch-based Q - V droop is adopted. The network-wide droop control can be described by

$$V_{Gi} = V_i^* - n_i Q_{Gi} + u_{com} + n_i Q_{i,dis} \quad (6.10)$$

where V_{Gi} is the per-unit droop voltage amplitude of i^{th} DER, normalised to network's phase peak voltage, V_i^* is the per-unit no-load voltage magnitude, n_i is the per-unit droop coefficients and Q_{Gi} are the per-unit reactive output power (normally low-pass filtered) normalised to a common base power S_B . The reactive power dispatch $Q_{i,dis}$ are individually commanded to affect the reactive power output through droop voltage amplitude adjustment. However, it is redundant to control all N DERs' Q_{dis} in a droop-controlled microgrid, instead only those of $(N-1)$ DERs are required. On the basis of this setting, a voltage correction term u_{com} commonly shared by all DERs is introduced to enable network-wide voltage regulation, without affecting the reactive power sharing accuracy among the DERs.

The voltage magnitude at N DER-buses can be expressed in term of DERs' reactive output power \mathbf{Q}_G and dispatch commands, in the compact matrix form, as

$$\mathbf{V}_G = \mathbf{V}^* - \Phi \mathbf{Q}_G + \Gamma \mathbf{u} \quad (6.11)$$

where

$$\begin{aligned} \mathbf{V}_G &= [V_{G1} \quad \cdots \quad V_{GN}]^T \\ \mathbf{V}^* &= [V_1^* \quad \cdots \quad V_N^*]^T \\ \Phi &= \begin{bmatrix} n_1 & \cdots & 0 & \cdots & 0 \\ \vdots & & \ddots & & \vdots \\ 0 & \cdots & 0 & \cdots & n_N \end{bmatrix} \\ \mathbf{Q}_G &= [Q_{G1} \quad \cdots \quad Q_{GN}]^T \end{aligned}$$

$$\mathbf{\Gamma} = \begin{bmatrix} 1 & n_1 & \cdots & 0 \\ \vdots & \vdots & \ddots & \vdots \\ 1 & 0 & \cdots & n_N \end{bmatrix}$$

$$\mathbf{u} = [u_{com} \quad Q_{1,dis} \quad \cdots \quad Q_{N,dis}]^T$$

The secondary control input vector \mathbf{u} consists of the common voltage correction term u_{com} and Q_{dis} of all DERs. The following assumptions are made to ease the integration of Q - V dispatch-droop scheme into DLPF:

- i. active and reactive power are sufficiently decoupled and the guaranteed accurate active power sharing of a droop-controlled islanded microgrid is less affected by reactive power correction; and
- ii. steady-state voltage angles remain relatively constant throughout the secondary control adjustment.

Then, the linear power flow equations in (6.9) can be simplified and be partitioned according to load- and DER-buses, i.e. $\mathbf{Q} = [\mathbf{Q}_L^T \mathbf{Q}_G^T]^T$, as

$$\begin{bmatrix} \mathbf{Q}_L \\ \mathbf{Q}_G \end{bmatrix}_{k+1} = - \begin{bmatrix} \mathbf{G}'_{LL} & \mathbf{G}'_{LG} \\ \mathbf{G}'_{GL} & \mathbf{G}'_{GG} \end{bmatrix} \begin{bmatrix} \delta_L \\ \delta_G \end{bmatrix}_{k+1} - \begin{bmatrix} \mathbf{B}_{LL} & \mathbf{B}_{LG} \\ \mathbf{B}_{GL} & \mathbf{B}_{GG} \end{bmatrix} \begin{bmatrix} \mathbf{V}_L \\ \mathbf{V}_G \end{bmatrix}_{k+1} \quad (6.12)$$

Substituting \mathbf{V}_G vector from (6.11) into (6.12), the load-bus voltage and DER-bus reactive power injection can be expressed as

$$\begin{aligned} \begin{bmatrix} \mathbf{Q}_L \\ \mathbf{Q}_G \end{bmatrix}_{k+1} &= - \begin{bmatrix} \mathbf{G}'_{LL} & \mathbf{G}'_{LG} \\ \mathbf{G}'_{GL} & \mathbf{G}'_{GG} \end{bmatrix} \begin{bmatrix} \delta_L \\ \delta_G \end{bmatrix}_k - \begin{bmatrix} \mathbf{B}_{LL} & \mathbf{B}_{LG} \\ \mathbf{B}_{GL} & \mathbf{B}_{GG} \end{bmatrix} \begin{bmatrix} \mathbf{V}_L \\ \mathbf{V}_G \end{bmatrix}_{k+1} \\ &= - \begin{bmatrix} \mathbf{G}'_{LL} & \mathbf{G}'_{LG} \\ \mathbf{G}'_{GL} & \mathbf{G}'_{GG} \end{bmatrix} \begin{bmatrix} \delta_L \\ \delta_G \end{bmatrix}_k - \begin{bmatrix} \mathbf{B}_{LL} \\ \mathbf{B}_{GL} \end{bmatrix} [\mathbf{V}_L]_{k+1} \\ &\quad - \begin{bmatrix} \mathbf{B}_{LG} \\ \mathbf{B}_{GG} \end{bmatrix} [\mathbf{V}^*] + \begin{bmatrix} \mathbf{B}_{LG} \Phi \\ \mathbf{B}_{GG} \Phi \end{bmatrix} [\mathbf{Q}_G]_{k+1} - \begin{bmatrix} \mathbf{B}_{LG} \Gamma \\ \mathbf{B}_{GG} \Gamma \end{bmatrix} [\mathbf{u}]_k \\ \begin{bmatrix} \mathbf{Q}_L \\ \mathbf{Q}_G \end{bmatrix}_{k+1} - \begin{bmatrix} \mathbf{B}_{LG} \Phi \\ \mathbf{B}_{GG} \Phi \end{bmatrix} [\mathbf{Q}_G]_{k+1} + \begin{bmatrix} \mathbf{B}_{LL} \\ \mathbf{B}_{GL} \end{bmatrix} [\mathbf{V}_L]_{k+1} &= - \begin{bmatrix} \mathbf{G}'_{LL} & \mathbf{G}'_{LG} \\ \mathbf{G}'_{GL} & \mathbf{G}'_{GG} \end{bmatrix} \begin{bmatrix} \delta_L \\ \delta_G \end{bmatrix}_k - \begin{bmatrix} \mathbf{B}_{LG} \\ \mathbf{B}_{GG} \end{bmatrix} [\mathbf{V}^*] - \begin{bmatrix} \mathbf{B}_{LG} \Gamma \\ \mathbf{B}_{GG} \Gamma \end{bmatrix} [\mathbf{u}]_k \quad (6.13) \\ \begin{bmatrix} \mathbf{I} \\ \mathbf{0} \end{bmatrix} [\mathbf{Q}_L]_k + \begin{bmatrix} \mathbf{B}_{LL} & -\mathbf{B}_{LG} \Phi \\ \mathbf{B}_{GL} & \mathbf{I} - \mathbf{B}_{GG} \Phi \end{bmatrix} \begin{bmatrix} \mathbf{V}_L \\ \mathbf{Q}_G \end{bmatrix}_{k+1} &= - \begin{bmatrix} \mathbf{G}'_{LL} & \mathbf{G}'_{LG} \\ \mathbf{G}'_{GL} & \mathbf{G}'_{GG} \end{bmatrix} \begin{bmatrix} \delta_L \\ \delta_G \end{bmatrix}_k - \begin{bmatrix} \mathbf{B}_{LG} \\ \mathbf{B}_{GG} \end{bmatrix} [\mathbf{V}^*] - \begin{bmatrix} \mathbf{B}_{LG} \Gamma \\ \mathbf{B}_{GG} \Gamma \end{bmatrix} [\mathbf{u}]_k \\ \begin{bmatrix} -\mathbf{B}_{LL} & \mathbf{B}_{LG} \Phi \\ -\mathbf{B}_{GL} & -\mathbf{I} + \mathbf{B}_{GG} \Phi \end{bmatrix} \begin{bmatrix} \mathbf{V}_L \\ \mathbf{Q}_G \end{bmatrix}_{k+1} &= \begin{bmatrix} \mathbf{G}'_{LL} & \mathbf{G}'_{LG} & \mathbf{I} & \mathbf{B}_{LG} \\ \mathbf{G}'_{GL} & \mathbf{G}'_{GG} & \mathbf{0} & \mathbf{B}_{GG} \end{bmatrix} \begin{bmatrix} \delta_L \\ \delta_G \\ \mathbf{Q}_L \\ \mathbf{V}^* \end{bmatrix}_k + \begin{bmatrix} \mathbf{B}_{LG} \Gamma \\ \mathbf{B}_{GG} \Gamma \end{bmatrix} [\mathbf{u}]_k \end{aligned}$$

Re-assemble the measurable sub-vectors and constant droop parameters into a single vector \mathbf{v} , (6.13) can be re-expressed as

$$\mathbf{y}(k+1) = \mathbf{C}\mathbf{v}(k) + \mathbf{D}\mathbf{u}(k) \quad (6.14)$$

where

$$\begin{aligned}
\mathbf{y} &= [\mathbf{V}_L^T \quad \mathbf{Q}_G^T]^T \\
\mathbf{v} &= [\delta_L^T \quad \delta_G^T \quad \mathbf{Q}_L^T \quad \mathbf{V}^{*T}]^T \\
\mathbf{u} &= [u_{com} \quad \mathbf{Q}_{dis}^T]^T \\
\mathbf{C} &= \begin{bmatrix} -\mathbf{B}_{LL} & \mathbf{B}_{LG}\Phi \\ -\mathbf{B}_{GL} & -\mathbf{I} + \mathbf{B}_{GG}\Phi \end{bmatrix}^{-1} \begin{bmatrix} \mathbf{G}'_{LL} & \mathbf{G}'_{LG} & \mathbf{I} & \mathbf{B}_{LG} \\ \mathbf{G}'_{GL} & \mathbf{G}'_{GG} & \mathbf{0} & \mathbf{B}_{GG} \end{bmatrix} \\
\mathbf{D} &= \begin{bmatrix} -\mathbf{B}_{LL} & \mathbf{B}_{LG}\Phi \\ -\mathbf{B}_{GL} & -\mathbf{I} + \mathbf{B}_{GG}\Phi \end{bmatrix}^{-1} \begin{bmatrix} \mathbf{B}_{LG}\Gamma \\ \mathbf{B}_{GG}\Gamma \end{bmatrix}
\end{aligned}$$

(6.14) serves as the model to estimate the behaviour of load-bus voltage and DER-bus reactive power output due to the control inputs of reactive power dispatch and the common voltage correction term.

6.3 Centralised optimal control for large-area islanded microgrids

In what follows, a centralised secondary optimal control is developed for reactive power and load-bus voltage regulation in a droop-controlled islanded microgrid through the *DIGSILENT-PowerFactory-Python* co-simulation platform. First, the microgrid network that is adopted for this study is described. It is followed by the illustration of the secondary estimation model with an integral-based corrective term to improve the accuracy of the linear power flow. Finally, the secondary control problem is framed into a quadratic programming problem that is solved using the *CVXOPT* module.

6.3.1 The multi-bus islanded microgrid network

An islanded microgrid network consisting of 5 DERs and 18 buses, as depicted in Fig. 6.1, is co-simulated to assess the feasibility and performance of the proposed control scheme. The microgrid size is decided/designed to limit the computational time to a reasonable duration. The long computational time is due primarily to the use of detailed primary control loop (inner current and voltage control loops, including power-electronic switching actions) of the power-electronic-interfaced DER under a standard workstation computing hardware. The primary control of a droop-controlled DER with dispatch, as already discussed in Section 3.2, and the proposed secondary optimal control scheme are shown in Fig. 6.2.

The network parameters, e.g., output feeder and line impedances, and the DERs' specification are tabulated in Table 6.1, along with the primary and secondary control parameters. The output feeder and line impedances are arbitrary set while ensuring that the corresponding X/R ratio is within a range of 2–10. Network state information such as reactive power, load-bus voltage magnitude and phase angle etc., are facilitated through *MatrikonOPC* for the secondary control implementation in *Python*. The load-bus voltage measurements in *DIGSILENT PowerFactory* are low-pass-filtered with

a chosen time constant of $\tau_{c,v}$. It is worth acknowledging here that some of the state information can be obtained through state estimator instead of from direct measurement. However, this subject is beyond the focus of this research work and hence all state information is obtained directly from the co-simulated network model in *PowerFactory* through *MatrikonOPC* at sampling time T_s (i.e. configuration as detailed in Appendix A).

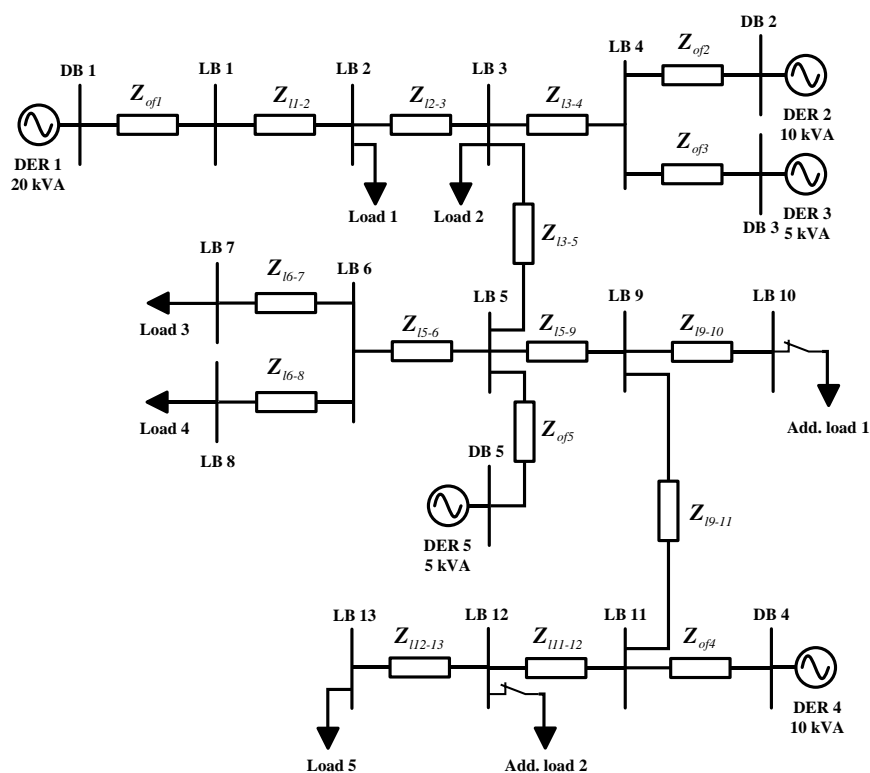


Fig. 6.1. Single-line diagram of the dispatch-droop-controlled islanded microgrid test network.

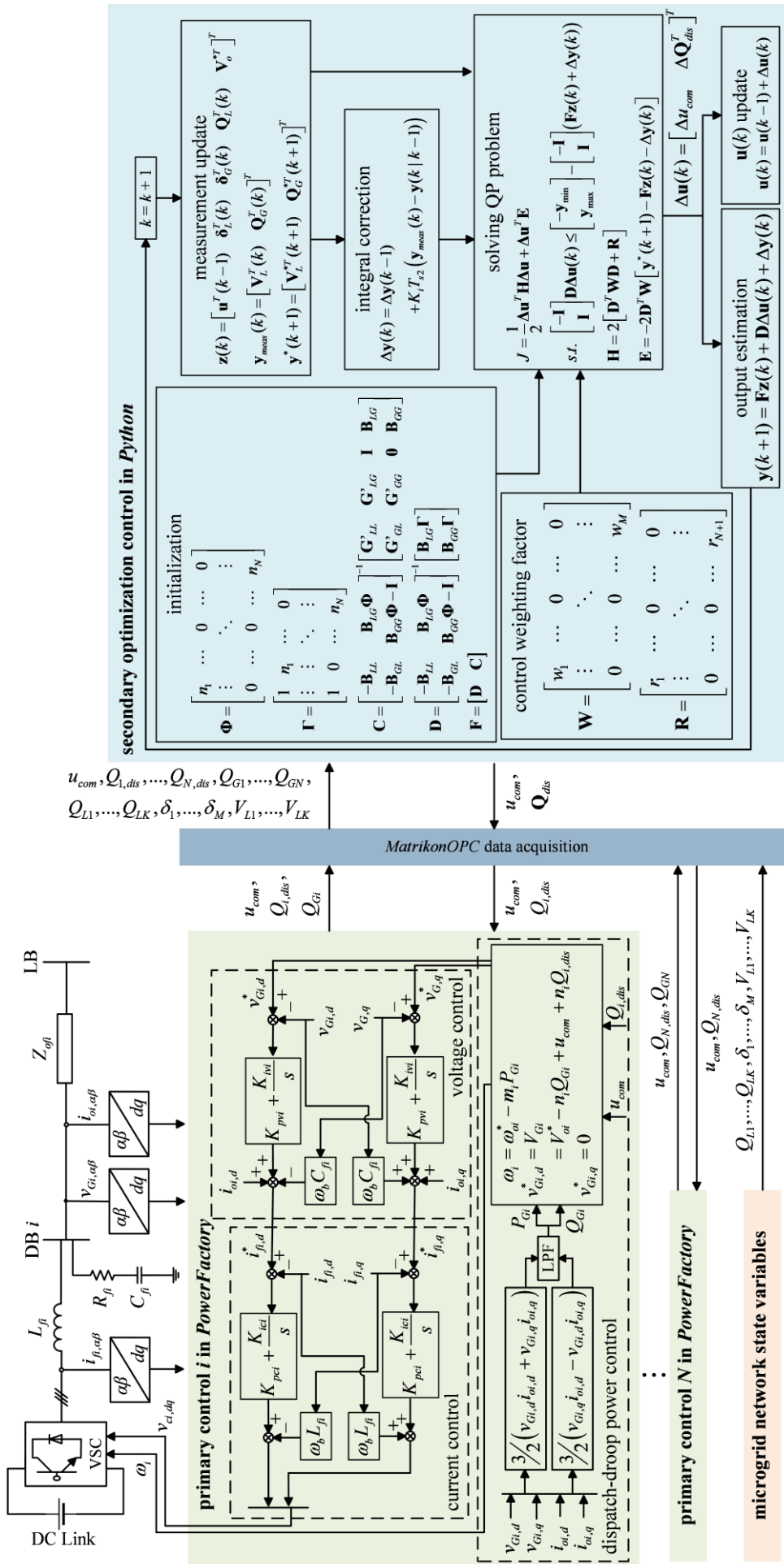


Fig. 6.2. Detailed block diagram of a DER's primary control and the proposed centralised multi-objective secondary optimal control for islanded microgrid.

Table 6.1. Specifications of the islanded microgrid network and proposed centralised secondary optimal control.

| Parameter | Value | DER primary control | | Value |
|------------------------------------|------------------------|---------------------------------|-------------------------------------|------------------|
| Network freq. | 50Hz | Voltage | K_v^P | 1.23 |
| Nominal voltage | 400V | control | K_v^I | 4.67 |
| DC voltage | 1kV | Current | K_c^P | 0.27 |
| Sw. freq. F_{sl} | 2.5kHz | control | K_c^I | 1.61 |
| DER ratings: | | P-f droop coefficient | | Q-V droop |
| Apparent power (pf) | | (pu) | | coefficient (pu) |
| DER 1 | 20 kVA (0.8) | 0.0625 | | 0.075 |
| DER 2 | 10 kVA (0.8) | 0.125 | | 0.15 |
| DER 3 | 5 kVA (0.8) | 0.25 | | 0.30 |
| DER 4 | 10 kVA (0.8) | 0.125 | | 0.15 |
| DER 5 | 5 kVA (0.8) | 0.25 | | 0.30 |
| Power-electronic-based DERs: | | Power-electronic-based DERs: | | |
| Output feeder impedances | | filter impedances L - RC | | |
| \mathbf{Z}_{of1} | 0.03 Ω , 0.35mH | \mathbf{Z}_{f1} | 7.62mH, 10 Ω , 3.32 μ F | |
| \mathbf{Z}_{of2} | 0.02 Ω , 0.45mH | \mathbf{Z}_{f2} | 15.24mH, 10 Ω , 1.66 μ F | |
| \mathbf{Z}_{of3} | 0.06 Ω , 0.35mH | \mathbf{Z}_{f3} | 30.48mH, 10 Ω , 0.83 μ F | |
| \mathbf{Z}_{of4} | 0.05 Ω , 0.56mH | \mathbf{Z}_{f4} | 15.24mH, 10 Ω , 1.66 μ F | |
| \mathbf{Z}_{of5} | 0.03 Ω , 0.42mH | \mathbf{Z}_{f5} | 30.48mH, 10 Ω , 0.83 μ F | |
| Line impedances | | | | |
| \mathbf{Z}_{l1-2} | 0.21 Ω , 1.50mH | \mathbf{Z}_{l6-8} | 0.31 Ω , 2.98mH | |
| \mathbf{Z}_{l2-3} | 0.26 Ω , 1.93mH | \mathbf{Z}_{l5-9} | 0.14 Ω , 1.03mH | |
| \mathbf{Z}_{l3-4} | 0.70 Ω , 3.70mH | \mathbf{Z}_{l9-10} | 0.10 Ω , 0.54mH | |
| \mathbf{Z}_{l3-5} | 0.28 Ω , 1.76mH | \mathbf{Z}_{l9-11} | 0.21 Ω , 0.78mH | |
| \mathbf{Z}_{l5-6} | 0.12 Ω , 1.18mH | \mathbf{Z}_{l11-12} | 0.47 Ω , 3.21mH | |
| \mathbf{Z}_{l6-7} | 0.19 Ω , 2.01mH | \mathbf{Z}_{l12-13} | 0.16 Ω , 3.06mH | |
| Proposed secondary optimal control | | | | |
| Parameter | Value | Parameter | Value | |
| Sampling freq. F_s | 0.2Hz | LPF time constant $\tau_{c,pq}$ | 0.2s | |
| Integral gain K_i | 0.02 | LPF time constant $\tau_{c,v}$ | 0.9s | |

6.3.2 Estimation model with integral correction

Subsequently, the secondary optimal control incorporates the modified DLPPF-based reactive power and bus voltage magnitude estimation model into a constrained quadratic programming problem. Foremost, the secondary estimation model (6.14) is augmented with $\mathbf{u}(k) = \mathbf{u}(k-1) + \Delta\mathbf{u}(k)$ into a quadratic programming problem, expressible as

$$\mathbf{y}(k+1) = \mathbf{F}\mathbf{z}(k) + \mathbf{D}\Delta\mathbf{u}(k) \quad (6.15)$$

where

$$\mathbf{z}(k) = \begin{bmatrix} \mathbf{u}(k-1) \\ \mathbf{v}(k) \end{bmatrix}$$

$$\mathbf{F} = [\mathbf{D} \quad \mathbf{C}]$$

The exploitation of linear power flow and the associated assumptions will usually entail small estimation errors – as expected in most linear power flow algorithms (Dvijotham and Molzahn, 2016; Yu, Cao and Li, 2018). Hence, it is proposed that an integral-based correction term is added to minimise the estimation error through available measurements. The proposed correction is achieved through

$$\Delta\mathbf{y}(k) = \Delta\mathbf{y}(k-1) + K_i T_s (\mathbf{y}_{meas}(k) - \mathbf{y}(k|k-1)) \quad (6.16)$$

where $\Delta\mathbf{y}(k)$ is the output estimation error at time k , \mathbf{y}_{meas} is the measured output vector, $\mathbf{y}(k|k-1)$ is the estimated output vector at $(k-1)^{\text{th}}$ time instant, and K_i is the integral gain with the secondary control sampling time T_s . Upon incorporating it into the secondary estimation model, (6.15) is modified to

$$\mathbf{y}(k+1) = \mathbf{F}\mathbf{z}(k) + \mathbf{D}\Delta\mathbf{u}(k) + \Delta\mathbf{y}(k) \quad (6.17)$$

The effectiveness of the integral-based corrective control in mitigating the estimation errors due to power flow linearisation is assessed in the co-simulation study. The result is summarised in Fig. 6.3. Before introducing (6.16), it can be clearly seen that the per-unit reactive power sharing remains slightly non-proportional; upon the activation of the integral correction with $K_i = 0.02$, the DERs reactive output powers are shared to the desired proportional ratio of $[4 : 2 : 1 : 2 : 1]$ – the ratio of their kVA ratings (as tabulated in Table 6.1). The absolute percentage estimation error is tabulated in Table 6.2 with DER 1 serving as a reference – realised through the simulation setting of “ $Q_{1,dis}$ disabled”, i.e. the dispatch command $Q_{1,dis}$ is deactivated due to $(N-1)$ consideration. The slight difference in individual reactive output powers between the two cases, i.e. “ $Q_{1,dis}$ disabled” and “ $Q_{4,dis}$ disabled”, is due to the voltage-dependent nature of the loads.

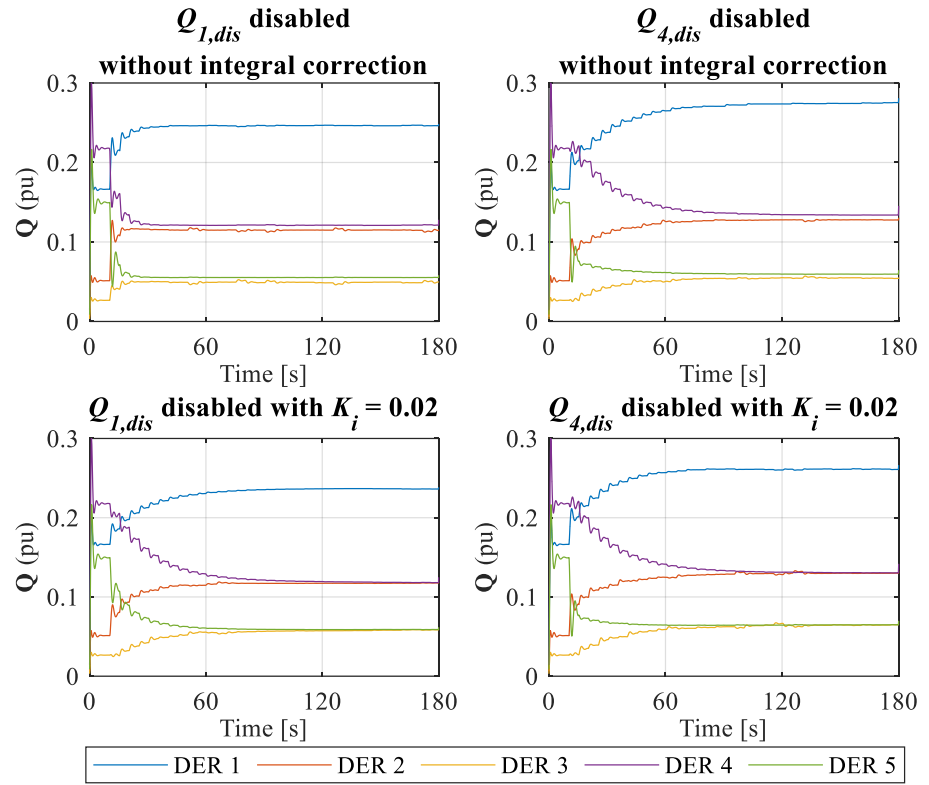


Fig. 6.3. Optimal reactive power sharing control with and without integral-based corrective control: DERs reactive output power.

Table 6.2. Steady state estimation error (absolute percentage) with/without integral-based correction control.

| | $Q_{1,dis}$ disabled (%) | | $Q_{4,dis}$ disabled (%) | |
|-------|--------------------------|--------------|--------------------------|--------------|
| | $K_i = 0$ | $K_i = 0.02$ | $K_i = 0$ | $K_i = 0.02$ |
| DER 1 | 0.00 | 0.00 | 2.69 | 0.23 |
| DER 2 | 8.84 | 0.13 | 4.94 | 0.00 |
| DER 3 | 22.32 | 0.23 | 23.25 | 0.40 |
| DER 4 | 1.23 | 0.13 | 0.00 | 0.00 |
| DER 5 | 11.32 | 0.23 | 12.45 | 0.40 |

6.3.3 Cost function with inequality constraints

With the estimation model represented in terms of secondary control input increment $\Delta \mathbf{u}$, the droop-controlled islanded microgrid reactive power and load-bus voltage regulation optimisation control problem is treated as a tracking problem through the quadratic cost function (3.13). Notably, \mathbf{W} weighting factor enables the possibility to adjust the priority between reactive power sharing and

load-bus voltage regulation while the penalty factor \mathbf{R} adjusts the control efforts among Δu_{com} and all $\Delta Q_{i,dis}$ in $\Delta \mathbf{Q}_{dis}$.

Next, the cost function of the multi-objective secondary optimal control in (3.13) is manipulated further using (6.17) to become:

$$\begin{aligned}
J &= \left(\mathbf{y}^*(k+1) - \mathbf{y}(k+1) \right)^T \mathbf{W} \left(\mathbf{y}^*(k+1) - \mathbf{y}(k+1) \right) + \Delta \mathbf{u}^T(k) \mathbf{R} \Delta \mathbf{u}(k) \\
&= \left\{ \mathbf{y}^*(k+1) - \mathbf{Fz}(k) - \mathbf{D} \Delta \mathbf{u}(k) - \Delta \mathbf{y}(k) \right\}^T \mathbf{W} \left\{ \mathbf{y}^*(k+1) - \mathbf{Fz}(k) - \mathbf{D} \Delta \mathbf{u}(k) \right\} + \Delta \mathbf{u}^T(k) \mathbf{R} \Delta \mathbf{u}(k) \\
&= \left\{ \left(\mathbf{y}^*(k+1) - \mathbf{Fz}(k) - \Delta \mathbf{y}(k) \right)^T - \Delta \mathbf{u}^T(k) \mathbf{D}^T \right\} \mathbf{W} \left\{ \left(\mathbf{y}^*(k+1) - \mathbf{Fz}(k) - \Delta \mathbf{y}(k) \right) - \mathbf{D} \Delta \mathbf{u}(k) \right\} + \Delta \mathbf{u}^T(k) \mathbf{R} \Delta \mathbf{u}(k) \\
&= \left(\mathbf{y}^*(k+1) - \mathbf{Fz}(k) - \Delta \mathbf{y}(k) \right)^T \mathbf{W} \left(\mathbf{y}^*(k+1) - \mathbf{Fz}(k) - \Delta \mathbf{y}(k) \right) - 2 \Delta \mathbf{u}^T(k) \mathbf{D}^T \mathbf{W} \left(\mathbf{y}^*(k+1) - \mathbf{Fz}(k) - \Delta \mathbf{y}(k) \right) \\
&\quad + \Delta \mathbf{u}^T(k) \mathbf{D}^T \mathbf{W} \mathbf{D} \Delta \mathbf{u}(k) + \Delta \mathbf{u}^T(k) \mathbf{R} \Delta \mathbf{u}(k) \\
&= \frac{1}{2} \Delta \mathbf{u}^T(k) \left\{ 2 \left(\mathbf{D}^T \mathbf{W} \mathbf{D} + \mathbf{R} \right) \right\} \Delta \mathbf{u}(k) + \Delta \mathbf{u}^T(k) \left\{ -2 \mathbf{D}^T \mathbf{W} \left(\mathbf{y}^*(k+1) - \mathbf{Fz}(k) - \Delta \mathbf{y}(k) \right) \right\} \\
&\quad + \left(\mathbf{y}^*(k+1) - \mathbf{Fz}(k) - \Delta \mathbf{y}(k) \right)^T \mathbf{W} \left(\mathbf{y}^*(k+1) - \mathbf{Fz}(k) - \Delta \mathbf{y}(k) \right)
\end{aligned} \tag{6.18}$$

Then, one can frame it into a quadratic programming problem (disregarding the last constant term) as

$$J = \frac{1}{2} \Delta \mathbf{u}^T(k) \mathbf{H} \Delta \mathbf{u}(k) + \Delta \mathbf{u}^T(k) \mathbf{h} \tag{6.19}$$

where

$$\begin{aligned}
\mathbf{H} &= 2 \left(\mathbf{D}^T \mathbf{W} \mathbf{D} + \mathbf{R} \right) \\
\mathbf{h} &= -2 \mathbf{D}^T \mathbf{W} \left(\mathbf{y}^*(k+1) - \mathbf{Fz}(k) - \Delta \mathbf{y}(k) \right)
\end{aligned}$$

The relevant network and DER constraints considered in this study are the bus voltage limits and the DERs reactive power capacity (i.e. the output vector \mathbf{y}). They can be framed based on (6.17) with the aid of (3.16c) as

$$\begin{bmatrix} -\mathbf{I} \\ \mathbf{I} \end{bmatrix} \mathbf{D} \Delta \mathbf{u}(k) \leq \begin{bmatrix} -\mathbf{y}_{\min} \\ \mathbf{y}_{\max} \end{bmatrix} - \begin{bmatrix} -\mathbf{I} \\ \mathbf{I} \end{bmatrix} (\mathbf{Fz}(k) + \Delta \mathbf{y}(k)) \tag{6.20}$$

6.3.4 Simulation results

The secondary optimisation control is investigated in conjunction with the islanded microgrid detailed in Subsection 6.3.1. The performance for different control settings, i.e. single-objective control e.g. accurate reactive power sharing among DERs, single load-bus voltage regulation, and multi-objective reactive power sharing and load-bus voltage regulation control, are assessed.

By default, the islanded microgrid is loaded with $15+j9$ kVA. Additional loads are connected to LB10 and LB12 at a chosen simulation time instant upon which the total load demand is increased to $22+j13$ kVA. In the secondary optimal controller, the weighting factor \mathbf{W} is a M -by- M diagonal matrix having the form of $\text{diag}(w_1, w_2, \dots, w_M)$, with elements corresponding to outputs $V_{L1}, V_{L2}, \dots, V_{LK}, Q_{G1}, \dots, Q_{GN}$, respectively. $K (= M-N)$ denotes the number of load-bus (which are labelled with LB in Fig. 6.1). On the other hand, the penalty factor \mathbf{R} is a $(N+1)$ -by- $(N+1)$ diagonal matrix in the

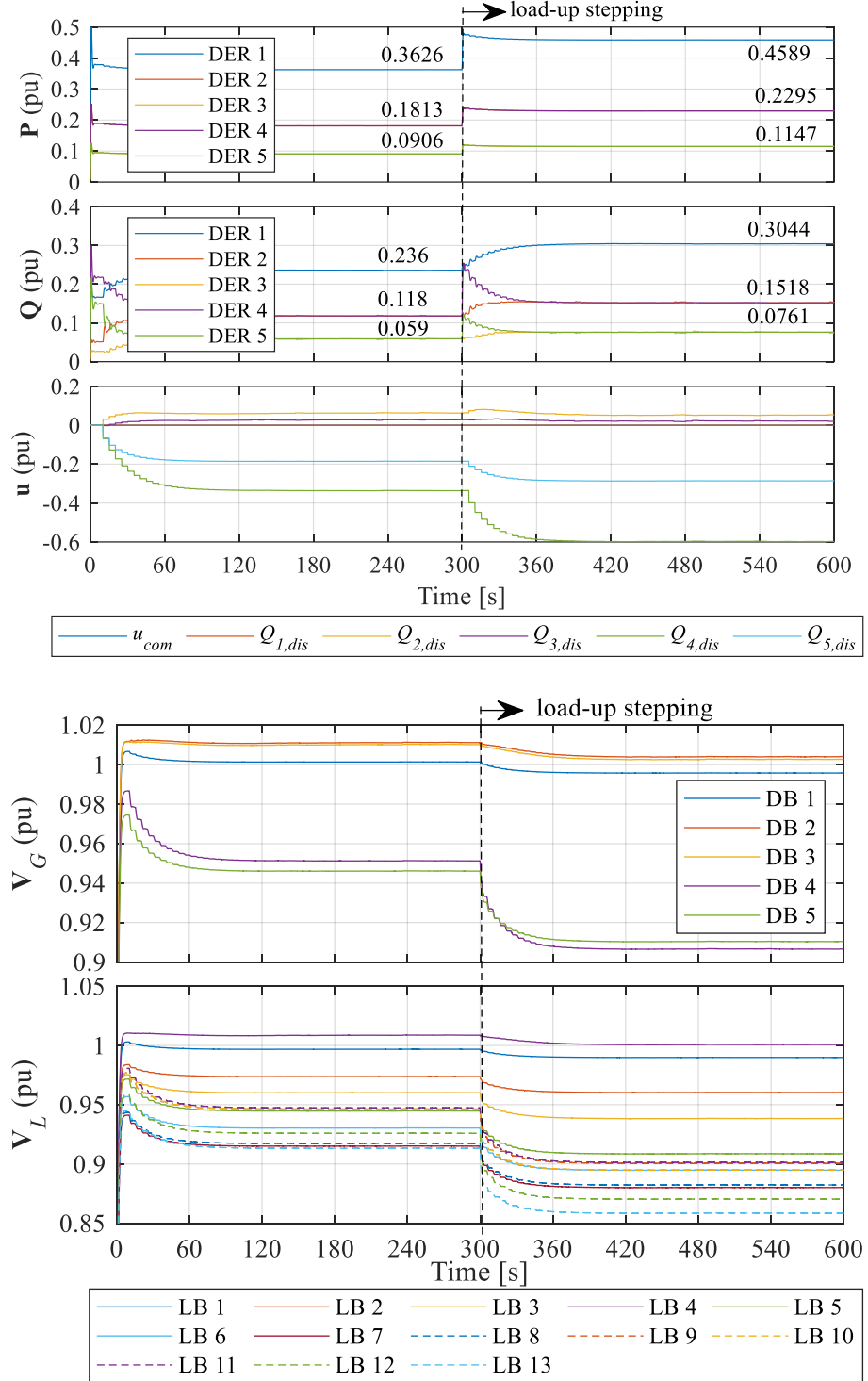


Fig. 6.4. Optimal reactive power sharing control: DERs active/reactive power, secondary droop dispatch input \mathbf{u} , DER droop voltage magnitudes and load-bus voltage magnitudes.

form of $\text{diag}(r_1, r_2, \dots, r_{N+1})$. Similarly, the r values correspond to the droop dispatch inputs Δu_{com} , $\Delta Q_{1,dis}$, \dots , and $\Delta Q_{N,dis}$, respectively. As mentioned, only those of $(N-1)$ DERs' Q_{dis} is required for reactive power sharing control. Hence, the corresponding r of the reference DER should be set significantly larger than the rest - DER 1 is chosen in the following studies.

In the first test scenario, optimal sharing of reactive load power among DERs is assessed. The DERs are initially droop-controlled with the secondary optimal control deactivated, i.e. without reactive power output correction. Fig. 6.4 shows that while the active power sharing is always proportionally shared, the reactive power is not. The proposed secondary optimal control with disabled voltage regulation is activated at $t = 10$ s. Penalty factor \mathbf{R} is set to $\text{diag}(10e10, 10e10, 5, 5, 5, 5)$ which essentially activates $Q_{2,dis}$ to $Q_{5,dis}$ for realising optimal reactive power sharing. As shown in Fig. 6.4 for time just before 300 s, the reactive power sharing among the DERs is significantly improved, giving a ratio of 4:2:1:2:1 at steady state. Note that u_{com} and $Q_{1,dis}$ are not functional at this stage. The corresponding voltages of the DER- and load-buses are also shown in Fig. 6.4 – they range from 0.9132 pu at LB 13 to 1.0112 pu at DB 2. Next, additional loads are connected at LB 10 and LB 12 at approximately $t = 300$ s. Proportional reactive power sharing is retained by the proposed secondary control after load increment with a minimum voltage magnitude of 0.8584 pu at LB 13 and a maximum voltage magnitude of 1.0027 pu at DB 2.

For single load-bus voltage regulation control, the islanded microgrid is loaded with the default loadings. Initially, the voltage magnitude at LB 12, V_{LI2} , “drooped” to 0.9584 pu. The optimal control is activated at $t = 10$ s with w_{12} (which corresponds to V_{LI2} regulation) set to 10 while the others are set to zero (which essentially means that the reactive power control is also disabled). \mathbf{R} is set as $\text{diag}(10, 10e10, 10e10, 10e10, 10e10, 10e10)$, signifying that only u_{com} is activated for this single-objective control problem. Fig. 6.5 shows that V_{LI2} is successfully regulated to $V^{ref} = 0.98$ pu through the adjustment of u_{com} without noticeable transient in the DERs' reactive output power. Upon load stepping-up at $t = 300$ s, the voltage magnitude at LB 12 remains regulated at 0.98 pu but the issue of non-proportional reactive power sharing persists, as expected.

For the assessment in conjunction with the multi-objective control, the first setting considered is the optimal reactive power sharing and single load-bus voltage regulation control. The DERs are initially droop-controlled at the default load condition. At $t = 10$ s, the optimal secondary control is activated by setting \mathbf{W} with $w_{12}, w_{14}-w_{18} = 10$ and \mathbf{R} as $\text{diag}(10, 10e10, 5, 5, 5, 5)$. Fig. 6.6 shows that proportional reactive power sharing is achieved among the DERs. In addition, V_{LI2} is regulated to $V^{ref} = 0.98$ pu, before and after step-up-loadings at $t = 300$ s.

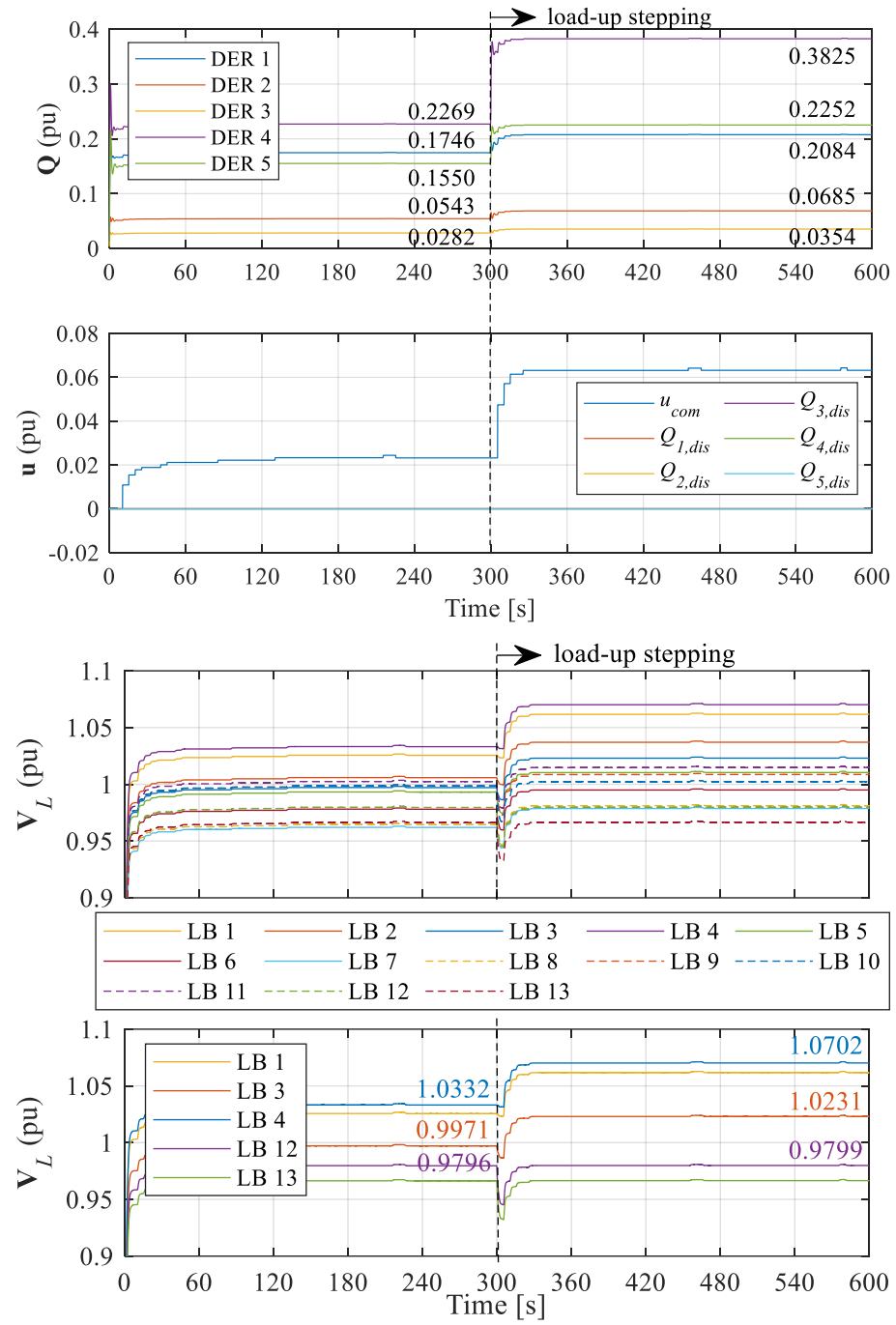


Fig. 6.5. Single load-bus voltage regulation control: DERs reactive output power, secondary droop dispatch input u and load-bus voltage magnitudes.

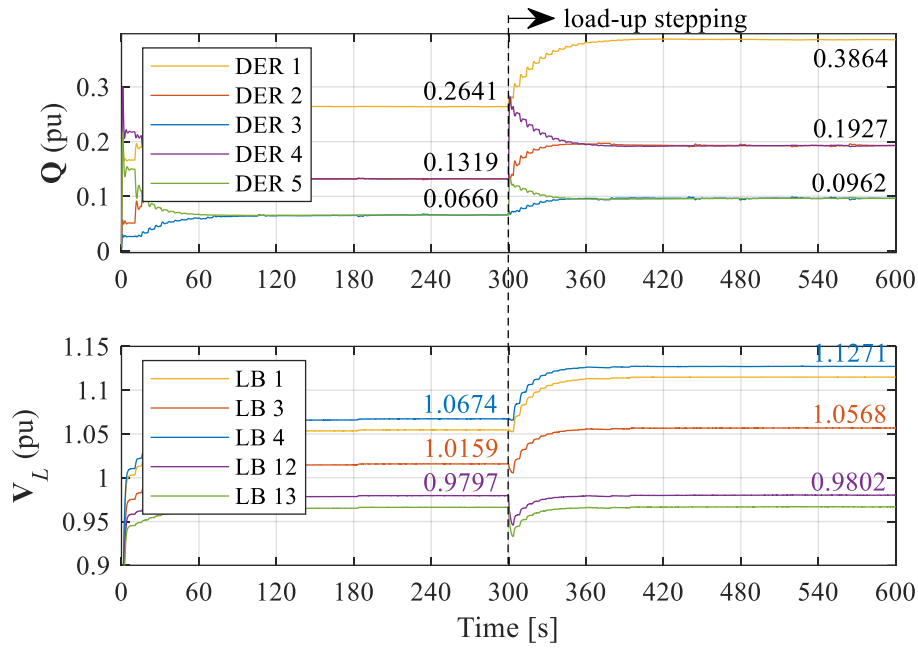


Fig. 6.6. Optimal reactive power sharing and single load-bus voltage regulation control: DERs reactive output power and selected load-bus voltage magnitudes.

Next, the performance of the secondary optimal control on simultaneous reactive power sharing and single-/multi-load-buses voltage regulation is examined. At default loading condition, i.e. before the activation of the secondary controller, voltage magnitudes at LB12 and LB 4 are 0.9584 pu and 1.0104 pu, respectively. At $t = 10$ s, the multi-objective secondary control in which load-bus voltage regulation is prioritised with an emphasis on reactive power sharing improvement is activated by setting \mathbf{W} with $w_{12} = 100$ and $w_{14-18} = 10$, and \mathbf{R} as $\text{diag}(10, 10e10, 5, 5, 5, 5)$. Subsequently, at $t = 300$ s, w_4 is changed from 0 to 100 to realise multi-bus voltage regulation. The trade-offs between optimal reactive power sharing among DERs and multi-bus voltage regulation is clearly demonstrated in Fig. 6.7. Precise single load-bus voltage regulation, i.e. V_{L12} being regulated to $V_{L12}^{ref} = 0.98$ pu and proportional reactive power sharing are achieved for $t < 300$ s. Upon the activation of the multi-bus voltage regulation, i.e. enabling the voltage reference V_{L4}^{ref} (i.e. 1.0 pu), it can be seen from Fig. 6.7 that although V_{L4} and V_{L12} are regulated close to their respective references, the proportionality of reactive power outputs among DERs is heavily compromised. This is due to the selection of \mathbf{W} , weighing more on voltage regulation (i.e., 100) than reactive power sharing (i.e. 10).

Next, both reactive power sharing and voltage regulation are weighted equally by setting w_4 , w_{12} and w_{14-18} to 10 with \mathbf{R} remains as $\text{diag}(10, 10e10, 5, 5, 5, 5)$. It can be clearly seen from Fig. 6.8 that the reactive power sharing ratio among the DERs is significantly improved while V_{L4} and V_{L12} are more loosely regulated from their references.

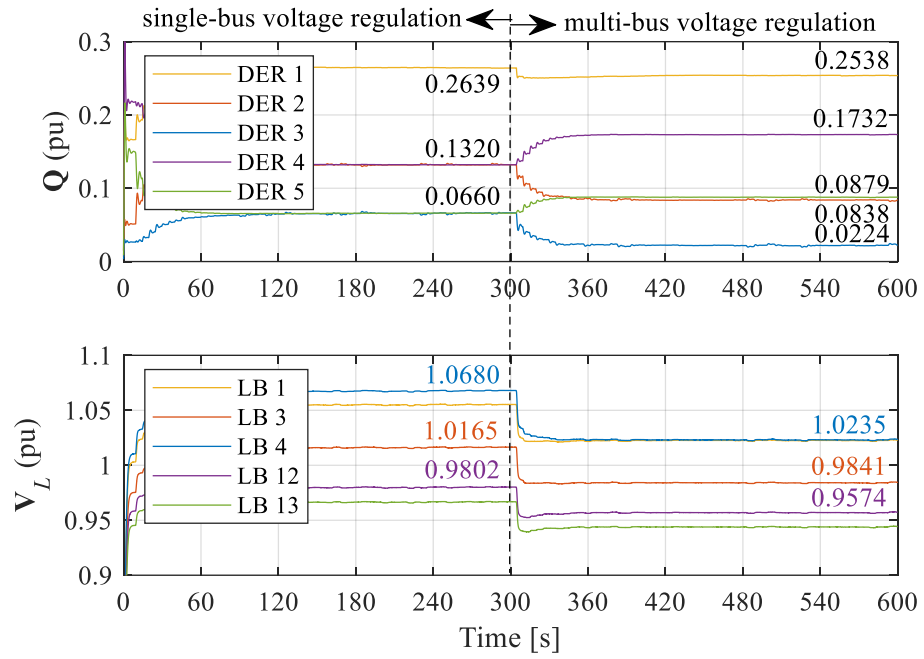


Fig. 6.7. Optimal reactive power sharing and prioritised multi-load-bus voltage regulation control: DERs reactive output power and selected load-bus voltage magnitudes.

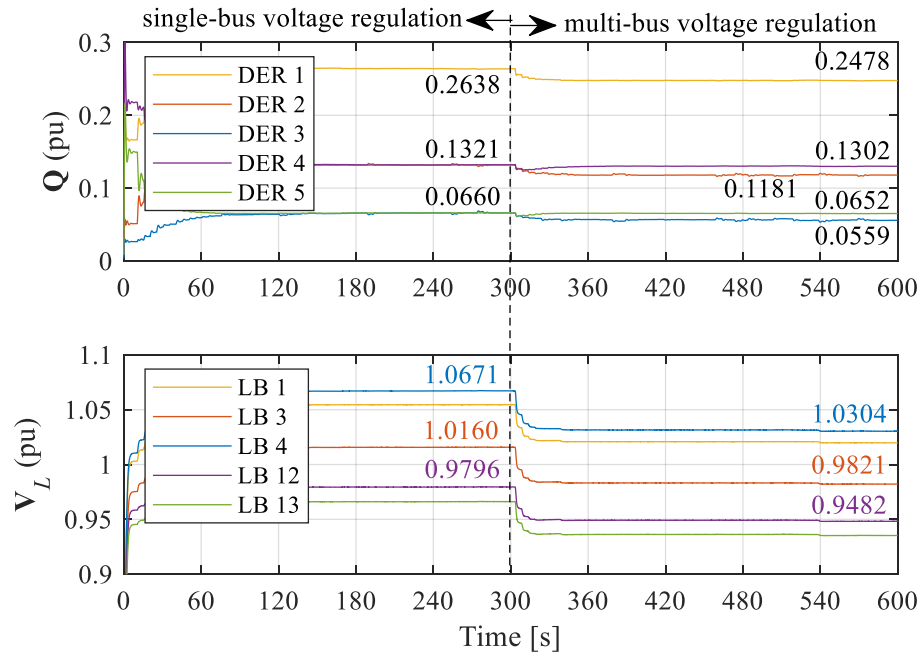


Fig. 6.8. Optimal reactive power sharing and multi-load-buses voltage regulation control: DERs reactive output power and selected load-bus voltage magnitudes.

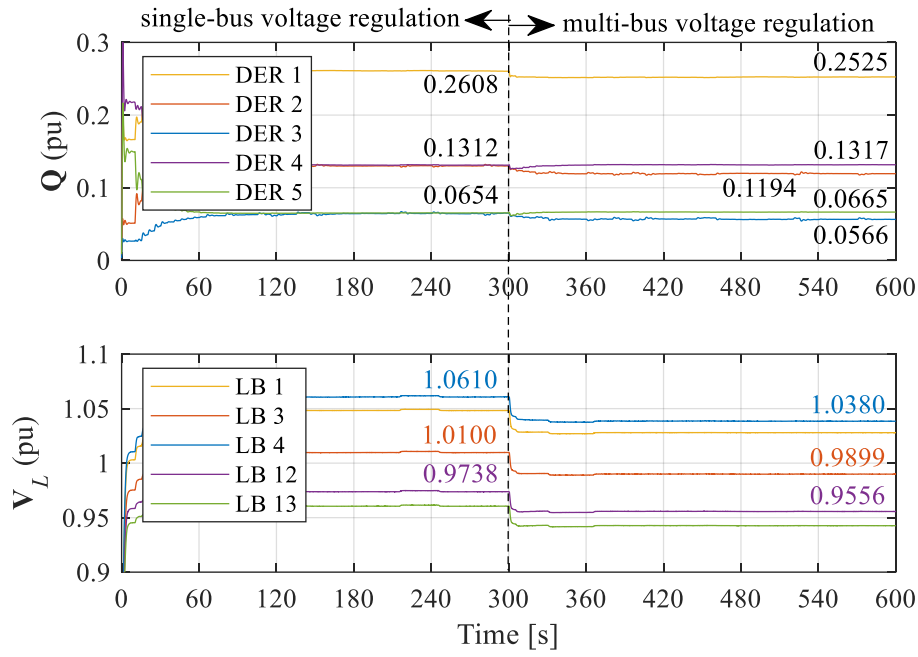


Fig. 6.9. Constrained optimal reactive power sharing and multi-load-buses voltage regulation: DERs reactive output power and selected load-buses voltage magnitudes.

Lastly, the ability of the quadratic-programming-based secondary optimal control in dealing with constraints is examined by activating the inequality constraints (6.20). The islanded microgrid is loaded with default loading condition and at $t = 10$ s, the secondary control with equally weighted voltage regulation and reactive power sharing control is activated. Weighting factor \mathbf{W} and penalty factor \mathbf{R} are set as per the last-used setting in the preceding unconstrained scenarios. LB 3 is selected as a “critical” bus where the voltage magnitude V_{L3} is to be constrained to within $\pm 1\%$ while the remaining buses are constrained loosely to $-6\%/+10\%$ (arbitrarily chosen value during simulation) from 1.0 pu. Moreover, the DERs reactive output powers are to be limited to within their respective capacity limits. It can be seen from Fig. 6.9 that, while V_{L12} is regulated close to 0.9738 pu ($V_{L12}^{ref} = 0.98$ pu) and the reactive power sharing ratio is improved to [0.2608 : 0.1312 : 0.0654 : 0.1312 : 0.0654], the unregulated V_{L3} (since $w_3 = 0$) is limited to 1.01 pu as opposed to the unconstrained scenario where V_{L3} became 1.016 pu (as in Fig. 6.8). At $t = 300$ s, the multi-load-bus voltage regulation control is activated by setting w_4 to 10, signifying an attempt to regulate the voltage at LB 4 to its reference V_{L4}^{ref} of 1.0 pu. It is evident that the proposed multi-objective secondary optimal control regulates V_{L4} and V_{L12} to 1.038 pu and 0.9556 pu, respectively, and maintains a near-proportional reactive power sharing while keeping the voltage of the critical bus LB 3 to approximately 0.99 pu. This result demonstrates the capability of the proposed multi-objective secondary optimal control in considering the network constraints.

6.4 Semi-distributed optimal control for intra- and inter-microgrids voltage and reactive power regulation

In Section 6.3, a centralised secondary optimal control is developed for realising multi-bus voltage and reactive power control. Although the intrinsic trade-off is successfully addressed in an optimal manner, the central controller poses the risk of single-point failure, reducing the system reliability. The computational complexity of a centralised, optimisation-based secondary control is expected to increase exponentially as the microgrid scales up. It is worth highlighting that the number of small-scale, controllable DERs in future microgrids will be of several orders higher than what is in today's power grid; this hints about the need for a more-efficient secondary control scheme. In what follows, on the basis of the theoretical treatment in Section 6.3, a semi-distributed secondary optimal control is proposed to improve the secondary optimal controller in terms of reliability and computational burden. First, it is proposed that the microgrid is segregated, in terms of the secondary control structure, into multiple sub-microgrid clusters. The dispatchable droop with modified DLPF is exploited to develop an estimation model for each sub-microgrid cluster. Then, the graph theory of cooperative control is exploited to design a novel quadratic cost function that will eventually enable the “semi-distributed” feature of the proposed secondary controller. Lastly, the performance of single- and multi-bus voltage regulation and reactive power sharing control will be assessed in conjunction with intra- and inter-cluster microgrids.

6.4.1 Clustering of multi-bus islanded microgrid network

Consider a large islanded microgrid network having N DERs, the microgrid network is proposed to be segregated, in terms of the secondary control structure, into M sub-microgrids with each sub-microgrid having N_D DERs and N_B buses. These DERs will be optimally controlled by the proposed secondary controller in a semi-distributed manner to realise load-bus voltage regulation and reactive power sharing. In the secondary controller of each sub-microgrid cluster, there are intra-cluster control objective and inter-cluster control objective that accounts for the interaction among neighbouring sub-microgrid clusters.

In order to incorporate the intra- and inter- microgrid cluster control objectives, the Q - V droop with dispatch is first modified as

$$V_{Gi,m} = V_{i,m}^* - n_{i,m} Q_{Gi,m} + n_{i,m} Q_{dis,i,m} + u_{com,m} + Q_{dcom,m} \quad (6.21)$$

where $V_{Gi,m}$ is the per-unit droop voltage amplitude (normalised to the network's phase peak voltage) of i^{th} DER in m^{th} sub-microgrid; $V_{i,m}^*$ is the per-unit no-load voltage magnitude, $n_{i,m}$ is the per-unit droop coefficient; $Q_{Gi,m}$ is the filtered per-unit reactive output power, normalised to a common base power S_B ; $Q_{dis,i,m}$ is the individual DER's reactive power dispatch command; and $u_{com,m}$ and $Q_{dcom,m}$ are the common voltage and sub-microgrid's total reactive power correction terms shared among the

DERs in m^{th} sub-microgrid. Note that although the dispatch terms u_{com} and Q_{dcom} share the same underlying working principle (on how they affect the droop function), they are intentionally separated so that the control means for voltage regulation and reactive power sharing can be clearly distinguished. For each m^{th} sub-microgrid, there is an intra-cluster and inter-cluster control means. For example, \mathbf{Q}_{dis} (i.e. $Q_{i,dis}$ within) and Q_{dcom} are meant for realising accurate reactive power sharing, respectively, within each cluster and among multiple sub-microgrid clusters.

Voltage magnitudes of N_D DER-buses in m^{th} sub-microgrid can be expressed in terms of droop parameters, DERs' reactive output powers, and dispatch commands as

$$\mathbf{V}_{G,m} = \mathbf{V}_m^* - \mathbf{\Phi}_m \mathbf{Q}_{G,m} + \mathbf{\Gamma}_m \mathbf{u}_m \quad (6.22)$$

where

$$\begin{aligned} \mathbf{V}_{G,m} &= [V_{G1} \quad \cdots \quad V_{GN_D}]_m^T \\ \mathbf{V}_m^* &= [V_1^* \quad \cdots \quad V_{N_D}^*]_m^T \\ \mathbf{\Phi}_m &= \begin{bmatrix} n_1 & \cdots & 0 & \cdots & 0 \\ \vdots & & \ddots & & \vdots \\ 0 & \cdots & 0 & \cdots & n_{N_D} \end{bmatrix}_m \\ \mathbf{Q}_G &= [Q_{G1} \quad \cdots \quad Q_{GN_D}]_m^T \\ \mathbf{\Gamma} &= \begin{bmatrix} 1 & n_1 & \cdots & 0 & 1 \\ \vdots & \vdots & \ddots & \vdots & \vdots \\ 1 & 0 & \cdots & n_N & 1 \end{bmatrix}_m \\ \mathbf{u} &= [u_{com} \quad Q_{1,dis} \quad \cdots \quad Q_{N_D,dis} \quad Q_{dcom}]_m^T \end{aligned}$$

in which the secondary control input vector \mathbf{u} consists of the common correction term u_{com} and Q_{dcom} , and Q_{dis} of all N_D DERs.

6.4.2 Estimation model with integral correction

Adopt the DLPI in (6.9), the voltage magnitude and phase angle of N_B buses in m^{th} sub-microgrid can be expressed as

$$\begin{bmatrix} \delta \\ \mathbf{V} \end{bmatrix}_m = \begin{bmatrix} \mathbf{H} & \mathbf{M} \\ \mathbf{N} & \mathbf{K} \end{bmatrix}_m \begin{bmatrix} \mathbf{P} \\ \mathbf{Q} \end{bmatrix}_m \quad (6.23)$$

where

$$\begin{bmatrix} \mathbf{H} & \mathbf{M} \\ \mathbf{N} & \mathbf{K} \end{bmatrix} = \begin{bmatrix} -\mathbf{B}' & \mathbf{G} \\ -\mathbf{G}' & -\mathbf{B} \end{bmatrix}^{-1}$$

Without loss of generality, the vectors are re-arranged correspondingly to load- and DER-buses. (6.23) is simplified and partitioned as

$$\begin{bmatrix} \mathbf{V}_L \\ \mathbf{V}_G \end{bmatrix}_m = \begin{bmatrix} \mathbb{N}_{LL} & \mathbb{N}_{LG} & \mathbb{K}_{LL} & \mathbb{K}_{LG} \\ \mathbb{N}_{GL} & \mathbb{N}_{GG} & \mathbb{K}_{GL} & \mathbb{K}_{GG} \end{bmatrix}_m \begin{bmatrix} \mathbf{P}_L \\ \mathbf{P}_G \\ \mathbf{Q}_L \\ \mathbf{Q}_G \end{bmatrix}_m \quad (6.24)$$

, assuming that the bus voltage phase angle in a droop-controlled islanded microgrid is a function of active power that is less affected by the reactive power correction (i.e. phase angle vector is disregarded with voltage magnitude being the variable of interest).

Assume that the constant-impedance active and reactive load powers, and the DERs active output power do not vary significantly during the secondary control regulation, the estimation model of m^{th} sub-microgrid can be obtained by substituting \mathbf{V}_G vector in (6.24) with (6.22)

$$\begin{aligned} \begin{bmatrix} \mathbf{I} \\ \mathbf{0} \end{bmatrix} [\mathbf{V}_L]_{m,k+1} + \begin{bmatrix} \mathbf{0} \\ \mathbf{I} \end{bmatrix} [\mathbf{V}_G]_{m,k+1} &= \begin{bmatrix} \mathbb{N}_{LL} & \mathbb{N}_{LG} & \mathbb{K}_{LL} & \mathbb{K}_{LG} \\ \mathbb{N}_{GL} & \mathbb{N}_{GG} & \mathbb{K}_{GL} & \mathbb{K}_{GG} \end{bmatrix}_m \begin{bmatrix} \mathbf{P}_L \\ \mathbf{P}_G \\ \mathbf{Q}_L \\ \mathbf{Q}_G \end{bmatrix}_{m,k+1} \\ \begin{bmatrix} \mathbf{I} \\ \mathbf{0} \end{bmatrix} [\mathbf{V}_L]_{m,k+1} + \begin{bmatrix} \mathbf{0} \\ \mathbf{I} \end{bmatrix} \{ \mathbf{v}_m^* - \Phi_m \mathbf{Q}_{G,m,k+1} + \Gamma_m \mathbf{u}_{m,k} \} &= \begin{bmatrix} \mathbb{N}_{LL} & \mathbb{N}_{LG} & \mathbb{K}_{LL} \\ \mathbb{N}_{GL} & \mathbb{N}_{GG} & \mathbb{K}_{GL} \end{bmatrix}_m \begin{bmatrix} \mathbf{P}_L \\ \mathbf{P}_G \\ \mathbf{Q}_L \end{bmatrix}_{m,k} + \begin{bmatrix} \mathbb{K}_{LG} \\ \mathbb{K}_{GG} \end{bmatrix}_m [\mathbf{Q}_G]_{m,k+1} \\ \begin{bmatrix} \mathbf{I} \\ \mathbf{0} \end{bmatrix} [\mathbf{V}_L]_{m,k+1} + \begin{bmatrix} \mathbf{0} \\ -\Phi \end{bmatrix}_m [\mathbf{Q}_G]_{m,k+1} + \begin{bmatrix} -\mathbb{K}_{LG} \\ -\mathbb{K}_{GG} \end{bmatrix}_m [\mathbf{Q}_G]_{m,k+1} &= \begin{bmatrix} \mathbb{N}_{LL} & \mathbb{N}_{LG} & \mathbb{K}_{LL} \\ \mathbb{N}_{GL} & \mathbb{N}_{GG} & \mathbb{K}_{GL} \end{bmatrix}_m \begin{bmatrix} \mathbf{P}_L \\ \mathbf{P}_G \\ \mathbf{Q}_L \end{bmatrix}_{m,k} + \begin{bmatrix} \mathbf{0} \\ -\mathbf{I} \end{bmatrix}_m [\mathbf{v}_m^*] + \begin{bmatrix} \mathbf{0} \\ -\Gamma \end{bmatrix}_m [\mathbf{u}]_{m,k} \\ \begin{bmatrix} \mathbf{I} & -\mathbb{K}_{LG} \\ \mathbf{0} & -\Phi - \mathbb{K}_{GG} \end{bmatrix} \begin{bmatrix} \mathbf{V}_L \\ \mathbf{Q}_G \end{bmatrix}_{m,k+1} &= \begin{bmatrix} \mathbb{N}_{LL} & \mathbb{N}_{LG} & \mathbb{K}_{LL} & \mathbf{0} \\ \mathbb{N}_{GL} & \mathbb{N}_{GG} & \mathbb{K}_{GL} & -\mathbf{I} \end{bmatrix}_m \begin{bmatrix} \mathbf{P}_L \\ \mathbf{P}_G \\ \mathbf{Q}_L \\ \mathbf{v}_m^* \end{bmatrix}_{m,k} + \begin{bmatrix} \mathbf{0} \\ -\Gamma \end{bmatrix}_m [\mathbf{u}]_{m,k} \end{aligned} \quad (6.25)$$

Then, by re-assembling the measurable/estimated sub-vectors and (constant) droop parameters into a single vector \mathbf{v} , the estimation model for secondary optimal control of sub-microgrid m , in short

$$\mathbf{y}_m(k+1) = \mathbf{C}_m \mathbf{v}_m(k) + \mathbf{D}_m \mathbf{u}_m(k) \quad (6.26)$$

where

$$\begin{aligned}
\mathbf{y}_m &= \begin{bmatrix} \mathbf{V}_L^T & \mathbf{Q}_G^T \end{bmatrix}_m^T \\
\mathbf{v}_m &= \begin{bmatrix} \mathbf{P}_L^T & \mathbf{P}_G^T & \mathbf{Q}_L^T & \mathbf{V}^{*T} \end{bmatrix}_m^T \\
\mathbf{u}_m &= \begin{bmatrix} u_{com} & \mathbf{Q}_{dis}^T & Q_{dcom} \end{bmatrix}_m^T \\
\mathbf{C}_m &= \begin{bmatrix} \mathbf{I} & -\mathbb{K}_{LG} \\ \mathbf{0} & -\Phi - \mathbb{K}_{GG} \end{bmatrix}_m^{-1} \begin{bmatrix} \mathbb{N}_{LL} & \mathbb{N}_{LG} & \mathbb{K}_{LL} & \mathbf{0} \\ \mathbb{N}_{GL} & \mathbb{N}_{GG} & \mathbb{K}_{GL} & -\mathbf{I} \end{bmatrix}_m \\
\mathbf{D}_m &= \begin{bmatrix} \mathbf{I} & -\mathbb{K}_{LG} \\ \mathbf{0} & -\Phi - \mathbb{K}_{GG} \end{bmatrix}_m^{-1} \begin{bmatrix} \mathbf{0} \\ -\Gamma \end{bmatrix}_m
\end{aligned}$$

It has been established from the literature review and in Section 6.3 that the exploitation of linear power flow will lead to slight estimation error. Therefore, an integral-based corrective term, similar to that in (6.16), is introduced. It essentially exploits the difference between the measured and estimated vectors within a sub-microgrid to improve the estimation output. (6.26) is modified, based on the integral-based correction term and the known relationship of $\mathbf{u}(k) = \mathbf{u}(k-1) + \Delta\mathbf{u}(k)$, as

$$\mathbf{y}_m(k+1) = \mathbf{F}_m \mathbf{z}_m(k) + \mathbf{D}_m \Delta\mathbf{u}_m(k) + \Delta\mathbf{y}_m(k) \quad (6.27)$$

where

$$\begin{aligned}
\mathbf{z}_m(k) &= \begin{bmatrix} \mathbf{u}(k-1) \\ \mathbf{v}(k) \end{bmatrix}_m \\
\mathbf{F}_m &= [\mathbf{D} \quad \mathbf{C}]_m
\end{aligned}$$

6.4.3 Cluster-oriented cost function

(6.27) is essentially an intra-cluster estimation model that accounts for the interaction of the DERs within m^{th} sub-microgrid. In order to realise proportional reactive power sharing among all DERs in the entire islanded microgrid, inter-cluster reactive power sharing, i.e. DERs reactive power sharing among sub-microgrid, is to be accounted for. Based on the distributed cooperative/consensus control theory, the reactive power of each sub-microgrid can assume first-order discrete-time dynamics, giving

$$Q_{mg,m}(k+1) = Q_{mg,m}(k) + \Delta Q_{dcom,m}(k) \quad (6.28)$$

where ΔQ_{dcom} is the inter-cluster control input increment that is commonly shared among all N_D DERs in a sub-microgrid cluster. It is crucial to note that in the context of cooperative/consensus control, the reactive power of each sub-microgrid is required to be normalised to its respective kVA base power. This essentially means that the reactive power sharing among sub-microgrids is proportionally shared when the locally normalised Q_{mg} are made equal upon correction.

Then, it is proposed that the semi-distributed optimal control of load-bus voltage regulation and intra- and inter-cluster reactive power sharing is framed as a tracking control problem. This is achieved by modifying cost function in (3.13) as

$$J_m = (\mathbf{y}_m^*(k+1) - \mathbf{y}_m(k+1))^T \mathbf{W}_m (\mathbf{y}_m^*(k+1) - \mathbf{y}_m(k+1)) + w_m \left(\sum_{n \in N_m} (Q_{mg,n}(k+1) - Q_{mg,m}(k+1))^2 \right) + \Delta \mathbf{u}_m^T(k) \mathbf{R}_m \Delta \mathbf{u}_m(k) \quad (6.29)$$

The first term in (6.29) weighs on the intra-cluster load-bus voltage and reactive power sharing errors, aiming to minimise the difference between the local output variables and their setpoints vector \mathbf{y}^* . \mathbf{W} enables the possibility of adjusting the control priority. The second term weighs on the inter-cluster reactive power difference, aiming to minimise the difference of total reactive power among neighbouring sub-microgrids (note: $Q_{mg,n}$ is the total reactive power of a neighbouring n^{th} sub-microgrid, where $n \in N_m$ in which N_m denotes the set of neighbours of m^{th} sub-microgrid). It is also assumed that the neighbours' total reactive output powers remain constant within the control cycle of m^{th} sub-microgrid such that $Q_{mg,n}(k+1) = Q_{mg,n}(k)$. The \mathbf{R} penalty factor in the last term is responsible to alter the control efforts among u_{com} , all $Q_{i,dis}$ in \mathbf{Q}_{dis} , and Q_{dcom} in m^{th} sub-microgrid.

Next, by adopting the first-order consensus dynamic (6.28) and the assumption of $Q_{mg,n}(k+1) = Q_{mg,n}(k)$, one can represent the total reactive power of m^{th} sub-microgrid and its neighbours in a single vector, as follows

$$\mathbf{y}_m'(k+1) = \mathbf{y}_m'(k) + \lambda_m \Delta \mathbf{u}_m(k) \quad (6.30)$$

where

$$\mathbf{y}_m' = [Q_{mg,1} \quad \cdots \quad Q_{mg,m} \quad \cdots \quad Q_{mg,N_m}]^T$$

$$\lambda_m = \begin{bmatrix} 0 & 0 & \cdots & 0 \\ \vdots & \vdots & \ddots & \vdots \\ 0 & 0 & \cdots & 1 \\ \vdots & \vdots & \ddots & \vdots \\ 0 & 0 & \cdots & 0 \end{bmatrix}$$

Then, the modified cost function in (6.29) can be expanded using (6.30), to become

$$\begin{aligned}
J_m &= (\mathbf{y}_m^*(k+1) - \mathbf{y}_m(k+1))^T \mathbf{W}_m (\mathbf{y}_m^*(k+1) - \mathbf{y}_m(k+1)) + w_m \left(\sum_{n \in N_m} (\mathcal{Q}_{mg,n}(k+1) - \mathcal{Q}_{mg,m}(k+1))^2 \right) \\
&\quad + \Delta \mathbf{u}_m^T(k) \mathbf{R}_m \Delta \mathbf{u}_m(k) \\
&= (\mathbf{y}_m^*(k+1) - \mathbf{y}_m(k+1))^T \mathbf{W}_m (\mathbf{y}_m^*(k+1) - \mathbf{y}_m(k+1)) + w_m (\mathbf{y}_m^{*T}(k+1) \mathbf{L}_m \mathbf{y}_m'(k+1)) + \Delta \mathbf{u}_m^T(k) \mathbf{R}_m \Delta \mathbf{u}_m(k) \\
&= \left((\mathbf{y}_m^*(k+1) - \mathbf{F}_m \mathbf{z}_m(k) - \Delta \mathbf{y}_m(k))^T - \Delta \mathbf{u}_m^T(k) \mathbf{D}_m^T \right) \mathbf{W}_m \left((\mathbf{y}_m^*(k+1) - \mathbf{F}_m \mathbf{z}_m(k) - \Delta \mathbf{y}_m(k)) - \mathbf{D}_m \Delta \mathbf{u}_m(k) \right) \\
&\quad + w_m \left((\mathbf{y}_m^T(k) + \Delta \mathbf{u}_m^T(k) \boldsymbol{\lambda}_m^T) \mathbf{L}_m (\mathbf{y}_m'(k) + \boldsymbol{\lambda}_m \Delta \mathbf{u}_m(k)) \right) + \Delta \mathbf{u}_m^T(k) \mathbf{R}_m \Delta \mathbf{u}_m(k) \\
&= (\mathbf{y}_m^*(k+1) - \mathbf{F}_m \mathbf{z}_m(k) - \Delta \mathbf{y}_m(k))^T \mathbf{W}_m (\mathbf{y}_m^*(k+1) - \mathbf{F}_m \mathbf{z}_m(k) - \Delta \mathbf{y}_m(k)) \\
&\quad - 2 \Delta \mathbf{u}_m^T(k) \mathbf{D}_m^T \mathbf{W}_m (\mathbf{y}_m^*(k+1) - \mathbf{F}_m \mathbf{z}_m(k) - \Delta \mathbf{y}_m(k)) + \Delta \mathbf{u}_m^T(k) \mathbf{D}_m^T \mathbf{W}_m \mathbf{D}_m \Delta \mathbf{u}_m(k) + w_m \mathbf{y}_m^{*T}(k) \mathbf{L}_m \mathbf{y}_m'(k) \\
&\quad + 2 w_m \Delta \mathbf{u}_m^T(k) \boldsymbol{\lambda}_m^T \mathbf{L}_m \mathbf{y}_m'(k) + w_m \Delta \mathbf{u}_m^T(k) \boldsymbol{\lambda}_m^T \mathbf{L}_m \boldsymbol{\lambda}_m \Delta \mathbf{u}_m(k) + \Delta \mathbf{u}_m^T(k) \mathbf{R}_m \Delta \mathbf{u}_m(k) \\
&= \frac{1}{2} \Delta \mathbf{u}_m^T(k) \left\{ 2 (\mathbf{D}_m^T \mathbf{W}_m \mathbf{D}_m + w_m \boldsymbol{\lambda}_m^T \mathbf{L}_m \boldsymbol{\lambda}_m + \mathbf{R}_m) \right\} \Delta \mathbf{u}_m(k) \\
&\quad + \Delta \mathbf{u}_m^T(k) \left\{ -2 (\mathbf{D}_m^T \mathbf{W}_m (\mathbf{y}_m^*(k+1) - \mathbf{F}_m \mathbf{z}_m(k) - \Delta \mathbf{y}_m(k)) - w_m \boldsymbol{\lambda}_m^T \mathbf{L}_m \mathbf{y}_m'(k)) \right\} \\
&\quad + (\mathbf{y}_m^*(k+1) - \mathbf{F}_m \mathbf{z}_m(k) - \Delta \mathbf{y}_m(k))^T \mathbf{W}_m (\mathbf{y}_m^*(k+1) - \mathbf{F}_m \mathbf{z}_m(k) - \Delta \mathbf{y}_m(k)) + w_m \mathbf{y}_m^{*T}(k) \mathbf{L}_m \mathbf{y}_m'(k)
\end{aligned} \tag{6.31}$$

where \mathbf{L}_m is the Laplacian matrix of the m^{th} sub-microgrid communication graph.

Lastly, the cost function of the proposed multi-objective semi-distributed secondary control can be expressed in the standard quadratic programming form as (note: the last constant term in (6.31) is disregarded)

$$J_m = \frac{1}{2} \Delta \mathbf{u}_m^T(k) \mathbf{H}_m \Delta \mathbf{u}_m(k) + \Delta \mathbf{u}_m^T(k) \mathbf{h}_m \tag{6.32}$$

where

$$\begin{aligned}
\mathbf{H}_m &= 2 (\mathbf{D}_m^T \mathbf{W}_m \mathbf{D}_m + w_m \boldsymbol{\lambda}_m^T \mathbf{L}_m \boldsymbol{\lambda}_m + \mathbf{R}_m) \\
\mathbf{h}_m &= -2 (\mathbf{D}_m^T \mathbf{W}_m (\mathbf{y}_m^*(k+1) - \mathbf{F}_m \mathbf{z}_m(k) - \Delta \mathbf{y}_m(k)) - w_m \boldsymbol{\lambda}_m^T \mathbf{L}_m \mathbf{y}_m'(k))
\end{aligned}$$

6.4.4 Simulation results

The semi-distributed secondary control designed in the preceding sections is tested in what follows on an islanded microgrid depicted in Fig. 6.11. The microgrid is first segregated (for control purpose) into two sub-microgrid, i.e. sub-microgrid *A* and *B*. The islanded microgrid is loaded with $(14+j6)$ kVA at LB 4 in sub-microgrid *A*, and $(13+j12)$ kVA at LB 2 in sub-microgrid *B*. The common base voltage V_B is 400 V and the base power $S_{B,com}$ is 20 kVA; the specification of all-participating DERs are tabulated in Table 6.3 together with the respective sets of secondary control parameters.

The feasibility of the proposed semi-distributed control scheme is assessed through the *MATLAB* platform instead of the *DIgSILENT-PowerFactory-Python* co-simulation platform (note:

all previous investigations, including the work in Section 6.3, have been conducted in the co-simulation platform). In *MATLAB*, the islanded microgrid is modelled using the general nonlinear power flow equations (6.5)-(6.6), adopting all necessary modifications to account for the modified Q - V droop scheme with dispatch. The microgrid network state variables e.g. load-bus voltage magnitude V_L , active/reactive load power P_L/Q_L etc are obtained by solving the non-linear power flow using *fsolve* function. These state variables are then made available to the secondary controller. The overall simulation platform in *MATLAB* is illustrated in Fig. 6.10.

Table 6.3. Specifications of the islanded microgrid network and proposed semi-distributed secondary optimal control.

| DER ratings: | | Q - V droop no-load | Q - V droop |
|---|-----------------|-------------------------|-------------------------|
| Apparent power (pf) | | voltage, V_i^* (pu) | coefficient, n_i (pu) |
| DER 1 | 20 kVA (0.8) | 1.02 | 0.075 |
| DER 2 | 10 kVA (0.8) | | 0.15 |
| DER 3 | 5 kVA (0.8) | | 0.30 |
| DER 4 | 10 kVA (0.8) | | 0.15 |
| DER output feeder impedances | | Line impedances | |
| Z_{of1} | 0.0300Ω, 0.35mH | Z_{l14} | 0.46Ω, 1.464mH |
| Z_{of2} | 0.0804Ω, 0.45mH | Z_{l23} | 0.46Ω, 2.928mH |
| Z_{of3} | 0.0560Ω, 0.35mH | Z_{l34} | 0.70Ω, 3.694mH |
| Z_{of4} | 0.0433Ω, 0.42mH | | |
| Sub-microgrid's secondary optimal control | | | |
| Parameter | Value | Parameter | Value |
| Sampling freq. F_s | 0.5Hz | Integral gain K_i | 0.2 |

Microgrid network in the form of general power flow equation

$$\begin{aligned}
 P_i &= V_i^2 Y_{ii} \cos \theta_{ii} + \sum_{j=1}^M V_i V_j Y_{ij} \cos(\delta_i - \delta_j - \theta_{ij}) \\
 &= V_i^2 G_{ii} + \sum_{j=1}^M V_i V_j [B_{ij} \sin(\delta_i - \delta_j) + G_{ij} \cos(\delta_i - \delta_j)] \\
 Q_i &= -V_i^2 Y_{ii} \sin \theta_{ii} + \sum_{j=1}^M V_i V_j Y_{ij} \sin(\delta_i - \delta_j - \theta_{ij}) \\
 &= -V_i^2 B_{ii} + \sum_{j=1}^M V_i V_j [G_{ij} \sin(\delta_i - \delta_j) - B_{ij} \cos(\delta_i - \delta_j)]
 \end{aligned}$$

which

$$\begin{aligned}
 P_i &= P_{Li} \quad Q_i = Q_{Li} \quad \left. \vphantom{\begin{matrix} P_i \\ Q_i \end{matrix}} \right\} i \in L \\
 P_i &= P_{Gi} \quad Q_i = Q_{Gi} \quad \left. \vphantom{\begin{matrix} P_i \\ Q_i \end{matrix}} \right\} i \in G
 \end{aligned}$$

incorporating the modified Q - V droop scheme with dispatch in Q_G , i.e. from (6.21) to solve for steady state variables e.g. voltage magnitude and phase angle of all buses using *fsolve* function

Semi-distributed optimal secondary control (detailed in Fig. 6.11)

data exchange
(state variables,
control inputs etc)

Fig. 6.10. Overall simulation platform of the semi-distributed optimal control within *MATLAB*.

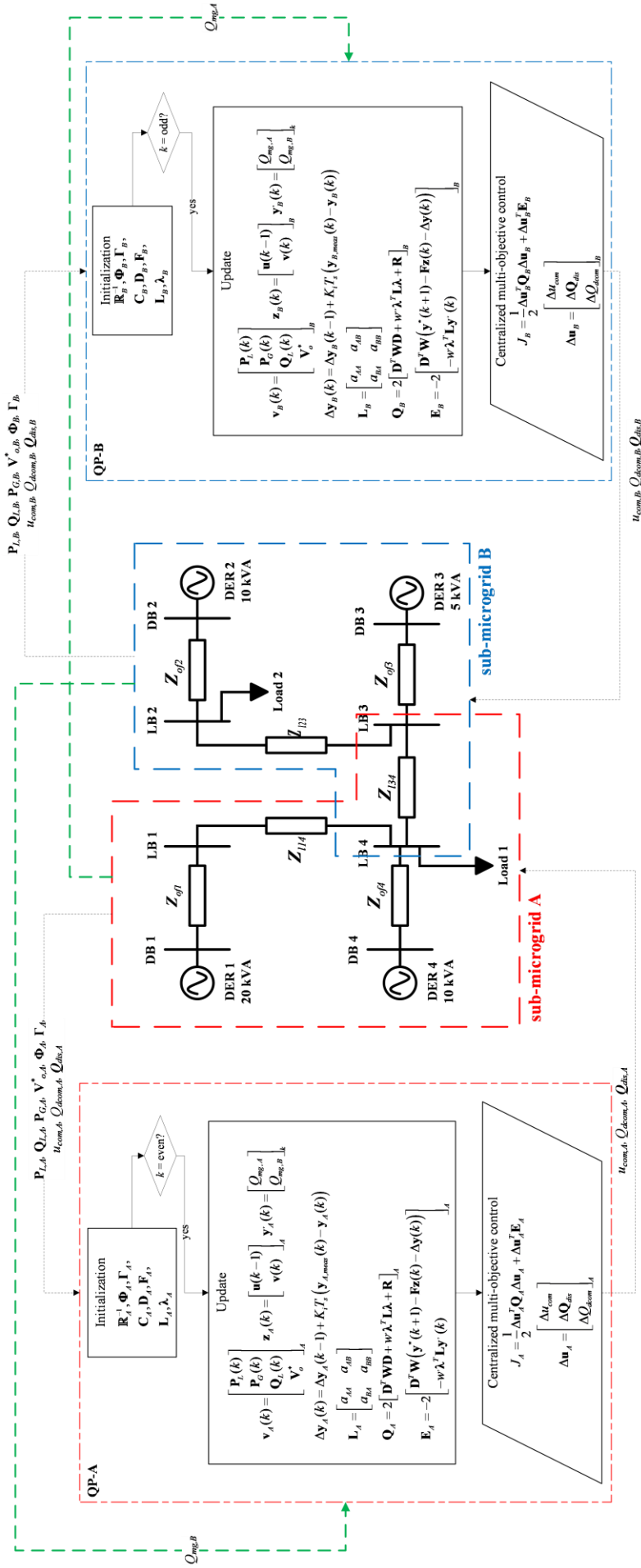


Fig. 6.11. Single line diagram of an islanded microgrid with detailed semi-distributed secondary control flowchart.

As for the semi-distributed optimisation control of each sub-microgrid, the weighting factor \mathbf{W}_m is a $N_{B,m}$ -by- $N_{B,m}$ diagonal matrix having the form of $\text{diag}(w_1, w_2, \dots, w_{N_{B,m}})$ and the penalty factor \mathbf{R}_m is a $(N_{D,m}+2)$ -by- $(N_{D,m}+2)$ diagonal matrix having the form of $\text{diag}(r_1, r_2, \dots, r_{N_{D,m}+2})$. For instance, in sub-microgrid A with $N_{B,A} = 5$ and $N_{D,A} = 2$, the individual w elements correspond to outputs V_{L1} , V_{L3} , V_{L4} , Q_{G1} and Q_{G4} , whereas the individual r elements correspond to control inputs $\Delta u_{com,A}$, $\Delta Q_{1,dis}$, $\Delta Q_{4,dis}$ and $\Delta Q_{dcom,A}$. Different control settings are considered in conjunction with the semi-distributed secondary control: (single-objective control) optimal reactive power sharing among DERs and, separately, single load-bus voltage regulation; (multi-objective control) single- and multi-bus voltage regulation with optimal reactive power sharing.

The islanded microgrid is initially droop-controlled with the secondary control disabled. It is shown in Fig. 6.12 that the reactive powers are not proportionally shared among DERs, neither in each sub-microgrid cluster nor among the sub-microgrids. The intra-reactive power sharing control is initiated in both secondary control A and B at $t = 60$ s by setting the corresponding weighting elements within \mathbf{W} to 1, and the penalty elements within \mathbf{R} that correspond to \mathbf{Q}_{dis} , to 10. Fig. 6.12 shows that the reactive power sharing among the DERs within each sub-microgrid is significantly improved, giving a steady-state sharing ratio of 2:1 (i.e. $Q_{G1}:Q_{G4}$ in sub-microgrid A , and $Q_{G2}:Q_{G3}$ in sub-microgrid B). The corresponding voltages of the DER- and load-buses are also shown in Fig. 6.12 – they range within 0.9416 pu (at LB 4) to 1.018 pu (at DB 1) despite that the total reactive power is not proportionally shared between the two sub-microgrid. The latter is as expected as the inter-cluster reactive power sharing feature is not enabled, i.e. $w'_m = 0$.

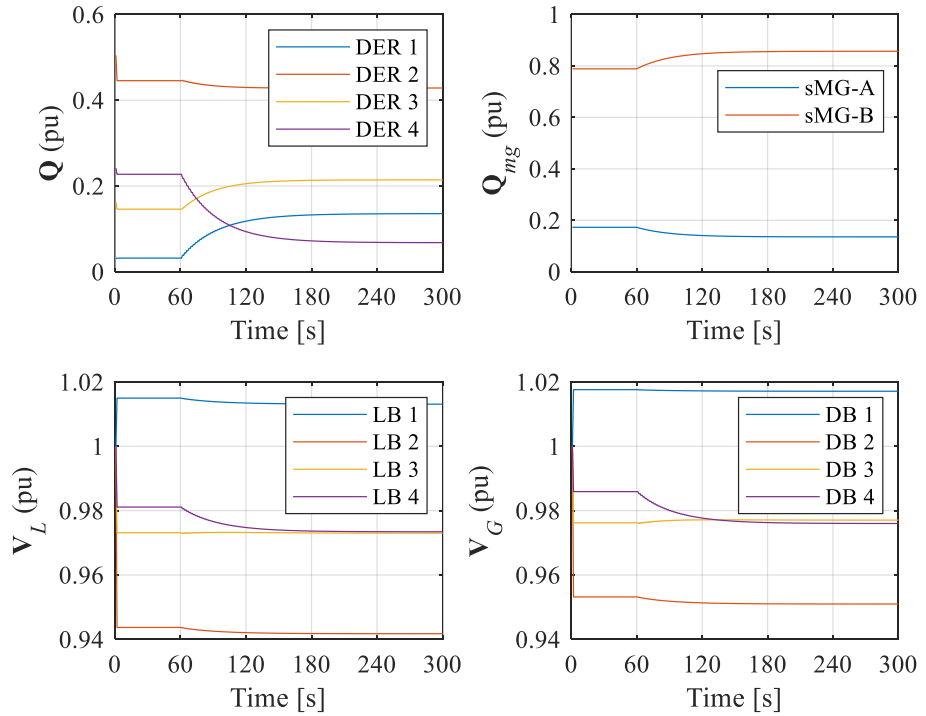


Fig. 6.12. Optimal intra-cluster reactive power sharing control: DERs reactive output power, sub-microgrids reactive output power, load-bus voltage magnitudes and DER-bus voltage magnitudes.

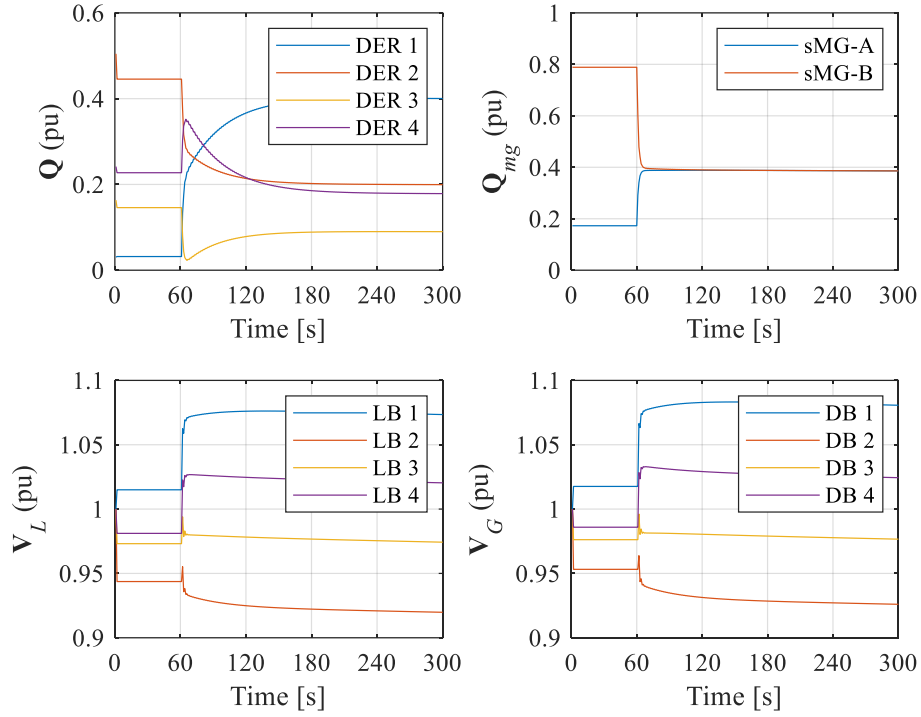


Fig. 6.13. Optimal intra- and inter-cluster reactive power sharing control without integral-based correction: DERs reactive output power, sub-microgrids reactive output power, load-bus voltage magnitudes and DER-bus voltage magnitudes.

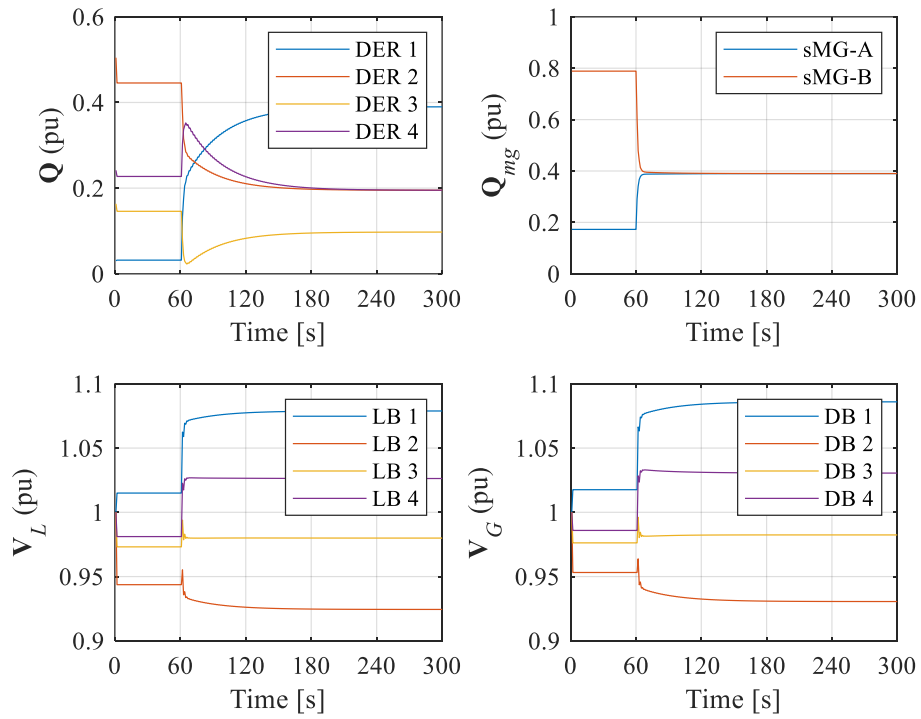


Fig. 6.14. Optimal intra- and inter-cluster reactive power sharing control: DERs reactive output power, sub-microgrids reactive output power, load-bus voltage magnitudes and DER-bus voltage magnitudes.

Next, the performance of intra- and inter-cluster reactive power sharing is examined along with the justification of integral-based correction control. The inter-reactive power sharing control is activated along with the intra-control at $t = 60$ s. The penalty elements within \mathbf{R} that correspond to individual DER's Q_{dis} and common Q_{dcom} are set to 10. In Fig. 6.13, the reactive power sharing of two sub-microgrids is significantly improved. However, without the integral-based correction control, the reactive power sharing between DER 2 and 4 remain slightly non-proportional (note: they are supposed to be equal, in pu with the common base S_B , as detailed in Table 6.3). Upon introducing the correction scheme with the setting of $K_i = 0.2$, the reactive power sharing among all DERs in the islanded microgrid is significantly improved. Fig. 6.14 shows that the reactive power is shared at a ratio of 4:2:1:2 while the bus voltages range from 0.9246 pu at LB 4 to 1.086 pu at DB 1.

The next control setting to be assessed is the single load-bus voltage regulation control. Initially, the voltage magnitude at LB 1 in sub-microgrid A and LB 2 in sub-microgrid B are “drooped”, respectively, to 1.015 pu and 0.9437 pu. First, two scenarios are examined. At $t = 60$ s, the load-bus voltage regulation control of the proposed optimal control is activated by (first scenario) setting $w_{L,A}$ that corresponds to V_{L1} in sub-microgrid A to 1, and (second scenario) setting $w_{L,B}$ that corresponds to V_{L2} in sub-microgrid B to 1. In both scenarios, the penalty factor \mathbf{R} is set such that only u_{com} is activated. It can be clearly seen from Fig. 6.15 and Fig. 6.16 that V_{L1} and V_{L2} are regulated to $V_{ref} = 1.0$ pu independently in both scenarios without noticeable improvement in reactive power sharing (this is expected since the reactive power sharing feature is disabled). Next, the third scenario of

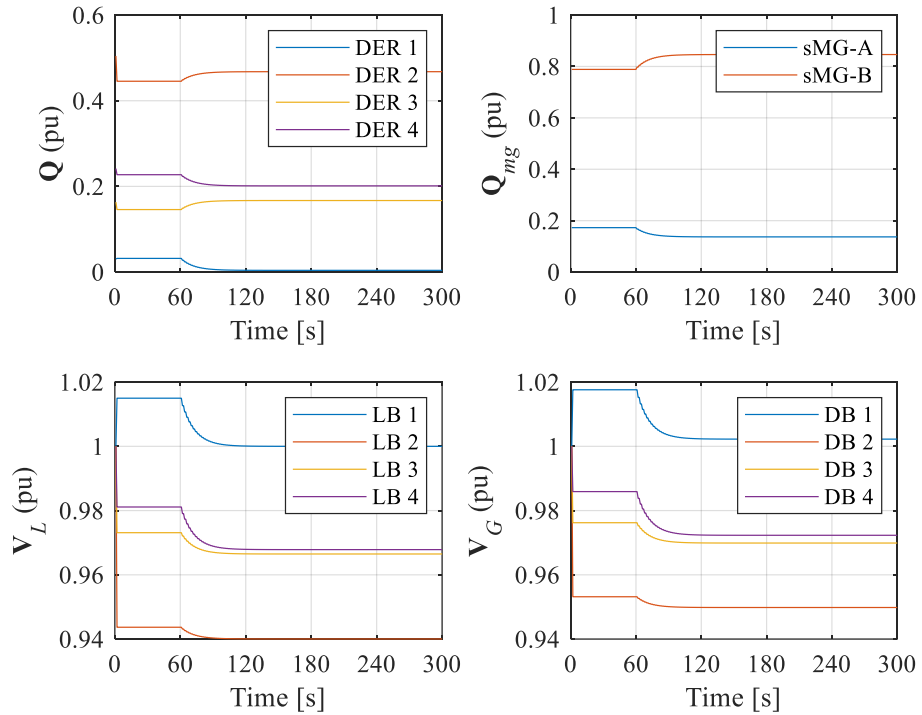


Fig. 6.15. Single load-bus voltage regulation control at sub-microgrid A: DERs reactive output power, sub-microgrids reactive output power, load-bus voltage magnitudes and DER-bus voltage magnitudes.

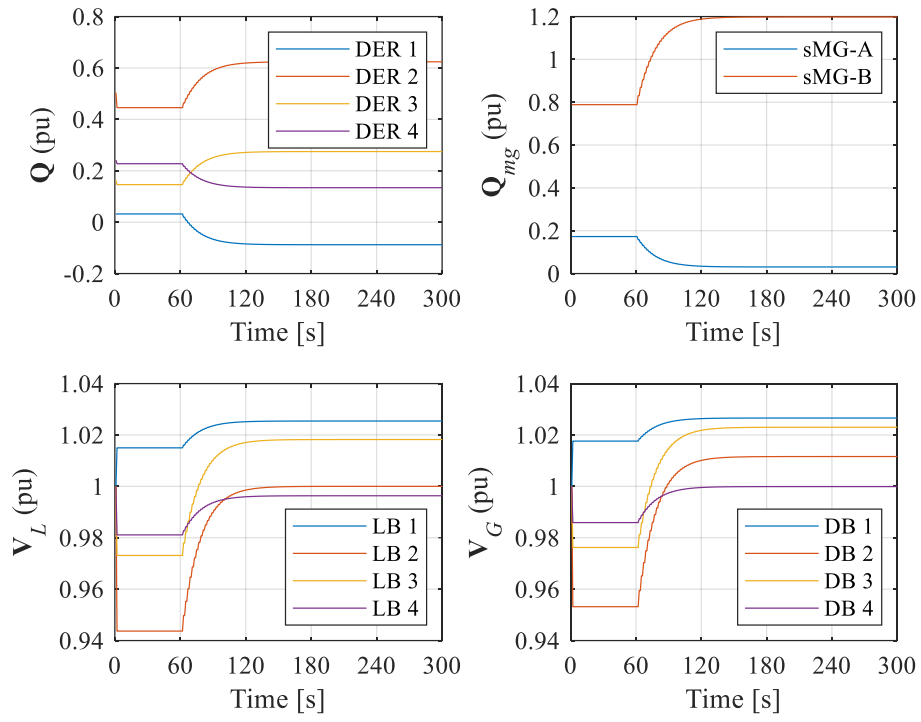


Fig. 6.16. Single load-bus voltage regulation control at sub-microgrid *B*: DERs reactive output power, sub-microgrids reactive output power, load-bus voltage magnitudes and DER-bus voltage magnitudes.

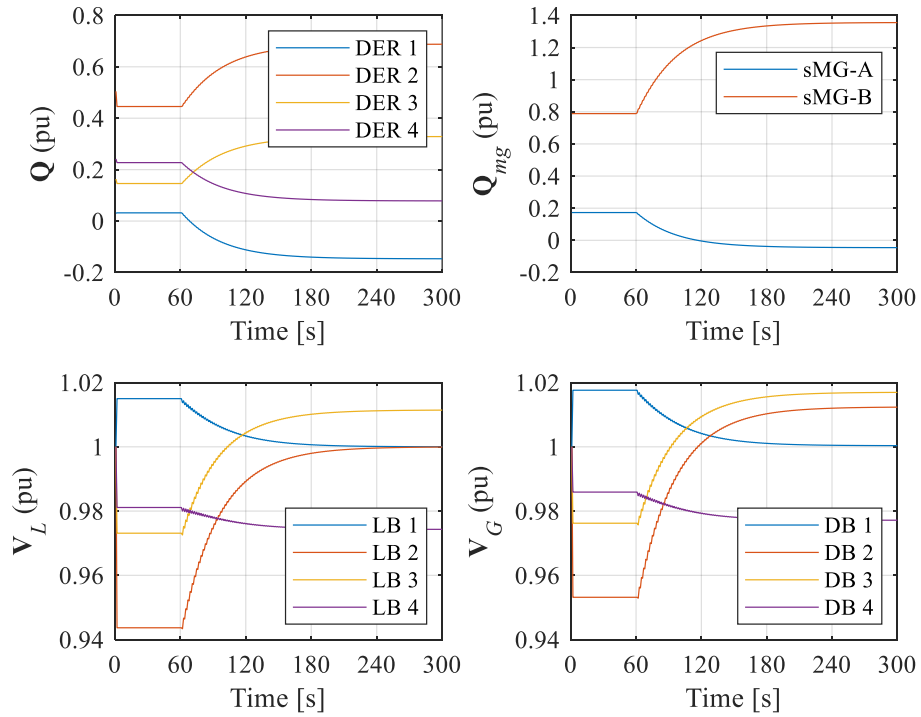


Fig. 6.17. Simultaneous single load-bus voltage regulation control in two sub-microgrids: DERs reactive output power, sub-microgrids reactive output power, load-bus voltage magnitudes and DER-bus voltage magnitudes.

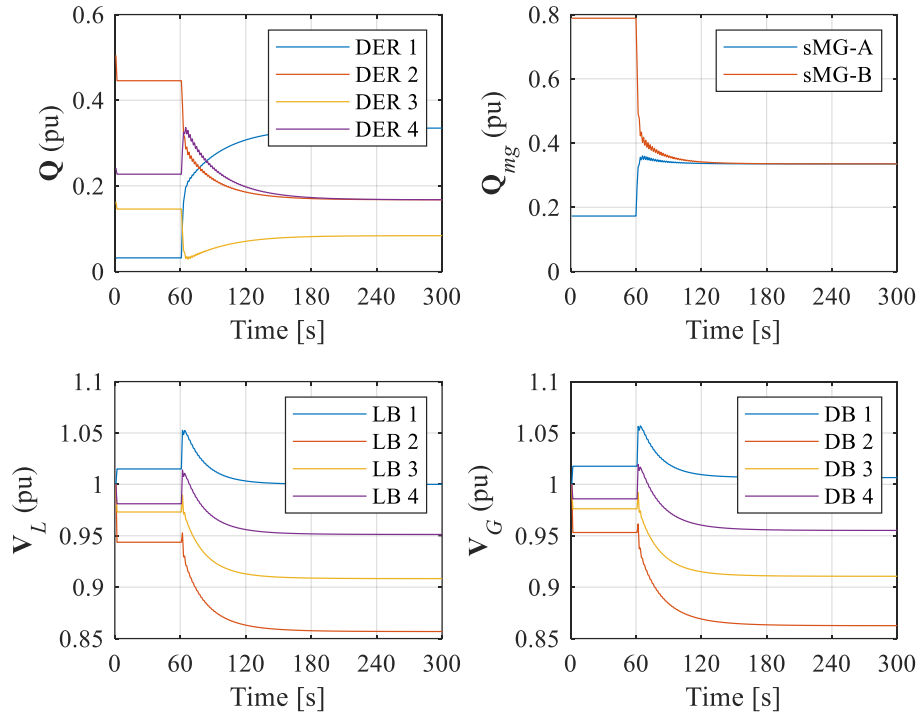


Fig. 6.18. Optimal intra- and inter-reactive power sharing and single load-bus voltage regulation control at sub-microgrid A: DERs reactive output power, sub-microgrids reactive output power, load- and DER-bus voltage magnitudes.

simultaneous single load-bus voltage regulation in both sub-microgrids, i.e. V_{L1} in sub-microgrid A and V_{L2} in sub-microgrid B, is examined. Both semi-distributed controllers are activated at $t = 60$ s by setting $w_{1,A} = w_{1,B} = 1$. It is shown in Fig. 6.17 that both V_{L1} and V_{L2} are regulated to $V_{ref} = 1.0$ pu, but with the non-proportional reactive power sharing, as per the theoretical expectation.

The third control setting focuses on the multi-objective control of voltage and reactive power. The first scenario to be examined is the single load-bus voltage regulation in sub-microgrid A with simultaneous intra- and inter-cluster reactive power sharing control. The semi-distributed optimal control has the following setting: $w_{4-5,A} = w_{4-5,B} = 1$ and $w' = 1$ (for, respectively, intra- and inter-reactive power sharing); $w_{1,A} = 1$ (for V_{L1} regulation in sub-microgrid A). All control inputs are utilised by setting the penalty factor $\mathbf{R}_{A/B}$ as $\text{diag}(10,10,10,10)$. Fig. 6.18 shows that the proportional reactive power sharing among all DERs within the entire islanded microgrid is achieved, and V_{L1} is regulated to $V_{ref} = 1.0$ pu. It is worth highlighting that this optimal outcome is achieved through two separated instances of secondary controllers – being the first proof of the feasibility of the proposed semi-distributed control scheme.

Next scenario is about prioritising the multi-load-bus voltage regulation in sub-microgrid A while maintaining the intra- and inter-cluster reactive power sharing. To be specific, in sub-microgrid A, voltage regulation at LB 1 is prioritised by setting $w_{1,A} = 10$ along with regulating V_{L3} through $w_{2,A} = 1$. Fig. 6.19 shows that $V_{L1} = 1.008$ pu is regulated close to V_{ref} (being 1.0) with V_{L3} is more loosely regulated to 0.9162 pu (also having $V_{ref} = 1.0$). Evidently, proportional reactive power sharing is

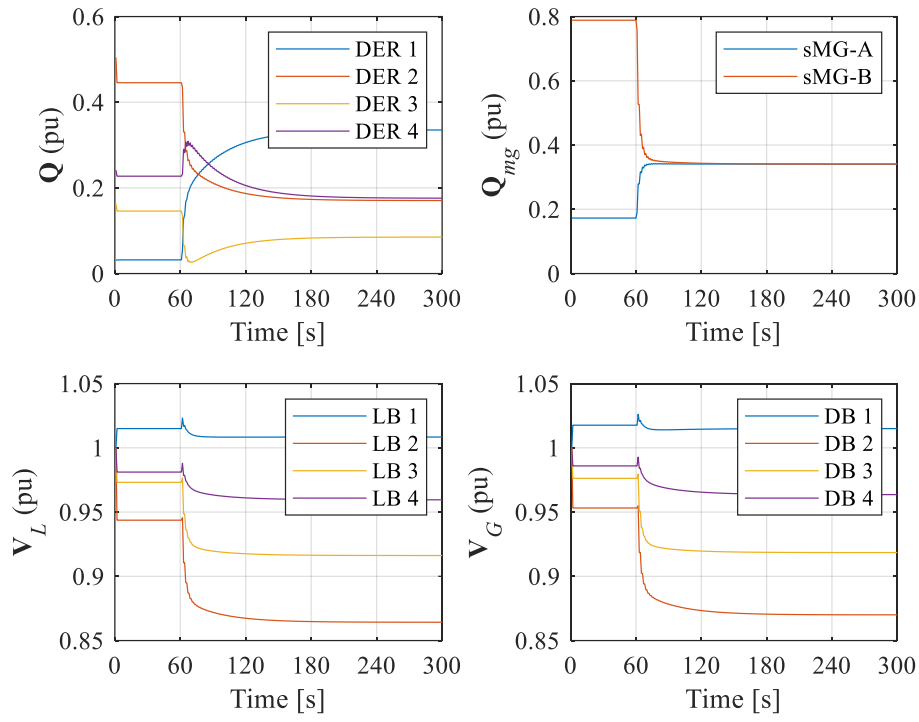


Fig. 6.19. Optimal intra- and inter-reactive power sharing and multi-load-bus voltage regulation control at sub-microgrid A: DERs reactive output power, sub-microgrids reactive output power, load- and DER-bus voltage magnitudes.

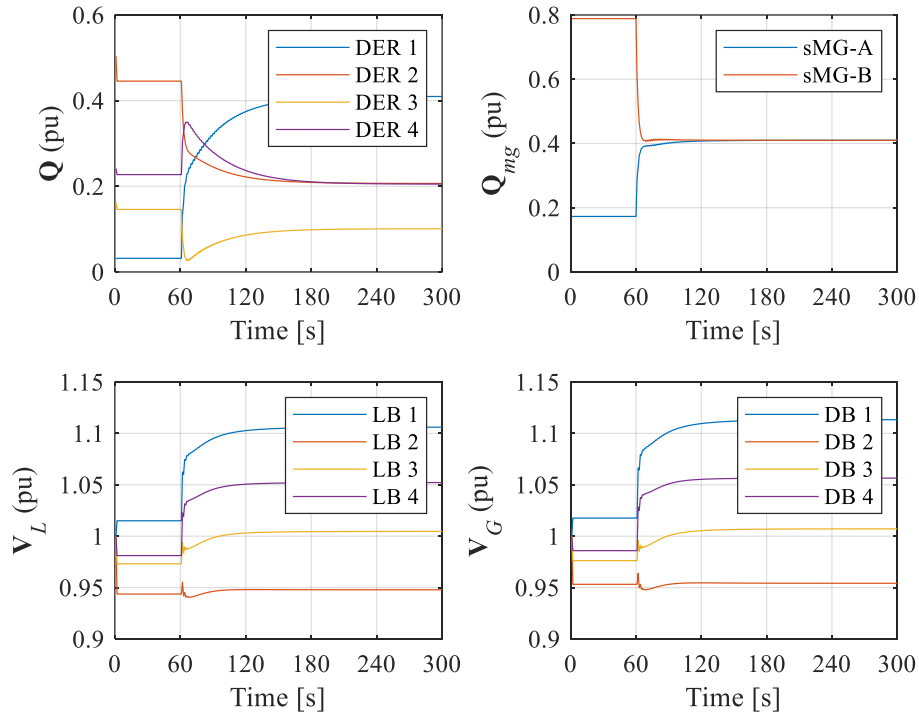


Fig. 6.20. Optimal intra- and inter-reactive power sharing and multi-load-bus voltage regulation control in sub-microgrid B: DERs reactive output power, sub-microgrids reactive output power, load- and DER-bus voltage magnitudes.

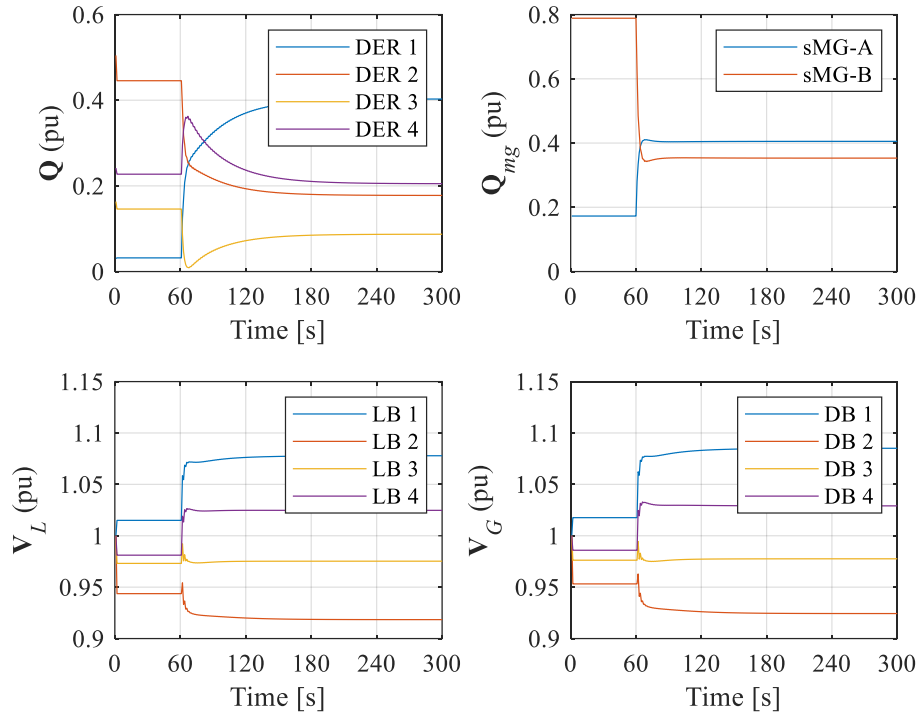


Fig. 6.21. Optimal intra- and inter-reactive power sharing and inter-multi-load-bus voltage regulation control: DERs reactive output power, sub-microgrids reactive output power, load- and DER-bus voltage magnitudes

now slightly compromised, being 0.3352:0.1705:0.0851:0.1760 instead of 4:2:1:2 ratio (as in the previous scenario). With multi-bus voltage regulation in sub-microgrid *B* and reactive power sharing weighted equally (by setting $w_{4-5,A}$, $w_{1,B}$, $w_{3-5,B}$ and w' to 1), Fig. 6.20 shows that reactive power sharing among all DERs is considerably improved, to a ratio of 0.4097:0.2067:0.1007:0.2051. However, V_{L2} and V_{L4} are more loosely regulated to 0.9479 and 1.052 pu ($V_{ref} = 1.0$ pu).

The last scenario focuses on the inter-cluster load-bus voltage regulation (i.e. one load-bus in each sub-microgrid) with intra- and inter-reactive power sharing. At $t = 60$ s, the semi-distributed control is activated through the setting of $w_{2,A} = w_{4-5,A} = 1$ in \mathbf{W}_A , $w_{3,B} = w_{4-5,B} = 1$ in \mathbf{W}_B , and $w' = 1$. It is seen in Fig. 6.21 that while V_{L3} in sub-microgrid *A* and V_{L4} in sub-microgrid *B* are regulated to 0.9753 pu and 1.025 pu (i.e. closed to the reference of 1.0 pu), both intra- and inter-cluster reactive power sharing accuracy is clearly compromised. The overall reactive power sharing ratio stands at 0.4028:0.1777:0.0871:0.2051, in pu. The reactive power ratio of the two sub-microgrids is 0.4053:0.3531 - slightly off from 1:1, being the ratio of their respective total kVA values. This agrees with the theoretical expectation.

Through the three control settings and the scenarios therewithin, the effectiveness of the proposed semi-distributed optimal control in managing trade-offs (of reactive power sharing and load-bus voltage regulation) among all the DERs across the sub-microgrid clusters, has been demonstrated. It is worth highlighting that this is achieved through separated instances of optimal secondary controllers for the sub-microgrids.

6.5 Summary

This chapter presents two quadratic-programming-based multi-objective secondary control for optimal reactive power sharing and voltage regulation in an islanded microgrid through the exploitation of Decoupled Linearised Power Flow.

Section 6.3 introduced a centralised, non-iterative-based multi-objective secondary control to address the intrinsic trade-off control objectives of optimal reactive power sharing among DERs and voltage regulation at multiple buses in droop-controlled microgrids. The multi-objective control problem is framed into a generic quadratic programming problem, enabling the deployment of established solver, e.g. *CVXOPT* module in *Python*. It is successfully demonstrated that the proposed secondary control is capable of realising single-objective control, i.e. optimal reactive power sharing or single bus voltage regulation, and accomplishing multi-objective control, i.e. optimal reactive power sharing and single load-bus voltage regulation without compromising reactive power sharing accuracy. In addition, the control scheme can also realise multi-load-buses voltage regulation with optimal trade-offs with the accurate reactive power sharing objective. The robustness of the centralised secondary control in constraining the relevant network variables, e.g. load-bus voltages and DERs' reactive output power, to within the predefined limits has also been demonstrated and verified.

Section 6.4 proposed and studied a semi-distributed, non-iterative-based multi-objective secondary control concept that exploits the use of optimal and cooperative control techniques. The motivation behind this is to improve the system reliability (relating to the risk of single point failure) and computational efficiency of the secondary control layer of future microgrids. The secondary optimal control is assessed in *MATLAB* through the use of *quadprog* function in a sequential approach. It is clearly demonstrated and verified that despite having separated instances of secondary controller, the novel semi-distributed optimal control concept is able to realise optimal reactive power sharing and/or voltage regulation, be it single- or multi-bus within the entire microgrid.

Lastly, it is worth highlighting again that both the secondary optimisation-based control schemes have adopted the Decoupled Linearised Power Flow. The non-iterative power flow has effectively improved the computational efficiency of the optimal control algorithm. The presented simulation proofs have confirmed that the proposed optimal control schemes can realise single-objective control, i.e. optimal reactive power sharing or single load-bus voltage regulation, and multi-objective control, i.e. load-bus voltage regulation with optimal trade-offs of reactive power sharing, in an optimal manner. It has also been proven that the weighting and penalty factors in the cost function are useful in setting the priority of the control objectives. This feature does not usually exist in the consensus control schemes (those in Chapter 5 and in other literature summarised in Chapter 2) and is believed to be another useful addition to the microgrid secondary control.

This part of the work has been published in a conference paper (Wong, Lim, A. J. Cruden, *et al.*, 2021) and a journal paper (Wong, Lim, Goh, *et al.*, 2021).

Chapter 7 Conclusion

7.1 Conclusions

This PhD thesis successfully designed, developed, and assessed novel secondary control schemes that aim to improve the voltage regulation and reactive power sharing among the power-electronic-interfaced DER in microgrids. Specifically, the targeted microgrids are those with a large number of DERs, which are common in large-area distribution microgrids. A *DIGSILENT-PowerFactory-Python* co-simulation platform with primary closed-loop control that is present in all power-electronic-interfaced DERs, is established and tested. It forms a reliable simulation platform to numerically assess the developed novel secondary control schemes.

In Chapter 2, a comprehensive review of the existing improved variants of droop-based reactive power schemes is presented. The relationship between the non-linear virtual-output-impedance-based droop scheme and the first-order consensus protocol is first established. To better articulate the open gaps and limitations, some of the major secondary control strategies are succinctly tabulated based on their main characteristics. It is concluded that the issue of consensus gain design is rarely discussed to date. Moreover, as far as secondary voltage regulation control is concerned, there have been very limited reactive power sharing schemes co-regulating voltages at multiple load-buses.

Chapter 3 first introduces the fundamental concepts, such as transformation, dynamical model for droop control, inverter current/voltage/power controls, consensus control, graph theory, optimal control, and quadratic programming. The adopted simplifications in the control analysis are comprehensively discussed. The dynamical model of power-electronic-interfaced DERs presented in this chapter has been published in a conference paper (Wong *et al.*, 2018) along with the *DIGSILENT-PowerFactory-Python* co-simulation platform established.

A comprehensive assessment of reactive-power-sharing-focused droop control schemes, i.e., standard droop control with dispatch and virtual-output-impedance-based droop control, is presented in Chapter 4. Their merits and demerits are clearly established. Apart from verifying the validity of the *DIGSILENT-PowerFactory-Python* co-simulation platform, the viability of the reactive-power-sharing-focused droop control schemes with full-graph distributed integral controllers are confirmed, and their main features are summarised accordingly. It is revealed that the static-dynamic VOI-droop variant tends to suffer from a larger voltage deviation than other control counterparts. Another important observation from the assessment is that, in the VOI-droop scheme, the droop output voltages of all participating DERs converged upon the reactive power sharing correction. This provided a basis to develop a novel control scheme in the next chapter.

In Chapter 5, distributed consensus-based VOI-droop schemes with sparse graph communication structure realising accurate reactive power sharing are developed and benchmarked against the dual-impedance consensus control reported by Zhang *et al.* (2017). From the investigation, it is concluded that the static component contributes to unnecessary virtual voltage drop, and that the dynamic component alone is sufficient to achieve an accurate sharing of reactive power. It is also found that the virtual-reactance-based scheme exhibits a faster reactive power correction dynamic as compared to the virtual-resistance-based counterpart. On the other hand, another novel consensus droop control scheme is also developed using the newly introduced droop equivalent impedance concept, on which the principle behind the single-virtual-impedance (i.e., with either virtual output reactance or resistance) droop mechanism is analysed and explained. It is also concluded that upon the convergence of the droop equivalent reactance (resistance) through the regulation of virtual output reactance (resistance), the other droop equivalent impedance counterpart will naturally be synchronised. This chapter also clarified the relationship among virtual output impedance, droop equivalent impedance and reactive power in facilitating a faster correction dynamic. Upon confirming that a poorly designed consensus coupling gain would destabilise the microgrid, a consensus gain tuning guideline for both distributed consensus control schemes is developed. With that, the extensive use of static VOI component and local *PI* controller in each DER is eliminated successfully. This can improve the practicality and relevance of consensus control schemes in future microgrids, especially those with a large amount of DERs (e.g. hundreds to tens of thousands). The presented works have been published in a conference paper (Wong, Lim, Cruden, *et al.*, 2020) and two journal papers (Wong, Lim, Rotaru, *et al.*, 2020; Wong, Lim, A. Cruden, *et al.*, 2021).

Chapter 6 presents two novel optimal secondary control strategies, i.e. centralised and semi-distributed multi-objective secondary controls, that address the intrinsic trade-offs between voltage and reactive power regulation in droop-controlled islanded microgrids. By adapting the non-iterative Decoupled Linearised Power Flow into the secondary control schemes, the computational efficiency is improved. The first control strategy successfully realises single-objective or multi-objective control while ensuring the compliance of some network limits. The system reliability (relating to the risk of single point failure) and computational efficiency of the secondary control scheme is further improved by conceptualising and developing a semi-distributed secondary optimal control scheme that uses both the optimal control and cooperative control techniques. In spite of having separated instances of secondary controllers, the novel semi-distributed optimal control is capable of realising optimal voltage and reactive power regulation in the entire microgrid. Through distributing the computational effort across multiple secondary controllers, the computational complexity and scalability issue is successfully eased. The works in this chapter have been published in a conference paper (Wong, Lim, A. J. Cruden, *et al.*, 2021) and a journal paper (Wong, Lim, Goh, *et al.*, 2021).

In summary, advanced secondary control strategies for voltage regulation and/or reactive power sharing correction in droop-controlled islanded microgrids are successfully developed and

verified in this thesis. It is believed that these control strategies will contribute to encouraging the adoption and realisation of future large-scale distribution microgrids.

7.2 Recommendation for Future Work

Drawing from the conclusions presented in previous chapters, future research of secondary control of voltage and reactive power for islanded microgrids with power-electronic-interfaced DERs should be directed to the following:

- i. The DC source in the power-electronic-interfaced DERs is considered ideal, which might be unrealistic in some practical applications as it is the nature of microgrids to integrate a variety of alternative energy resources. Therefore, it is recommended that the development of secondary control strategy should be combined with the development of realistic micro-source models, e.g., micro-turbine and energy storage. Characteristic and dynamical responses of micro-sources should be incorporated into the control design to better reflect the overall dynamic of the microgrids. This includes, but not limited to, fluctuating power generation from intermittent weather nature and state-of-charge of energy storage systems.
- ii. The primary control dynamic of the power-electronic-interfaced DERs is disregarded in the conceptualising and development of semi-distributed optimal secondary control strategy in MATLAB simulation software. Hence, it is suggested that the primary control dynamic should be included through proper dynamical modelling in an appropriate simulation platform. This can help to further verify the overall stability and performance of the semi-distributed optimal secondary control strategy with the power-electronic-based DERs. In addition, the semi-distributed control strategy can be extended to a large-scale network in future very-large-area microgrids. This can better reflect the usability of the semi-distributed control strategy. Furthermore, the semi-distributed control concept should be benchmarked against recent advanced control techniques, e.g., distributed model predictive control and ADMM. The criteria should focus on the strength and weaknesses of the control strategies and their practicality in actual microgrids.
- iii. Only linear load type is considered in this thesis. The load disturbances can be extended to include both nonlinear and unbalanced loads. Consequently, secondary control strategy can be extended to account for these loads. Their potential in addressing the voltage unbalances and poor power quality issues (e.g., intermittent changes in weather) can then be assessed.

Appendix A *DIgSILENT-PowerFactory-Python* co-simulation platform configuration

Co-simulation enables specialist simulation packages in different domains to efficiently collaborate in a complex system, allowing the study of the behaviour of the overall system. For this research work, *DIgSILENT PowerFactory* is identified as a suitable industrial-grade power system specialist simulation package. It offers a wide set of interfaces that enable the possibility of processing parallel simulations with external controller platform through the establishment of communication links. This research work is made possible with the time-limited thesis license and the grant of license is renewed on a yearly basis. The analysis functions required are defined according to the scope of work of the thesis with the OPC interface at an additional cost. On the other hand, *Python* is selected as the external control environment due to its open-source, large and comprehensive standard library. The *Python*'s Integrated Development and Learning Environment (IDLE) is used in this work for secondary control design and development. The use of open-source *Python* reduces the license requirement of the co-simulation, making repeatability more possible. In order to establish the *DIgSILENT PowerFactory-Python* co-simulation platform, the supported *Python* versions, i.e., 3.3, 3.4 and 3.5 are recommended. Lastly, OPC interface *ComLink* offered in

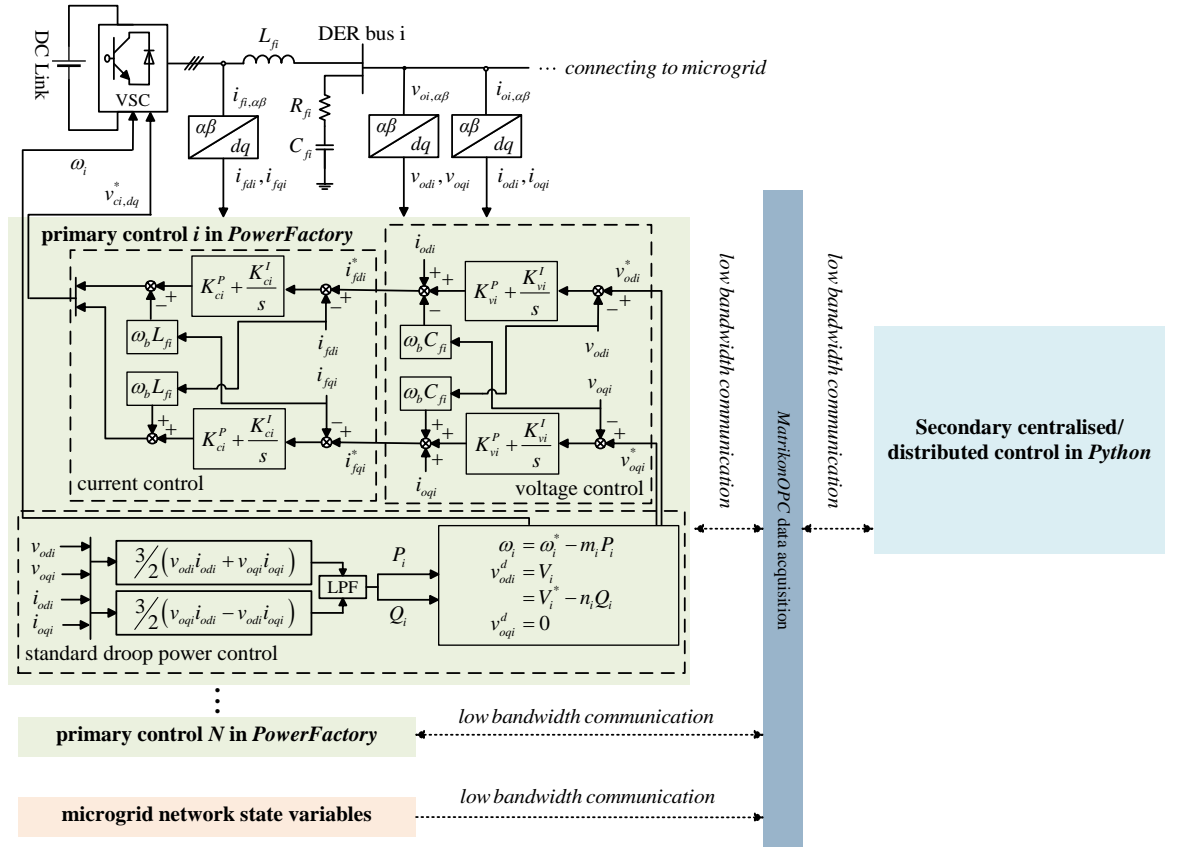


Fig. A.1. Illustration of the *DIgSILENT-PowerFactory-Python* co-simulation platform with detailed primary control of a standard droop-controlled DER.

Appendix A

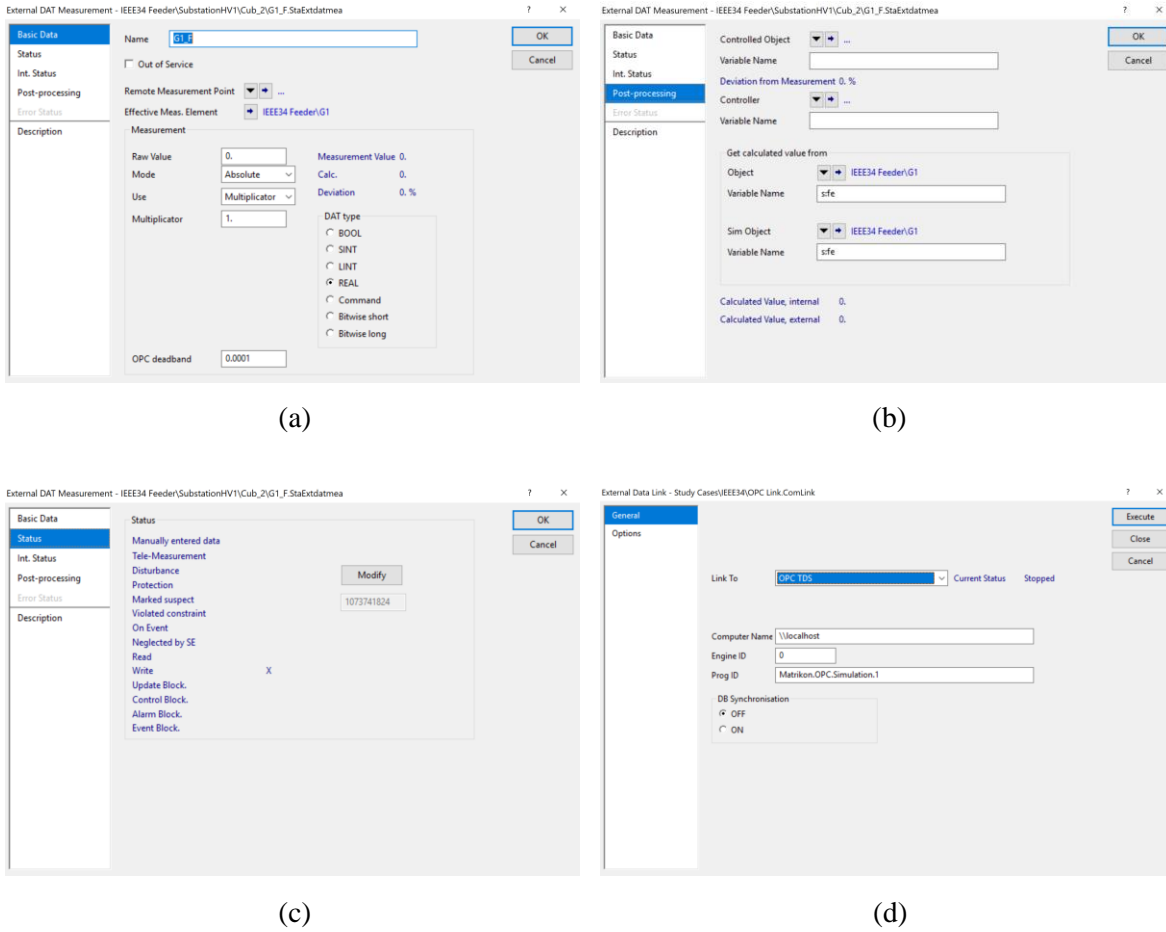
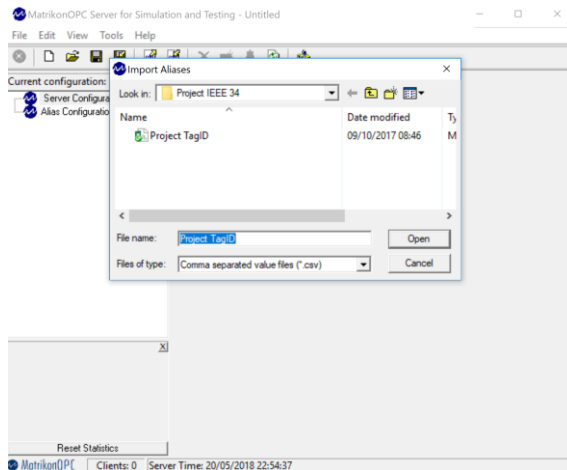


Fig. A.2. External data measurement setup (a) basic data; (b) post-processing; (c) status; (d) external data link setup in *DigSILENT PowerFactory*.

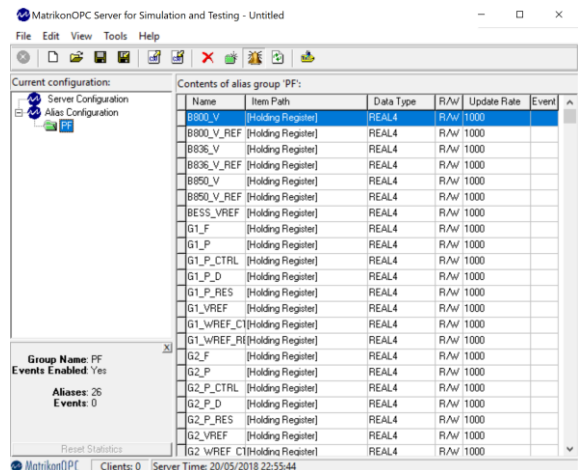
the *DigSILENT PowerFactory* is used to serve as the data acquisition interface for the microgrid network and the corresponding DERs primary control in *DigSILENT PowerFactory* while the secondary control in *Python* exploits the open-source *OpenOPC* module. *MatrikonOPC* is an industrial-grade automation software interface. It is used as the OPC server to facilitate the data acquisition and transfer between the two clients. The established co-simulation platform (with a sample of detailed primary control loop) is as illustrated in Fig. A.1.

The configuration of the *DigSILENT-PowerFactory-Python* co-simulation platform will be explained in what follows. The mapping of OPC tags to *DigSILENT PowerFactory*'s variables is done by setting up external tags through the *External measurement* tool provided in *DigSILENT PowerFactory*. Each OPC tag that is supposed to be processed by *DigSILENT PowerFactory* must be created and configured. For example, Fig. A.2 shows the external data measurement setup, e.g., the operating frequency of *synchronous generator 1* in *DigSILENT PowerFactory*. The frequency variable, default named *s:fe* in *DigSILENT PowerFactory* is written to the user-defined external tag *G1_F*. The post-processing tab (Fig. A.2(b)) allows the user to configure from which object/variable in the *DigSILENT PowerFactory* does the value of the OPC tag is read and/or write to. On the status tab (Fig. A.2 (c)), “read status” indicates that the OPC tag value is read by *DigSILENT PowerFactory*

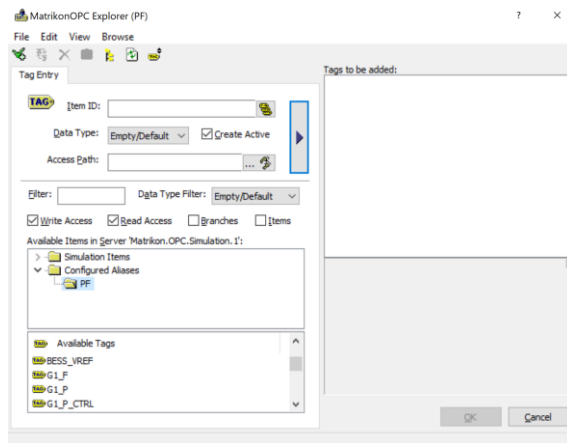
whilst “write status” indicates that *DigSILENT PowerFactory* writes the value to the corresponding OPC tag. Upon the completion of identifying the control variables, it is recommended that all control variables are externally compiled in an excel’s csv file to ease the tags import process to *MatrikonOPC*. The connection to an OPC server is established by a *ComLink* class offered in *DigSILENT PowerFactory*, as shown in Fig. A.2(d). This link object holds the OPC client configuration and is responsible for data exchange and transfer. *OPC TDS* link allows a complex simulation of the dynamic behaviour in the time domain. The pre-configured OPC tags are imported from the excel’s csv file to *MatrikonOPC* and go live/online (during co-simulation) with *MatrikonOPC* server, as depicted in Fig. A.3.



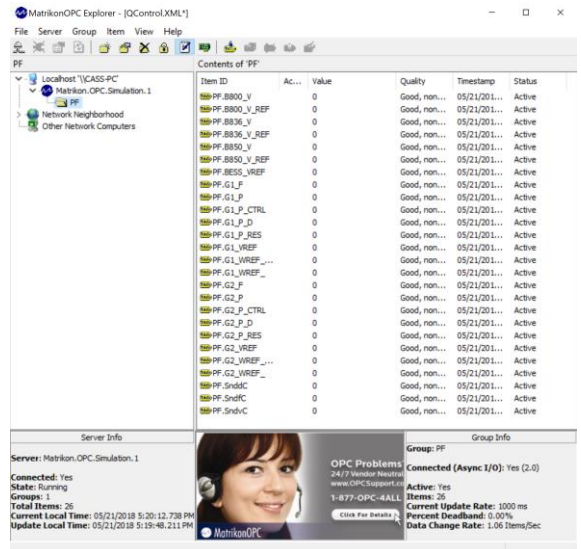
(a)



(b)



(c)



(d)

Fig. A.3. (a) Pre-configured tags importing to *MatrikonOPC*; (b) an alias group *PF* containing OPC tags; (c) uploading *PF* group OPC tags onto *MatrikonOPC* server; (d) parallel execution with *MatrikonOPC*.

Appendix A

For more information, documentation is provided by *DIgSILENT PowerFactory* to describe details of the configuration and setup along with case examples.

Appendix B Publications from the thesis

Journal publications:

1. Wong, Y. C. C., Lim, C. S., Rotaru, M. D., Cruden, A. and Kong, X. (2020) ‘Consensus virtual output impedance control based on the novel droop equivalent impedance concept for a multi-bus radial microgrid’, *IEEE Transactions on Energy Conversion*, 35(2), pp. 1078–1087.
2. Wong, Y. C. C., Lim, C. S., Cruden, A., Rotaru, M. D. and Ray, P. K. (2021) ‘A consensus-based adaptive virtual output impedance control scheme for reactive power sharing in radial microgrids’, *IEEE Transactions on Industry Applications*, 57(1), pp. 784–794.
3. Wong, Y. C. C., Lim, C. S., Goh, H. H., Cruden, A., Rotaru, M. D. and Kong, X. (2021) ‘An optimal secondary multi-bus voltage and reactive power sharing control based on non-iterative decoupled linearized power flow for islanded microgrids’, *IEEE Access*, 9, pp. 105242-105254.

Conference publications:

4. Wong, Y. C. C., Lim, C. S., Rotaru, M. D., Cruden, A. and Kong, X. (2018) ‘Reactive power sharing study of an islanded microgrid in DigSILENT PowerFactory’, *International Conference on Renewable Energy Research and Applications*. Paris, France, 14–17 October. Paper No. 68.
5. Wong, Y. C. C., Lim, C. S., Cruden, A., Rotaru, M. D. and Ray, P. K. (2020) ‘A consensus-based adaptive virtual output impedance control scheme for reactive power sharing in meshed microgrids’, *IEEE International Conference on Power Electronics, Smart Grid and Renewable Energy*. Cochin, India, 2–4 January. Paper No. 323.
6. Wong, Y. C. C., Lim, C. S., Cruden, A., Rotaru, M. D. and Kong, X. (2021) ‘Semi-distributed optimal secondary control based on decoupled linearized power flow for large-area droop-controlled microgrids’, *International Conference on Green Energy, Computing and Sustainable Technology*. Sarawak, Malaysia, 7–9 July. Paper No. 1570727021. (Best Paper Award in Track 4: Green Energy and Power System, Smart Grid)

Consensus Virtual Output Impedance Control Based on the Novel Droop Equivalent Impedance Concept for a Multi-Bus Radial Microgrid

Yi Chyn Cassandra Wong, *Student Member, IEEE*, Chee Shen Lim[✉], *Senior Member, IEEE*, Mihai Dragos Rotaru, *Member, IEEE*, Andrew Cruden[✉], and Xin Kong

Abstract—Most of the existing reactive power sharing schemes that assume parallel architecture are known to be less effective for multi-bus radial microgrids. This article proposes an improved reactive power sharing scheme that exploits the novel concept of droop equivalent impedance into designing a consensus virtual-output-impedance-based droop control scheme. The control scheme leads to two notable improvements: (a) it proves that only either virtual resistance or virtual reactance is sufficient to restore proportional reactive power sharing; (b) only a global coupling gain needs to be tuned and no proportional-integral controller is required. A systematic guideline that establishes the approximate range of stable coupling gain is developed. This simplifies the tuning process of the coupling gain. The power correction performance, the resulting bus voltage behavior, consensus control stability, and the robustness to time delay have been investigated in conjunction with an islanded microgrid modified from the IEEE 34 Node Test Feeder. It is shown that the consensus control scheme is capable to demonstrate accurate power sharing regardless of the changes in the network topology, network impedances, loading conditions, and communication delay.

Index Terms—Droop control, radial microgrid, reactive power sharing, adaptive virtual output impedance.

I. INTRODUCTION

IN ORDER to facilitate the requirement of autonomous power sharing among distributed energy resources (DERs) in a microgrid, droop control mechanism has been widely adopted. However, it is known that although the load active power can be proportionately shared among the DERs, the load reactive

power tends to suffer from the problem of non-proportional sharing. This is due fundamentally to non-negligible voltage discrepancies at the points of coupling [1]–[3].

Various reactive power sharing improvement techniques have been developed in the past and, in the authors' opinion, they can be broadly categorized to communication-less and communication-based techniques. The former is typically developed for parallel DERs (i.e., those share a point of common coupling through respective feeder impedances) and is based predominantly on the fundamental principle of improving the droop control design. One example being the cross-coupled droop control reported in [4]. Though with higher reliability, they cannot be directly extended to multi-bus radial microgrid cases, especially the ones with the plug-and-play requirement [1]. The problem has been solved predominantly through the communication-based techniques (with some exception, as will be explained next). It is worth highlighting that multi-bus radial architecture is in practice very relevant for large-area distribution microgrids. Summarily, the improved communicated-based reactive power correction techniques are based primarily on two types of correction mechanisms: one based on the adjustment of droop parameters (e.g., droop coefficient or dispatch command); one based on virtual output impedance (VOI) integrated droop control and through adjusting the VOI value. Examples of the former type include the decentralized control based dispatch command adjustment [5], adaptively tuned droop coefficient [6], optimal no-load reference through primal-dual interior-point method [7], a two-layer consensus algorithm with no-load reference adjustment [8], a distributed-averaging droop control with adjustable dispatch [9], and a consensus control with local voltage restoration and reactive power mismatch correction [10]. Differently, a consensus-based power sharing control is proposed in [11] and [12] through output currents mismatch. In addition, [13] has introduced a fundamentally-different distributed control scheme that uses the output voltage reference derived directly from the distributed errors instead of following the usual droop mechanism. It was however reported that the system's equilibrium and stability has subsequently become heavily dependent on the choice of control parameters.

VOI based control schemes were first introduced in [14] and [15]. These methods have assumed a parallel architecture and therefore only considered the mismatch of output/feeder impedances but not network impedances. A similar fixed-

Manuscript received September 11, 2019; revised December 10, 2019; accepted January 28, 2020. Date of publication February 6, 2020; date of current version May 20, 2020. This work was supported by the Fundamental Research Grant Scheme under Grant FRGS/1/2016/TK07/USMC/02/1 awarded by the Ministry of Higher Education, Malaysia. Paper no.-TEC00932-2019 (*Corresponding author: Chee Shen Lim.*)

Yi Chyn Cassandra Wong and Chee Shen Lim are with the University of Southampton Malaysia, Iskandar Puteri 79200, Malaysia (e-mail: y.c.c.wong@soton.ac.uk; c.s.lim@soton.ac.uk).

Mihai Dragos Rotaru is with the Institute of Microelectronics, A*STAR 627590, Singapore (e-mail: mihai_dragos_rotaru@ime.a-star.edu.sg).

Andrew Cruden is with Energy Technologies Research Group, University of Southampton, Southampton SO17 1BJ, U.K. (e-mail: a.j.cruden@soton.ac.uk).

Xin Kong is with Experimental Power Grid Centre of ERI@N, Nanyang Technological University, Singapore 627590, Singapore (e-mail: xin.kong@ntu.edu.sg).

Color versions of one or more of the figures in this article are available online at <http://ieeexplore.ieee.org>.

Digital Object Identifier 10.1109/TEC.2020.2972002

virtual-impedance techniques have been reported in [3] and [16] but only for microgrids with unchanging, i.e., non-plug-and-play, parallel architecture (owing to the line impedance parameter requirement). A communication-less offline genetic-algorithm-based VOI scheme for a radial microgrid is proposed in [17]. Similarly, [18] has reported a communication-less particle-swarm-optimization-based droop control with fixed-VOI for power sharing improvement. However, their extension to microgrids with changing topology is also not possible. Some other schemes that focus on unbalance and/or harmonic power sharing can be found in [2], [19], [20]. In addition, [21] has shown that the virtual impedance value is critical in grid-connected mode (not within the scope of this work) and they should be designed to be kept within the desired range to prevent instability.

As far as accurate reactive power sharing in an islanded radial microgrid is concerned, [17], [22]–[26] are relevant ([26] only focuses on non-changing network topology). Note that some literature (e.g., [23]) have used the term “mesh” instead of “radial” [27]. The latter seems to be a more usual definition to describe the topology of the network under consideration, and hence is the one being used in what follows. An adaptive VOI control with centralized secondary integrator control is presented in [25]. The work has shown that by equating the virtual resistance to the virtual reactance and by adjusting their values through integral control, the reactive power can be made equal. Another similar centralized scheme is proposed in [22]. This work concludes that reactive power sharing can be corrected by adjusting the virtual resistance alone (through proportional-integral control) but keeping the virtual reactance constant. Another centralized secondary control supplemented adaptive VOI scheme is proposed in [23]. The work achieves the correction by adjusting the virtual reactance (through proportional-integral control) while keeping the ratio of virtual resistance/reactance constant. In the distributed VOI scheme proposed by [24], it is shown that reactive power sharing correction can be realized by adjusting both the virtual resistance and reactance based on the distributed reactive power sharing errors (again, through proportional-integral control). Two practical issues are concluded here: there is no systematic way in determining the ratio of virtual reactance/resistance; tuning of the coupling and proportional-integral gains have not been discussed comprehensively (e.g., [25] highlighted that the integral gain has to be set small to ensure stability; [22]–[24] reported that, with a fixed static component, the dynamic component is deliberately tuned via a small integral gain).

The work intends to contribute in three aspects. Firstly, this work will visit the problem through the concept of droop equivalent impedance. It will be shown that, as far as reactive power sharing of an islanded radial microgrid is concerned, there is never a need to have both virtual reactance and resistance, but only either of them is sufficient to correct the reactive power sharing. Secondly, the proposed control scheme adopts a single consensus integral action without needing any proportional-integral controllers. This simplifies the gain tuning process of the distributed system. Thirdly, as mentioned in [9], pure-droop-based power control is non-linear, hence some

forms of linearization are required to establish the behavior of the voltage/power towards the coupling gain. The proposed adaptive-VOI-based power control has an additional non-linear behavior due to the adaptive VOI nature. Hence the coupling gain tuning would be a more critical issue. This work establishes a systematic guideline that determines the approximate range of stable coupling gain. In essence, the guideline first linearizes the non-linear system about the probable operating regions, then establishes the range of coupling gain that ensures convergence through the standard linear consensus theorem.

The remaining of this paper is organized as follows. Section II introduces the fundamentals of consensus algorithm. Section III introduces the novel droop equivalent impedance together with other commonly known impedances. Section IV discusses the consensus VOI-based control scheme and the coupling gain tuning guideline. Section V introduces the islanded microgrid network, the selected primary controls, and the results under three test cases: static and transient load, plug-and-play capability, and communication delay. Section VI concludes the paper.

II. PRELIMINARIES OF CONSENSUS CONTROL

The communication network of a microgrid can be modeled as a graph with edges corresponding to the information flow between the DERs, denoted as the nodes. The graph is generally expressed as $G = (V_G, E_G, A_G)$ with a set of N nodes $V_G = \{v_1, v_2, \dots, v_N\}$, a set of edges $E_G \subset V_G \times V_G$ and an adjacency matrix $A_G = [a_{ij}] \in \mathbb{R}^{N \times N}$. The edges E_G denote the communication links between DERs and each edge $(v_j, v_i) \in E_G$ represents the information flow from node j to node i , is associated with a weight a_{ij} with $a_{ij} > 0$ if $(v_j, v_i) \in E_G$, otherwise $a_{ij} = 0$. Node j is called a neighbor of node i if $(v_j, v_i) \in E_G$ and the set of neighbors of node i is denoted as $N_i = \{v_j: (v_j, v_i) \in E_G\}$. The graph is termed to be undirected if $(v_j, v_i) \Rightarrow (v_i, v_j) \in E_G$; otherwise directed. The in-degree matrix is defined as $D = \text{diag}\{d_i\} \in \mathbb{R}^{N \times N}$ with $d_i = \sum_{j \in N_i} a_{ij}$ and hence, the Laplacian matrix of the graph is defined as $L_G = D - A_G$.

Consider the first-order discrete-time consensus algorithm

$$\begin{aligned} x_i(k+1) &= x_i(k) + \delta_i(k) \\ \delta_i(k) &= -c \sum_{j \in N_i} a_{ij} [x_i(k) - x_j(k)] \end{aligned} \quad (1)$$

where x_i and δ_i denote the state variable and control input. It is established that consensus is guaranteed if the coupling gain c satisfies the sufficient condition [28]

$$c < \frac{1}{d_{\max}} \quad (2)$$

where $d_{\max} = \max(D)$. Suppose that information is passed between the DERs with a time-delay $\tau > 0$, the consensus algorithm can be written as

$$\begin{aligned} x_i(k+1) &= x_i(k) + \delta_i(k) \\ \delta_i(k) &= -c \sum_{j \in N_i} a_{ij} [x_i(k-\tau) - x_j(k-\tau)] \end{aligned} \quad (3)$$

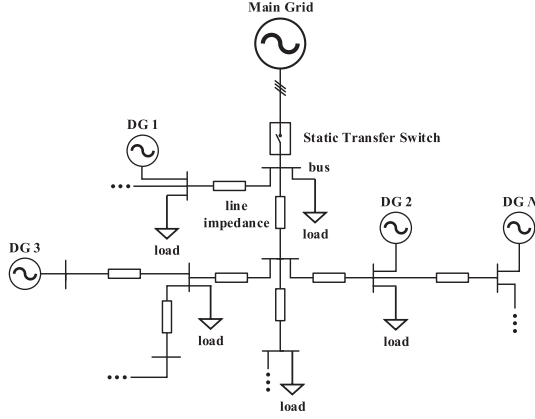


Fig. 1. Architecture of a multi-bus radial microgrid.

The time-delayed consensus control is said to be globally asymptotically stable if and only if [24], [29]–[31]

$$0 < \tau < \frac{\pi}{2\lambda_{max}c} \quad (4)$$

where λ_{max} is the maximum eigenvalue of the communication graph's Laplacian matrix L_G .

III. CONTROL MODELING AND ANALYSIS OF MULTI-BUS RADIAL MICROGRID

A microgrid is considered radial structured with DERs and/or loads connected to the local distributed network at various nodes. Fig. 1 depicts the configuration/topology of an islanded multi-bus radial microgrid composed of N number of DERs and loads.

A. Primary Control and Virtual Output Impedance Integrated Droop Control

The primary control of a VOI-controlled DER includes a power control, an output voltage control, an inverter current control and a virtual output impedance control, as shown in Fig. 2. During islanded operation, DERs achieve autonomous power sharing through the standard active power-frequency (P - f) and reactive power-voltage (Q - V) droop control [1], [32], [33], expressed as

$$\begin{aligned} \omega_i &= \omega_i^* - mP_i \\ V_i &= V_i^* - nQ_i \end{aligned} \quad (5)$$

where ω_i and V_i are the per-unit operating frequency and the droop voltage amplitude (normalized to network's phase peak voltage) of i th DER, ω_i^* and V_i^* are corresponding per-unit no-load frequency and voltage reference, and m and n are the per-unit droop coefficients. Typically, m and n are commonly shared among the DERs in the same microgrid. P_i and Q_i are the filtered per-unit active and reactive output powers (normalized to the respective kVA rating).

Since all the inner-loop controllers operate in the synchronous reference frame, the direct (d) and quadrature (q) notations will be used in what follows. In each DER, the synchronous reference frame is made aligned to the droop output voltage vector ($u_{odi}^d =$

$u_{od}^d + ju_{oqi}^d$, u_{odi}^d and u_{oqi}^d being the d - and q -axis components normalized to the phase peak voltage), the voltage components can be expressed as:

$$\begin{aligned} u_{odi}^d &= V_i \\ &= V_i^* - nQ_i \\ u_{oqi}^d &= 0 \end{aligned} \quad (6)$$

The synchronous reference frame's angular position is obtainable from the respective droop frequency in (5) after synchronizing with the microgrid during first connection.

The active and reactive output powers with low-pass filtering (and with amplitude-invariant rotational transformation) can be written as

$$\begin{aligned} \tau_c \frac{dP_i}{dt} + P_i &= \frac{3}{2} (u_{odi}i_{odi} + u_{oqi}i_{oqi}) \\ \tau_c \frac{dQ_i}{dt} + Q_i &= \frac{3}{2} (u_{oqi}i_{odi} - u_{odi}i_{oqi}) \end{aligned} \quad (7)$$

where τ_c is the low pass filter's cutoff period and u_{odi} , u_{oqi} , i_{odi} , and i_{oqi} are the d - and q -axis measured output voltage and current components.

VOI control works by regulating the output voltage references from the standard droop control, given as

$$\begin{aligned} u_{odi}^* &= u_{odi}^d - u_{vdi} \\ u_{oqi}^* &= -u_{vqi} \end{aligned} \quad (8)$$

where u_{odi}^* and u_{oqi}^* are the output voltage references after the VOI, and u_{vdi} and u_{vqi} are the voltage drop components across the VOI. The electrical steady state values (i.e., \bar{u}_{vdi} and \bar{u}_{vqi} , after assuming $d/dt = 0$) are calculated as

$$\begin{aligned} \bar{u}_{vdi} &= R_{vi}i_{odi} - \omega_s L_{vi}i_{oqi} \\ \bar{u}_{vqi} &= R_{vi}i_{oqi} + \omega_s L_{vi}i_{odi} \end{aligned} \quad (9)$$

where ω_s is the nominal angular frequency in rad/s, and R_{vi} and L_{vi} are the virtual resistance and inductance.

B. Reactive Power Sharing Strategy Based on the Droop Equivalent Impedance Concept

In per-phase quantity, we first introduce the following impedance terms: droop equivalent impedance ($Z_{ei}^d = R_{ei}^d + jX_{ei}^d$), physical equivalent output impedance ($Z_{ei} = R_{ei} + jX_{ei}$), virtual output impedance ($Z_{vi} = R_{vi} + jX_{vi}$), and feeder impedance ($Z_{ofi} = R_{ofi} + jX_{ofi}$) of i th DER. The latter three can be seen directly from Fig. 3. In Fig. 3(a), a commonly seen single-line diagram that consists of the virtual output impedance and the physical feeder impedance is shown. In Fig. 3(b), an equivalent single-line diagram that replaces both the feeder impedance and the grid connection with a physical equivalent impedance, is shown. Since the voltage vector at node A is synchronized to the droop angular position (i.e., $u_{oqi}^d = 0$ V), the phase voltage amplitude can be obtained directly from the d -axis component, which in turn equals to the droop output voltage reference (as reflected in Eq. (6)). The concept of droop equivalent impedance is introduced by first defining the

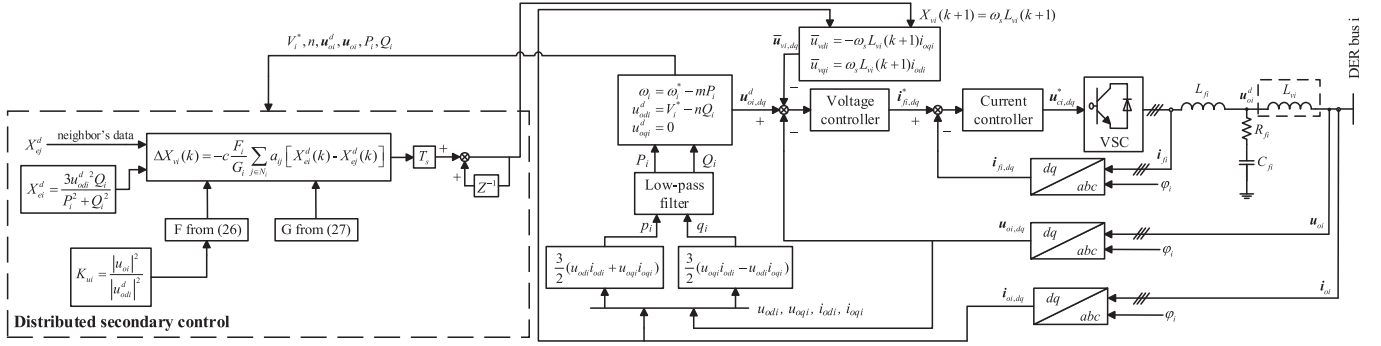


Fig. 2. Schematic diagram of the proposed consensus virtual output impedance control of a droop-based distributed energy resource.

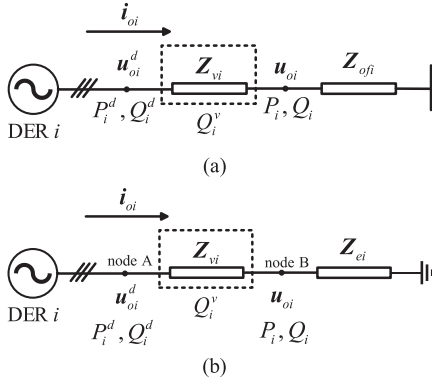


Fig. 3. (a) Single line diagram for an inverter-based DER with a virtual output impedance (Z_{vi}) and a feeder impedance (Z_{ofi}); (b) the corresponding single line diagram with the virtual output impedance and a physical equivalent impedance as seen by the DER output towards the microgrid network, Z_{ei} .

following:

$$Z_{ei}^d = \frac{3u_{odi}^2}{S_i^*} = \frac{3u_{odi}^2}{P_i - jQ_i} \quad (10)$$

where $S_i (= P_i + jQ_i)$ is the fundamental apparent power at node B and u_{odi} is droop output voltage at node A. It is important to highlight that this impedance is different from the commonly known physical equivalent impedance Z_{ei} , defined below (with u_{oi} being the normalized output voltage after VOI):

$$Z_{ei} = \frac{3u_{oi}^2}{S_i^*} = \frac{3u_{oi}^2}{P_i - jQ_i} \quad (11)$$

A common design principle of droop control is that all the generating sources should be adopting the same droop profile (although it is acknowledged here that some variations do exist in some microgrid literature). Upon steady state before reactive power correction, since droop frequency is a global uniform variable, the active power can always be accurately (i.e., proportionately) shared among DERs [1], [9], [23], [25]. This gives (with t represents time):

$$\lim_{t \rightarrow \infty} [P_1(t) = P_2(t) = \dots = P_N(t)] \quad (12)$$

However, owing to potentially significant voltage discrepancies at their points of coupling in a multi-bus radial microgrid, the reactive power, if left uncompensated, will not be proportionately shared among the DERs. Upon success correction by the VOI-based control schemes, one can expect that

- i) the reactive power will be proportionately shared:

$$\lim_{t \rightarrow \infty} [Q_1(t) = Q_2(t) = \dots = Q_N(t)] \quad (13)$$

- ii) the droop output voltage reference for all DERs will have a common value:

$$\lim_{t \rightarrow \infty} [u_{od1}^d(t) = u_{od2}^d(t) = \dots = u_{odN}^d(t)] \quad (14)$$

With conditions (12–14), it can be realised from (10) that the droop equivalent impedances of all DERs must also converge to a common value:

$$\lim_{t \rightarrow \infty} [Z_{e1}^d(t) = Z_{e2}^d(t) = \dots = Z_{eN}^d(t)] \quad (15)$$

Some previous works [6], [16], [26], [31] have exploited the concept of converging the DERs' equivalent impedance of ($Z_{vi} + Z_{ofi}$) (see Fig. 3(a)) to a common value to realise proportional reactive power sharing. However, since the concept requires a common point of coupling, it can be deduced that the method is not applicable to a multi-bus radial microgrid. The work intends to introduce a novel concept to address this limitation, as explained next. One useful observation of (15) is that if the virtual output impedance Z_{vi} can be controlled in such a way that the droop equivalent impedance Z_{ei}^d equalizes, then the reactive power will be shared proportionately. On this basis, we propose that the following consensus protocol:

$$\begin{aligned} \dot{Z}_{ei}^d &= \delta_i \\ \delta_i &= -c_i \sum_{j \in N_i} a_{ij} (Z_{ei}^d - Z_{ej}^d) \end{aligned} \quad (16)$$

Based on (16), it can be deduced that one can drive Z_{ei}^d towards a consensus value, then the proportional reactive power sharing will be achieved. Nevertheless, it was found that (16) can be simplified further. This is explained by first expanding (10):

$$R_{ei}^d + jX_{ei}^d = \left(\frac{3u_{odi}^2 P_i}{P_i^2 + Q_i^2} \right) + j \left(\frac{3u_{odi}^2 Q_i}{P_i^2 + Q_i^2} \right) \quad (17)$$

Based on (12), (14) and (17), it can be deduced that:

- i) if the droop equivalent reactance (X_e^d) of all DERs were to converge to a common value, a proportional reactive power sharing will be achieved. With these conditions, the droop equivalent resistance (R_e^d) will also equalize;
- ii) if the droop equivalent resistance (R_e^d) of all DERs were to converge to a common value, a proportional reactive power sharing will be achieved. With these conditions, the droop equivalent reactance (X_e^d) will also equalize.

In essence, this means that as far as reactive power correction is concerned, there is seldom a need to regulate both droop equivalent impedance components. In fact, any attempt to regulate both together would be an ill-posed problem and will result in control instability. This observation somewhat agrees with most previous works, e.g., changing R_v fixed X_v [17], [22], [34]; fixed R_v/X_v ratio [23]–[25]. In [24], although there are individual virtual resistance and reactance control loops, however, the two virtual impedance components are inherently coupled since their integral loop are common (which leads to an approximately fixed dynamic R_v/X_v ratio). Therefore, moving forward, it is proposed here that only the droop equivalent reactance is considered, i.e.:

$$\dot{X}_{ei}^d = -c \sum_{j \in N_i} a_{ij} (X_{ei}^d - X_{ej}^d) \quad (18)$$

Note that one may also use the droop equivalent resistance as the consensus error, but it can be seen from (17) that the droop equivalent reactance has a more direct impact on the control of reactive power and hence is the preferred choice.

IV. ADAPTIVE VIRTUAL OUTPUT IMPEDANCE CONTROL BASED ON DROOP EQUIVALENT IMPEDANCE CONSENSUS

A. Proposed Consensus-VOI Control Based on Droop Equivalent Impedance

Most of the existing consensus-based reactive power correction schemes are based on the reactive power values, e.g., Q_i as in [5], [8], [13]; and $n_i Q_i$ [10], [24], [31]. Based on the deduction in Section III, it is therefore proposed here that the consensus protocol is applied to the droop equivalent reactance X_{ei}^d . However, it can be easily confirmed that (18) is still not suitable for implementation as there is no direct mean to control X_{ei}^d but only X_{vi} is directly controllable. Hence, their relationship is first analyzed in what follows.

One can define the reactive power injected by the DER (from node A) in terms of the virtual output impedance and the physical equivalent impedance (as shown in Fig. 3(b)):

$$Q_i^d = \frac{3u_{odi}^2 (X_{ei} + X_{vi})}{R_{ei}^2 + (X_{ei} + X_{vi})^2} \quad (19)$$

where the physical equivalent resistance R_{ei} and reactance X_{ei} can be expanded from (11) to become

$$R_{ei} = \frac{3u_{oi}^2 P_i}{P_i^2 + Q_i^2} \quad \text{and} \quad X_{ei} = \frac{3u_{oi}^2 Q_i}{P_i^2 + Q_i^2} \quad (20)$$

Then, the virtual reactive power across X_{vi} can be written as

$$Q_i^v = \frac{3i_{oi}^2 X_{vi}^2}{X_{vi}} \quad (21)$$

where the normalized output current i_{oi} can be expressed in terms of u_{odi}^d and the physical equivalent impedance as:

$$i_{oi}^2 = \frac{u_{odi}^2}{R_{ei}^2 + (X_{ei} + X_{vi})^2} \quad (22)$$

Then, a relationship between X_{vi} and the reactive output power Q_i can be expressed as

$$Q_i = Q_i^d - Q_i^v = \frac{3u_{odi}^2 X_{ei}}{R_{ei}^2 + (X_{ei} + X_{vi})^2}$$

$$X_{vi} = \sqrt{\frac{3u_{odi}^2 X_{ei}}{Q_i} - R_{ei}^2 - X_{ei}} \quad (23)$$

Substitute (6) and (20) into (23) results in

$$X_{vi} = \sqrt{\frac{3(V_i^* - nQ_i)^2 K_{ui} \frac{3(V_i^* - nQ_i)^2 Q_i}{P_i^2 + Q_i^2}}{Q_i} - \left(K_{ui} \frac{3(V_i^* - nQ_i)^2 P_i}{P_i^2 + Q_i^2} \right)^2 - K_{ui} \frac{3(V_i^* - nQ_i)^2 Q_i}{P_i^2 + Q_i^2}} \quad (24)$$

A factor K_{ui} is introduced into the expression in order to simplify the relationship between X_{vi} and Q_i .

$$K_{ui} = \frac{R_{ei}}{R_{ei}^d} = \frac{X_{ei}}{X_{ei}^d} = \frac{|u_{oi}|^2}{|u_{odi}^d|^2} \quad (25)$$

Notice that K_{ui} value remains typically near to one as the virtual voltage drop is typically kept small as compared to the rated voltage value. On this basis, if both K_{ui} and P_i do not change significantly during Q_i correction (due to X_{vi} adjustment), the dynamical relationship between X_{vi} and Q_i can be approximated to a linear, operating-point-dependent relation through time-derivative of (24):

$$\dot{X}_{vi} = F_i(V_i^*, n, P_{oi}, Q_{oi}, K_{ui}) \cdot \dot{Q}_i \quad (26)$$

where the full expression of F_i is given in the appendix. P_{oi} and Q_{oi} are the power values at the steady state operating point about which the linearization is made.

Next, the relationship between X_{ei}^d and Q_i is to be established. From X_{ei}^d expression in (17), and assume that the active power P_i does not change significantly during Q_i correction, the dynamical relationship between X_{ei}^d and Q_i can again be approximated to a linear, operating-point-dependent relationship:

$$\dot{X}_{ei}^d = G_i(V_i^*, n, P_{oi}, Q_{oi}) \cdot \dot{Q}_i \quad (27)$$

where the full expression of G_i is given in the appendix. Then, with (26) and (27), the relationship between X_{vi} and X_{ei}^d can be given by

$$\dot{X}_{vi} = H_i(V_i^*, n, P_{oi}, Q_{oi}, K_{ui}) \cdot \dot{X}_{ei}^d \quad (28)$$

where $H_i = F_i/G_i$. Based on the basic principle of linearization about an operating point, (28) gives a simplified linear relationship between the time-derivative of X_{vi} and time-derivative of X_{ei}^d . By substituting (28) into (18), and rewrite the consensus algorithm, we get:

$$\dot{X}_{vi} = -\kappa_i \sum_{j \in N_i} a_{ij} (X_{ei}^d - X_{ej}^d) \quad (29)$$

where $\kappa_i = cH_i(V_i^*, n, P_{oi}, Q_{oi}, K_{ui})$. Reactive power correction through adaptive VOI is fundamentally a non-linear control problem. This is reflected in the coupling gain κ_i (29) through its operating-point dependent nature. Upon first-order discretization, the virtual output reactance can be found:

$$\begin{aligned} X_{vi}(k+1) &= X_{vi}(k) + T_s \Delta X_{vi}(k) \\ \Delta X_{vi}(k) &= -\kappa_i \sum_{j \in N_i} a_{ij} [X_{ei}^d(k) - X_{ej}^d(k)] \end{aligned} \quad (30)$$

It is well-established that consensus stability is guaranteed if sufficient condition (2) is met. However, as revealed from (29), the effective local gain κ_i for a given global coupling gain c is essentially dependent on the local operating point. There are two possible ways of setting the local gain κ_i : (i) compute the local H_i value on the fly and update κ_i accordingly; (ii) consider the smallest value of $H_{i,\min}$ for a given range of operating points and use $cH_{i,\min}$ as the global gain κ (common to all DERs). This work considers the second way as it is expected to give a more reliable consensus control but with a small penalty on the correction dynamics. The possible values of κ for a given range of operating points (i.e., different P_o and Q_o , with a rated power factor of 0.8) is summarized in Table I. The calculation assumes that u_{oi} is fixed at 0.9 and the load power factor is always kept equal or above 0.8 (grey-shaded column is below 0.8). Based on the previous analysis, it is recommended that the coupling gain κ_i should be chosen at low-loading (e.g., one with 10% P_{rated} and 5% Q_{rated}).

Lastly, communication delay is inevitable in practice. Based on (3), the proposed consensus control with communication delay can be expressed as:

$$\Delta X_{vi}(k) = -\kappa_i \sum_{j \in N_i} a_{ij} [X_{ei}^d(k-\tau) - X_{ej}^d(k-\tau)] \quad (31)$$

V. RESULTS AND DISCUSSION

An islanded microgrid network and the corresponding DERs' local controllers are implemented in *DIgSILENT PowerFactory* while the distributed secondary control is in *Python*. *MatriconOPC* is used as the OPC server to facilitate the information exchange among the DERs. *DIgSILENT PowerFactory* and *Python* are the OPC clients and they interface with the OPC server through respective interfaces (*ComLink* in *PowerFactory* and *OpenOPC* in *Python*). See [35] and reference therein for details.

The proposed secondary reactive power sharing control is verified on an islanded microgrid modified from the IEEE 34 Node Test Feeder [36]. Basic parameters of the DERs and the

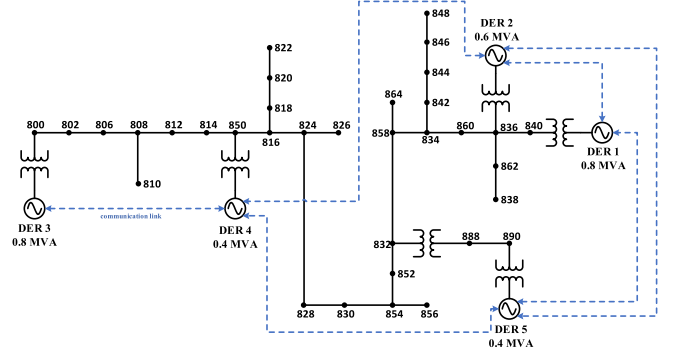


Fig. 4. A large-area islanded microgrid modified from the IEEE 34 Node Test Feeder (with actual network impedances).

modified microgrid network are tabulated in Table II. Some of the network features are highlighted below:

- a) DERs with different power ratings are connected to the islanded microgrid via Y-Y, 400 V/24.9 kV (4.16 kV for the short lateral) transformer. Their placement in the network, as shown in Fig. 4, are based on *PV* curve analysis of *PowerFactory* [37];
- b) Shunt capacitors from the original IEEE 34 Node Test Feeder are kept in the network (at bus 844 and 848) and they are of a total rating of 0.75 MVar;
- c) *LC* filters with resistive damping are used as the switching harmonic filters,
- d) The Laplacian matrix of the communication graph is

$$L_G = \begin{bmatrix} 2 & -1 & 0 & 0 & -1 \\ -1 & 3 & 0 & -1 & -1 \\ 0 & 0 & 1 & -1 & 0 \\ 0 & -1 & -1 & 3 & -1 \\ -1 & -1 & 0 & -1 & 3 \end{bmatrix} \quad (32)$$

Fig. 4 depicts the single-line diagram of the large-area microgrid modified from IEEE 34 Node Test Feeder.

As explained in Section III-B, Fig. 5 provides an evidence proving that the system will become unstable if one attempts to converge, through consensus control, the DERs' droop equivalent impedances (by independently regulating both virtual impedance components). It has also been verified in the simulation that the droop equivalent resistance can regulate the reactive power and produce a result somewhat similar to Figs. 6–8. However, as explained, this work recommends the use of droop equivalent reactance, which entails the derivation of (19)–(30). With this choice, the steady state and load change with coupling gain consideration, the plug-and-play feature, and the effect of communication link delay will be examined further.

A. Case Study 1: Default Steady State and Load Change With Coupling Gain Consideration

A total load of 1.52 MW and 1.27 MVar passive load are present in the islanded microgrid network. Before $t = 10$ s, the DERs are initially controlled through the standard droop scheme

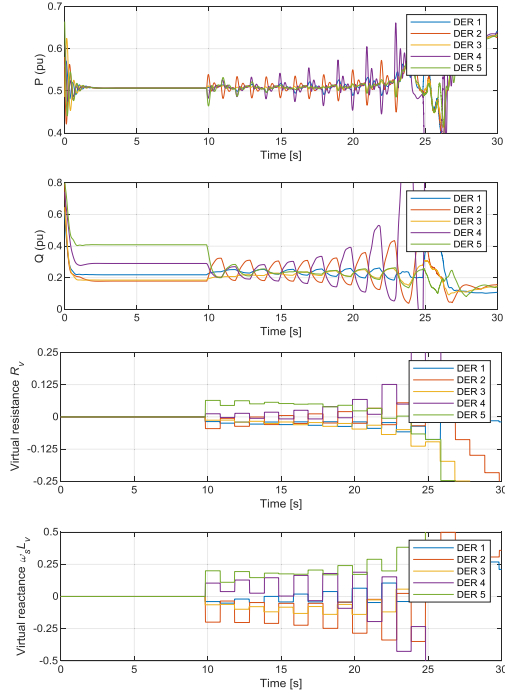


Fig. 5. System instability caused by the attempt to converge the droop equivalent impedances by regulating both virtual impedances independently.

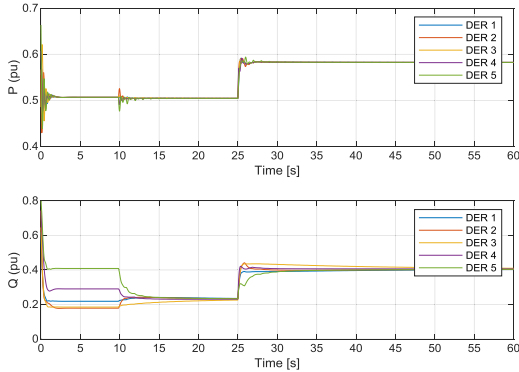


Fig. 6. Default steady state and load up-stepping with fixed κ : active and reactive output power of DERs for the standard droop control (before 10 s) without correction (after 10 s) with correction and (at 25 s) load step change.

without any reactive power sharing correction. It can be established from Fig. 6 that the active power is always proportionally shared, but the reactive power is not. At $t = 10$ s, the proposed reactive power sharing control scheme is activated. Based on the established tuning guideline, κ is globally tuned to 0.103. It is seen clearly that the load reactive power is now proportionally shared among the DERs. The corresponding virtual reactance profiles in Fig. 7 show that the virtual reactance can take both positive and negative values.

Traces in Fig. 8 show that upon steady state the droop voltage references also equalize but the MV bus voltages have been lowered further. Subsequently, an additional load is connected to bus 814 at $t = 25$ s during which the total load demand of the islanded microgrid is increased to $1.75 + j1.66$ MVA. Figs. 6–8

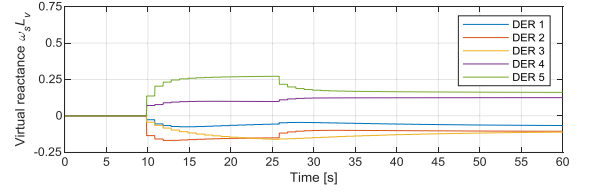


Fig. 7. Default steady state and load up-stepping with fixed κ : adaptive virtual reactance generated.

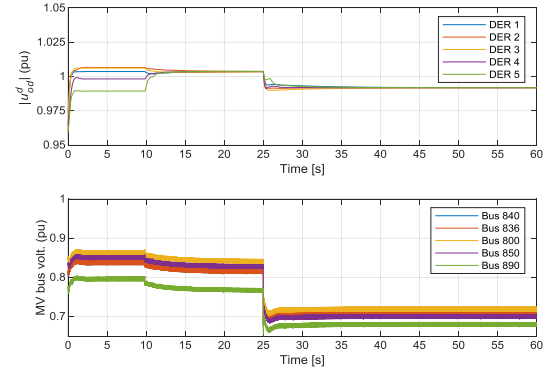


Fig. 8. Default steady state and load up-stepping with fixed κ : the corresponding droop output voltage references and voltage magnitudes at respective MV buses.

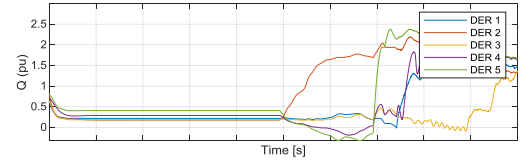


Fig. 9. Default steady state with fixed $\kappa = 0.3$: DERs' reactive output power.

show that the proposed control scheme responds accordingly without noticeable large transients.

Fig. 9 shows that control instability occurs when κ is globally tuned to 0.3 despite that κ is less than $1/d_{\max}$ (as in (2)). This is due to the fact that the dynamical relationship between X_{vi} and X_{ei}^d has not been accounted for in the consensus protocol (30), the consensus theorem, e.g., (2), therefore cannot be applied directly. On the other hand, the performance of an adaptively tuned control scheme (i.e. with local κ_i gain defined by the local operating points of u_{odi}^d , K_{ui} , P_{oi} , and Q_{oi}) is shown in Fig. 10. A stable, underdamped performance is noted. This finding agrees with the theoretical expectation in Section IV. However, as mentioned, in order to ensure a stable consensus control, it is preferable to tune gain κ globally to the smallest value (i.e., being 0.103 in Table I). This is done for subsequent studies.

B. Case Study 2: Plug-and-Play Capability

The dynamic performance of the proposed VOI control scheme considering the plug-and-play capability is studied here.

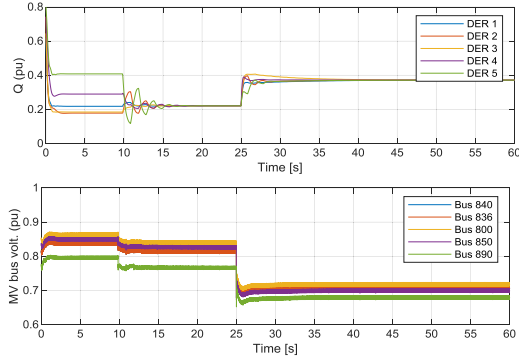


Fig. 10. Default steady state and load up-stepping with adaptively tuned κ : DERs' reactive output power and voltage magnitudes at respective MV buses.

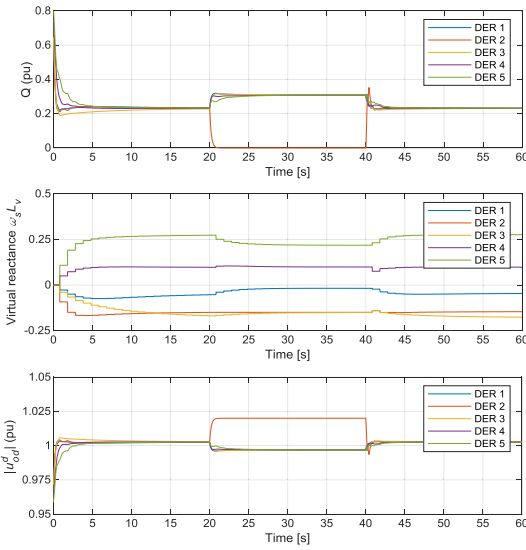


Fig. 11. DER 2 plug-and-play capability: DERs' reactive output power, adaptive virtual reactance generated and the corresponded droop output voltage references.

Notice that a DER's disconnection means that all communication links between the DER and the remaining DERs are lost. In order to ensure a stable consensus system, it is assumed that the communication links among the remaining DERs still maintain a connected graph.

The islanded microgrid operates under default loading condition with the proposed control scheme activated from $t = 0$ s. At $t = 20$ s, DER 2's circuit breaker is opened, and it is re-closed at $t = 40$ s. As seen in Fig. 11, proportional reactive power sharing is retained by the remaining DERs. It can be noticed that the reactive powers of the remaining DERs increase and their corresponding droop voltage reference decreases. With the reconnection of DER 2 at $t = 40$ s, the reactive load power is almost instantaneously re-distributed among the DERs with some small overshoots.

C. Case Study 3: Effect of Communication Link Delays

The robustness of the distributed control scheme against communication link delays is examined next. Based on the consensus

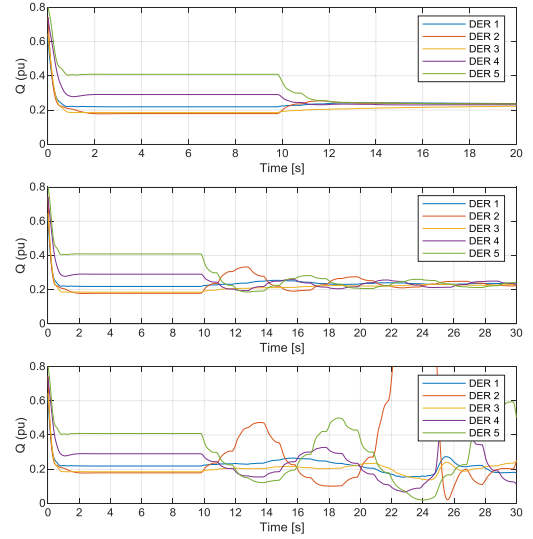


Fig. 12. DERs' reactive output power with communication link time delay of (top) 0.6 s (mid) 1.4 s and (bottom) 1.8 s.

theorem (3–4) and (31), the maximum allowable time delay is $\tau_{\max} = 1.75$ s (i.e., with the maximum eigenvalue of $\lambda_{\max} = 4.48$ and the coupling gain $c = 0.2$). In this case study, the time delay τ is set to be 0.6, 1.4 and 1.8 s, respectively. Fig. 12 shows the corresponding reactive output powers of the DERs with the proposed control scheme activated at $t = 10$ s. It can be seen that proportional reactive power sharing is achieved for the case of $\tau = 0.6$ s ($\ll \tau_{\max}$). For the case of $\tau = 1.4$ s, power oscillation can be seen before the final steady state. However, for the case of $\tau = 1.8$ s ($> \tau_{\max}$), the islanded microgrid is unable to maintain a stable operation. This essentially verifies the communication delay discussion described in Sections II and III. It is worth highlighting here that the compliance is only possible if the control gain κ is tuned by the proposed tuning guideline; if one were not to consider the operating-point-dependent H , or were to append proportional-integral controllers subsequent to the consensus control, (4) will not be applicable.

VI. CONCLUSION

In this paper, we propose a novel droop-equivalent-reactance-based consensus adaptive VOI control to realize accurate reactive power sharing among DERs in a radial microgrid. The control scheme only needs a sparse communication structure and eliminates the needs for a central control. The proposed control scheme does not rely on the local proportional-integral controllers and therefore there is effectively one coupling gain to be tuned. A systematic tuning guideline with linearization about practical operating points is established and proven. The proposed control scheme has been tested for different test scenarios: steady state, transients (load up-stepping), plug-and-play, and communication delay, and the results successfully justify the claims.

APPENDIX

$$\begin{aligned}
F_i = & -\frac{9}{\sqrt{\frac{9K_{ui}(V_i^* - nQ_{oi})^4}{P_{oi}^2 + Q_{oi}^2} - \frac{9K_{ui}^2 P_{oi}^2 (V_i^* - nQ_{oi})^4}{(P_{oi}^2 + Q_{oi}^2)^2}}} \\
& \times \left[\frac{K_{ui}Q_{oi}(V_i^* - nQ_{oi})^4}{(P_{oi}^2 + Q_{oi}^2)^2} - \frac{2K_{ui}^2 P_{oi}^2 Q_{oi}(V_i^* - nQ_{oi})^4}{(P_{oi}^2 + Q_{oi}^2)^3} \right. \\
& + \frac{2K_{ui}(V_i^{*2}n - 3V_i^{*2}n^2Q_{oi} + 3V_i^*n^3Q_{oi}^2 - n^4Q_{oi}^3)}{P_{oi}^2 + Q_{oi}^2} \\
& \left. - \frac{2K_{ui}^2 P_{oi}^2 (V_i^{*2}n - 3V_i^{*2}n^2Q_{oi} + 3V_i^*n^3Q_{oi}^2 - n^4Q_{oi}^3)}{(P_{oi}^2 + Q_{oi}^2)^2} \right] \\
& + \frac{6K_{ui}Q_{oi}^2(V_i^* - nQ_{oi})^2}{(P_{oi}^2 + Q_{oi}^2)^2} \\
& - \frac{3K_{ui}(V_i^{*2} - 4V_i^*nQ_{oi} + 3n^2Q_{oi}^2)}{P_{oi}^2 + Q_{oi}^2} \quad (33)
\end{aligned}$$

$$\begin{aligned}
G_i = & \frac{3V_i^{*2}P_{oi}^2 - 3V_i^{*2}Q_{oi}^2 - 12V_i^*nP_{oi}^2Q_{oi} + 9n^2P_{oi}^2Q_{oi}^2 + 3n^2Q_{oi}^4}{(P_{oi}^2 + Q_{oi}^2)^2} \quad (34)
\end{aligned}$$

REFERENCES

- [1] Y. Han, H. Li, P. Shen, E. A. A. Coelho, and J. M. Guerrero, "Review of active and reactive power sharing strategies in hierarchical controlled microgrids," *IEEE Trans. Power Electron.*, vol. 32, no. 3, pp. 2427–2451, Mar. 2017.
- [2] Y. Han, P. Shen, X. Zhao, and J. M. Guerrero, "An enhanced power sharing scheme for voltage unbalance and harmonics compensation in an islanded AC microgrid," *IEEE Trans. Energy Convers.*, vol. 31, no. 3, pp. 1037–1050, Sep. 2016.
- [3] Y. W. Li and C. N. Kao, "An accurate power control strategy for power-electronics-interfaced distributed generation units operating in a low-voltage multibus microgrid," *IEEE Trans. Power Electron.*, vol. 24, no. 12, pp. 2977–2988, Dec. 2009.
- [4] T. Qunais and M. K. Gharthamani, "Systematic modeling of a class of microgrids and its application to impact analysis of cross-coupling droop terms," *IEEE Trans. Energy Convers.*, vol. 34, no. 3, pp. 1632–1643, Sep. 2019.
- [5] Q. Shafiee, J. M. Guerrero, and J. C. Vasquez, "Distributed secondary control for islanded microgrids—a novel approach," *IEEE Trans. Power Electron.*, vol. 29, no. 2, pp. 1018–1031, Feb. 2014.
- [6] H. Mahmood, D. Michaelson, and J. Jiang, "Reactive power sharing in islanded microgrids using adaptive voltage droop control," *IEEE Trans. Smart Grid*, vol. 6, no. 6, pp. 3052–3060, Nov. 2015.
- [7] X. Yang, Y. Du, J. Su, L. Chang, Y. Shi, and J. Lai, "An optimal secondary voltage control strategy for an islanded multibus microgrid," *IEEE J. Emerg. Sel. Top. Power Electron.*, vol. 4, no. 4, pp. 1236–1246, Dec. 2016.
- [8] A. Bidram, A. Davoudi, and F. L. Lewis, "A multiobjective distributed control framework for islanded AC microgrids," *IEEE Trans. Ind. Inform.*, vol. 10, no. 3, pp. 1785–1798, Aug. 2014.
- [9] J. W. S.-Porco, Q. Shafiee, F. Dorfler, J. C. Vasquez, J. M. Guerrero, and F. Bullo, "Secondary frequency and voltage control of islanded microgrids via distributed averaging," *IEEE Trans. Ind. Electron.*, vol. 62, no. 11, pp. 7025–7038, Nov. 2015.
- [10] R. Han, L. Meng, G. F. Trecate, E. A. A. Coelho, J. C. Vasquez, and J. M. Guerrero, "Containment and consensus-based distributed coordination control to achieve bounded voltage and precise reactive power sharing in islanded AC microgrids," *IEEE Trans. Ind. Appl.*, vol. 53, no. 6, pp. 5187–5199, Dec. 2017.
- [11] M. A. Mahmud, M. J. Hossain, H. R. Pota, and A. M. T. Oo, "Robust nonlinear distributed controller design for active and reactive power sharing in islanded microgrids," *IEEE Trans. Energy Convers.*, vol. 29, no. 4, pp. 893–903, Dec. 2014.
- [12] M. S. Golsorkhi, Q. Shafiee, D. D. C. Lu, and J. M. Guerrero, "Distributed control of low-voltage resistive AC microgrids," *IEEE Trans. Energy Convers.*, vol. 34, no. 2, pp. 573–584, Jun. 2019.
- [13] J. Schiffer, T. Seel, J. Raisch, and T. Sezi, "Voltage stability and reactive power sharing in inverter-based microgrids with consensus-based distributed voltage control," *IEEE Trans. Control Syst. Technol.*, vol. 24, no. 1, pp. 96–109, Jan. 2016.
- [14] J. M. Guerrero, L. G. de Vicuna, J. Matas, M. Castilla, and J. Miret, "Output impedance design of parallel-connected UPS inverters with wireless load-sharing control," *IEEE Trans. Ind. Electron.*, vol. 52, no. 4, pp. 1126–1135, Aug. 2005.
- [15] J. M. Guerrero, J. Matas, L. G. de Vicuna, M. Castilla, and J. Miret, "Decentralized control for parallel operation of distributed generation inverters using resistive output impedance," *IEEE Trans. Ind. Electron.*, vol. 54, no. 2, pp. 994–1004, Apr. 2007.
- [16] J. He, Y. W. Li, J. M. Guerrero, F. Blaabjerg, and J. C. Vasquez, "An islanding microgrid power sharing approach using enhanced virtual impedance control scheme," *IEEE Trans. Power Electron.*, vol. 28, no. 11, pp. 5272–5282, Nov. 2013.
- [17] Y. Zhu, F. Zhuo, F. Wang, B. Liu, R. Gou, and Y. Zhao, "A virtual impedance optimization method for reactive power sharing in networked microgrid," *IEEE Trans. Power Electron.*, vol. 31, no. 4, pp. 2890–2904, Apr. 2016.
- [18] Z. Peng *et al.*, "Droop control strategy incorporating coupling compensation and virtual impedance for microgrid application," *IEEE Trans. Energy Convers.*, vol. 34, no. 1, pp. 277–291, Mar. 2019.
- [19] M. Savaghebi, A. Jalilian, J. C. Vasquez, and J. M. Guerrero, "Autonomous voltage unbalance compensation in an islanded droop-controlled microgrid," *IEEE Trans. Ind. Electron.*, vol. 60, no. 4, pp. 1390–1402, Apr. 2013.
- [20] M. Savaghebi, A. Jalilian, J. C. Vasquez, and J. M. Guerrero, "Secondary control scheme for voltage unbalance compensation in an islanded droop-controlled microgrid," *IEEE Trans. Smart Grid*, vol. 3, no. 2, pp. 797–807, Jun. 2012.
- [21] J. He and Y. W. Li, "Analysis, design, and implementation of virtual impedance for power electronics interfaced distributed generation," *IEEE Trans. Ind. Appl.*, vol. 47, no. 6, pp. 2525–2538, Dec. 2011.
- [22] Y. Zhu, B. Liu, F. Wang, F. Zhuo, and Y. Zhao, "A virtual resistance based reactive power sharing strategy for networked microgrid," in *Proc. Int. Conf. Power Electron. ECCE Asia*, 2015, pp. 1564–1572.
- [23] T. V. Hoang and H. H. Lee, "An adaptive virtual impedance control scheme to eliminate the reactive-power-sharing errors in an islanding meshed microgrid," *IEEE J. Emerg. Sel. Top. Power Electron.*, vol. 6, no. 2, pp. 966–976, Jun. 2018.
- [24] H. Zhang, S. Kim, Q. Sun, and J. Zhou, "Distributed adaptive virtual impedance control for accurate reactive power sharing based on consensus control in microgrids," *IEEE Trans. Smart Grid*, vol. 8, no. 4, pp. 1749–1761, Jul. 2017.
- [25] H. Mahmood, D. Michaelson, and J. Jiang, "Accurate reactive power sharing in an islanded microgrid using adaptive virtual impedances," *IEEE Trans. Power Electron.*, vol. 30, no. 3, pp. 1605–1617, Mar. 2015.
- [26] B. Liu, Z. Liu, J. Liu, R. An, and S. Song, "A novel microgrid power sharing scheme enhanced by a non-intrusive feeder impedance estimation method," in *Proc. Int. Power Electron. Conf.*, 2018, pp. 3924–3928.
- [27] D. K. Dheer, O. V. Kulkarni, S. Doolia, and A. K. Rathore, "Effect of reconfiguration and meshed networks on the small-signal stability margin of droop-based islanded microgrids," *IEEE Trans. Ind. Appl.*, vol. 54, no. 3, pp. 2821–2833, May 2018.
- [28] A. Stanoev and D. Smilkov, "Consensus theory in networked systems," in *Consensus and Synchronization in Complex Networks*, L. Kocarev, Ed. Berlin, Germany: Springer-Verlag, 2013, pp. 1–22.
- [29] R. Olfati-Saber and R. M. Murray, "Consensus problems in networks of agents with switching topology and time-delays," *IEEE Trans. Automat. Control*, vol. 49, no. 9, pp. 1520–1533, Sep. 2004.
- [30] R. O.-Saber, J. A. Fax, and R. M. Murray, "Consensus and cooperation in networked multi-agent systems," *Proc. IEEE*, vol. 95, no. 1, pp. 215–233, Jan. 2007.
- [31] J. Zhou, S. Kim, H. Zhang, Q. Sun, and R. Han, "Consensus-based distributed control for accurate reactive, harmonic, and imbalance power sharing in microgrids," *IEEE Trans. Smart Grid*, vol. 9, no. 4, pp. 2453–2467, Jul. 2018.

- [32] J. M. Rey, C. X. Rosero, M. Velasco, P. Marti, J. Miret, and M. Castilla, "Local frequency restoration for droop-controlled parallel inverters in islanded microgrids," *IEEE Trans. Energy Convers.*, vol. 34, no. 3, pp. 1232–1241, Sep. 2018.
- [33] N. Pogaku, M. Prodanović, and T. C. Green, "Modeling, analysis and testing of autonomous operation of an inverter-based microgrid," *IEEE Trans. Power Electron.*, vol. 22, no. 2, pp. 613–625, Mar. 2007.
- [34] Y. Zhu, Q. Fan, B. Liu, and T. Wang, "An enhanced virtual impedance optimization method for reactive power sharing in microgrids," *IEEE Trans. Power Electron.*, vol. 33, no. 12, pp. 10390–10402, Sep. 2018.
- [35] Y. C. C. Wong, C. S. Lim, M. D. Rotaru, A. Cruden, and K. Xin, "Reactive power sharing study of an islanded microgrid in DiGSILENT PowerFactory," in *Proc. Int. Conf. Renew. Energy Res. Appl.*, 2018, pp. 1–6.
- [36] IEEE Power and Energy Society, "IEEE 34 node test feeder," 2010. [Online]. Available: <http://sites.ieee.org/pes-testfeeders/resources/>
- [37] Q. Fu *et al.*, "Microgrid generation capacity design with renewables and energy storage addressing power quality and surety," *IEEE Trans. Smart Grid*, vol. 3, no. 4, pp. 2019–2027, Sep. 2012.



ment, optimization control, and distributed cooperative control in microgrid.

Yi Chyn Cassandra Wong (Student Member, IEEE) received the B.Eng. (Hons.) degree in electrical power engineering from Curtin University, Miri, Malaysia, in 2016. She is currently working toward the split-site Ph.D. degree with the University of Southampton, Southampton, U.K., and the University of Southampton Malaysia, Gelang Patah, Malaysia. She was a Research Intern with the Experimental Power Grid Centre, Agency for Science, Technology, and Research (A*STAR), Singapore, from August to October 2017. Her research interests include power quality improvement, optimization control, and distributed cooperative control in microgrid.



Assistant Professor of electrical and electronic engineering with the University of Southampton Malaysia, Gelang Patah, Malaysia. His research interests include advanced model predictive control design, multiphase motor drives, grid-connected converter control, and microgrid hierarchical control. He also serves as an Associate Editor for the *IET Electric Power Applications*.

Chee Shen Lim (Senior Member, IEEE) received the B.Eng. degree (Hons.) in electrical engineering from the University of Malaya, Kuala Lumpur, Malaysia, in 2009, and the joint-university Ph.D. degrees in power electronics and drives from the University of Malaya and Liverpool John Moores University, Liverpool, U.K., in 2013. From 2009 to 2013, he was a Research Assistant with the Power Energy Dedicated Advanced Centre, University of Malaya. From 2013 to 2015, he was a Research Scientist with the Experimental Power Grid Centre, A*STAR, Singapore. He is currently an



University of Southampton Malaysia from 2013 to 2019. He is currently a Senior Scientist with the Institute of Microelectronics, A*STAR, Singapore. His research interests and expertise include simulation and modeling of complex applied electromagnetic problems.

Mihai Dragos Rotaru (Member, IEEE) received the B.Eng. and M.Sc. degrees in electrical engineering from the Technical University Cluj Napoca, Cluj-Napoca, Romania, in 1996 and 1997, respectively, and the Ph.D. degree in electrical engineering from the University of Southampton, Southampton, U.K., in 2001. He was an Assistant Professor then an Associate Professor with the School of Electronics and Computer Science, University of Southampton from 2007 to 2019. He also served as the Electrical and Electronic Engineering Program Leader with the



previously worked with fuel cell technology and condition monitoring of wind turbines. He is a member of the Training and Diversity Panel of the UK's Faraday Institution and Co-Director of the EPSRC Centre for Doctoral Training in Energy Storage and its Applications.

Andrew Cruden received the B.Eng., M.Sc., and Ph.D. degrees from the University of Strathclyde, Glasgow, U.K., in 1989, 1990, and 1998, respectively, all in electronic and electrical engineering. He is currently the Head of the Energy Technologies Research Group and a Professor of Energy Technology with the University of Southampton, U.K. He has significant experience in the field of energy storage and electric vehicles, covering vehicle-to-grid, new battery technologies (e.g., Aluminium-ion cells), and flow cells (e.g., soluble lead flow battery). He






design and control for grid application.

Xin Kong received the B.Eng. and M.Eng. degrees from Xi'an Jiaotong University, Xi'an, China, in 1994 and 1997, respectively, and the Ph.D. degree from the National University of Singapore, Singapore, in 2009, all in electrical engineering. She currently serves as a Senior Research Scientist and the Deputy Program Director in Energy Research Institute with ERI@N, Nanyang Technological University, Singapore. Her research interests include modern power system modelling and analysis, renewable energy integration, distributed microgrid control, and power electronic

Erratum

Erratum to “Consensus Virtual Output Impedance Control Based on the Novel Droop Equivalent Impedance Concept for a Multi-Bus Radial Microgrid”

Yi Chyn Cassandra Wong, *Student Member, IEEE*, Chee Shen Lim , *Senior Member, IEEE*,
Mihai Dragos Rotaru, *Member, IEEE*, Andrew Cruden , and Xin Kong 

In [1], Table I and Table II are cited at page 1083–1084 but are missing in the published article. These tables are provided next.

TABLE I
THE CORRESPONDING κ_i VALUES FOR DIFFERENT OPERATING
POINTS WITH $C = 0.2$

| Q_o (% of Q_{rated}) | K_u | P_o (% of P_{rated}) (Note: $S_{rated} = 1$ p.u. and $pf_{rated} = 0.8$) | | | | | | |
|---------------------------|-------|--|-------|-------|-------|-------|-------|-------|
| | | 5 | 10 | 30 | 50 | 70 | 90 | 95 |
| 5 | 0.782 | 0.159 | 0.103 | 0.134 | 0.146 | 0.152 | 0.156 | 0.151 |
| 10 | 0.786 | | 0.161 | 0.115 | 0.131 | 0.141 | 0.148 | 0.149 |
| 30 | 0.800 | | | 0.167 | 0.105 | 0.111 | 0.120 | 0.122 |
| 50 | 0.814 | | | | 0.174 | 0.110 | 0.107 | 0.107 |
| 70 | 0.837 | | | | | 0.181 | 0.116 | 0.112 |
| 90 | 0.844 | | | | | | 0.188 | 0.158 |
| 95 | 0.848 | | | | | | 0.244 | 0.189 |

TABLE II
SYSTEM PARAMETERS

| Parameter | Value | Parameter | Value |
|---|-------------------------|---|---|
| System freq. | 60 Hz | P - f droop coeff. (pu) | 0.0625 |
| MV levels | 24.9/ 4.16 kV | No-load freq. (pu) | 1.02 |
| Inverter DC bus | 1 kV | Q - V droop coeff. (pu) | 0.075 |
| Sw. freq. F_{s1} | 10 kHz | No-load voltage (pu) | 1.02 |
| DER ratings: | | Inverter output filter impedances: | |
| Apparent power (rated pf) | | L-RC | |
| DER 1 | 0.8 MVA (0.8) | | 0.1905 mH, 10 Ω , 132.96 μ F |
| DER 2 | 0.6 MVA (0.8) | | 0.2540 mH, 10 Ω , 88.64 μ F |
| DER 3 | 0.8 MVA (0.8) | | 0.1905 mH, 10 Ω , 132.96 μ F |
| DER 4 | 0.4 MVA (0.8) | | 0.3810 mH, 10 Ω , 66.48 μ F |
| DER 5 | 0.4 MVA (0.8) | | 0.3810 mH, 10 Ω , 66.48 μ F |
| Feeder impedances | | | |
| Z_{of1} | 0.03 Ω , 0.35 mH | Z_{of4} | 0.03 Ω , 0.30 mH |
| Z_{of2} | 0.06 Ω , 0.35 mH | Z_{of5} | 0.04 Ω , 0.35 mH |
| Z_{of3} | 0.05 Ω , 0.40 mH | | |
| Secondary Consensus Control ($F_{s2} = 1$ Hz) | | Prim. Voltage Control | |
| τ_c | 0.2 s | K_{pvi} | 1.23 |
| c | 0.2 | K_{ivi} | 4.67 |
| | | Prim. Current Control | |
| | | K_{pci} | 0.27 |
| | | K_{ici} | 1.61 |

REFERENCE

- [1] Y. C. C. Wong, C. S. Lim, M. D. Rotaru, A. Cruden, and X. Kong, “Consensus virtual output impedance control based on the novel droop equivalent impedance concept for a multi-bus radial microgrid,” in *IEEE Trans. Energy Conversion*, vol. 35, no. 2, pp. 1078–1087, Jun. 2020.

Manuscript received May 28, 2020; accepted May 28, 2020. Date of current version August 20, 2020. This work was supported by the Fundamental Research Grant Scheme under Grant FRGS/1/2016/TK07/USMC/02/1 awarded by the Ministry of Higher Education, Malaysia. Paper no. TEC00932-2019. (Corresponding author: Chee Shen Lim.)

Yi Chyn Cassandra Wong and Chee Shen Lim are with the University of Southampton Malaysia, Iskandar Puteri 79200, Malaysia (e-mail: y.c.c.wong@soton.ac.uk; c.s.lim@soton.ac.uk).

Mihai Dragos Rotaru is with the Institute of Microelectronics, A*STAR, Singapore 627590, Singapore (e-mail: mihai_dragos_rotaru@ime.a-star.edu.sg).

Andrew Cruden is with the Energy Technologies Research Group, University of Southampton, Southampton SO17 1BJ, U.K. (e-mail: a.j.cruden@soton.ac.uk).

Xin Kong is with the Experimental Power Grid Centre of ERI@N, Nanyang Technological University, Singapore 627590, Singapore (e-mail: xin.kong@ntu.edu.sg).

Digital Object Identifier 10.1109/TEC.2020.2998887

A Consensus-Based Adaptive Virtual Output Impedance Control Scheme for Reactive Power Sharing in Radial Microgrids

Yi Chyn Cassandra Wong, *Student Member, IEEE*, Chee Shen Lim[✉], *Senior Member, IEEE*, Andrew Cruden[✉], Mihai Dragos Rotaru, *Member, IEEE*, and Pravat Kumar Ray[✉], *Senior Member, IEEE*

I. INTRODUCTION

Abstract—This article presents a distributed secondary control scheme for accurate reactive power sharing in an islanded multi-bus radial microgrid. The scheme employs consensus control to adaptively tune the virtual output impedance (VOI) into achieving reactive power correction. The adaptive VOI-based control structure is essentially nonlinear. However, this work shows that the approximate range of stable coupling gain can be established by linearizing the problem about every probable operating point of the distributed energy resources (DERs). On the basis of islanding mode, it is also shown that only the dynamic VOI component is needed while the static component, which has been used extensively to date, can be nullified. It will also be shown that under the established gain tuning guideline, the virtual reactance typically results in quicker correction dynamics as compared to the virtual resistance. The proposed control scheme can realize an accurate power sharing among the DERs regardless of the microgrid topology, load condition, and communication delay (within the allowable limits defined by the consensus theorem). This study is carried out in conjunction with an islanded microgrid model modified from the IEEE 34 Node Test Feeder.

Index Terms—Consensus control, droop control, reactive power sharing, virtual output impedance (VOI).

MICROGRIDS have the capability to ease the problems caused by the ever increasing penetration of distributed energy resources (DERs) into the main electricity grid. They can operate in either grid-connected or islanded mode. In the islanded mode, a common requirement is to share the load power among the DERs in proportion to their respective power capacities. To facilitate autonomous power sharing, standard frequency-active power (P - f) and voltage-reactive power (Q - V) droop control has been widely adopted in the early stage. However, although accurate active power is guaranteed, it is known that poor reactive power sharing results, especially in a paralleled microgrid with different feeder impedances and in a multibus radial microgrid. This is due fundamentally to the voltage discrepancies at the points of coupling of the DERs in the microgrid network [1]–[3].

Numerous control schemes focusing on accurate reactive power sharing have been reported to date. Compared to the dispatch-based methods, virtual output impedance (VOI) control methods, which are relatively newer, have been reported to have improved decoupling of active and reactive power, as well as enhanced stability and transient dynamics [4], [5]. VOI control essentially exploits the additional degree of freedom enabled by the inner voltage control loop. Owing to the nature of embedding the VOI into the inner control loop, it is reportedly more robust under communication interruption [5] as compared to the conventional dispatch-based method (which depends almost entirely on the communication to adjust the correction). In [6] and [7], the same control method was used to improve both the power control stability and sharing accuracy. These methods, however, only consider the mismatch of DERs' output/feeder impedances but not the network impedances, which are typical in radial microgrids. From the literature, it has also been established that the static-only VOI will not be able to solve the reactive power sharing problem in multibus radial microgrids [5], [8], especially in the ones with plug-and-play requirement.

A centralized droop control with a static virtual output reactance (X_v) and proportional-integral(PI)-tuned virtual output resistance (R_v) is proposed in [9]. Other similar centralized techniques can be found in [8] and [10] with arbitrarily chosen X_v/R_v ratios (five in [8] and one in [10]). These centralized methods (e.g., [8]–[10]) centrally manage the DERs based on the

Manuscript received May 30, 2020; revised August 20, 2020; accepted October 10, 2020. Date of publication October 21, 2020; date of current version December 31, 2020. Paper 2020-SECSC-0340.R1, presented at the 2020 IEEE International Conference on Power Electronics, Smart Grid and Renewable Energy (PESGRE2020), Cochin, India, Jan. 02–04, and approved for publication in the IEEE TRANSACTIONS ON INDUSTRY APPLICATIONS by the Renewable and Sustainable Energy Conversion Systems Committee of the IEEE Industry Applications Society. This work was supported by the Fundamental Research Grant Scheme under Grant FRGS/1/2016/TK07/USMC/02/1 awarded by the Ministry of Higher Education, Malaysia. (Corresponding author: Chee Shen Lim.)

Yi Chyn Cassandra Wong and Chee Shen Lim are with the University of Southampton Malaysia, Iskandar Puteri 79200, Malaysia (e-mail: y.c.c.wong@soton.ac.uk; c.s.lim@soton.ac.uk).

Andrew Cruden is with the Energy Technologies Research Group, University of Southampton, SO17 1BJ Southampton, U.K. (e-mail: a.j.cruden@soton.ac.uk).

Mihai Dragos Rotaru is with the Institute of Microelectronics, A*STAR, 627590 Singapore (e-mail: mihai_dragos_rotaru@ime.a-star.edu.sg).

Pravat Kumar Ray is with the Department of Electrical Engineering, National Institute of Technology Rourkela, Rourkela 769008, India (e-mail: rayp@nitrkl.ac.in).

Color versions of one or more of the figures in this article are available online at <https://ieeexplore.ieee.org>.

Digital Object Identifier 10.1109/TIA.2020.3031884

system-wide information and complete-graph communication network. These features are known to affect the system's flexibility and configurability, as any change in the grid topology (e.g., due to plug-and-play of DERs) would require reconfiguration of the central controller. Apart from the risk of having single point failure, the increasing penetration of DERs over a wide geographical span would aggravate the overall computational burden and communication requirement.

There exists another group of VOI-based reactive power correction techniques with no communication requirement [11]–[14]. In [11] and [12], the control schemes are developed primarily for parallel-connected DERs hence their extension to radial microgrid is conjectured to be difficult. In [13], although the control scheme can estimate feeder impedance without knowing the network parameters, it inherently requires the voltage at the same point of common coupling (PCC) for all DERs, which is not available in microgrids with multibus radial structure. In [14], the reactive power sharing in a radial microgrid can be improved through an adaptive virtual resistance function with coefficients tuned using offline genetic algorithm. However, this method cannot fully eliminate the power sharing error. Owing to the use of network model, its extension to a larger microgrid with plug-and-play requirement is likely to be difficult.

Distributed control has recently been introduced into VOI-based power sharing control [5]. With sparse communication network, distributed control is essentially a tradeoff between the centralized and communication-less decentralized methods, and hence carries the advantages of improved performance and reliability (somewhat similar to the distributed dispatch-based droop control [2], [15], [16]). In [5], both X_v and R_v are adaptively tuned through PI control. Similar to [8]–[10], these proposals share a commonality of having both static and dynamic components of the VOI. According to [4], which focuses on designing the VOI for microgrids with parallel structure, the dynamic component is introduced to improve the transient power decoupling under the grid-connected mode, whereas the static component is, in general, responsible for ensuring an always-inductive VOI.

This postconference work extends the work in [17] to focus on developing a consensus-based adaptive VOI control for an islanded radial microgrid. The proposed technique is different from the previous works in several aspects: 1) instead of utilizing both VOI components cooperatively (which means there are more static impedance values, reactance/resistance ratio, and other controller gains to tune; aggravated further by the potentially-large number of DERs in the microgrid), this scheme uses individual resistance/reactance component of the VOI to achieve the same accurate reactive power sharing performance; 2) the control scheme does not use PI controllers, leading to a simpler tuning of the coupling gain for stability; 3) with a simpler control structure, the approximate range of stable coupling gain is successfully established. This is achieved by analyzing the range of stable coupling gain for every probable operating point while considering some simplifying assumptions such as minimum power factor and maximum voltage drop ratio. On the basis that a microgrid operates in the islanded mode, it will be

demonstrated that only either of the dynamic virtual resistance or reactance component is needed and the static component, which has been used extensively to date for reactive power sharing correction, in e.g., [3], [5], [6], [8], can be nullified. This significantly reduces the number of parameters to be tuned and therefore increases the practicality of the consensus-based adaptive VOI control schemes.

The rest of the article is organized as follows. Section II introduces the fundamentals of adaptive VOI control for reactive power sharing improvement. Section III presents the consensus control and the coupling gain's tuning guideline. Section IV shows the results for various test scenarios: static load, load stepping, plug-and-play test, and communication time delay. A recently reported consensus VOI control scheme with dual-impedance control loops [5] is used as the benchmark for performance evaluation. Section V discusses the bounds of the VOI value and Section VI concludes the article.

II. REACTIVE POWER SHARING ANALYSIS

A. Primary Droop Control

The primary control of a VOI-controlled DER includes a droop control, an output voltage control, an inverter current control, and a VOI control, as shown in Fig. 1. Typically, during islanded operation, DERs achieve autonomous power sharing through the P - f and Q - V droop control, expressed as

$$\begin{aligned}\omega_i &= \omega_i^* - mP_i \\ u_i &= u_i^* - nQ_i\end{aligned}\quad (1)$$

where ω_i and u_i are the per-unit operating frequency and the droop voltage amplitude of i th DER, ω_i^* and u_i^* are the per-unit no-load frequency and voltage reference, and m and n are the per-unit droop coefficients commonly shared among the DERs in the microgrid. P_i and Q_i are the filtered per-unit active and reactive output power. The common base voltage is peak voltage V_B and the base power S_i is the respective DER's kVA rating. The output voltage vector is aligned to the corresponding synchronous reference frame, giving

$$\begin{aligned}u_{odi}^d &= u_i^* - nQ_i \\ u_{oqi}^d &= 0\end{aligned}\quad (2)$$

where u_{odi}^d and u_{oqi}^d are the synchronous d - and q -axis output voltage references for the output voltage control. The synchronous reference frame's angular position is obtainable from the respective droop frequency (1) after synchronizing with the microgrid during connection. The active and reactive output powers with low-pass filtering are

$$\begin{aligned}\tau_c \frac{dP_i}{dt} + P_i &= \frac{3}{2} (u_{odi}^d i_{odi} + u_{oqi}^d i_{oqi}) \\ \tau_c \frac{dQ_i}{dt} + Q_i &= \frac{3}{2} (u_{oqi}^d i_{odi} - u_{odi}^d i_{oqi})\end{aligned}\quad (3)$$

where τ_c is the low pass filter's cutoff period and u_{odi} , u_{oqi} , i_{odi} , and i_{oqi} are the d - and q -axis (with amplitude-invariant rotational transformation) measured output voltage and current components.

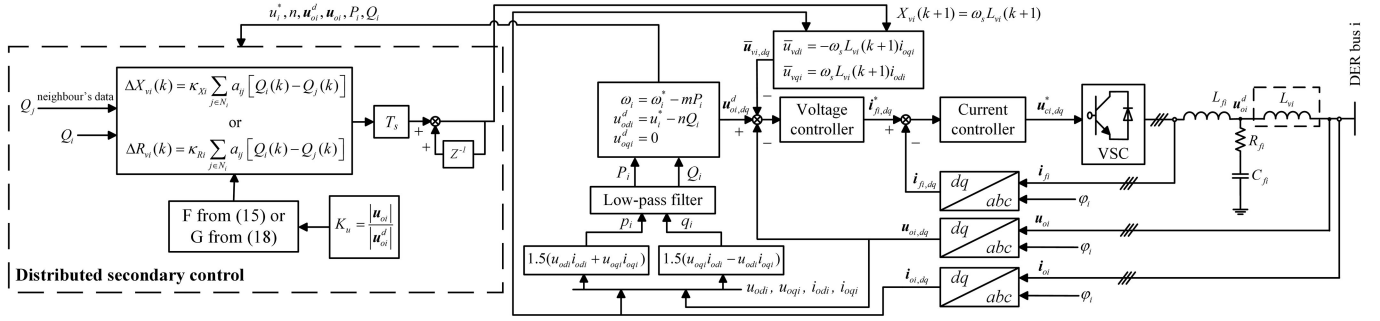


Fig. 1. Schematic diagram of the local control of a VOI-based droop-controlled DER with distributed secondary control for reactive power sharing.

B. Virtual Output Impedance Scheme

VOI control scheme works by regulating the output voltage references from the standard droop control

$$\begin{aligned} u_{odi}^* &= u_{odi}^d - u_{vdi} \\ u_{oqi}^* &= -u_{vqi} \end{aligned} \quad (4)$$

where u_{odi}^* and u_{oqi}^* are the output voltage references after the VOI, and u_{vdi} and u_{vqi} are the virtual voltage magnitude. The electrical steady-state values (i.e., \bar{u}_{vdi} and \bar{u}_{vqi} , after assuming $d/dt = 0$) are calculated as

$$\begin{aligned} \bar{u}_{vdi} &= R_{vi} i_{odi} - \omega_s L_{vi} i_{oqi} \\ \bar{u}_{vqi} &= R_{vi} i_{oqi} + \omega_s L_{vi} i_{odi} \end{aligned} \quad (5)$$

where ω_s is the nominal angular frequency in rad/s and R_{vi} and L_{vi} are the virtual resistance and inductance. Primary voltage and current control through *PI* controllers are implemented. The *PI* controllers are tuned empirically, such that the voltage and current control bandwidth are decoupled, and the voltage control dynamic is much faster than the outermost droop power control dynamic [3]. In principle, the innermost current control loop is tuned first with the assumption of a constant current reference (i.e., normally being the output of voltage controller), followed by the tuning of voltage controller by assuming a constant voltage reference (i.e., normally being the output of droop control). The design details are not included and interested readers are referred to [2], [3], and [18].

Typically, the VOI is comprised of two impedance components: static and dynamic, as in [3], [5], [6], and [8]. The static component ensures that the DER equivalent impedance is predominantly resistive/inductive, and the dynamic component is adaptively adjusted

$$\begin{aligned} R_{vi}(k) &= R_{vi,static} + R_{vi,dyn}(k) \\ X_{vi}(k) &= X_{vi,static} + X_{vi,dyn}(k) \end{aligned} \quad (6)$$

where $X_{vi} = \omega_s L_{vi}$, and the subscripts *static* and *dyn* indicate the static and dynamic components, respectively. However, it is anticipated that the abovementioned VOI method will result in poorer (lower) voltage profile due to the presence of static component (by causing additional voltage drops). This work therefore proposes a VOI method that uses only the dynamic

component, which indirectly leads to tuning effort reduction (relevant when the number of DERs is large). It will be shown later that, as far as the reactive power sharing of a droop-controlled islanded microgrid is concerned, this is indeed sufficient and it is not necessary to constrain the reactance to purely inductive (but a capacitive reactance is also feasible).

III. CONSENSUS-BASED ADAPTIVE VIRTUAL OUTPUT IMPEDANCE CONTROL DESIGN

A. Preliminary of Graph Theory

The communication network of a microgrid can be modeled as a graph with edges corresponding to the information flow between the DERs, denoted as the nodes in the graph. The graph is generally expressed as $G = (V_G, E_G, A_G)$ with a set of N nodes $V_G = \{v_1, v_2, \dots, v_N\}$, a set of edges $E_G \subset V_G \times V_G$ and an adjacency matrix $A_G = [a_{ij}] \in \mathbb{R}^{N \times N}$. The edges E_G denote the communication links between DERs and each edge $(v_j, v_i) \in E_G$ represents the information flow from node j to node i . Associated with a weight a_{ij} of edge (v_j, v_i) , $a_{ij} > 0$ if $(v_j, v_i) \in E_G$, otherwise $a_{ij} = 0$. Node j is called a neighbor of node i if $(v_j, v_i) \in E_G$ and the set of neighbors of node i is denoted as $N_i = \{v_j : (v_j, v_i) \in E_G\}$. The graph is termed to be undirected if $(v_j, v_i) \in E_G \Rightarrow (v_i, v_j) \in E_G$; otherwise directed. The in-degree matrix is defined as $D = \text{diag}\{d_i\} \in \mathbb{R}^{N \times N}$ with $d_i = \sum_{j \in N_i} a_{ij}$ and hence, the Laplacian matrix of the graph is defined as $L_G = D - A_G$.

B. Consensus-Based Adaptive VOI Control

The necessary condition to achieve proportional reactive power sharing among the DERs is

$$\lim_{t \rightarrow \infty} [Q_1(t) = Q_2(t) = \dots = Q_N(t)] \quad (7)$$

where Q_i is i th DER's output reactive power normalized to its kVA rating. This work chooses the widely-used linear first-order consensus control protocol for realizing reactive power correction [17]

$$\begin{aligned} \dot{Q}_i &= \delta_i \\ \delta_i &= -c \sum_{j \in N_i} a_{ij} [Q_i - Q_j] \end{aligned} \quad (8)$$

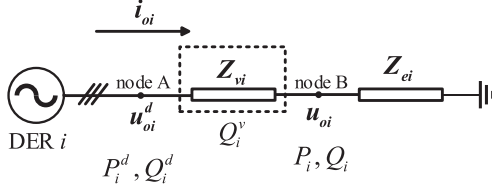


Fig. 2. Single line diagram of a three-phase DER at an arbitrary operating point and with the physical equivalent impedance that represents the loading connected at the output terminal. The virtual output impedance Z_{vi} will be configured as either reactive (i.e., setting $R_{vi} = 0$) or resistive (i.e., setting $X_{vi} = 0$) nature.

TABLE I
CORRESPONDING κ_X VALUES FOR DIFFERENT OPERATING
POINTS WITH $c = 0.2$

| Q_o (% of Q_{rated}) | K_U | P_o (% of P_{rated}) Note: $S_{rated} = 1.0$ p.u. | | | | | | | |
|---------------------------|-------|--|-------|------|------|------|------|------|--|
| | | 5 | 10 | 30 | 50 | 70 | 90 | 95 | |
| 5 | 0.884 | 54.52 | 32.89 | 6.86 | 2.77 | 1.48 | 0.93 | 0.84 | |
| 10 | 0.887 | | 13.49 | 5.06 | 2.35 | 1.33 | 0.86 | 0.78 | |
| 30 | 0.894 | | | 1.43 | 1.05 | 0.76 | 0.57 | 0.53 | |
| 50 | 0.902 | | | | 0.49 | 0.41 | 0.34 | 0.33 | |
| 70 | 0.915 | | | | | 0.23 | 0.21 | 0.20 | |
| 90 | 0.919 | | | | | | 0.13 | 0.13 | |
| 95 | 0.921 | | | | | | | 0.12 | |

TABLE II
CORRESPONDING κ_R VALUES FOR DIFFERENT OPERATING
POINTS WITH $c = 0.2$

| Q_o (% of Q_{rated}) | K_U | P_o (% of P_{rated}) Note: $S_{rated} = 1.0$ p.u. | | | | | | | |
|---------------------------|-------|--|-------|-------|-------|-------|-------|-------|--|
| | | 5 | 10 | 30 | 50 | 70 | 90 | 95 | |
| 5 | 0.884 | 3.285 | 0.534 | 0.055 | 0.027 | 0.018 | 0.014 | 0.013 | |
| 10 | 0.887 | | 0.850 | 0.069 | 0.030 | 0.019 | 0.014 | 0.013 | |
| 30 | 0.894 | | | 0.106 | 0.038 | 0.021 | 0.015 | 0.014 | |
| 50 | 0.902 | | | | 0.041 | 0.022 | 0.015 | 0.014 | |
| 70 | 0.915 | | | | | 0.022 | 0.015 | 0.013 | |
| 90 | 0.919 | | | | | | 0.014 | 0.012 | |
| 95 | 0.921 | | | | | | | 0.012 | |

where $c > 0$ is the scalar coupling gain and δ denotes the control input. Since a balanced-graph communication topology is assumed [17], [19], $a_{ij} = [0, 1]$. In the classical dispatch-droop method without VOI control [2], [15], [16], the consensus output will directly control the dispatch power command. However, in this work with VOI control, the reactive power Q_i is not directly controllable by the consensus control but is done through the adjustment of R_{vi} or X_{vi} . It is well established that the control of reactive power through adaptive VOI is essentially nonlinear [20], as reflected also in Fig. 1 where the virtual voltage drop is clearly a function of two sets of time-varying variables (current and VOI). In [20], it was mentioned that the stability of the VOI-based power control can be analyzed through the small-signal linear dynamic model. However, the effect of time-varying VOI (during adaptive adjustment) has not been taken into account. In this work, since the VOI value will be adaptively tuned by the secondary consensus control, it is therefore relevant to investigate the effect of such adjustment on the consensus control. Secondary control typically has a much reduced sampling frequency in order to commensurate with the practical communication bandwidth, therefore 1 Hz is chosen here (Table III). On the other hand, the inner's voltage control, current control, and droop control (with low-pass filtering) have 10 kHz control sampling frequency. Following the standard

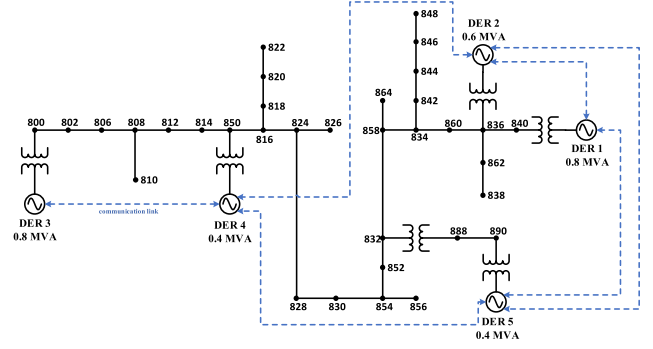


Fig. 3. Islanded microgrid test system (modified from IEEE 34 Feeder [21]).

TABLE III
SYSTEM PARAMETERS

| Parameter | Value | Parameter | Value |
|---|--------------------------|---|--------------------------|
| System freq. | 60 Hz | P - f droop coeff. (pu) | 0.0625 |
| MV levels | 24.9/4.16 kV | No-load freq. (pu) | 1.02 |
| Inverter DC bus | 1 kV | Q - V droop coeff. (pu) | 0.075 |
| Sw. freq. F_{s1} | 10 kHz | No-load voltage (pu) | 1.02 |
| DER ratings: | | Inverter output filter impedances: | |
| Apparent power (pf) | | L-RC | |
| DER 1 | 0.8 MVA (0.8) | 0.1905 mH, 10 Ω , 132.96 μ F | |
| DER 2 | 0.6 MVA (0.8) | 0.2540 mH, 10 Ω , 88.64 μ F | |
| DER 3 | 0.8 MVA (0.8) | 0.1905 mH, 10 Ω , 132.96 μ F | |
| DER 4 | 0.4 MVA (0.8) | 0.3810 mH, 10 Ω , 66.48 μ F | |
| DER 5 | 0.4 MVA (0.8) | 0.3810 mH, 10 Ω , 66.48 μ F | |
| Feeder impedances | | | |
| Z_{o1} | 0.030 Ω , 0.35 mH | Z_{o4} | 0.043 Ω , 0.35 mH |
| Z_{o2} | 0.056 Ω , 0.35 mH | Z_{o5} | 0.043 Ω , 0.35 mH |
| Z_{o3} | 0.030 Ω , 0.35 mH | | |
| Secondary consensus control ($F_{s2} = 1$ Hz) | | Primary voltage control | |
| τ_c | 0.2 s | K_{pvi} | 1.23 |
| c | 0.2 | K_{ivi} | 4.67 |
| | | Primary current control | |
| | | K_{pci} | 0.27 |
| | | K_{ici} | 1.61 |

practice of bandwidth separation, the analysis of the inner and outer loops can be effectively decoupled, and the focus here will be on the outer's secondary consensus control considering the presence of adaptive VOI. In what follows, the nonlinear relationship between the VOI and reactive power is first defined. Then, the approximated linear relationship at a wide range of operating points is derived to inform on the secondary consensus gain tuning.

Fig. 2 shows the single line diagram of a DER along with the VOI Z_{vi} (being $R_{vi} + jX_{vi}$), and the physical equivalent impedance Z_{ei} (being $R_{ei} + jX_{ei}$) as seen by the DER. Z_{ei} can be derived from the voltage and power terms, as

$$R_{ei} = \frac{3u_{oi}^2 P_i}{P_i^2 + Q_i^2}$$

$$X_{ei} = \frac{3u_{oi}^2 Q_i}{P_i^2 + Q_i^2} \quad (9)$$

where u_{oi} is the output voltage magnitude at node B (Fig. 2).

If one were to choose X_{vi} as the control input, the reactive power injected by the DER before Z_{vi} and the virtual reactive power across the virtual output reactance can be expressed as

(where $u_{oi}^d = u_{odi}^d + ju_{oqi}^d$)

$$\begin{aligned} Q_i^d &= \frac{3u_{oi}^{d^2}(X_{ei} + X_{vi})}{R_{ei}^2 + (X_{ei} + X_{vi})^2} \\ Q_i^v &= \frac{3i_{oi}^2 X_{vi}^2}{X_{vi}} \end{aligned} \quad (10)$$

in which the squared output current magnitude can be given as

$$i_{oi}^2 = \frac{u_{oi}^{d^2}}{R_{ei}^2 + (X_{ei} + X_{vi})^2}. \quad (11)$$

Then, X_v -based VOI-controlled DER's reactive output power $Q_i (= Q_i^d - Q_i^v)$ can be expressed as

$$Q_i = \frac{3u_{oi}^{d^2} X_{ei}}{R_{ei}^2 + (X_{ei} + X_{vi})^2}. \quad (12)$$

With (2), (9), and (12), the virtual reactance X_{vi} can be derived as

$$\begin{aligned} X_{vi} &= \sqrt{\frac{9K_{ui}^2(u_i^* - nQ_i)^4}{(P_i^2 + Q_i^2)} - \left(3K_{ui}^2 \frac{(u_i^* - nQ_i)^2 P_i}{P_i^2 + Q_i^2}\right)^2} \\ &\quad - 3K_{ui}^2 \frac{(u_i^* - nQ_i)^2 Q_i}{P_i^2 + Q_i^2} \end{aligned} \quad (13)$$

where the detailed manipulation is given in Appendix A. An operating-point-dependent voltage factor K_{ui} is introduced to approximate the ratio of output voltage magnitude u_{oi} to output voltage reference magnitude u_{oi}^d . If one were to assume that the voltages throughout the network remain close to the nominal value during the correction, K_{ui} can be approximated as a constant (that is close to "1"). In (13), it can be seen that X_{vi} is a function of K_{ui} , P_i , and Q_i (note: u_i^* and n are set the same for DERs in the same microgrid). Then, the nonlinear dynamical relationship of X_{vi} with respect to K_{ui} , P_i , and Q_i can be derived

$$\dot{X}_{vi} = \frac{\partial X_{vi}}{\partial P_i} \dot{P}_i + \frac{\partial X_{vi}}{\partial Q_i} \dot{Q}_i + \frac{\partial X_{vi}}{\partial K_{ui}} \dot{K}_{ui}. \quad (14)$$

Provided that the active and reactive power are sufficiently decoupled (which gives a small $\partial X_{vi}/\partial P_i$), and knowing that the steady-state active power in an islanded microgrid will not be affected by the reactive power correction (regardless of network topology), the first term of the RHS of (14) can be approximated to zero. On the other hand, since the changes of u_{oi} usually remain close to the changes in u_{oi}^d during correction, one may also approximate the last term of the RHS of (14) to zero. On this basis, the dynamical relationship between X_{vi} and Q_i can then be simplified to a linear, operating-point-dependent relationship, at an arbitrary operating point of K_{ui} , P_{oi} , and Q_{oi}

$$\begin{aligned} \dot{X}_{vi} &\approx \frac{\partial X_{vi}}{\partial Q_i} \dot{Q}_i \\ &= F_i(K_{ui}, P_{oi}, Q_{oi}) \dot{Q}_i \end{aligned} \quad (15)$$

where the full expression of F_i is given in Appendix B.

Next, the adaptive virtual output resistance-based control is considered. By configuring VOI as a pure resistive term, the R_v -based VOI-controlled DER's reactive output power (with

$Q_i^v = 0$ as $X_{vi} = 0$) can be expressed as

$$Q_i = \frac{3u_{oi}^{d^2} X_{ei}}{(R_{ei} + R_{vi})^2 + X_{ei}^2} \quad (16)$$

where (16) is essentially the counterpart of (12). By substituting (2) and (9) into (16), R_{vi} is given by

$$\begin{aligned} R_{vi} &= \sqrt{\frac{9K_{ui}^2(u_i^* - nQ_i)^4}{(P_i^2 + Q_i^2)} - \left(3K_{ui}^2 \frac{(u_i^* - nQ_i)^2 Q_i}{P_i^2 + Q_i^2}\right)^2} \\ &\quad - 3K_{ui}^2 \frac{(u_i^* - nQ_i)^2 P_i}{P_i^2 + Q_i^2}. \end{aligned} \quad (17)$$

By adopting the assumptions of nonchanging steady-state active power P_i and near-zero \dot{K}_{ui} , the dynamical relationship between R_{vi} and Q_i can be approximated to a linear, operating-point-dependent relationship

$$\dot{R}_{vi} = G_i(K_{ui}, P_{oi}, Q_{oi}) \dot{Q}_i \quad (18)$$

where G_i is given in Appendix B.

Lastly, substitute (15) and (18) to (8), and apply forward-Euler discretization, the consensus-based reactive power sharing control schemes can be expressed as

$$\Delta X_{vi}(k) = \kappa_{Xi} \sum_{j \in N_i} a_{ij} [Q_i(k) - Q_j(k)] \quad (19)$$

$$\Delta R_{vi}(k) = \kappa_{Ri} \sum_{j \in N_i} a_{ij} [Q_i(k) - Q_j(k)] \quad (20)$$

where $\kappa_{Xi} = -c_i F_i(K_{ui}, P_{oi}, Q_{oi})$ and $\kappa_{Ri} = -c_i G_i(K_{ui}, P_{oi}, Q_{oi})$. Subsequently, the individual VOI values for each of the consensus control scheme can be calculated from from (where T_s is the consensus control sampling period)

$$X_{vi}(k+1) = X_{vi}(k) + T_s \Delta X_{vi}(k) \quad (21)$$

$$R_{vi}(k+1) = R_{vi}(k) + T_s \Delta R_{vi}(k). \quad (22)$$

C. Coupling Gain Design

It is well established that consensus stability is guaranteed if the following sufficient condition is met

$$c < \frac{1}{d_{\max}} \quad (23)$$

where $d_{\max} = \max(\mathbf{D})$ [19]. However, as revealed from (19) and (20), the effective coupling gain for a given scalar coupling gain essentially depends on the operating point. Hence, going forward, there are two possible ways of setting the gain κ_{Xi} or κ_{Ri} values: 1) Compute the local F_i or G_i values on the fly and update the local gain κ_{Xi} or κ_{Ri} (in each DER); 2) consider the smallest value F_{\min} or G_{\min} for a given range of practical operating points and use $-cF_{\min}$ or $-cG_{\min}$ values as the global gain κ_X or κ_R (common to all DERs). For all practical purposes, this work considers the second way as it is expected to give a more reliable consensus control but with a small penalty on the correction dynamics (to be elaborated later). The possible values of κ_X or κ_R for a given range of operating points (i.e., of different P_o and Q_o values, and with

a rated power factor of 0.8) are summarized in Tables I and II. The calculation assumes that u_{oi} is fixed at 0.9 and that the load power factor is always kept equal or above 0.8 (note: grey-shaded column represents the operating points with below 0.8 power factor). The tables clearly show that κ changes quite significantly especially towards the low-loading region. It is recommended here that the fixed global coupling gain κ should be chosen at high-loading operating point (e.g., $P_o = 95\%$ of P_{rated} and $Q_o = 95\%$ of Q_{rated}) to ensure a stable secondary consensus control for most operating points. However, it is expected that such a choice would entail a slower correction dynamic at low load regions since the effective coupling gain κ at these regions will be very low. For example, based on Table I, if one were to fix the effective coupling gain κ_X as 0.12, then the equivalent scalar coupling gain c at low 5% P_{rated} loading point would be around $0.12 \times 0.2/54.52 = 4 \times 10^{-4}$. However, since nonproportional power sharing is naturally less of a concern at low-load regions, it makes practical sense to use κ_X or κ_R considering mainly the high-load regions.

D. Communication Delay

With the introduction of F_i and G_i in Section III-B, one can readily set the coupling gain of the first-order consensus protocol (8) based on (23). In practical application, time-delays are inevitable in communication-based systems, which effectively means that each DER's distributed control is unable to obtain its neighbors' information in a timely manner. To account for communication delay, the delay in this control problem is assumed to take the standard form with a constant delay for all DERs, similar to the standard time delay consideration [5], [19], [22], [23]. This gives

$$\Delta X_{vi}(k) = \kappa_{Xi} \sum_{j \in N_i} a_{ij} [Q_i(k - \tau) - Q_j(k - \tau)] \quad (24)$$

$$\Delta R_{vi}(k) = \kappa_{Ri} \sum_{j \in N_i} a_{ij} [Q_i(k - \tau) - Q_j(k - \tau)] \quad (25)$$

where τ denotes time delay. Based on the consensus stability theorem [5], [22]–[24], The delayed system would be asymptotically stable if and only if

$$0 < \tau < \frac{\pi}{2\lambda_{\max}c} \quad (26)$$

where λ_{\max} is the maximum eigenvalue of the communication graph's Laplacian matrix.

IV. SIMULATION RESULTS

An islanded microgrid network of five VOI-controlled DERs, modified from the IEEE 34 Node Test Feeder is depicted in Fig. 3 (see [21] for detailed network parameters). The network model, together with the primary voltage, current, droop control, and virtual output impedance control have been constructed in the *DigSILENT PowerFactory* environment (see [3] for modeling details). In addition, the performance of the proposed consensus-based reactive power sharing control scheme is benchmarked against a recently reported consensus control scheme [5], which adopts nonzero static VOI components and is known in what

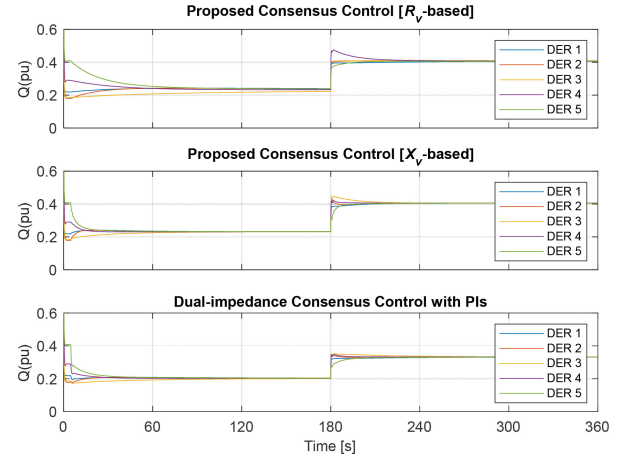


Fig. 4. (Case study 1) Steady-state and load step change: reactive output power of the DERs before and after reactive power sharing correction, and with load up-stepping.

follows as the dual-impedance consensus control. The basic parameters of the DERs and the islanded microgrid network are tabulated in Table III. For the consensus control, the associated communication graph's Laplacian matrix is as below

$$L_G = \begin{bmatrix} 2 & -1 & 0 & 0 & -1 \\ -1 & 3 & 0 & -1 & -1 \\ 0 & 0 & 1 & -1 & 0 \\ 0 & -1 & -1 & 3 & -1 \\ -1 & -1 & 0 & -1 & 3 \end{bmatrix}. \quad (27)$$

A. Case Study 1: Default Steady-State and Load Change

A total load of 1.52 MW and 1.27 MVar passive load are present in the islanded microgrid network. Before $t = 5$ s, the DERs are initially controlled through standard droop scheme without any reactive power sharing correction. It can be established from Fig. 4 that prior to 5 s the reactive power is not proportionally shared among the DERs. At $t = 5$ s, the proposed control scheme is activated with the global effective consensus gain κ set to 0.12 for X_v -based and 0.012 for R_v -based control schemes (note: these κ_X and κ_R values are chosen at high-loading operating points, as explained in Section III-C). Fig. 5 depicts a flowchart example for the consensus X_v -based reactive power sharing control scheme with the abovementioned gain setting. Similarly, the flowchart for R_v -based control that uses consensus equations (20) and (22) can also be easily constructed but this is not shown here. On the other hand, the controller gains of the dual-impedance consensus control are tuned in such a way that a similar settling time as the X_v -based scheme is obtained. The controller gains are summarized here: $C_Q = 4$, $D_P = 0.03$, $D_I = 1.2$, $K_{Q-L} = 0.15$, and $K_{Q-R} = 0.02$ (see [5] for details). It is seen clearly that the load reactive power can now be shared proportionally among the DERs. The corresponding VOI values for all three control schemes are shown in Fig. 6. Notice that in the control schemes without the static impedance components,

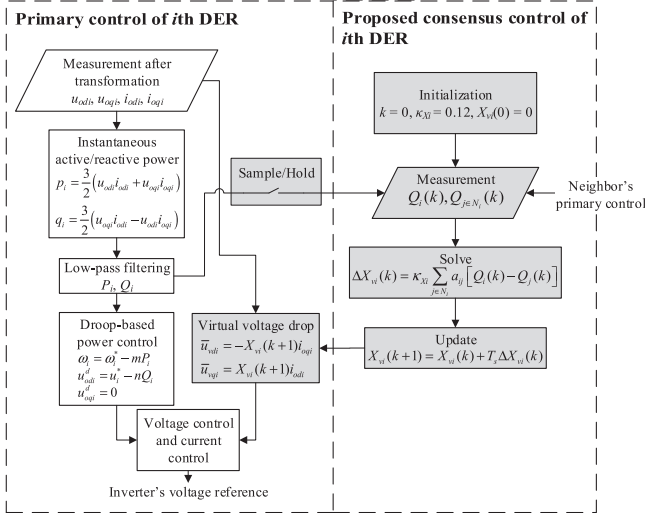


Fig. 5. Flowchart example of the consensus X_v -based reactive power sharing control.

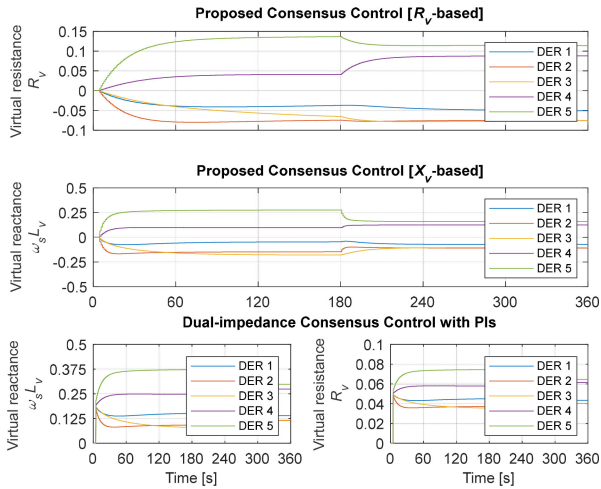


Fig. 6. (Case study 1) Default steady-state and load step change: virtual output impedance values of the DERs before and after reactive power sharing correction, and with load up-stepping.

the X_v and R_v can be positive or negative, whereas the dual-impedance scheme's X_v and R_v are always positive in value.

Next, an additional load is connected to bus 814 at $t = 180$ s. The total load demand of the islanded microgrid is therefore increased to $1.75 + j1.66$ MVA. Fig. 4 shows that control schemes continue to enable proportional power sharing regardless of load changing. However, Fig. 7 shows that the dual-impedance consensus control has resulted in larger bus voltage deviations as compared to those in the proposed control schemes, and this is due primarily to the nonzero static impedance (both resistive and inductive) components.

It can be clearly seen from Figs. 4, 6, and 7 that R_v -based scheme achieves proportional reactive power sharing at a much slower pace than that of X_v -based scheme. Note that both κ_X and κ_R have been chosen at the same high-loading operating

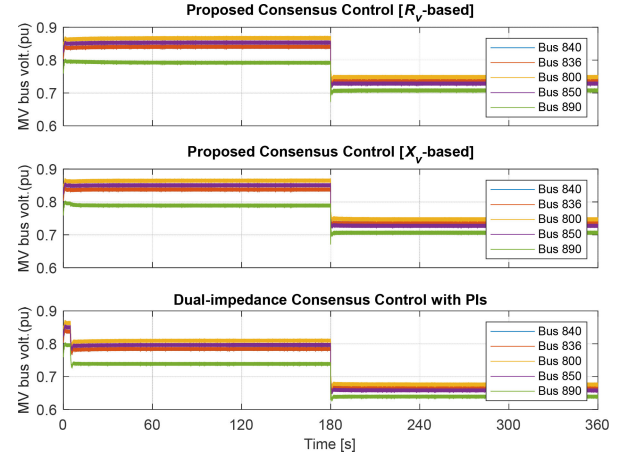


Fig. 7. (Case study 1) Default steady-state and load step change: voltage magnitudes at respective MV buses of the DERs. The base voltage of bus 890 is 4.16 kV and the rest are 24.9 kV.

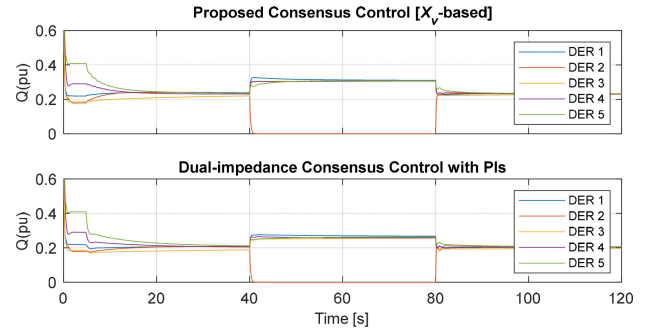


Fig. 8. (Case study 2) Plug-and-play of DER 2: reactive output power of the DERs with DER 2 disconnected at 40 s and reconnected at 80 s.

point. This hints that, as compared to the X_v -based control counterpart, R_v -based control is somewhat inferior in this medium-voltage microgrid with line impedances of moderate X/R ratio. This somewhat agrees with the observation in [9] and [25], where it was shown that a similar R_v -based control scheme is proven to be more relevant for resistive-lines-dominated low-voltage microgrids (i.e., with line impedances of low X/R ratio).

Therefore, in this medium-voltage microgrid, although both R_v -based and X_v -based control schemes result in the same voltage profile (as shown in Fig. 7), X_v -based control scheme is preferred as it results in a faster correction dynamic. Subsequent studies therefore only focus on the X_v -based control scheme.

B. Case Study 2: Plug-and-Play DER

The performance of the proposed reactive power sharing control scheme considering the plug-and-play feature of a microgrid is investigated next. The islanded microgrid operates under the default loading condition as in the case of case study 1 (after 5 s). At $t = 40$ s, DER 2 is disconnected arbitrarily, which means that the communication in and out of DER 2 (i.e., to and from other DERs) are lost. As seen in Fig. 8, proportional reactive power sharing is retained in both control

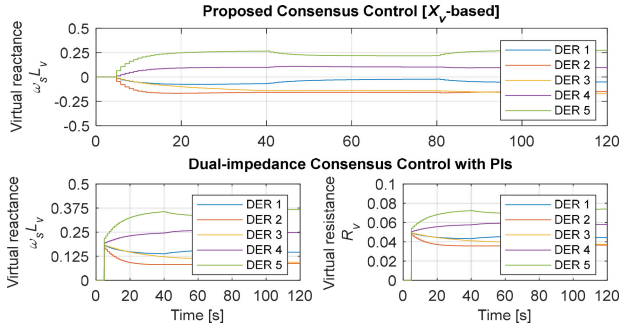


Fig. 9. (Case study 2) Plug-and-play of DER 2: virtual output impedance values with DER 2 disconnected at 40 s and reconnected at 80 s.

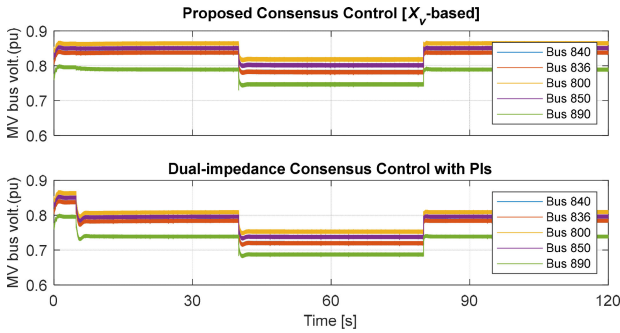


Fig. 10. (Case study 2) Plug-and-play of DER 2: voltage magnitudes at respective MV buses of all DERs.

schemes as expected, regardless of the network topology. In Fig. 9, during the disconnection, the VOI values of DER 2 prior to the disconnection point is kept constant to ensure stability. Upon disconnecting DER 2, it can be seen from Fig. 8 that the remaining DERs deliver higher reactive power to meet the load demand, which is accompanied by lowering of the MV bus voltages, as shown in Fig. 10. Prior to the reconnection of DER 2 at $t = 80$ s, the voltage angle of the incoming DER 2 is first synchronized with the point of coupling through the use of phase lock loop (embedded into the primary control layer), and followed by the eventual reclosing of the circuit breaker. Upon steady state, the bus voltages are restored (elevated) without any noticeable compromise of the reactive power sharing accuracy. Fig. 10 shows once again that the dual-impedance consensus control exhibits larger bus voltage deviations.

C. Case Study 3: Communication Link Delays

Lastly, the robustness of the proposed control scheme against communication time delays is examined. Based on the Laplacian matrix of the communication graph and the developed consensus control protocol, the maximum allowable time delay defined in (26) is $\tau_{\max} = 1.75$ s (i.e., with $\lambda_{\max} = 4.48$ and $c = 0.2$). Therefore, time delays of 1.4 and 1.8 s are tested under the default network setting (as in case study 1, after 5 s). Fig. 11 shows that the proposed control scheme remains stable for $\tau = 1.4$ s but the consensus control would become unstable for $\tau = 1.8$ s. It is worth highlighting that if the effective consensus gain κ

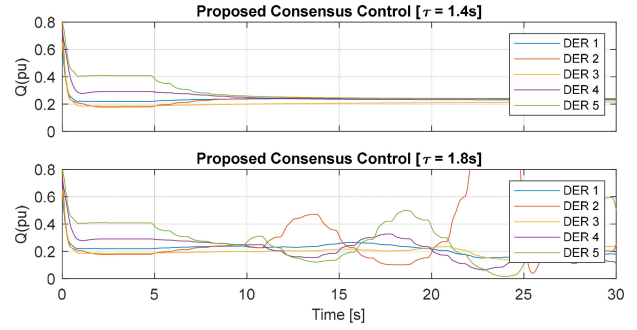


Fig. 11. (Case study 3) DERs' reactive output power with communication link delays.

is not tuned according to (15) or (18), but kept as the scalar coupling gain c , it is confirmed in the simulation study that the consensus VOI control schemes will not comply to the time delay limit defined in (26). This would reduce the practicality of the consensus VOI control scheme, and the proposed analysis in Sections III-B and III-C essentially help to improve this aspect.

V. DISCUSSION

In the preceding sections, as per the standard cascade control design, the primary control (inner's voltage, current, and droop) has been designed to have much higher control bandwidth than the secondary consensus control. This is achieved through the tuning of the primary's voltage and current controller, as well as the low-pass filter used in the droop control. This allows the analysis to only focus on the stability aspect of the secondary consensus control. It is acknowledged here that, if the microgrid is of a paralleled structure, some small-signal-based stability analyses [4], [20] do exist. They can help to define the VOI values in meeting the desired and critical stability requirements. Although those analyses are not directly applicable in this case with the multibus radial microgrid structure, what follows attempts to briefly analyze the results based on the approaches in [4] and [20].

Consider a simple DER-PCC model (e.g., as in Fig. 3 of [4]), the total output impedance as seen by the DER equipped with the VOI control can be defined as $Z_{\text{total}}(j\omega) = Z_{of}(j\omega) + Z_v(j\omega) + Z_o(j\omega)$, where Z_{of} is the physical feeder impedance and Z_o is the output impedance introduced by the inner voltage control loop. It can be easily proven that for a closed-loop voltage control, regardless of the type of inner voltage controller (stationary reference frame's proportional-resonant controllers [4] or synchronous reference frame's PI controllers, as in this work), Z_o at the fundamental frequency would effectively be zero magnitude (i.e., no steady-state error at the fundamental frequency). This allows one to approximate the VOI as $Z_v(j\omega) \approx Z_{\text{total}}(j\omega) - Z_{of}(j\omega)$. Then, it is proven in [4] that the stability of an islanded microgrid with paralleled DERs can be obtained from a wide range of Z_{total} value (i.e., almost the entire positive-value regions in Fig. 8 of [4]). Note that there is a small region of "unstable" Z_{total} in the figure near the origin, which is in principle caused by the fact that under the parallel structure, and with very small physical feeder impedances, the

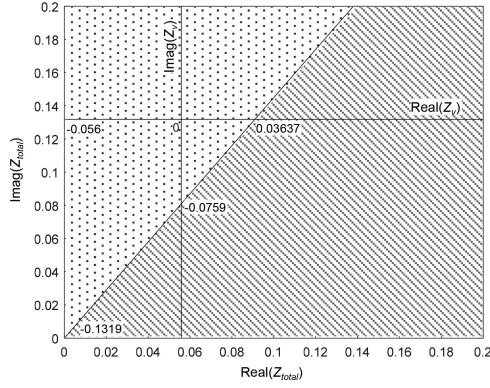


Fig. 12. Example of the lower bounds of Z_{v3} values obtainable using the analysis in [4] and [20], based on the single-DER-PCC model.

voltage-controlled DERs practically attempt to simultaneously regulate the voltage at the same PCC, leading to instability. In the case with a wide-area multibus radial network topology, this scenario naturally does not arise as there are always line impedances among the DER-connected buses. This simple analysis in some ways supports the observation made throughout the investigation, where it is found out that there is indeed no clear correlation between the overall system stability and the VOI values, instead, the stability is found to depend almost entirely on the effective consensus control gain.

What follows attempts to establish the saturation limits of the consensus output's Z_v (specifically the lower bound), which has not been considered in Sections III and IV. For example, referring to Fig. 12, one can establish Z_{v3} 's lower limit by using the Z_{of3} value. Fig. 12 shows two regions of X/R ratios which are separated by the line that represents unity decoupling coefficient with a maximum of 10° phase angle difference between the DER and PCC voltages (see [4, Sec. III] or [20, Sec. V-B] for details). Broadly speaking, it can be said that dotted-region has strong power decoupling whereas line-shaded region has strong power coupling which, in practical terms, means that the power regulation would be affected more severely during transients. Nevertheless, if the power coupling transient is of less concern (e.g., when the bandwidth separation of the primary and secondary control is clearly established), both regions are indeed usable. From Fig. 12, it is clearly seen that the lower bounds of Z_v are negative in value, which again substantiate the proposal of nullifying the static component of Z_v (together with the results in Section IV). If necessary, one may also consider including these saturation limits, approximated using the much simplified single-DER-PCC model [4], into the secondary consensus control design to further improve the overall system stability. However, provided a stable consensus control (i.e., with bounded inputs), it is unlikely that Z_v will be driven beyond the lower bounds defined above.

VI. CONCLUSION

This article presents a consensus-based adaptive VOI secondary control for accurate reactive power sharing for an islanded, multibus radial microgrid. The proposed control scheme

only requires a sparse communication structure and avoids the needs of a central control, which effectively mitigates the risk of single point failure. Instead of the widely used dual-impedance (both virtual resistance and reactance) consensus control, this work shows that virtual resistance or reactance alone is sufficient to ensure an accurate sharing of reactive power. In addition, instead of the usual static-dynamic impedance components, only the dynamic component is used here. The stability aspect of this work focuses primarily on the secondary consensus control and it is verified that the effective consensus coupling gain is a dominant factor in ensuring a stable system. This work proposes a systematic tuning guideline that establishes the approximate range of the effective consensus coupling gain to ensure a better system stability. It was revealed that, if the relationship between the virtual output reactance/resistance and the reactive power is not considered, the consensus protocol, especially in terms of coupling gain tuning, would not be able to meet the theoretical expectation. It is proven here that the proposed consensus control with adaptive virtual reactance/resistance and without the extensive use of proportional-integral control structure, can be appropriately tuned using the developed coupling gain tuning guideline to realize a stable accurate reactive power sharing among the DERs in an islanded, multibus radial microgrid. It is believed that this would improve the practicality of the consensus-based VOI control schemes for industrial adoption.

APPENDIX

A. Derivation of X_{vi} Expression in (13)

Replace the R_{ei} and X_{ei} terms in (12) with (9), the X_v -controlled DERs' reactive output power Q_i can be expressed as

$$Q_i = \frac{3u_{oi}^{d2} \left(\frac{3u_{oi}^2 Q_i}{P_i^2 + Q_i^2} \right)}{\left(\frac{3u_{oi}^2 P_i}{P_i^2 + Q_i^2} \right)^2 + \left(\frac{3u_{oi}^2 Q_i}{P_i^2 + Q_i^2} + X_{vi} \right)^2}. \quad (28)$$

The virtual output reactance X_{vi} can be expressed as

$$X_{vi} = \sqrt{\frac{9u_{oi}^{d2} (K_{ui} u_{oi}^d)^2}{P_i^2 + Q_i^2} - \left(\frac{3(K_{ui} u_{oi}^d)^2 P_i}{P_i^2 + Q_i^2} \right)^2} - \frac{3(K_{ui} u_{oi}^d)^2 Q_i}{P_i^2 + Q_i^2} \quad (29)$$

where the operating-point-dependent voltage factor $K_{ui} = u_{oi}/u_{oi}^d$. Then, substitute (2) into (29) (i.e., to express u_{oi}^d in terms of u_i^* , n and Q_i) and after manipulation, (13) is obtained.

B. Operating-Point-Dependent F_i and G_i

The operating-point-dependent function F_i in (15) for X_{vi} -based consensus control can be expressed as

$$F_i = - \frac{9}{\sqrt{\frac{9K_{ui}^2 (u_i^* - nQ_{oi})^4}{P_{oi}^2 + Q_{oi}^2} - \frac{9K_{ui}^4 P_{oi}^2 (u_i^* - nQ_{oi})^4}{(P_{oi}^2 + Q_{oi}^2)^2}}}$$

$$\begin{aligned}
& \left[\frac{K_{ui}^2 Q_{oi} (u_i^* - nQ_{oi})^4}{(P_{oi}^2 + Q_{oi}^2)^2} - \frac{2K_{ui}^4 P_{oi}^2 Q_{oi} (u_i^* - nQ_{oi})^4}{(P_{oi}^2 + Q_{oi}^2)^3} \right. \\
& + \frac{2K_{ui}^2 (u_i^{*2}n - 3u_i^{*2}n^2Q_{oi} + 3u_i^*n^3Q_{oi}^2 - n^4Q_{oi}^3)}{P_{oi}^2 + Q_{oi}^2} \\
& \left. - \frac{2K_{ui}^4 P_{oi}^2 (u_i^{*2}n - 3u_i^{*2}n^2Q_{oi} + 3u_i^*n^3Q_{oi}^2 - n^4Q_{oi}^3)}{(P_{oi}^2 + Q_{oi}^2)^2} \right] \\
& + \frac{6K_{ui}^2 Q_{oi}^2 (u_i^* - nQ_{oi})^2}{(P_{oi}^2 + Q_{oi}^2)^2} - \frac{3K_{ui}^2 (u_i^{*2} - 4u_i^*nQ_{oi} + 3n^2Q_{oi}^2)}{P_{oi}^2 + Q_{oi}^2} \quad (30)
\end{aligned}$$

The operating-point-dependent function G_i in (18) for the R_v -based consensus control can be expressed as

$$\begin{aligned}
G_i = & - \frac{9}{\sqrt{\frac{9K_{ui}^2 (u_i^* - nQ_{oi})^4}{P_{oi}^2 + Q_{oi}^2} - \frac{9K_{ui}^4 Q_{oi}^2 (u_i^* - nQ_{oi})^4}{(P_{oi}^2 + Q_{oi}^2)^2}}} \\
& \left[\frac{K_{ui}^2 Q_{oi} (u_i^* - nQ_{oi})^4}{(P_{oi}^2 + Q_{oi}^2)^2} + \frac{2K_{ui}^2 n (u_i^* - nQ_{oi})^3}{P_{oi}^2 + Q_{oi}^2} \right. \\
& - \frac{2K_{ui}^4 Q_{oi}^2 n (u_i^* - nQ_{oi})^3 - K_{ui}^4 Q_{oi} (u_i^* - nQ_{oi})^4}{(P_{oi}^2 + Q_{oi}^2)^2} \\
& \left. - \frac{2K_{ui}^4 Q_{oi}^3 (u_i^* - nQ_{oi})^4}{(P_{oi}^2 + Q_{oi}^2)^3} \right] + \frac{6K_{ui}^2 P_{oi} Q_{oi} (u_i^* - nQ_{oi})^2}{(P_{oi}^2 + Q_{oi}^2)^2} \\
& + \frac{6K_{ui}^2 P_{oi} n (u_i^* - nQ_{oi})}{P_{oi}^2 + Q_{oi}^2} \quad (31)
\end{aligned}$$

REFERENCES

- [1] Y. Han, H. Li, P. Shen, E. A. A. Coelho, and J. M. Guerrero, "Review of active and reactive power sharing strategies in hierarchical controlled microgrids," *IEEE Trans. Power Electron.*, vol. 32, no. 3, pp. 2427–2451, Mar. 2017.
- [2] A. Bidram, A. Davoudi, and F. L. Lewis, "A multiobjective distributed control framework for islanded AC microgrids," *IEEE Trans. Ind. Inform.*, vol. 10, no. 3, pp. 1785–1798, Aug. 2014.
- [3] Y. C. C. Wong, C. S. Lim, M. D. Rotaru, A. Cruden, and K. Xin, "Reactive power sharing study of an islanded microgrid in DigSILENT PowerFactory," in *Proc. 7th Int. Conf. Renewable Energy Res. Appl.*, 2018, Paper 68.
- [4] J. He and Y. W. Li, "Analysis, design, and implementation of virtual impedance for power electronics interfaced distributed generation," *IEEE Trans. Ind. Appl.*, vol. 47, no. 6, pp. 2525–2538, Nov./Dec. 2011.
- [5] H. Zhang, S. Kim, Q. Sun, and J. Zhou, "Distributed adaptive virtual impedance control for accurate reactive power sharing based on consensus control in microgrids," *IEEE Trans. Smart Grid*, vol. 8, no. 4, pp. 1749–1761, Jul. 2017.
- [6] J. M. Guerrero, L. Gracia de Vicuna, J. Matas, M. Castilla, and J. Miret, "Output impedance design of parallel-connected UPS inverters with wireless load-sharing control," *IEEE Trans. Ind. Electron.*, vol. 52, no. 4, pp. 1126–1135, Aug. 2005.
- [7] J. M. Guerrero, J. Matas, L. Gracia de Vicuna, M. Castilla, and J. Miret, "Decentralized control for parallel operation of distributed generation inverters using resistive output impedance," *IEEE Trans. Ind. Electron.*, vol. 54, no. 2, pp. 994–1004, Apr. 2007.
- [8] T. V. Hoang and H. H. Lee, "An adaptive virtual impedance control scheme to eliminate the reactive-power-sharing errors in an islanding meshed microgrid," *IEEE J. Emerg. Sel. Top. Power Electron.*, vol. 6, no. 2, pp. 966–976, Jun. 2018.
- [9] Y. Zhu, B. Liu, F. Wang, F. Zhuo, and Y. Zhao, "A virtual resistance based reactive power sharing strategy for networked microgrid," in *Proc. 9th Int. Conf. Power Electron. ECCE*, 2015, pp. 1564–1572.
- [10] H. Mahmood, D. Michaelson, and J. Jiang, "Accurate reactive power sharing in an islanded microgrid using adaptive virtual impedances," *IEEE Trans. Power Electron.*, vol. 30, no. 3, pp. 1605–1617, Mar. 2015.
- [11] S. Liu and Y. Zhang, "Voltage compensation strategy using adaptive virtual impedance for reactive power sharing in an islanded microgrid," in *Proc. Int. Conf. Elect. Mach. Syst.*, 2017, pp. 1–6.
- [12] B. Wang, S. Liu, and Y. Zhang, "Reactive power sharing control based on voltage compensation strategy in microgrid," in *Proc. 36th Chinese Control Conf.*, 2017, pp. 10745–10750.
- [13] B. Liu, Z. Liu, J. Liu, R. An, and S. Song, "A novel microgrid power sharing scheme enhanced by a non-intrusive feeder impedance estimation method," in *Proc. Int. Power Electron. Conf.*, 2018, pp. 3924–3928.
- [14] Y. Zhu, F. Zhuo, F. Wang, B. Liu, R. Gou, and Y. Zhao, "A virtual impedance optimization method for reactive power sharing in networked microgrid," *IEEE Trans. Power Electron.*, vol. 31, no. 4, pp. 2890–2904, Apr. 2016.
- [15] A. Bidram, A. Davoudi, F. L. Lewis, and J. M. Guerrero, "Distributed cooperative secondary control of microgrids using feedback linearization," *IEEE Trans. Power Syst.*, vol. 28, no. 3, pp. 3462–3470, Aug. 2013.
- [16] R. Han, L. Meng, G. Ferrari-Trecate, E. A. A. Coelho, J. C. Vasquez, and J. M. Guerrero, "Containment and consensus-based distributed coordination control to achieve bounded voltage and precise reactive power sharing in islanded AC microgrids," *IEEE Trans. Ind. Appl.*, vol. 53, no. 6, pp. 5187–5199, Dec. 2017.
- [17] Y. C. C. Wong, C. S. Lim, A. J. Cruden, M. D. Rotaru, and P. K. Ray, "A consensus-based adaptive virtual output impedance control scheme for reactive power sharing in meshed microgrids," in *Proc. IEEE Int. Conf. Power Electron., Smart Grid Renewable Energy*, 2020, Paper 323.
- [18] R. Kabiri, D. G. Holmes, and B. P. McGrath, "Inverter control modelling for distributed generation feeding into a utility network," in *Proc. Australasian Univ. Power Eng. Conf.*, 2013, pp. 1–6.
- [19] F. L. Lewis, H. Zhang, K. Hengster-Movric, and A. Das, "Algebraic graph theory and cooperative control consensus," in *Cooperative Control of Multi-Agent Systems*. 1st ed., London, U.K.: Springer-Verlag, 2014, pp. 23–71.
- [20] X. Wu, C. Shen, and R. Iravani, "Feasible range and optimal value of the virtual impedance for droop-based control of microgrids," *IEEE Trans. Smart Grid*, vol. 8, no. 3, pp. 1242–1251, May 2017.
- [21] IEEE Power and Energy Society. Piscataway, NJ, USA, *IEEE 34 Node Test Feeder*. 2010. [Online]. Available: <http://sites.ieee.org/pes-testfeeders/resources/>
- [22] R. Olfati-Saber and R. M. Murray, "Consensus problems in networks of agents with switching topology and time-delays," *IEEE Trans. Autom. Control*, vol. 49, no. 9, pp. 1520–1533, Sep. 2004.
- [23] R. Olfati-Saber, J. A. Fax, and R. M. Murray, "Consensus and cooperation in networked multi-agent systems," *Proc. IEEE*, vol. 95, no. 1, pp. 215–233, Jan. 2007.
- [24] J. Zhou, S. Kim, H. Zhang, Q. Sun, and R. Han, "Consensus-based distributed control for accurate reactive, harmonic, and imbalance power sharing in microgrids," *IEEE Trans. Smart Grid*, vol. 9, no. 4, pp. 2453–2467, Jul. 2018.
- [25] Y. Zhu, Q. Fan, B. Liu, and T. Wang, "An enhanced virtual impedance optimization method for reactive power sharing in microgrids," *IEEE Trans. Power Electron.*, vol. 33, no. 12, pp. 10390–10402, Dec. 2018.



Yi Chyn Cassandra Wong (Student Member, IEEE) received the B.Eng. (Hons.) degree in electrical power engineering from the Curtin University Malaysia, Miri, Malaysia, in 2016. She is currently working toward the split-site Ph.D. degree with the University of Southampton, U.K., and University of Southampton Malaysia, Iskandar Puteri, Malaysia.

She was a Research Intern with the Experimental Power Grid Centre, Agency for Science, Technology, and Research (A*STAR), Singapore, in 2017. Her research interests include power quality improvement,

optimization control, and distributed cooperative control in microgrid.



Chee Shen Lim (Senior Member, IEEE) received the B.Eng. degree (Hons.) in electrical engineering from the University of Malaya, Kuala Lumpur, Malaysia, in 2009, and the joint-university Ph.D. degrees in power electronics and drives from the University of Malaya and Liverpool John Moores University, Liverpool, U.K., in 2013.

He was a Research Scientist with the Experimental Power Grid Centre, A*STAR, Singapore, from 2013 to 2015. He is with the University of Southampton Malaysia, Iskandar Puteri, Malaysia, since November 2015, and he is currently an Associate Professor of electrical and electronic engineering. His research interests include advanced model predictive control design, multiphase motor drives, grid-connected converter control, and micro-grid hierarchical control.

Dr. Lim serves as an Associate Editor for the *IET Electric Power Applications*.



Mihai Dragos Rotaru (Member, IEEE) received the B.Eng. and M.Sc. degrees in electrical engineering from the Technical University Cluj Napoca, Cluj-Napoca, Romania, in 1996 and 1997, respectively, and the Ph.D. degree in electrical engineering from the University of Southampton, U.K., in 2001.

He was an Assistant Professor then Associate Professor with the School of Electronics and Computer Science of University of Southampton, from 2007 to 2019. He also served as the Electrical and Electronic Engineering Program Leader at the University of Southampton Malaysia, from 2013 to 2019. He is currently a Senior Scientist with the Institute of Microelectronics, A*STAR, Singapore. His research interests and expertise include simulation and modeling of complex applied electromagnetic problems.



Andrew Cruden received the B.Eng., M.Sc., and Ph.D. degrees from the University of Strathclyde, Glasgow, U.K., in 1989, 1990, and 1998, respectively, all in electronic and electrical engineering.

He is currently the Head of the Energy Technologies Research Group and a Professor of Energy Technology with the University of Southampton, U.K. He has significant experience in the field of energy storage and electric vehicles, covering vehicle-to-grid (V2G), new battery technologies (e.g., aluminium-ion cells), and flow cells (e.g., soluble lead flow battery). He has previously worked with fuel cell technology and condition monitoring of wind turbines.

Prof. Cruden is a member of the Training and Diversity Panel of the UK's Faraday Institution and Co-Director of the EPSRC Centre for Doctoral Training (CDT) in Energy Storage and its Applications.



Pravat Kumar Ray (Senior Member, IEEE) received the B.S. degree from Indira Gandhi Institute of Technology, Sarang, Odisha, India, in 2000, the M.E. degree from Indian Institute of Engineering Science and Technology, Shibpur, Howrah, India, in 2003, and the Ph.D. degree from National Institute of Technology (NIT) Rourkela, India, in 2011, all in electrical engineering.

He is currently an Associate Professor with the Department of Electrical Engineering, NIT Rourkela. He was also a Postdoctoral Fellow at Nanyang Technological University, Singapore, during January 2016 to June 2017. His research interests include signal processing and soft computing applications to power system, power quality, and grid integration of renewable energy systems.

Received July 10, 2021, accepted July 19, 2021, date of publication July 26, 2021, date of current version August 2, 2021.

Digital Object Identifier 10.1109/ACCESS.2021.3099432

An Optimal Secondary Multi-Bus Voltage and Reactive Power Sharing Control Based on Non-Iterative Decoupled Linearized Power Flow for Islanded Microgrids

YI CHYN CASSANDRA WONG^{1,2}, (Student Member, IEEE),
CHEE SHEN LIM¹, (Senior Member, IEEE),
HUI HWANG GOH³, (Senior Member, IEEE), ANDREW CRUDEN²,
MIHAI DRAGOS ROTARU⁴, (Member, IEEE), AND XIN KONG⁵

¹University of Southampton Malaysia, Iskandar Puteri, Johor 79200, Malaysia

²School of Engineering, University of Southampton, Southampton SO17 1BJ, U.K.

³School of Electrical Engineering, Guangxi University, Nanning 530015, China

⁴Institute of Microelectronics, Agency for Science, Technology and Research, Singapore 138634

⁵Energy Research Institute at NTU, Nanyang Technological University, Singapore 627590

Corresponding author: Hui Hwang Goh (hhgoh@gxu.edu.cn)

This work was supported in part by the School of Engineering, University of Southampton, U.K., and in part by the School of Electrical Engineering, Guangxi University, China.

ABSTRACT The subject of optimal secondary control of power-electronic-interfaced distributed energy resources (DERs) in droop-controlled microgrids has garnered significant research attention in recent years. While the feasibility of optimal secondary control based on non-linear power flow has been proven, the power flow algorithm is essentially iterative in nature. This work proposes an optimal secondary control with non-iterative power flow to regulate multi-bus voltages and DERs' reactive powers. The control scheme incorporates a modified Decoupled Linearized Power Flow that is known to be superior in terms of reactive power and bus voltage magnitude estimation, as compared to classical DC power flow, into a constrained quadratic programming. Q -V droop is integrated into the linear power flow in place of the slack bus. The proposed optimal scheme is provably accurate for maintaining reactive power sharing while regulating multiple load-bus voltages. The additional degrees of freedom enabled by the weighting factors significantly improve the control flexibility of the secondary controller. The allowable bus voltages and DER kVar capacity limits have also been considered by the control algorithm. The work is proven through an accurate co-simulation study comprising an 18-bus network and a full primary control models in *PowerFactory*, interfaced through industrial communication tool *MatrikonOPC*.

INDEX TERMS Microgrid, droop control, reactive power sharing, voltage regulation, optimal secondary control, decoupled linearized power flow.

I. INTRODUCTION

Accurate reactive power sharing of distributed energy resources (DERs) in distribution microgrids can be achieved through improved droop schemes based on dispatch mechanisms [1], synchronous-axis voltage droop mechanisms [2], enhanced droop techniques [3], and virtual output impedance (VOI) mechanisms [4], [5]. In applications where

bus voltages within the droop-based microgrids are to be regulated concurrently (e.g. being the critical buses or the main points of common coupling with the wider AC grid), advanced secondary voltage control schemes are relevant. In general, these secondary control schemes can be categorized to the types of targeted buses: (i) DER-bus scheme; (ii) load-bus scheme.

In recent years, DER-bus-targeted secondary control schemes for droop-controlled microgrids (i.e. with reactive power sharing correction/control) have been actively

The associate editor coordinating the review of this manuscript and approving it for publication was Shihong Ding¹.

researched in conjunction with centralized, decentralized, and distributed control structures. Reference [6] adopts a full-graph dispatch droop (with high-bandwidth finite-control-set model predictive voltage controller) to realize average DER-voltage restoration. Reference [7] proposed a non-linear state estimator to realize decentralized secondary DER-voltage control [8]–[14] (with [8] adopting VOI-based primary control) have investigated on consensus-based secondary controls that restore the average DER-voltage while maintaining accurate reactive power sharing. Reference [11] proposed a voltage-consensus scheme to maintain the averaged DER-bus voltage to the rated value. [12], [15] proposed a *PI*-consensus based secondary voltage controller for regulating averaged-*DER*-bus voltage without the needs of external reference. Different from the typical average-voltage scheme, [16] proposed an observer-based distributed secondary voltage control that can regulate *DER* voltages to a weighted-average value (while considering constraints on reactive powers). References [13], [14] reported on a tunable consensus control to address the conflicting objectives of multi-*DER*-bus voltage regulation and reactive power sharing. Reference [17] proposed a consensus-based containment control attempting to keep the *DER*-bus voltages within upper and lower bounds. Reference [18] proposed and studied a two-layer, iterative consensus control strategy that minimizes overall *DER*-bus voltage deviation while attempting to maintain accurate reactive power sharing.

On the other hand, load-bus schemes are also relevant. It has been established in [19] that the single load-bus secondary voltage control can be achieved, through *PI*-consensus control, without compromising the accurate sharing of reactive power. However, it was acknowledged in [20] that the reactive power sharing accuracy may be affected if the *DER* control gains are coupled. In [21], a *PI*-based, two-layer consensus control scheme realizing single load-bus voltage control with intra- and inter-microgrid reactive power sharing correction, was reported. These works, together with previously mentioned works [6]–[14], [16]–[18], have proven that the secondary voltage control with reactive power sharing consideration (of both centralized and non-centralized types) can readily regulate multiple *DER*-bus and single load-bus voltages. It is also worth noting that some recent works have investigated microgrid's secondary voltage control without emphasizing on reactive power sharing, e.g. single-load-bus-targeted fuzzy-logic-based scheme [22], distributed feedback linearization-approach [23], [24], finite-time distributed control approach [25], and event-triggered-based [26]. Recently, advanced algorithms have been exploited for multi-load-bus voltage regulation. For example, [27] substituted the primary droop-based power control with a neural-network-based control. Reference [28] proposed a multi-objective evolutionary algorithm based on decomposition technique that restores load-bus voltage while considering reactive power sharing.

As far as islanded operating mode is concerned, multi-load-bus voltage regulation schemes embedded with

power flow algorithms have also been investigated, e.g. non-linear power flow [29], [30] (which are fitted as non-linear constraints of the optimization problem), Jacobian-based method [31], [32] (specifically, Newton Raphson [33]; Newton-trust region [31]; modified Newton Raphson [32]), neural-network-based non-linear mapping method [34], and virtual-impedance-integrated linear power flow [35]. However, it was learnt that optimal secondary control with non-linear power flow [29], [30] will confront with the issue of slow convergence. This was evidently acknowledged in [29], despite that the work only studied a three-*DER* network. On the other hand, the convergence issue resulted from the attempt to fit the iterative-based Jacobian power flow into an optimal control problem [33], [34] will aggravate further due to the large number of *DER*s/buses in future microgrids. On this background, this work sets out to develop an optimal secondary control strategy realizing multi-load-bus voltage and accurate reactive power sharing control, with non-iterative power flow algorithm, for droop-controlled microgrids. (Note: [30], [33] have similar multi-load-bus voltage consideration but have not considered the issue of accurate reactive power sharing, instead, e.g. in [30], network efficiency is considered together).

This work proposes and investigates an optimal secondary control based on modified Decoupled Linearized Power Flow (DLPF) for multi-load-bus voltages and reactive power sharing regulation. Linearized power flow model has always been the preferred algorithm for large-scale power system studies such as contingency analyses and reliability assessments [36], [37]. DLPF was proposed originally in [36] as an alternative to classical DC power flow (which is known to be slightly inferior in terms of bus voltage estimation [36]). In this work, the linear power flow is modified to account for the islanded microgrid's droop control and is then fitted as the linearity constraint of the quadratic programming (QP) problem. Moreover, the allowable voltage and reactive power limits are imposed through the inequality constraints. An 18-bus islanded microgrid has been modelled in detail into *DIGSILENT PowerFactory*, accounting for the primary voltage and current control loops of the power electronic control. The secondary control algorithm is realistically implemented (in terms of communication structure, sampling time and data exchange) in a co-simulated, *Python*-based platform. The secondary controller is interfaced with the network model running in parallel in *PowerFactory* through *MatrikonOPC* – an interoperability standard for data exchange in industrial automation.

The rest of the paper is organized as follows. Section II discusses the fundamentals of network power flow and the DLPF. Section III discusses the aggregation of dispatchable droop control with the DLPF and formulates the constrained QP optimization problem. Section IV details the *PowerFactory-Python* co-simulation platform. Section V investigates the system performance under different practical scenarios such as optimal power sharing, multi-objective optimal power sharing with single/multi-bus

voltage regulation, optimal regulation under voltage and DER capacity limits, as well as communication failure. Section VI discusses and summarizes the main findings and relate them to practical contexts. Section VII concludes the paper.

II. NETWORK POWER FLOW

A. BASIC EQUATIONS

A network with M buses can be modelled by forming the network nodal equation

$$\begin{bmatrix} I_{\sim 1} \\ \vdots \\ I_{\sim i} \\ \vdots \\ I_{\sim M} \end{bmatrix} = \begin{bmatrix} Y_{\sim 11} & \cdots & Y_{\sim 1i} & \cdots & Y_{\sim 1M} \\ \vdots & \ddots & \vdots & \ddots & \vdots \\ Y_{\sim i1} & \cdots & Y_{\sim ii} & \cdots & Y_{\sim iM} \\ \vdots & \ddots & \vdots & \ddots & \vdots \\ Y_{\sim M1} & \cdots & Y_{\sim M1} & \cdots & Y_{\sim MM} \end{bmatrix} \times \begin{bmatrix} V_{\sim 1} \\ \vdots \\ V_{\sim i} \\ \vdots \\ V_{\sim M} \end{bmatrix} \quad \text{or} \quad \mathbf{I} = \mathbf{Y} \mathbf{V} \quad (1)$$

where the subscript i represents the bus number; and V_i and I_i are the voltage and current injection at i^{th} bus. \mathbf{Y} is the nodal admittance matrix with its element $Y_{ij} \in \mathbf{Y}$ obtainable from

$$Y_{\sim ij} = \begin{cases} y_{\sim i0} + \sum_{k=1}^M y_{\sim ik} & \text{if } i = j \\ -y_{\sim ij} & \text{otherwise} \end{cases} \quad (2)$$

where y_{i0} is the shunt admittance and y_{ij} is the admittance between bus i and bus j where $y_{ij} = g_{ij} + jb_{ij}$, with g and b being the conductance and susceptance, is the reciprocal of the corresponding complex line impedance z_{ij} ($= r_{ij} + jx_{ij}$, with r and x being the resistance and reactance). Note that any off-diagonal element Y_{ij} is non-zero if and only if there is a branch linking bus i and j . If there are l branches in an M -bus system then \mathbf{Y} would have M^2 elements, of which $(2l + M)$ elements are non-zero.

The current injection at i^{th} bus can be extracted from (1) as

$$I_{\sim i} = Y_{\sim ii} V_{\sim i} + \sum_{j=1}^M Y_{\sim ij} V_{\sim j} \quad (3)$$

where the general form of the complex voltage and admittance can be written as $V_{\sim i} = V_i \angle \delta_i$ and $Y_{\sim ij} = Y_{ij} \angle \theta_{ij}$. Then, the apparent power injected at i^{th} bus can be expressed as [38]

$$\begin{aligned} S_{\sim i} &= P_{\sim i} + jQ_{\sim i} = V_{\sim i} I_{\sim i}^* \\ &= V_i^2 Y_{ii} e^{-j\theta_{ii}} + V_i \sum_{j=1}^M V_j Y_{ij} e^{j(\delta_i - \delta_j - \theta_{ij})} \end{aligned} \quad (4)$$

where $Y_{ij} = G_{ij} + jB_{ij}$. Classical iterative techniques such as Gauss-Seidel, Newton-Raphson and fast-decoupled methods are commonly adopted to solve the nonlinear power

flow equations. Standard power flow algorithms are not applicable for islanded operation due to two known reasons: the inexistence of slack bus and the dependence of active/reactive power on frequency/voltage due to droop action. In addition, the nonlinearity of basic power flow equations is known for their iterative nature and therefore slow in convergence [36], [39]. Since future microgrids will consist of a significantly large number of DERs (several orders higher than present state of the arts), a more computationally efficient algorithm will be beneficial. Alternatively, the DC power flow algorithm is a convenient option to approximate the linearity between active power injection P and phase angle δ [37]. However, since it is established based on the assumption of constant bus voltages, reactive power injection is practically neglected [36].

As reported in Fig. 8 of [40], although the classical DC power flow (i.e. Model II in [40]) has the most significant advantages in computational efficiency, computational accuracy is expected to be low in large-area network as voltage magnitude is disregarded. On the other hand, non-iterative DLPF (i.e. Model IV in [40]) exhibits high computational efficiency in term of calculation time compared to the classical AC power flow with accurate voltage magnitude calculation (i.e. Model I in [40]). This provides a basis to this work to evaluate DLPF further in the optimal control algorithm.

B. DECOUPLED LINEARIZED POWER FLOW ALGORITHM

For microgrids with secondary voltage restoration control, the bus voltage magnitudes are approximately 1.0 pu, i.e. $V_i \approx V_j \approx 1.0$. The angle difference between the adjacent nodes' voltage phasors tends to remain below 20° , which results in $\cos(\delta_i - \delta_j) \approx 1$ and $\sin(\delta_i - \delta_j) \approx 0$. On this basis, this work adopts a non-iterative, linearized power flow model proposed originally in [36] and [37] (it was known as *Decoupled Linearized Power Flow* (DLPF); mathematical manipulation is detailed in Appendix A, [36] and [37]). Expressing the DLPF in the matrix form, we have

$$\begin{bmatrix} \mathbf{P} \\ \mathbf{Q} \end{bmatrix} = \begin{bmatrix} -\mathbf{B}' & \mathbf{G} \\ -\mathbf{G}' & -\mathbf{B} \end{bmatrix} \begin{bmatrix} \delta \\ \mathbf{V} \end{bmatrix} \quad (5)$$

where \mathbf{G} and \mathbf{B} are the real and imaginary part of the admittance matrix, and \mathbf{G}' and \mathbf{B}' are the corresponding matrices without the shunt element.

III. MODIFIED DLPF AND QP-BASED OPTIMAL SECONDARY CONTROL

A. MODIFIED DLPF FOR DROOP-CONTROLLED MICROGRIDS

The active and reactive power injection at i^{th} bus can be defined as

$$\begin{aligned} P_i &= P_{Li} + P_{Gi} \\ Q_i &= Q_{Li} + Q_{Gi} \end{aligned} \quad (6)$$

where the subscripts L and G represent those of load and generation. Hence, load- and DER-connected buses are hereafter

known as load-bus and droop-bus, respectively. To enable reactive power sharing correction and voltage regulation in an islanded microgrid with N DERs, a dispatch-based $Q - V$ droop scheme is adopted in the primary control with the standard $P - f$ droop control, and are given by

$$\begin{aligned}\omega_i &= \omega_{oi}^* - m_i P_{Gi} \\ V_{Gi} &= V_{oi}^* - n_i Q_{Gi} + u_{com} + n_i Q_{i,dis}\end{aligned}\quad (7)$$

where ω_i and V_{Gi} are the per-unit operating frequency and the droop voltage amplitude (normalized to network's phase peak voltage) of i^{th} DER, ω_{oi}^* and V_{oi}^* are the per-unit no-load frequency and voltage magnitude, m_i and n_i are the per-unit droop coefficients, and P_{Gi} and Q_{Gi} are the filtered per-unit active and reactive output power, normalized to a common base power S_B . The reactive power dispatch command $Q_{i,dis}$ of DERs are individually tuned to adaptively adjust the droop voltage amplitude for accurate reactive power sharing. However, since autonomous power sharing is essentially guaranteed by droop control, it is redundant to control all N DERs' $Q_{i,dis}$, instead only $(N-1)$ DERs are required (to be elaborated later). Subsequently, a commonly shared voltage correction term u_{com} is introduced to enable network-wide voltage regulation without affecting the reactive power sharing accuracy among the DERs.

From (7), the voltage magnitude at N droop buses can be manipulated in term of reactive power injection \mathbf{Q}_G as

$$\begin{bmatrix} V_{G1} \\ \vdots \\ V_{GN} \end{bmatrix} = \begin{bmatrix} V_{o1}^* \\ \vdots \\ V_{oN}^* \end{bmatrix} - \Phi \begin{bmatrix} Q_{G1} \\ \vdots \\ Q_{GN} \end{bmatrix} + \Gamma \begin{bmatrix} u_{com} \\ Q_{1,dis} \\ \vdots \\ Q_{N,dis} \end{bmatrix} \quad (8)$$

$\mathbf{V}_G \qquad \mathbf{V}_o^* \qquad \mathbf{Q}_G \qquad \mathbf{u}$

where

$$\Phi = \begin{bmatrix} n_1 & \cdots & 0 & \cdots & 0 \\ \vdots & & \ddots & & \vdots \\ 0 & \cdots & 0 & \cdots & n_N \end{bmatrix}$$

and

$$\Gamma = \begin{bmatrix} 1 & n_1 & \cdots & 0 \\ \vdots & \vdots & \ddots & \vdots \\ 1 & 0 & \cdots & n_N \end{bmatrix}$$

where \mathbf{u} consists of the common voltage correction term u_{com} and $Q_{i,dis}$ of all DERs. Assumed that the active and reactive power are sufficiently decoupled and knowing that the accurate active power sharing in a droop-controlled islanded microgrid is guaranteed and less affected by the reactive power correction, (5) can be simplified and partitioned (with $\mathbf{Q} = [\mathbf{Q}_L^T \ \mathbf{Q}_G^T]^T$, correspond respectively to reactive power injection at load and droop buses) as

$$\begin{bmatrix} \mathbf{Q}_L \\ \mathbf{Q}_G \end{bmatrix}_{k+1} = - \begin{bmatrix} \mathbf{G}'_{LL} & \mathbf{G}'_{LG} \\ \mathbf{G}'_{GL} & \mathbf{G}'_{GG} \end{bmatrix} \begin{bmatrix} \delta_L \\ \delta_G \end{bmatrix}_{k+1} - \begin{bmatrix} \mathbf{B}_{LL} & \mathbf{B}_{LG} \\ \mathbf{B}_{GL} & \mathbf{B}_{GG} \end{bmatrix} \begin{bmatrix} \mathbf{V}_L \\ \mathbf{V}_G \end{bmatrix}_{k+1} \quad (9)$$

By assuming that the load- and droop-buses' steady-state voltage angle remain relatively constant during secondary control, the estimation model for secondary optimization can be determined by replacing \mathbf{V}_G vector in (9) with (8) (detailed manipulation and full expression in Appendix B), expressible as

$$\mathbf{y}(k+1) = \mathbf{C}\mathbf{v}(k) + \mathbf{D}\mathbf{u}(k) \quad (10)$$

with the aid of the measurable sub-vectors δ_L , δ_G and \mathbf{Q}_L , and constant droop parameters, where

$$\begin{aligned}\mathbf{y} &= [\mathbf{V}_L^T \ \mathbf{Q}_G^T]^T \\ \mathbf{v} &= [\delta_L^T \ \delta_G^T \ \mathbf{Q}_L^T \ \mathbf{V}_o^{*T}]^T \\ \mathbf{u} &= [u_{com} \ \mathbf{Q}_{dis}^T]^T\end{aligned}$$

B. QUADRATIC PROGRAMMING BASED OPTIMAL SECONDARY CONTROL

The secondary estimation model can be augmented with $\mathbf{u}(k) = \mathbf{u}(k-1) + \Delta\mathbf{u}(k)$ into a standard quadratic programming problem, given by

$$\mathbf{y}(k+1) = \underbrace{[\mathbf{D} \ \mathbf{C}]}_{\mathbf{F}} \underbrace{\begin{bmatrix} \mathbf{u}(k-1) \\ \mathbf{v}(k) \end{bmatrix}}_{\mathbf{z}(k)} + \mathbf{D}\Delta\mathbf{u}(k) \quad (11)$$

Then, the microgrid voltage regulation and reactive power sharing optimization problem can now be treated as a tracking problem through the following cost function

$$J = (\mathbf{y}^*(k+1) - \mathbf{y}(k+1))^T \mathbf{W} (\mathbf{y}^*(k+1) - \mathbf{y}(k+1)) + \Delta\mathbf{u}^T \mathbf{R} \Delta\mathbf{u} \quad (12)$$

where \mathbf{y}^* is the output setpoint vector. Notably, \mathbf{W} weighting factor enables the possibility of adjusting the priority between reactive power sharing and voltage regulation. On the other hand, \mathbf{R} can adjust the control efforts among Δu_{com} and all $\Delta Q_{i,dis}$ in $\Delta \mathbf{Q}_{dis}$. It will be shown that the control objectives of reactive power sharing and multi-bus voltage regulation can be conveniently tuned through \mathbf{W} and \mathbf{R} . The cost function (12) of the multi-objective secondary control problem can be formulated into a standard quadratic programming problem, as below:

$$J = \frac{1}{2} \Delta\mathbf{u}^T \mathbf{H} \Delta\mathbf{u} + \Delta\mathbf{u}^T \mathbf{E} \quad (13)$$

where

$$\begin{aligned}\mathbf{H} &= 2 [\mathbf{D}^T \mathbf{W} \mathbf{D} + \mathbf{R}] \\ \mathbf{E} &= -2\mathbf{D}^T \mathbf{W} [\mathbf{y}^*(k+1) - \mathbf{F}\mathbf{z}(k)]\end{aligned} \quad (14)$$

Apart from the adjustable control priority using weighting factors, network and DER constraints can also be considered in QP (as will be demonstrated in Section V). The most relevant constraints in this control problem are the inequality constraints on the outputs (being the bus voltage limits and the DER reactive power). They can be written as

$$\mathbf{y}_{\min} \leq \mathbf{y}(k+1) \leq \mathbf{y}_{\max} \quad (15)$$

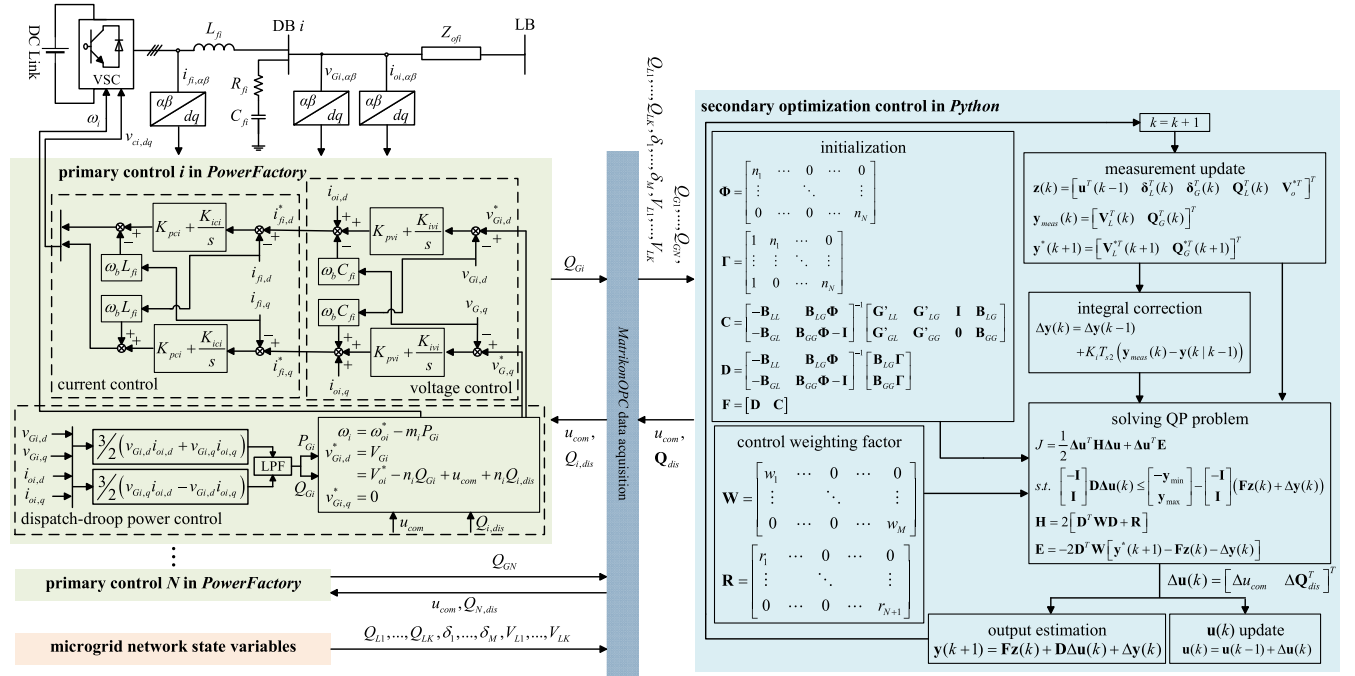


FIGURE 1. Detailed block diagram of DER's primary control and the proposed multi-objective optimal secondary control for islanded microgrid.

In order to fit the inequality constraints into the QP formulation, the constraints are decomposed into lower and upper limit [41]

$$\begin{bmatrix} -\mathbf{I} \\ \mathbf{I} \end{bmatrix} \mathbf{y}(k+1) \leq \begin{bmatrix} -\mathbf{y}_{\min} \\ \mathbf{y}_{\max} \end{bmatrix} \quad (16)$$

Based on (11), the inequality constraints can be re-expressed as

$$\begin{bmatrix} -\mathbf{I} \\ \mathbf{I} \end{bmatrix} \mathbf{D}\Delta\mathbf{u}(k) \leq \begin{bmatrix} -\mathbf{y}_{\min} \\ \mathbf{y}_{\max} \end{bmatrix} - \begin{bmatrix} -\mathbf{I} \\ \mathbf{I} \end{bmatrix} \mathbf{Fz}(k) \quad (17)$$

C. INTEGRAL-BASED CORRECTIVE TERM

The simulation work in Section V (and Fig. 3, in next pages) will show that the adoption of linear power flow (together with associated assumptions) does entail some estimation errors that may be as large as ten percent. This agrees with the general expectation of linear power flow adoption [40], [42]. To improve the estimation, this work subsequently proposes an integral-based corrective term aiming to utilize the available measurements to improve the estimation error. This is done by adding $\Delta\mathbf{y}$ into \mathbf{y} in (11), which gives

$$\Delta\mathbf{y}(k) = \Delta\mathbf{y}(k-1) + K_i T_{s2} (\mathbf{y}_{meas}(k) - \mathbf{y}(k|k-1)) \quad (18)$$

where $\Delta\mathbf{y}(k)$ is the output estimation error at time k , \mathbf{y}_{meas} is the measured output vector, $\mathbf{y}(k|k-1)$ is estimated output vector at time $k-1$ and K_i is the integral gain with the secondary sampling time T_{s2} . This expression is somewhat similar to output feedback corrective term which can be found in standard "discrete-time observer". The main difference here is that, instead of system's time dynamics, the optimal

control here focuses on real-time dispatch of DERs [43]. The issue of voltage offset has also been identified in other linearized power flow, e.g. [44] where non-integral offset correction technique that is rather computationally intensive (for real-time dispatch problems), is proposed. To incorporate the proposed corrective term into the optimal control, (11), (14) and (17) shall be modified to:

$$\mathbf{y}(k+1) = \mathbf{Fz}(k) + \mathbf{D}\Delta\mathbf{u}(k) + \Delta\mathbf{y}(k)$$

$$\mathbf{E} = -2\mathbf{D}^T \mathbf{W} [\mathbf{y}^*(k+1) - \mathbf{Fz}(k) - \Delta\mathbf{y}(k)]$$

$$\begin{bmatrix} -\mathbf{I} \\ \mathbf{I} \end{bmatrix} \mathbf{D}\Delta\mathbf{u}(k) \leq \begin{bmatrix} -\mathbf{y}_{\min} \\ \mathbf{y}_{\max} \end{bmatrix} - \begin{bmatrix} -\mathbf{I} \\ \mathbf{I} \end{bmatrix} (\mathbf{Fz}(k) + \Delta\mathbf{y}(k)) \quad (19)$$

IV. POWERFACTORY-PYTHON CO-SIMULATION PLATFORM

A *PowerFactory-Python* co-simulation platform has been established to investigate the proposed optimal secondary control scheme. *MatrikonOPC* is used as the OPC server to facilitate the data acquisition and transfer between the two software instances (being the clients, through *ComLink* and *OpenOPC* interfaces, respectively). The primary control of a DER and the proposed secondary control is detailed in Fig. 1. The primary controller of each DER is modelled entirely from basic block models of sampling clock, sample-and-hold, $\alpha\beta$ -dq transformation, and etc.

The default voltage and current measurement in *PowerFactory* is in the $\alpha\beta$ reference frame. The entire primary control is comprised of a dispatch-droop power control, output voltage control and an inverter current control - all are performed in the dq reference frame. The DER output voltage vector is

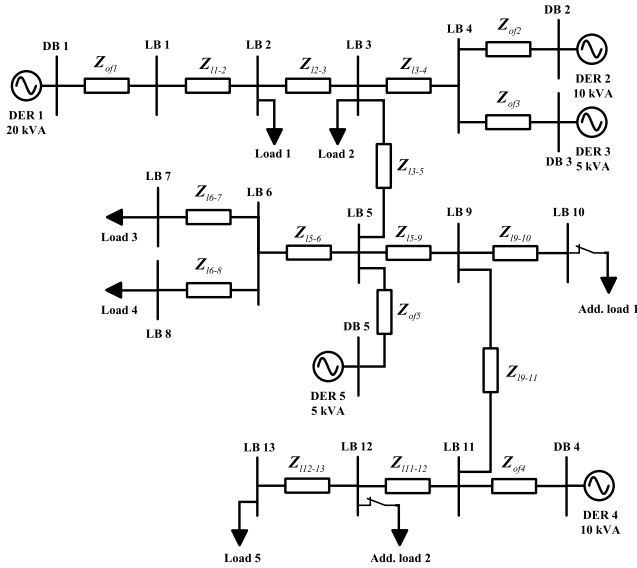


FIGURE 2. Single-line diagram of the islanded microgrid test system.

aligned to its synchronous reference frame, as shown below

$$\begin{aligned} v_{Gi,d}^* &= V_{oi}^* - n_i Q_{Gi} + u_{com} + n_i Q_{i,dis} \\ v_{Gi,q}^* &= 0 \end{aligned} \quad (20)$$

The d -axis reference is the reference for the inner voltage control loop. The primary voltage and current control are controlled by PI controllers, which are tuned in such a way that the control bandwidths are decoupled and the voltage control dynamic having higher bandwidth than the dispatch-droop power control. The tuning steps can be briefly described as follows: the innermost current control loop is tuned first with the assumption of a constant current reference (i.e., typically being the output of voltage control loop), followed by the tuning of voltage controller by assuming a constant output voltage reference (i.e., normally being the output of droop-based power control). The design details are depicted in Fig. 1 but interested readers may also refer to [45], [46] for details.

As for the secondary controller in *Python*, live information such as reactive powers, load-bus voltages, etc., are facilitated through *MatrikonOPC*. Note that in actual implementation some of the state information may be obtained from network state estimation instead of direct measurement. This subject is beyond the focus of the current work hence all state information is obtained directly from the co-simulated network model (Fig. 2) in *PowerFactory*. Each measurement is configured with an OPC tag in *PowerFactory* and is updated to the OPC server at a preset interval while the secondary control reads from the server at a regular period T_{s2} ($= 1/F_{s2}$). Note that the proposed optimal secondary control is designed with prerequisite information such as the constant droop parameters and the network \mathbf{G}' and \mathbf{B} matrices. Upon successful iterations of QP (set to a maximum of 100 iterations in the CVXOPT solver) in each control cycle, provided that $\Delta \mathbf{u}(k)$

TABLE 1. Specifications of the islanded microgrid network and proposed control.

| Parameter | Value | Parameter | Value |
|---|---------------------------------------|--|-------------------------|
| Sw. freq. F_{s1} | 2.5 kHz | Primary voltage control | K_{pvi} 1.23 |
| System freq. | 50 Hz | K_{ivi} | 4.67 |
| Inverter DC bus | 1 kV | Primary current control | K_{pci} 0.27 |
| AC voltage levels | 400 V | K_{ici} | 1.61 |
| DER ratings: | | | |
| Apparent pow. (rated pf) | | P-f droop coefficients (pu) | |
| DER 1 | 20 kVA (0.8) | | 0.0625 |
| DER 2 | 10 kVA (0.8) | | 0.125 |
| DER 3 | 5 kVA (0.8) | | 0.25 |
| DER 4 | 10 kVA (0.8) | | 0.125 |
| DER 5 | 5 kVA (0.8) | | 0.25 |
| Q-V droop coefficients (pu) | | | |
| DER 1 | | | 0.075 |
| DER 2 | | | 0.15 |
| DER 3 | | | 0.30 |
| DER 4 | | | 0.15 |
| DER 5 | | | 0.30 |
| Inverter filter impedances: L-RC | | | |
| Z_{f1} | 7.62 mH, 10 Ω , 3.32 μF | DER output feeder impedances | |
| Z_{f2} | 15.24 mH, 10 Ω , 1.66 μF | Z_{of1} | 0.03 Ω , 0.35 mH |
| Z_{f3} | 30.48 mH, 10 Ω , 0.83 μF | Z_{of2} | 0.02 Ω , 0.45 mH |
| Z_{f4} | 15.24 mH, 10 Ω , 1.662 μF | Z_{of3} | 0.06 Ω , 0.35 mH |
| Z_{f5} | 30.48 mH, 10 Ω , 0.83 μF | Z_{of4} | 0.05 Ω , 0.56 mH |
| | | Z_{of5} | 0.03 Ω , 0.42 mH |
| Line impedances | | | |
| Z_{l1-2} | 0.21 Ω , 1.50 mH | Z_{l6-8} | 0.31 Ω , 2.98 mH |
| Z_{l2-3} | 0.26 Ω , 1.93 mH | Z_{l5-9} | 0.14 Ω , 1.03 mH |
| Z_{l3-4} | 0.70 Ω , 3.70 mH | Z_{l9-10} | 0.10 Ω , 0.54 mH |
| Z_{l3-5} | 0.28 Ω , 1.76 mH | Z_{l9-11} | 0.21 Ω , 0.78 mH |
| Z_{l5-6} | 0.12 Ω , 1.18 mH | Z_{l11-12} | 0.47 Ω , 3.21 mH |
| Z_{l6-7} | 0.19 Ω , 2.01 mH | Z_{l12-13} | 0.16 Ω , 3.06 mH |
| Proposed optimal secondary control | | | |
| Parameter | Value | Parameter | Value |
| Sampling freq. F_{s2} | 0.2 Hz | LPF time constant $\tau_{c,pq}$ | 0.2 s |
| Integral gain K_i | 0.02 | LPF time constant $\tau_{c,v}$ | 0.9 s |

is greater than a pre-defined minimum threshold (being a very small value), the optimal droop dispatch input \mathbf{u} , i.e. u_{com} and all $Q_{i,dis}$, will be updated based on $\mathbf{u}(k) = \mathbf{u}(k-1) + \Delta \mathbf{u}(k)$.

It is worth noting that the investigation is conducted through the comprehensively developed co-simulation platform, which can be regarded as a “software-in-the-loop” technique. The accuracy of the co-simulation is supported by the state-of-the-art network and DER’s primary closed-loop control modelling in *PowerFactory*, and the interoperability data-exchange industrial standard *MatrikonOPC*.

V. RESULTS

Fig. 2 depicts the single-line diagram of the microgrid network. The co-simulated network has 5 DERs (3 is used in [29]) and 18 buses – these settings are chosen in order to limit the wait time due to computational burden encountered (owing to the use of detailed primary control loops) when running the network model in a standard computing workstation. The DER specification are tabulated in Table 1 along with primary control (refer to [46] and [47] for details) and secondary control (e.g. F_{s2} , K_i , etc.) parameters. The power and voltage readings are low-pass filtered at time constants of $\tau_{c,pq}$ and $\tau_{c,v}$, respectively, before being deployed into the secondary control algorithm (in *Python*). DER 1 at droop bus 1 (i.e. DB 1 in Fig. 2) is taken as the reference unit.

In the QP optimization, the weighting factor \mathbf{W} is a M -by- M (i.e. $M = K+N$) diagonal matrix having the form of

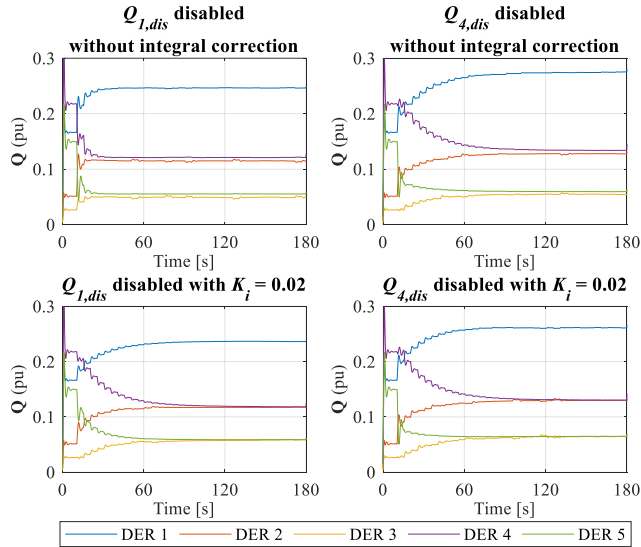


FIGURE 3. Optimal reactive power sharing control with and without integral-based error correction: DER reactive output power.

TABLE 2. Steady state estimation error (absolute percentage) without/with integral correction.

| | $Q_{1,dis}$ disabled [%] | | $Q_{4,dis}$ disabled [%] | |
|-------|--------------------------|--------------|--------------------------|--------------|
| | $K_i = 0$ | $K_i = 0.02$ | $K_i = 0$ | $K_i = 0.02$ |
| DER 1 | 0.00 | 0.00 | 2.69 | 0.23 |
| DER 2 | 8.84 | 0.13 | 4.94 | 0.00 |
| DER 3 | 22.32 | 0.23 | 23.25 | 0.40 |
| DER 4 | 1.23 | 0.13 | 0.00 | 0.00 |
| DER 5 | 11.32 | 0.23 | 12.45 | 0.40 |

$\text{diag}(w_1, w_2, \dots, w_M)$. K is the number of load-bus (labelled as LB in Fig. 2) and N is the number of DERs. In this work with $K = 13$ and $N = 5$, the individual w weighting factors essentially correspond to outputs V_{L1}, \dots, V_{LK} , Q_{G1}, \dots , and Q_{GN} , respectively. Penalty factor \mathbf{R} is a $(N + 1)$ -by- $(N + 1)$ diagonal matrix of the form $\text{diag}(r_1, r_2, \dots, r_{N+1})$. Similarly, the individual r penalty factors correspond, respectively, to control inputs Δu_{com} , $\Delta Q_{1,dis}$, \dots , and $\Delta Q_{N,dis}$.

Fig. 3 first demonstrates the effectiveness of the proposed error correction technique (as explained in Section III-C) in mitigating errors due to power flow linearization. Before introducing (18)-(19), the reactive power sharing remains slightly non-proportional, in pu (with respect to their ratings, Table 1); upon correction with $K_i = 0.02$, they are restored to the proportional ratio of 4:2:1:2:1 (Fig. 3). The absolute percentage estimation error is tabulated in Table 2 with DER 1 acted as the reference for the case “ $Q_{1,dis}$ disabled” and vice versa. The slight difference in individual reactive output powers (between the “ $Q_{1,dis}$ disabled” and “ $Q_{4,dis}$ disabled” cases) is due to the voltage-dependent nature of the loads.

Next, the secondary control scheme in conjunction with different control settings is investigated. By default, a total passive load of 15 kW and 9 kVar are present in the islanded microgrid. Additional loads are connected to LB 10 and

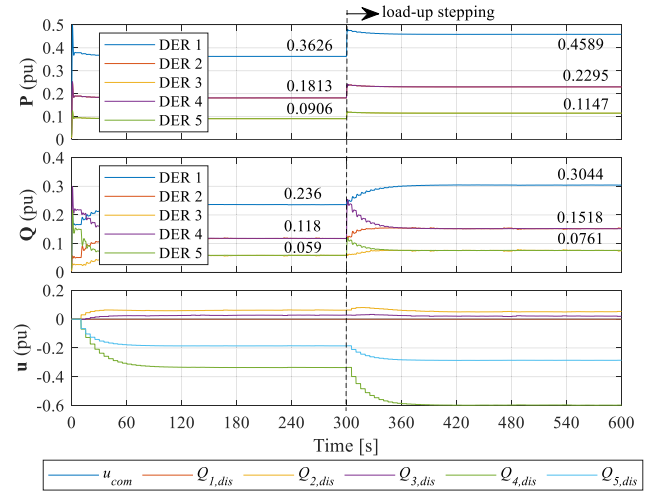


FIGURE 4. Case A: Optimal reactive power sharing control: DERs active/reactive output power and secondary control input u .

LB 12 at a chosen simulation time instant, upon which, the total load demand increases to $22 + j13$ kVA.

A. OPTIMAL SHARING OF REACTIVE POWER

Initially, the DERs are controlled through the standard droop control without the proposed secondary control. It can be established from Fig. 4 that while the active power is always proportionally shared, the reactive power is not. As explained in Section III-A, it is redundant to utilize all N DERs’ $Q_{i,dis}$ for reactive power sharing correction control, instead only those for $(N-1)$ DERs are required. Hence, the r_i value of a DER should be set significantly large (DER 1 is chosen in subsequent studies).

At $t = 10$ s, the proposed optimal secondary control layer with deactivated voltage regulation (achieved by setting $w_{14} - w_{18}$ to 10) is started. Penalty factor \mathbf{R} is set to $\text{diag}(10e10, 10e10, 5, 5, 5, 5)$, which essentially activates $Q_{2,dis}$ to $Q_{5,dis}$ for reactive power sharing correction. The reactive power sharing among the DERs (with $K_i = 0.02$) is significantly improved, giving the ratio of 4:2:1:2:1 at steady state. The corresponding voltages of the droop- and load-buses are shown in Fig. 5, ranging from 0.9132 pu (i.e., LB 13) to 1.0112 pu (i.e., DB 2). Subsequently, additional loads are connected to LB 10 and LB 12 at (approx.) $t = 300$ s. Figs. 4-5 show that proportional reactive power sharing can be retained by the proposed control even after load increase, with the minimum and maximum voltage magnitudes being $V_{L13} = 0.8584$ pu and $V_{G2} = 1.0027$ pu.

B. SINGLE LOAD-BUS VOLTAGE REGULATION

The islanded microgrid is loaded with the default loadings, and the voltage magnitude at LB 12, V_{L12} has “drooped” to 0.9584 pu. At $t = 10$ s, the proposed control is activated with w_{12} (corresponds to V_{L12}) set to 10, and others set to zero (which means the reactive power control is deactivated). \mathbf{R} is set as $\text{diag}(10, 10e10, 10e10, 10e10, 10e10, 10e10)$, which

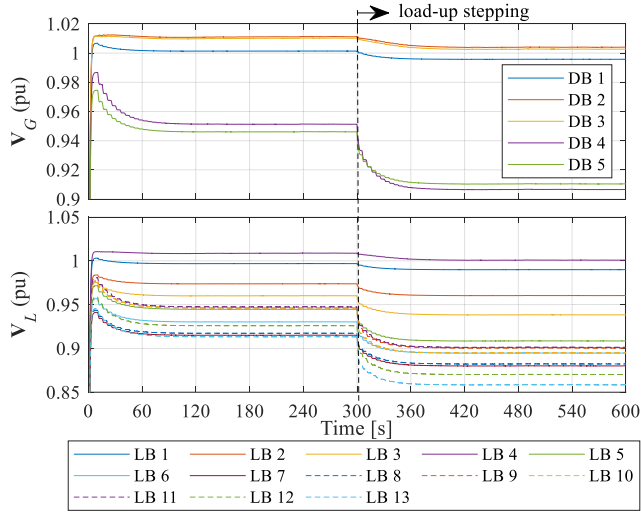


FIGURE 5. Case A: Optimal reactive power sharing control: DER droop voltage magnitudes and load-bus voltage magnitudes.

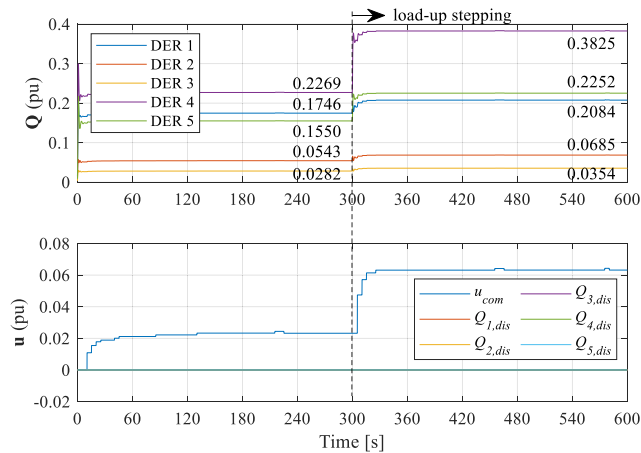


FIGURE 6. Case B: Single load bus voltage regulation control: DERs reactive output power and secondary control input u .

means only u_{com} is activated. It can be clearly seen from Figs. 6 and 7 that V_{L12} is regulated to $V^{ref} = 0.98$ pu through adjustment of the voltage correction term u_{com} without any noticeable transient in the DERs' reactive output power. Upon loads up-stepping at $t = 300$ s, the voltage magnitude at load-bus LB 12 is retained at 0.98 pu but the issue of non-proportional reactive power sharing persists, as expected.

C. OPTIMAL REACTIVE POWER SHARING AND VOLTAGE REGULATION

The case of simultaneous optimal reactive power sharing and voltage regulation is investigated next. Initially, the DERs are allowed to droop at the default load condition. At $t = 10$ s, the optimal secondary control is activated by setting \mathbf{W} as $w_{12}, w_{14} - w_{18} = 10$ and \mathbf{R} as $\text{diag}(10, 10e10, 5, 5, 5, 5, 5)$. Fig. 8 shows, despite loads up-stepping (at $t = 300$ s), proportional reactive power sharing can be achieved among the DERs and V_{L12} is always regulated to $V^{ref} = 0.98$ pu.

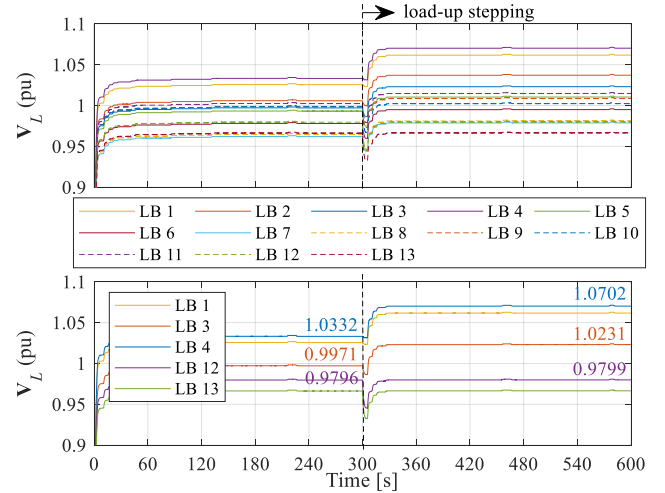


FIGURE 7. Case B: Single load bus voltage regulation control: load-bus voltage magnitudes.

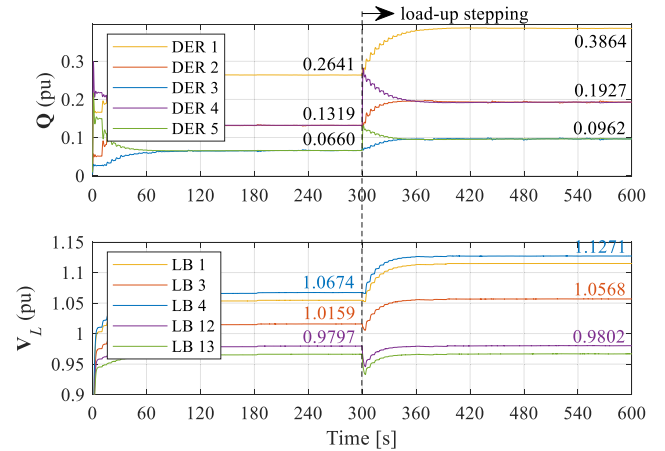


FIGURE 8. Case C: Optimal reactive power sharing and single load-bus voltage regulation control: reactive output power and load-bus voltage magnitudes.

This confirms the viability of the proposed optimal secondary control for the case with single load-bus.

Next, the performance of optimal reactive power sharing and multi-load-buses voltage regulation is examined. At default loading condition, the voltage magnitude at LB 12 is of 0.9584 pu with $V_{L4} = 1.0104$ pu. In case C-I, multi-load-buses voltage regulation control is prioritized but with an emphasis on reactive power sharing improvement. At $t = 10$ s, the proposed control is activated by setting \mathbf{W} with $w_{12} = 100$ and $w_{14} - w_{18} = 10$, and \mathbf{R} as $\text{diag}(10, 10e10, 5, 5, 5, 5, 5)$.

Subsequently, at $t = 300$ s, w_4 is changed from 0 to 100 in order to realize multi-bus voltage (V_{L4} and V_{L12}) regulation. Fig. 9 clearly demonstrates the trade-offs between optimal reactive power sharing among the DERs and multi-bus voltage regulation. Precise single-bus voltage regulation (i.e. V_{L12} be regulated to $V_{L12}^{ref} = 0.98$ pu) and proportional reactive power sharing are achieved before 300 s. Upon

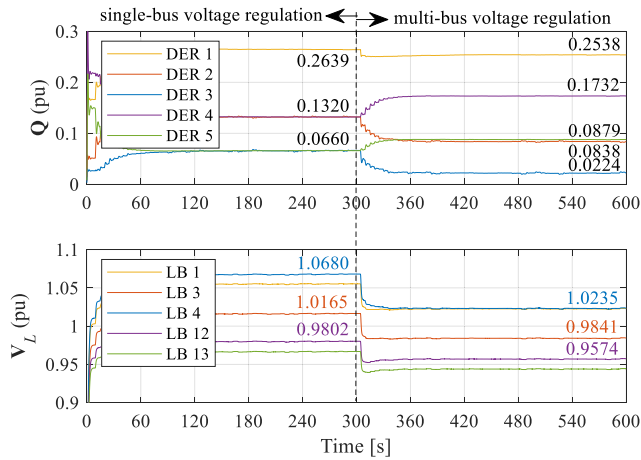


FIGURE 9. Case C-I: Optimal reactive power sharing and prioritized multi-load-bus voltage regulation control: DERs reactive output power and load-bus voltage magnitudes.

the multi-load-bus voltage regulation (i.e. $V_{L4}^{ref} = 1.0$ pu), although V_{L4} and V_{L12} are both regulated close to their references (1.0235 pu and 0.9574 pu), proportional reactive power sharing is compromised. This is because \mathbf{W} weighs voltage regulation heavier than reactive power sharing (100 vs 10).

The robustness of the proposed optimal control against communication failure is examined next in case C-II. Specifically, DER 2 is chosen as the subject, and the “communication failure” is realistically simulated by “freezing” the communication in and out of DER 2, leaving DER 2 to operate under droop control with fixed dispatch commands. The proposed control is activated with multi-bus voltage regulation and reactive power sharing at $t = 10$ s. Weighting/penalty factors \mathbf{W} and \mathbf{R} are set the same as that in case C-I. Communication in and out of DER 2 are lost at $t = 120$ s and the optimal controller retains the last available DER 2’s reactive power. As shown in Fig. 10, the reactive power ratio and bus voltages have been slightly affected after 120 s (until 300 s), as compared to the result in case C-I (Fig. 9). This result nevertheless confirms the robustness of the proposed optimal control towards communication loss even for a sustained period. In practical scenarios, communication loss is usually detected (and mitigated) in a much shorter time duration.

In scenario C-III, both the voltage regulation and reactive power sharing are weighted equally (by setting $w_4, w_{12}, w_{14} - w_{18}$ to 10) with \mathbf{R} remains as $\text{diag}(10, 10e10, 5, 5, 5, 5)$. It can be clearly seen from Fig. 11 that the reactive power sharing error among the DERs is significantly improved (ratio as shown in Fig. 11) while V_{L4} and V_{L12} are more loosely regulated.

D. CONSTRAINED OPTIMAL REACTIVE POWER SHARING AND MULTI-BUS VOLTAGE REGULATION

Next, the ability of the QP-based secondary control in dealing with limits (by activating the inequality constraints (19)) is examined. The islanded microgrid is loaded with the default

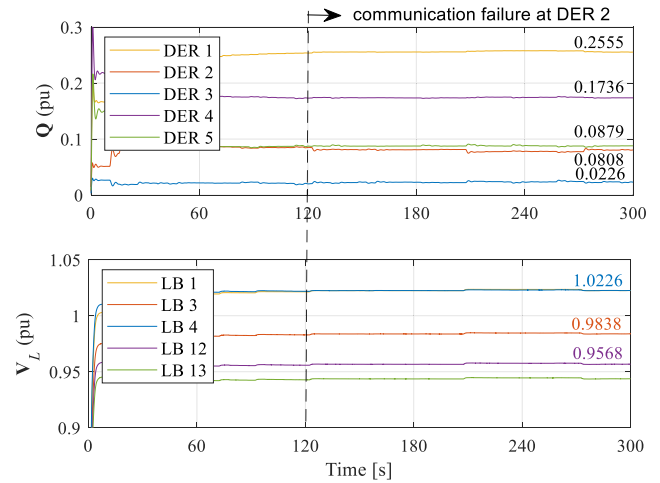


FIGURE 10. Case C-II: Optimal reactive power sharing and multi-load-bus voltage regulation control with communication failure: DERs reactive output power and load-bus voltage magnitudes.

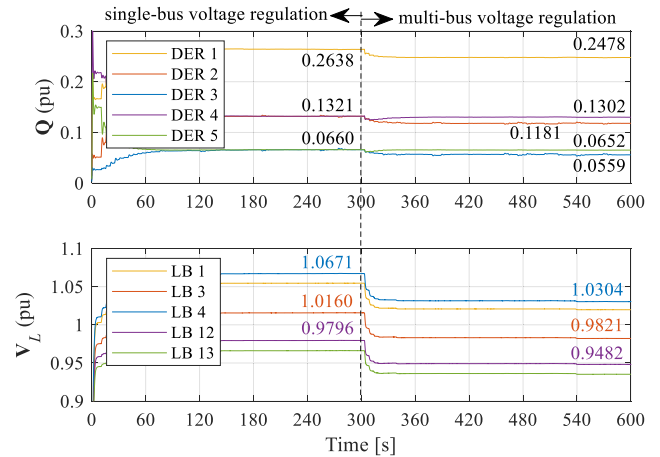


FIGURE 11. Case C-III: Optimal reactive power sharing and multi-load-bus voltage regulation control: DERs reactive output power and load-bus voltage magnitudes.

loading and at $t = 10$ s, the secondary control with equal weighting of voltage regulation and reactive power sharing, is activated. Weighting/penalty factors \mathbf{W} and \mathbf{R} are set the same as scenario C-III and LB 3 is selected as a critical bus with the desire to achieve a voltage tolerance of $\pm 1\%$ (and with the DERs reactive output power limited to their respective capacity limit; the remaining buses are limited loosely to $-6\%/+10\%$ from 1.0 pu). It can be seen from Fig. 12 that, while V_{L12} is regulated to 0.9738 pu (with $V_{L12}^{ref} = 0.98$ pu) and the reactive power sharing ratio is improved to 0.2608:0.1312:0.0654, the unregulated V_{L3} (since $w_3 = 0$) is maintained at 1.01 pu (as opposed to the unconstrained scenario in case C-III, $V_{L3} = 1.016$ pu, as in Fig. 11). Then, at $t = 300$ s, multi-bus voltage regulation is activated by setting w_4 as 10 (i.e., activating V_{L4} regulation with $V_{L4}^{ref} = 1.0$ pu). It is shown that the proposed QP-based optimal control can regulate V_{L4} and V_{L12} to, respectively, 1.038 pu and 0.9556 pu, and maintain near-proportional reactive power sharing. Voltage of the critical bus LB 3 is kept at approximately 0.99 pu.

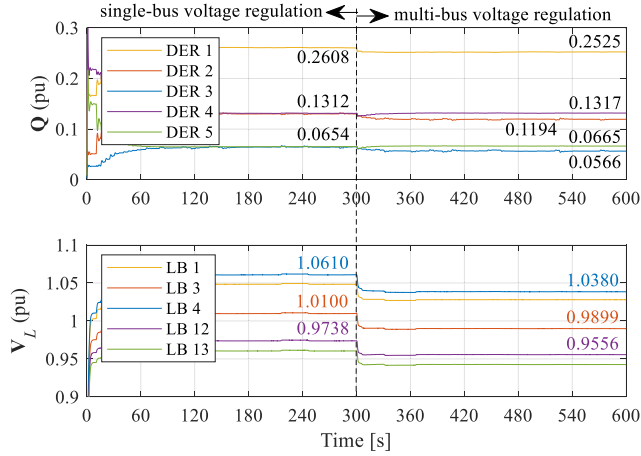


FIGURE 12. Case D: Constrained optimal reactive power sharing and multi-load-bus voltage regulation control: DERs reactive output power and load-bus voltage magnitudes.

This result fully demonstrates the capability of the QP-based multi-objective optimal secondary control in considering the network constraints.

VI. DISCUSSION

In the preceding sections, the optimal secondary control has been tested in conjunction with three distinctive cases: reactive power sharing correction without voltage regulation, single-load bus voltage regulation without reactive power sharing correction, and lastly, optimal reactive power sharing and single-/multi-bus voltage regulation. These results have verified the performance of the proposed optimal control in handling the intrinsic trade-offs between reactive power sharing and voltage regulation in droop-controlled islanded microgrids. The ability of the proposed QP-based secondary control in handling practical constraints is also fully verified. The load-bus voltage and DERs' reactive power limits consideration are practically relevant to the scenarios of critical buses and physically limited kVA capacities of e.g. grid battery system (being a dispatchable DER).

Possible applications of the proposed control strategy include but not limited to the following: the single load-bus voltage regulation is relevant to the context of synchronizing the islanded microgrid's point of interconnection with the wider AC grid, specifically, during the transition from islanded mode to grid-connected mode; for islanded microgrids with multiple critical/sensitive buses, apart from maintaining a fairly accurate reactive power sharing (means whenever physically possible) among the DERs, the multi-bus voltage regulation will be useful in keeping the voltage magnitude of those critical buses within the desired limits, either through the direct voltage regulation feature or the constraint-handling feature of the optimal secondary controller.

Lastly, discussion on the relevance of extending the proposed control scheme for frequency regulation, e.g. [48], and power oscillation, e.g. [49], [50], is due. Frequency regulation/restoration can be readily achieved (in either central

or distributed manner) by correcting the frequency droop deviation through a modified $P - f$ droop equation in (7). On the other hand, if one intends to improve the active power oscillation, the common approach is through the intervention at the primary control [49], [50], owing to the control bandwidth requirement. Therefore, the proposed DLDPF-based optimal secondary control (even after augmenting it to include active-power-frequency droop) is likely not suitable for these purposes.

VII. CONCLUSION

In this paper, we propose a non-iterative based multi-objective optimal secondary control scheme based on modified Decoupled Linearized Power Flow to address the control objectives with intrinsic trade-off: optimal reactive power sharing among DERs and voltage regulation at multiple load-buses in droop-controlled islanded microgrids. The constrained secondary control is framed into a generic QP problem with linear constraints to enable the deployment of established solver, e.g. CVXOPT. The proposed secondary control not only capable to realize single-objective control, i.e. optimal reactive power sharing or single-bus voltage regulation, it can also accomplish multi-objective control, e.g. single load-bus voltage regulation and optimal reactive power sharing without compromising proportional reactive power sharing. The control scheme can also optimally regulate multiple load-bus voltages with tradeoffs of reactive power sharing. It is provably capable to keep the network variables, e.g. load-bus voltages and DERs' reactive power outputs, to within the predefined limits. The priority among the output objectives and control efforts can also be flexibly adjusted through weighting and penalty factors (being \mathbf{W} and \mathbf{R} here). All the claims have been supported by theoretical derivation and substantiated with extensive simulation proofs.

Lastly, for future works, the proposed non-iterative based optimal secondary control scheme should be benchmarked against relevant control techniques, e.g., iterative-based counterpart. Moreover, in order to alleviate the risk of single-point failure of centralized control and ease the computational load of the optimal control strategy, the next logical step is to develop the optimal secondary control scheme into a distributed architecture.

APPENDIX A

DECOUPLED LINEARIZED POWER FLOW ALGORITHM

The terms \mathbf{B} , \mathbf{B}' , \mathbf{G} and \mathbf{G}' in (8) can be extracted from the following expressions (see [36] for detailed steps):

$$\begin{aligned}
 P_i &= V_i^2 G_{ii} + \sum_{j=1, j \neq i}^M V_i V_j [B_{ij} \sin(\delta_i - \delta_j) + G_{ij} \cos(\delta_i - \delta_j)] \\
 &= V_i^2 G_{ii} + \sum_{j=1, j \neq i}^M V_i V_j [B_{ij} \sin \Delta \delta_{ij} + G_{ij} \cos \Delta \delta_{ij}] \\
 &= V_i^2 G_{ii} + \sum_{j=1, j \neq i}^M V_i V_j [B_{ij} \Delta \delta_{ij} + G_{ij}] \\
 &= \sum_{j=1}^M G_{ij} V_j - \sum_{j=1}^M B'_{ij} \delta_j
 \end{aligned} \tag{21}$$

$$\begin{aligned}
Q_i &= -V_i^2 B_{ii} + \sum_{j=1, j \neq i}^M V_i V_j [G_{ij} \sin(\delta_i - \delta_j) - B_{ij} \cos(\delta_i - \delta_j)] \\
&= -V_i^2 B_{ii} + \sum_{j=1, j \neq i}^M V_i V_j [G_{ij} \sin \Delta \delta_{ij} - B_{ij} \cos \Delta \delta_{ij}] \\
&= -V_i^2 B_{ii} + \sum_{j=1, j \neq i}^M V_i V_j [G_{ij} \Delta \delta_{ij} - B_{ij}] \\
&= -\sum_{j=1}^M B_{ij} V_j - \sum_{j=1}^M G'_{ij} \delta_j
\end{aligned} \quad (22)$$

APPENDIX B

SECONDARY ESTIMATION MODEL IN (10)

DER-bus voltage terms in (8) are substituted into (9) to express \mathbf{V}_G in terms of reactive power injection, constant droop parameters, and control inputs \mathbf{u} , i.e., u_{com} and \mathbf{Q}_{dis} , with the assumption that the steady-state voltage angle δ (obtainable from measurement) remain relatively constant during the secondary control adjustment. This gives

$$\begin{aligned}
&\begin{bmatrix} -\mathbf{B}_{LL} & \mathbf{B}_{LG}\Phi \\ -\mathbf{B}_{GL} & \mathbf{B}_{GG}\Phi - \mathbf{I} \end{bmatrix} \underbrace{\begin{bmatrix} \mathbf{V}_L \\ \mathbf{Q}_G \end{bmatrix}}_{\mathbf{y}(k+1)} \\
&= \begin{bmatrix} \mathbf{G}'_{LL} & \mathbf{G}'_{LG} & \mathbf{I} & \mathbf{B}_{LG} \\ \mathbf{G}'_{GL} & \mathbf{G}'_{GG} & \mathbf{0} & \mathbf{B}_{GG} \end{bmatrix} \underbrace{\begin{bmatrix} \delta_L \\ \delta_G \\ \mathbf{Q}_L \\ \mathbf{V}_o^* \end{bmatrix}}_{\mathbf{v}(k)} \\
&+ \underbrace{\begin{bmatrix} \mathbf{B}_{LG}\Gamma \\ \mathbf{B}_{GG}\Gamma \end{bmatrix} \begin{bmatrix} u_{com} \\ \mathbf{Q}_{1,dis} \\ \vdots \\ \mathbf{Q}_{N,dis} \end{bmatrix}}_{\mathbf{u}(k)}
\end{aligned} \quad (23)$$

By re-assembling the known sub-vectors, i.e. δ_L , δ_G , \mathbf{Q}_L and \mathbf{V}_o^* , into a single vector \mathbf{v} , one can obtain (10), where \mathbf{C} is a $M \times 2M$ matrix and \mathbf{D} is a $M \times (N + 1)$ matrix, which can be expressed as

$$\begin{aligned}
\mathbf{C} &= \begin{bmatrix} -\mathbf{B}_{LL} & \mathbf{B}_{LG}\Phi \\ -\mathbf{B}_{GL} & \mathbf{B}_{GG}\Phi - \mathbf{I} \end{bmatrix}^{-1} \begin{bmatrix} \mathbf{G}'_{LL} & \mathbf{G}'_{LG} & \mathbf{I} & \mathbf{B}_{LG} \\ \mathbf{G}'_{GL} & \mathbf{G}'_{GG} & \mathbf{0} & \mathbf{B}_{GG} \end{bmatrix} \\
\mathbf{D} &= \begin{bmatrix} -\mathbf{B}_{LL} & \mathbf{B}_{LG}\Phi \\ -\mathbf{B}_{GL} & \mathbf{B}_{GG}\Phi - \mathbf{I} \end{bmatrix}^{-1} \begin{bmatrix} \mathbf{B}_{LG}\Gamma \\ \mathbf{B}_{GG}\Gamma \end{bmatrix}
\end{aligned}$$

REFERENCES

- [1] H. Mahmood, D. Michaelson, and J. Jiang, "Reactive power sharing in islanded microgrids using adaptive voltage droop control," *IEEE Trans. Smart Grid*, vol. 6, no. 6, pp. 3052–3060, Nov. 2015.
- [2] R. M. Imran, S. Wang, and F. M. F. Flaih, "DQ-voltage droop control and robust secondary restoration with eligibility to operate during communication failure in autonomous microgrid," *IEEE Access*, vol. 7, pp. 6353–6361, 2019.
- [3] S. Zhang, C. Chen, L. Dong, Y. Li, J. Zhao, H. Nian, and L. Kong, "An enhanced droop control strategy for accurate reactive power sharing in islanded microgrids," in *Proc. IEEE Innov. Smart Grid Technol.-Asia (ISGT Asia)*, May 2019, pp. 2352–2356.
- [4] T. V. Hoang and H.-H. Lee, "An adaptive virtual impedance control scheme to eliminate the reactive-power-sharing errors in an islanding meshed microgrid," *IEEE J. Emerg. Sel. Topics Power Electron.*, vol. 6, no. 2, pp. 966–976, Jun. 2018.
- [5] Y. C. C. Wong, C. S. Lim, A. J. Cruden, M. D. Rotaru, and P. K. Ray, "A consensus-based adaptive virtual output impedance control scheme for reactive power sharing in meshed microgrids," in *Proc. IEEE Int. Conf. Power Electron., Smart Grid Renew. Energy (PESGRE)*, Jan. 2020, pp. 1–6.
- [6] R. Heydari, T. Dragicevic, and F. Blaabjerg, "High-bandwidth secondary voltage and frequency control of VSC-based AC microgrid," *IEEE Trans. Power Electron.*, vol. 34, no. 11, pp. 11320–11331, Nov. 2019.
- [7] W. Gu, G. Lou, W. Tan, and X. Yuan, "A nonlinear state estimator-based decentralized secondary voltage control scheme for autonomous microgrids," *IEEE Trans. Power Syst.*, vol. 32, no. 6, pp. 4794–4804, Nov. 2017.
- [8] H. Zhang, S. Kim, Q. Sun, and J. Zhou, "Distributed adaptive virtual impedance control for accurate reactive power sharing based on consensus control in microgrids," *IEEE Trans. Smart Grid*, vol. 8, no. 4, pp. 1749–1761, Jul. 2017.
- [9] J. Schiffer, T. Seel, J. Raisch, and T. Sezi, "Voltage stability and reactive power sharing in inverter-based microgrids with consensus-based distributed voltage control," *IEEE Trans. Control Syst. Technol.*, vol. 24, no. 1, pp. 96–109, Jan. 2016.
- [10] H.-J. Yoo, T.-T. Nguyen, and H.-M. Kim, "Consensus-based distributed coordination control of hybrid AC/DC microgrids," *IEEE Trans. Sustain. Energy*, vol. 11, no. 2, pp. 629–639, Apr. 2020.
- [11] Q. Shafiee, V. Nasirian, J. C. Vasquez, J. M. Guerrero, and A. Davoudi, "A multi-functional fully distributed control framework for AC microgrids," *IEEE Trans. Smart Grid*, vol. 9, no. 4, pp. 3247–3258, Jul. 2018.
- [12] M. Shi, X. Chen, J. Zhou, Y. Chen, J. Wen, and H. He, "PI-consensus based distributed control of AC microgrids," *IEEE Trans. Power Syst.*, vol. 35, no. 3, pp. 2268–2278, May 2020.
- [13] J. W. Simpson-Porco, Q. Shafiee, F. Dörfler, J. C. Vasquez, J. M. Guerrero, and F. Bullo, "Secondary frequency and voltage control of islanded microgrids via distributed averaging," *IEEE Trans. Ind. Electron.*, vol. 62, no. 11, pp. 7025–7038, Nov. 2015.
- [14] J. Liu, J. Li, H. Song, A. Nawaz, and Y. Qu, "Nonlinear secondary voltage control of islanded microgrid via distributed consistency," *IEEE Trans. Energy Convers.*, vol. 35, no. 4, pp. 1964–1972, Dec. 2020.
- [15] J. Lai, X. Lu, X. Li, and R.-L. Tang, "Distributed multiagent-oriented average control for voltage restoration and reactive power sharing of autonomous microgrids," *IEEE Access*, vol. 6, pp. 25551–25561, May 2018.
- [16] X. Lu, X. Yu, J. Lai, Y. Wang, and J. M. Guerrero, "A novel distributed secondary coordination control approach for islanded microgrids," *IEEE Trans. Smart Grid*, vol. 9, no. 4, pp. 2726–2740, Jul. 2018.
- [17] R. Han, L. Meng, G. Ferrari-Trecate, E. A. A. Coelho, J. C. Vasquez, and J. M. Guerrero, "Containment and consensus-based distributed coordination control to achieve bounded voltage and precise reactive power sharing in islanded AC microgrids," *IEEE Trans. Ind. Appl.*, vol. 53, no. 6, pp. 5187–5199, Nov. 2017.
- [18] Y. Xu, Q. Guo, H. Sun, and Z. Fei, "Distributed discrete robust secondary cooperative control for islanded microgrids," *IEEE Trans. Smart Grid*, vol. 10, no. 4, pp. 3620–3629, Jul. 2019.
- [19] X. Wu, C. Shen, and R. Iravani, "A distributed, cooperative frequency and voltage control for microgrids," *IEEE Trans. Smart Grid*, vol. 9, no. 4, pp. 2764–2776, Jul. 2018.
- [20] A. Bidram, A. Davoudi, and F. L. Lewis, "A multiobjective distributed control framework for islanded AC microgrids," *IEEE Trans. Ind. Informat.*, vol. 10, no. 3, pp. 1785–1798, Aug. 2014.
- [21] X. Wu, Y. Xu, X. Wu, J. He, J. M. Guerrero, C.-C. Liu, K. P. Schneider, and D. T. Ton, "A two-layer distributed cooperative control method for islanded networked microgrid systems," *IEEE Trans. Smart Grid*, vol. 11, no. 2, pp. 942–957, Mar. 2020.
- [22] R. V. A. Neves, R. Q. Machado, V. A. Oliveira, X. Wang, and F. Blaabjerg, "Multitask fuzzy secondary controller for AC microgrid operating in stand-alone and grid-tied mode," *IEEE Trans. Smart Grid*, vol. 10, no. 5, pp. 5640–5649, Sep. 2019.
- [23] A. Bidram, A. Davoudi, F. L. Lewis, and J. M. Guerrero, "Distributed cooperative secondary control of microgrids using feedback linearization," *IEEE Trans. Power Syst.*, vol. 28, no. 3, pp. 3462–3470, Aug. 2013.
- [24] N. M. Dehkordi, N. Sadati, and M. Hamzeh, "Fully distributed cooperative secondary frequency and voltage control of islanded microgrids," *IEEE Trans. Energy Convers.*, vol. 32, no. 2, pp. 675–685, Jun. 2017.
- [25] F. Guo, C. Wen, J. Mao, and Y. D. Song, "Distributed secondary voltage and frequency restoration control of droop-controlled inverter-based microgrids," *IEEE Trans. Ind. Electron.*, vol. 62, no. 7, pp. 4355–4364, Jul. 2015.

- [26] M. Chen, X. Xiao, and J. M. Guerrero, "Secondary restoration control of islanded microgrids with a decentralized event-triggered strategy," *IEEE Trans. Ind. Informat.*, vol. 14, no. 9, pp. 3870–3880, Sep. 2018.
- [27] Z. Afshar, M. Mollayousefi, S. M. T. Bathaee, M. T. Bina, and G. B. Gharehpetian, "A novel accurate power sharing method versus droop control in autonomous microgrids with critical loads," *IEEE Access*, vol. 7, pp. 89466–89474, Jul. 2019.
- [28] F. Qiao and J. Ma, "Voltage/var control for hybrid distribution networks using decomposition-based multiobjective evolutionary algorithm," *IEEE Access*, vol. 8, pp. 12015–12025, Jan. 2020.
- [29] X. Yang, Y. Du, J. Su, L. Chang, Y. Shi, and J. Lai, "An optimal secondary voltage control strategy for an islanded multibus microgrid," *IEEE J. Emerg. Sel. Topics Power Electron.*, vol. 4, no. 4, pp. 1236–1246, Dec. 2016.
- [30] G. Agundis-Tinajero, N. L. D. Aldana, A. C. Luna, J. Segundo-Ramírez, N. Visairo-Cruz, J. M. Guerrero, and J. C. Vazquez, "Extended-optimal-power-flow-based hierarchical control for islanded AC microgrids," *IEEE Trans. Power Electron.*, vol. 34, no. 1, pp. 840–848, Jan. 2019.
- [31] M. M. A. Abdelaziz, H. E. Farag, E. F. El-Saadany, and Y. A.-R. I. Mohamed, "A novel and generalized three-phase power flow algorithm for islanded microgrids using a Newton trust region method," *IEEE Trans. Power Syst.*, vol. 28, no. 1, pp. 190–201, Feb. 2013.
- [32] F. Mumtaz, M. H. Syed, M. A. Hosani, and H. H. Zeineldin, "A novel approach to solve power flow for islanded microgrids using modified Newton Raphson with droop control of DG," *IEEE Trans. Sustain. Energy*, vol. 7, no. 2, pp. 493–503, Apr. 2016.
- [33] A. La Bella, S. R. Cominesi, C. Sandroni, and R. Scattolini, "Hierarchical predictive control of microgrids in islanded operation," *IEEE Trans. Autom. Sci. Eng.*, vol. 14, no. 2, pp. 536–546, Apr. 2017.
- [34] H. R. Baghaee, M. Mirsalim, and G. B. Gharehpetian, "Power calculation using RBF neural networks to improve power sharing of hierarchical control scheme in multi-DER microgrids," *IEEE J. Emerg. Sel. Topics Power Electron.*, vol. 4, no. 4, pp. 1217–1225, Dec. 2016.
- [35] E. E. Pompodakis, G. C. Karyonidis, and M. C. Alexiadis, "A comprehensive load flow approach for grid-connected and islanded AC microgrids," *IEEE Trans. Power Syst.*, vol. 35, no. 2, pp. 1143–1155, Mar. 2020.
- [36] J. Yang, N. Zhang, C. Kang, and Q. Xia, "A state-independent linear power flow model with accurate estimation of voltage magnitude," *IEEE Trans. Power Syst.*, vol. 32, no. 5, pp. 3607–3617, Sep. 2017.
- [37] Y. Liu, N. Zhang, Y. Wang, J. Yang, and C. Kang, "Data-driven power flow linearization: A regression approach," *IEEE Trans. Smart Grid*, vol. 10, no. 3, pp. 2569–2580, May 2019.
- [38] J. Machowski, J. W. Bialek, and J. R. Bumby, *Power System Dynamics: Stability and Control*, 2nd ed. West Sussex, U.K.: Wiley, 2008.
- [39] Y. Liu, Y. Wang, N. Zhang, D. Lu, and C. Kang, "A data-driven approach to linearize power flow equations considering measurement noise," *IEEE Trans. Smart Grid*, vol. 11, no. 3, pp. 2576–2587, May 2020.
- [40] D. Yu, J. Cao, and X. Li, "Review of power system linearization methods and a decoupled linear equivalent power flow model," in *Proc. Int. Conf. Electron. Technol. (ICET)*, May 2018, pp. 232–239.
- [41] L. Wang, *Model Predictive Control System Design and Implementation Using MATLAB*. London, U.K.: Springer-Verlag, 2009.
- [42] K. Dvijotham and D. K. Molzahn, "Error bounds on the DC power flow approximation: A convex relaxation approach," in *Proc. IEEE 55th Conf. Decis. Control (CDC)*, Dec. 2016, pp. 2411–2418.
- [43] D. Van Hertem, J. Verboomen, K. Purchala, R. Belmans, and W. L. Kling, "Usefulness of DC power flow for active power flow analysis with flow controlling devices," in *Proc. 8th IEEE Int. Conf. AC DC Power Transmiss. (ACDC)*, 2006, pp. 58–62.
- [44] Y. Wang, H. Wu, H. Xu, Q. Li, and S. Liu, "A general fast power flow algorithm for transmission and distribution networks," *IEEE Access*, vol. 8, pp. 23284–23293, Feb. 2020.
- [45] A. Bidram, V. Nasirian, A. Davoudi, and F. L. Lewis, "Control of AC microgrids," in *Cooperative Synchronization in Distributed Microgrid Control*. Cham, Switzerland: Springer, 2017, pp. 32–36.
- [46] Y. C. C. Wong, C. S. Lim, M. D. Rotaru, and K. Xin, "Reactive power sharing study of an islanded microgrid in DiGSILENT Power-Factor," in *Proc. 7th Int. Conf. Renew. Energy Res. Appl. (ICRERA)*, Oct. 2018, pp. 1–6.
- [47] N. Pogaku, M. Prodanovic, and T. C. Green, "Modeling, analysis and testing of autonomous operation of an inverter-based microgrid," *IEEE Trans. Power Electron.*, vol. 22, no. 2, pp. 613–625, Mar. 2007.
- [48] Z. Li, Z. Cheng, J. Liang, J. Si, L. Dong, and S. Li, "Distributed event-triggered secondary control for economic dispatch and frequency restoration control of droop-controlled AC microgrids," *IEEE Trans. Sustain. Energy*, vol. 11, no. 3, pp. 1938–1950, Jul. 2020.
- [49] H. Lahiji, J. Mohammadi, F. B. Ajaei, and R. Boudreau, "Damping power oscillations in the inverter-dominated microgrid," in *Proc. IEEE Electr. Power Energy Conf. (EPEC)*, Oct. 2018, pp. 1–7.
- [50] Y. Sun, X. Hou, J. Yang, H. Han, M. Su, and J. M. Guerrero, "New perspectives on droop control in AC microgrid," *IEEE Trans. Ind. Electron.*, vol. 64, no. 7, pp. 5741–5745, Jul. 2017.



YI CHYN CASSANDRA WONG (Student Member, IEEE) received the B.Eng. degree (Hons.) in electrical power engineering from Curtin University, Malaysia, in 2016. She is currently pursuing the split-site Ph.D. degree with the University of Southampton, U.K., and the University of Southampton Malaysia.

She was a Research Intern with the Experimental Power Grid Centre, Agency for Science, Technology and Research (A*STAR), Singapore, in 2017. Her research interests include power quality improvement, optimization control, and distributed cooperative control in microgrid.



CHEE SHEN LIM (Senior Member, IEEE) received the B.Eng. degree (Hons.) in electrical engineering from the University of Malaya, Malaysia, in 2009, and the joint-university Ph.D. degree in power electronics and drives from the University of Malaya and Liverpool John Moores University, U.K., in 2013.

He was a Research Scientist with the Experimental Power Grid Centre, A*STAR, Singapore, from 2013 to 2015. He joined the University of Southampton Malaysia, in November 2015, as an Assistant Professor of electrical and electronic engineering, and he is currently an Associate Professor. His research interests include advanced model predictive control design, multiphase motor drives, grid-connected converter control, and microgrid's hierarchical control. He serves as an Associate Editor for the *IET Electric Power Applications*.



HUI HWANG GOH (Senior Member, IEEE) received the B.Eng. degree (Hons.) in electrical engineering, the M.Eng. degree in electrical engineering, and the Ph.D. degree from Universiti Teknologi Malaysia (UTM), Johor, Malaysia, in 1998, 2002, and 2007, respectively.

He is currently a Professor of electrical engineering with the School of Electrical Engineering, Guangxi University, Nanning, China. His research interests include embedded power generation modeling and simulation, power quality studies, wavelet analysis, multi-criteria decision-making, renewable energies, and dynamic equivalent. He is a fellow of the Institution of Engineering and Technology (IET), U.K. He is also a fellow of the ASEAN Academy of Engineering and Technology (AAET) and the Chinese Society of Electrical Engineering (CSEE). He is a Chartered Engineer under the Engineering Council United Kingdom (ECUK). He is a Professional Engineer under the Board of Engineers, Malaysia (BEM).



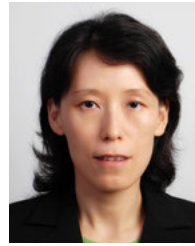
ANDREW CRUDEN received the B.Eng., M.Sc., and Ph.D. degrees in electronic and electrical engineering from the University of Strathclyde, Glasgow, U.K., in 1989, 1990, and 1998, respectively.

He is currently the Associate Dean (Infrastructure) of the Faculty of Engineering and Physical Sciences (FEPS) and a Professor of energy technology with the University of Southampton, U.K. He has significant experience in the field of energy storage and electric vehicles, covering vehicle-to-grid (V2G), new battery technologies, such as aluminium-ion cells, and flow cells, such as soluble lead flow battery. He has previously worked in fuel cell technology and condition monitoring of wind turbines. He is a member of the Training and Diversity Panel of the U.K.'s Faraday Institution and the Co-Director of the EPSRC Centre for Doctoral Training (CDT) in energy storage and its applications.



MIHAI DRAGOS ROTARU (Member, IEEE) received the B.Eng. and M.Sc. degrees in electrical engineering from the Technical University of Cluj-Napoca, Romania, in 1996 and 1997, respectively, and the Ph.D. degree in electrical engineering from the University of Southampton, U.K., in 2001.

He was an Assistant Professor then an Associate Professor with the School of Electronics and Computer Science, University of Southampton, from 2007 to 2019. He served as the Electrical and Electronic Engineering Program Leader for the University of Southampton Malaysia, from 2013 to 2019. He is currently a Senior Scientist with the Institute of Microelectronics, A*STAR, Singapore. His research interests and expertise include simulation and modeling of complex applied electromagnetic problems.



XIN KONG received the B.Eng. and M.Eng. degrees in electrical engineering from Xi'an Jiaotong University, China, in 1994 and 1997, respectively, and the Ph.D. degree in electrical engineering from the National University of Singapore, Singapore, in 2009.

She is currently a Principal Research Scientist and the Deputy Program Director of the Energy Research Institute at NTU (ERI@N), Nanyang Technological University, Singapore. Her research interests include modern power system modeling and analysis, renewable energy integration, distributed microgrid control, and power electronic design and control for grid application.

...

Reactive Power Sharing Study of an Islanded Microgrid in DIgSILENT PowerFactory

Yi Chyn Cassandra Wong^{1,2}, Chee Shen Lim^{1,2}, Mihai D. Rotaru^{1,2}, Andrew Cruden², Kong Xin³

¹University of Southampton Malaysia (UoSM), Johor Bahru, Malaysia

²University of Southampton (UoS), Southampton, United Kingdom

³Experimental Power Grid Centre (EPGC), A*STAR, Singapore

y.c.c.wong@soton.ac.uk, c.s.lim@soton.ac.uk, A.J.Cruden@soton.ac.uk

Abstract— In an islanded microgrid, it has been reported that owing to the nature of low reactance/resistance ratio line impedances, additional provision is usually required at the primary/secondary control level to maintain an accurate power sharing among DERs. Several microgrid-theme techniques such as virtual output impedance methods and adjustable power dispatch methods have been reported but most of them had only been investigated using heavily simplified networks in first principle simulation packages such as Matlab. However, in a large-scale microgrid with many DERs, it has become increasing apparent that the nature of interaction among the DERs on, for example, power sharing performance or individual controller interaction, is becoming important to be known in advance. Hence, this work develops an inverter-based DER model suitable for microgrid studies in the DIgSILENT PowerFactory simulation environment. A power sharing study based on a four-DER islanded microgrid with adjustable virtual output impedance scheme and on the use of standard P - f and Q - V droop scheme is presented here to demonstrate the viability of the developed model and platform.

INTRODUCTION

Microgrids can be regarded as one of the building blocks of smart grid technology which can ease the integration of a large number of distribution energy resources (DERs). Common DERs include wind, solar, biomass and biogas renewable resources, battery energy storage systems, and fuel-based distributed generation. Microgrids can operate either in the grid-connected mode where the voltage and frequency dynamics are dominated by the large-inertia main grid, or in the islanded mode where the voltage and frequency are to be governed by the local DERs while they meet the local active and reactive load power demands.

Standard frequency-active-power (P - f) and voltage-reactive-power (Q - V) droop control is an established technique for power sharing among the generators in a power grid with large inertia and high reactance/resistance (X/R) ratio (e.g. transmission network). Nevertheless, it has been established that owing to the low X/R ratio in a microgrid distribution network, the standard droop control suffers from

crossing coupling of active and reactive power control, which subsequently leads to disproportionate sharing of power among the generators or DERs. It was also hinted in some literature [1-12] that the reactive power is usually more susceptible to the cross-coupling issue, depending on the value of the X/R ratio. To date, various droop-based accurate power sharing methods have been proposed [1-12], and they can be broadly categorized as follows: P - V and Q - f droop control technique [14-15]; virtual-output-impedance-based droop (VOI-droop) control technique [1-9]; and, standard droop control with centralized/distributed power dispatch [15]. Typically, some of these methods require some modification or changes at the primary or secondary control level and this renders most of the default packages in the power system specialist software not usable and this work intends to contribute towards this aspect. However, since the P - V and Q - f droop technique relies on the assumption of very low X/R ratio (i.e. X being negligible) which is not common in large-area distribution microgrid, it will not be considered further and the focus will therefore be on the VOI-droop control.

This work focuses on the development of an inverter-based DER model suitable for the implementation of VOI-droop technique in the DIgSILENT PowerFactory simulation environment. The model and the platform are examined using an adjustable-VOI-based reactive power sharing study. The rest of the paper is organized as follows: Section II discusses the standard droop control principle and gives some mathematical insight into the reactive power sharing problem in a microgrid. Section III illustrates the inverter-based DER model with VOI scheme. Section IV shows the results of an adjustable VOI-based reactive power sharing scheme for scenarios such as load stepping and DER disconnection. Lastly, section V discusses and concludes the adjustable-VOI-based reactive power sharing study.

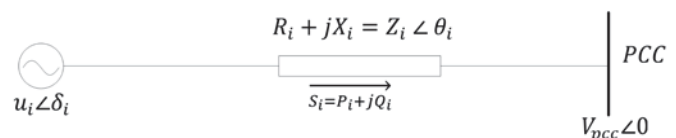


Fig. 1: An inverter-based DER connects to the microgrid at the point of common coupling PCC.

The conference expenses are financed in part by the Fundamental Research Grant Scheme (FRGS) of the Ministry of Higher Education Malaysia, and in part by the Centre for Doctoral Training in Sustainable Infrastructure Systems, UK. The studentship for Ms. Wong is funded in part by the FRGS Malaysia and in part by the Faculty of Engineering and Environment, University of Southampton, UK.

BASIC CONSIDERATION

A. Standard Droop Control in a Distribution Microgrid

Fig. 1 shows that the i^{th} inverter-based DER that connects to an AC bus through a line impedance Z_i . The active and reactive power delivered to the AC bus can be calculated from

$$P_i = \frac{V_{pcc}u_i}{Z_i} \cos(\theta_i - \delta_i) - \frac{V_{pcc}^2}{Z_i} \cos \theta_i \quad (1)$$

$$Q_i = \frac{V_{pcc}u_i}{Z_i} \sin(\theta_i - \delta_i) - \frac{V_{pcc}^2}{Z_i} \sin \theta_i \quad (2)$$

where V_{pcc} and u_i are the i^{th} PCC bus voltage magnitude and the i^{th} DER output/feeder voltage magnitude, δ_i is the power angle between the two voltage phasors, and Z_i and θ_i are the magnitude and the phase angle of the line impedance phasor. With some manipulation, they become

$$P_i = \left(\frac{V_{pcc}u_i}{Z_i} \sin \delta_i \right) \sin \theta_i + \left(\frac{V_{pcc}u_i}{Z_i} \cos \delta_i - \frac{V_{pcc}^2}{Z_i} \right) \cos \theta_i \quad (3)$$

$$Q_i = \left(\frac{V_{pcc}u_i}{Z_i} \cos \delta_i - \frac{V_{pcc}^2}{Z_i} \right) \sin \theta_i - \left(\frac{V_{pcc}u_i}{Z_i} \sin \delta_i \right) \cos \theta_i \quad (4)$$

On the other hand, the standard P - f and Q - V droop control can be expressed mathematically as follows:

$$\omega_i = \omega_i^* - m_i P_i \quad (5)$$

$$u_i = u_i^* - n_i Q_i \quad (6)$$

where ω_i^* and u_i^* are the no-load angular frequency and no-load RMS output voltage of i^{th} DER, and P_i and Q_i are the actual active and reactive power delivered by the i^{th} DER. The active and reactive power droop coefficients m_i and n_i are usually set based on the i^{th} DER rating and the maximum allowable voltage and frequency deviation. The standard droop control assumes that the voltage angle is very small (i.e. $\sin \delta \approx \delta$ and $\cos \delta \approx 1$) and that X/R is large (or R is negligible, i.e. $\sin \theta \approx 1$ and $\cos \theta \approx 0$), which then simplifies the active and reactive power terms from (3)-(4) to

$$P_{i,droop} = \frac{V_{pcc}u_i}{Z_i} \delta_i \quad (7)$$

$$Q_{i,droop} = \frac{V_{pcc}(u_i - V_{pcc})}{Z_i} \quad (8)$$

B. Reactive Power Sharing Analysis

In a microgrid, however, the standard droop control becomes inaccurate as the distribution lines usually have much lower X/R ratio (i.e. low X , non-negligible R) than the assumption. This leads to occurrence of the well-known coupling phenomenon between active and reactive power loops [13, 15]. From the existing literature, it has been found that for some range of X/R ratio, the reactive power sharing is more susceptible than the active power counterpart. Hence, one of the objectives of this work is to provide some mathematical insight into this phenomenon: assume that the voltage angle is small and the line impedance angle θ_i is no longer $\pi/2$ (non-negligible R) but slightly below $\pi/2$ (say $\sin \theta_i$ still $\approx 0.9 \sim 1$ for $X/R > 2$) while the line impedance magnitude remains the same as $|Z_i|$, the power expressions become:

$$P_i \approx \frac{V_{pcc}u_i}{Z_i} \delta_i + \left(\frac{V_{pcc}u_i}{Z_i} - \frac{V_{pcc}^2}{Z_i} \right) \cos \theta_i \quad (9)$$

$$Q_i \approx \frac{V_{pcc}(u_i - V_{pcc})}{Z_i} - \left(\frac{V_{pcc}u_i}{Z_i} \delta_i \right) \cos \theta_i \quad (10)$$

By taking the ratio of the power deviation (i.e. $\Delta P_i = P_i - P_{i,droop}$ and $\Delta Q_i = Q_i - Q_{i,droop}$) to the standard droop's power terms, we have:

$$\frac{\Delta P_i}{P_{i,droop}} \approx \left(\frac{u_i - V_{pcc}}{u_i} \right) \frac{\cos \theta_i}{\delta_i} \quad (11)$$

$$\frac{\Delta Q_i}{Q_{i,droop}} \approx \left(\frac{u_i}{u_i - V_{pcc}} \right) \frac{\delta_i}{\cos \theta_i} \quad (12)$$

The expression will now be evaluated with some realistic test values: if a voltage drop of 10% across the line impedance is assumed, and δ assumes a value of 0.1 rad or 5.7° , and $\cos \theta_i$ assumes the range of values of 0.1~0.45 (corresponds to X/R value from 2~10), $\Delta P_i/P_{i,droop}$ value falls in the range of 0.1~0.45 and $\Delta Q_i/Q_{i,droop}$ falls in the range of 2.2~10. The large reactive power change ratio signifies that the reactive power would be affected much more than the active power as the X/R ratio reduces from a large value (i.e. complying with the ideal droop assumption) to any smaller value that is still, in this analysis, greater than 2, and this X/R ratio range of 2 to 10 corresponds essentially to most line impedance ratios of large-area low-voltage distribution network. The reactive power disproportionate deviation will be verified again by the simulation results in Section IV. For even lower X/R ratio, such as that of building microgrids, it is expected that P - V and Q - f droop technique [14, 15] should be considered, but this is not the focus of this paper.

C. Virtual Output Impedance for Reactive Power Sharing

One of the reported techniques to overcome the issue of reactive power sharing in an islanded microgrid is by integrating virtual output impedance (VOI) into the inverter-based DERs' primary control. This VOI scheme attempts to modify the effective output/network impedance as seen by the inverter-based DER through close-loop control. In principle, if all the droop-participating inverter-based DERs are equipped with the VOI technique, and if a network-wide impedance modification scheme is applied (e.g. [3, 8, 9]), the droop-based power sharing accuracy among the DERs can then be improved while the standard P - f and Q - V droop profiles continue to be applicable.

The virtual voltage drops in i^{th} DER's primary control can be expressed in the stationary reference frame as

$$u_{vi,\alpha\beta} = (R_{vi} + j\omega L_{vi})(i_{oi,\alpha} + j i_{oi,\beta}) \quad (13)$$

where R_{vi} and L_{vi} are the desired virtual resistance and inductance, and $i_{oi,\alpha}$ and $i_{oi,\beta}$ are the output currents expressed in the stationary reference frame. In order to adaptively tune the virtual resistance and inductance, a secondary controller is developed and integrated onto the primary controllers of the DERs in the microgrid. Only a central, integrator-based secondary controller is used here as the focus of this work is primarily on the modelling of PowerFactory-based primary control with virtual output impedance and on the evaluation of the effectiveness of the platform for reactive power sharing study using modern microgrid-based control techniques.

IMPLEMENTATION IN DIGSILENT POWERFACTORY

Fig. 2 shows the single line representation of i^{th} inverter-based DER equipped with an LC output filter. The output of the DER is connected to the main network at feeder i . The

schematic of the entire primary control for this voltage-controlled DER is summarised in Fig. 3. It can be seen that there are essentially four sub-control modules: a droop-based power control, a virtual output impedance control/calculation, a three-phase output voltage (v_o) controller, and a three-phase filter current (i_i) controller. It can also be noticed that the control of three-phase quantities are done primarily in the synchronous reference frame, i.e. $d-q$ reference frame, through the use of standard proportional-integral (PI) controllers (stationary frame quantities are used only in the VOI calculation). The synchronous reference frame's angular position, φ_i , can be obtained based on one of the two start-up mechanisms: if the i^{th} DER is supposed to black-start, φ_i will be obtained from the internal calculation in the droop control block; if the i^{th} DER is supposed to start with a live grid, then φ_i will be first made equal to the grid voltage vector's angular position through the use of phase locked loop.

Fig. 4 shows an overview of the controller blocks implemented in DiGSILENT PowerFactory. PowerFactory default measurement block *Power Measurement Device* is used to measure the inverter-based DER delivered active and reactive power at the DER terminal. The DER's operating

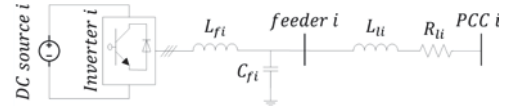


Fig 2: Single line representation of a three-phase voltage source inverter.

frequency and reference output voltage for the voltage controller are calculated using the measured active and reactive power (usually low-pass filtered, but this is not done here for simplicity) through the power controller through the P - f and Q - V droop profiles. Default measurement block *Current Measurement Devices* are placed before and after the LC filter to measure the inverter current and output current respectively.

D. Feeder's Power Control

In an islanded microgrid, power control of DERs (voltage-controlled type) are typically achieved through droop control since the voltage and frequency stability are inherently guaranteed. Standard P - f and Q - V droop profiles are adopted in this work, as summarized by eqns. (5)-(6) and Fig. 5. Since the synchronous reference frame is synchronously aligned to the feeder voltage vector of i^{th}

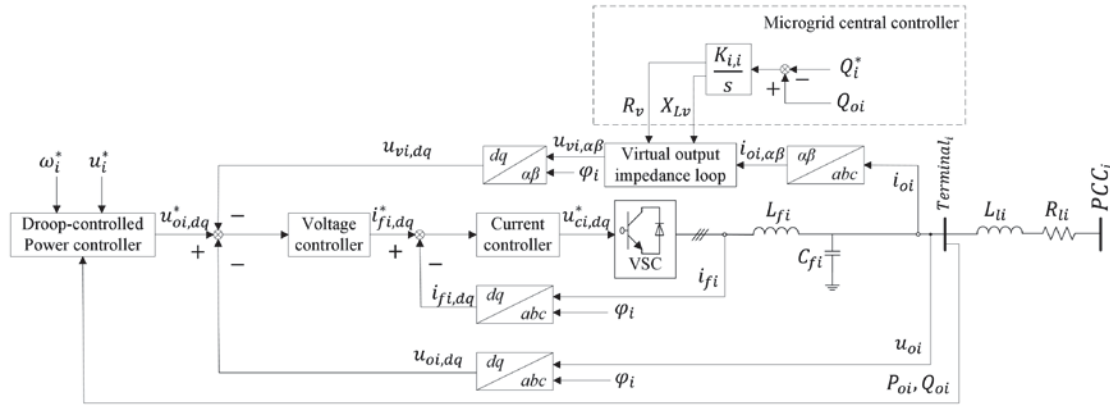


Fig. 3: Schematic diagram of an inverter-based DER local controller with microgrid central controller.

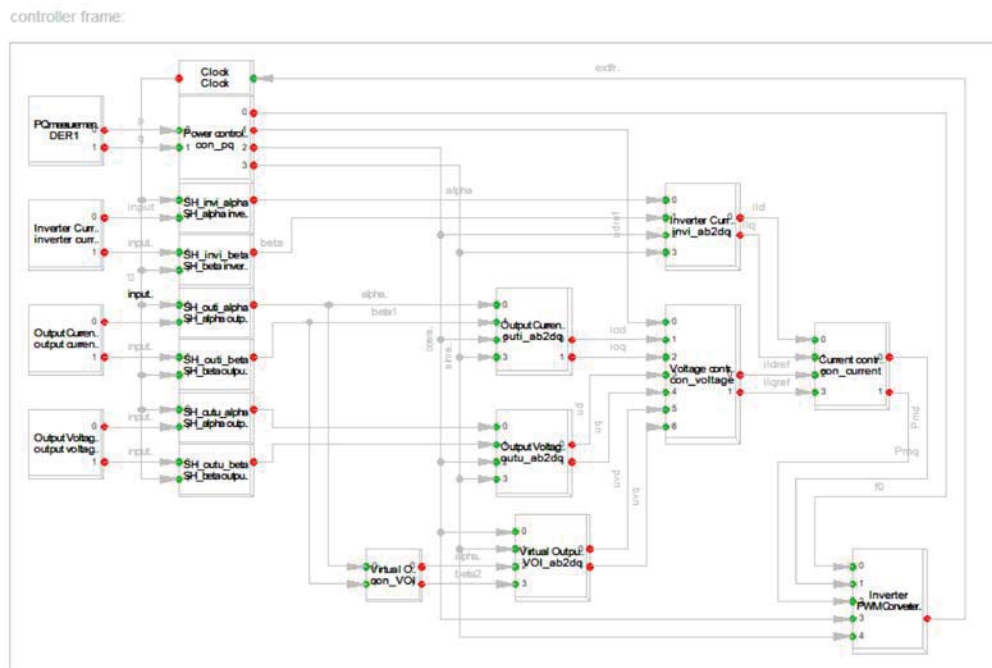


Fig. 4: Local controller block implemented in DiGSILENT PowerFactory.

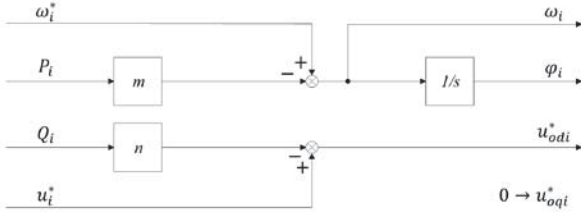


Fig. 5: Power controller block diagram.

DER, the output voltage can be given by

$$u_{odi}^* = u_i^* - n_i Q_i \quad (14)$$

$$u_{oqi}^* = 0 \quad (15)$$

where u_{odi}^* and u_{oqi}^* are the voltage references for the output voltage controller in i^{th} DER. On the other hand, the corresponding operating frequency ω_i is obtained from eqn. (5) and the synchronous reference frame angular position ϕ_i is calculated from

$$\phi_i = \int \omega_i \cdot dt \quad (16)$$

Since all DERs considered in this work are of the dispatchable type and are involved in supporting the voltage and frequency of the islanded microgrid, each DER would have its own angular position calculated from its respective droop coefficients. It is acknowledged that the synchronization mechanism of DER during their first connection to the microgrid will usually require additional provision on the angular position ϕ_i calculation (as already discussed above).

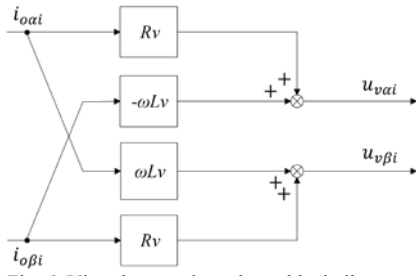


Fig. 6: Virtual output impedance block diagram.

E. Feeder/Output Voltage Control

On the basis of eqn. (13), the block diagram of the VOI voltage terms calculation is depicted graphically in Fig. 6. This calculation block calculates the additional virtual output voltage drop u_{vi} that will be feedforwarded to the voltage controller after being rotationally transformed into the synchronous reference frame – a reference frame is being used by the output voltage controller (and the filter current controller, see below). Fig. 7 shows the block diagram of the feeder/output voltage controller model. PI controllers are used as the regulator to compare the output voltage reference from the power controller against the measured i^{th} inverter-based DER output voltages and the feedforwarded virtual output voltages from the VOI controller to command the required changes in the inverter currents. Subsequently, the measured output voltage is feedforwarded through the admittance to improve the output dynamics.

F. Filter Current Control

The filter current control block diagram is depicted graphically in Fig. 8. The reference inverter currents are provided by the feeder/output voltage controller with PI

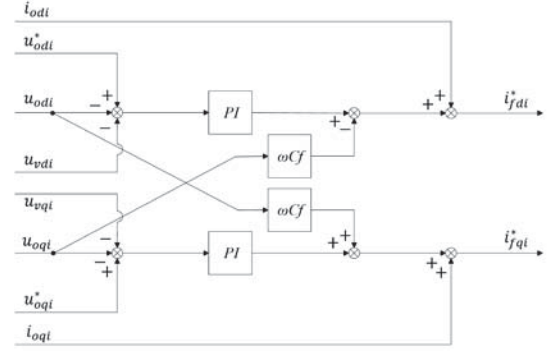


Fig. 7: Voltage controller block diagram.

controllers that determine the tracking error from the desired reference and the measured inverter currents. In order to improve the control dynamics, the cross-decoupling terms are feedforwarded. The reference inverter voltages will then be inversely rotational-transformed to the stationary frame to match with the DigSILENT PowerFactory inverter block model.

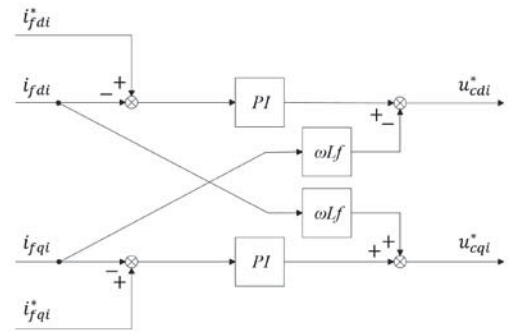


Fig. 8: Current controller block diagram.

G. Secondary Control for Virtual Impedance Adjustment

If all the grid network parameters and the loads are fixed, then the VOIs can be suitably set and kept constant, and the reactive power required by all the loads in the microgrid can be proportionately shared among the DERs. However, fixed distribution network configuration is rarely the case in practice. Therefore, in order to account for changes in the network (e.g. addition or removal of DERs/loads), the VOIs should be appropriately adjusted. For simplicity, this work adopts a central secondary controller, which means low-bandwidth (tens of seconds or minutes) communication between the DERs' local/primary controllers and the secondary control is expected to be present. Then, real-time information such as kVA rating, the reactive power measurement, and VOI values will be exchanged between the central secondary controller and the local controllers. Accordingly, the load-adjustable virtual inductance is calculated through

$$L_{vi} = \frac{K_{Li}}{s} (Q_i - Q_i^*) \quad (17)$$

where K_{Li} is the integral gain to regulate the virtual inductance. Note that only virtual reactance is used here as the main concern here is on the reactive power sharing. Virtual resistance, which could be used for active damping purpose, is less relevant and hence is assumed to be zero.

SIMULATION RESULTS

The simulation test system of a four inverter-based DERs islanded microgrid is depicted in Fig. 9. Two balanced loads

are connected to the microgrid at PCC bus 1 and 2 respectively. The parameters of the four DERs are tabulated in Table I. Series RL impedances are used for each feeder. The desired ratio of the active and reactive power of the four DER units is respectively 4:2:1:2.

For the first case study, the DERs are supplying the total load of 19.3 kW and 12.2 kVar. The respective active and

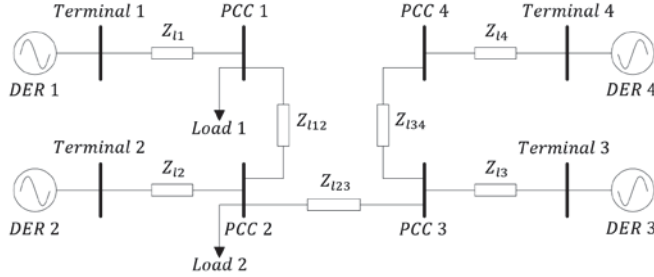


Fig. 9: Single line diagram of the microgrid test system.

TABLE I. INVERTER-BASED DERs PARAMETERS

| Parameter | Value | Parameter | Value |
|----------------------------|----------|---------------------|-----------------------------|
| System frequency | 50 Hz | Switching frequency | 10 kHz |
| Inverter-based DER ratings | | Line impedances | |
| DER 1 | 20 kVA | Z_{11} | 0.03000 Ω , 0.350 mH |
| DER 2 | 10 kVA | Z_{12} | 0.04334 Ω , 0.350 mH |
| DER 3 | 5 kVA | Z_{13} | 0.05597 Ω , 0.350 mH |
| DER 4 | 10 kVA | Z_{14} | 0.08040 Ω , 0.350 mH |
| Voltage ratings | | Z_{12} | 0.23000 Ω , 0.732 mH |
| DC voltage | 1.0 kV | Z_{23} | 0.35000 Ω , 1.847 mH |
| AC voltage | 400 V | Z_{34} | 0.23000 Ω , 1.464 mH |
| Output filters | | | |
| L_{f1} | 7.62 mH | C_{f1} | 30 μ F |
| L_{f2} | 15.24 mH | C_{f2} | 15 μ F |
| L_{f3} | 30.24 mH | C_{f3} | 7.5 μ F |
| L_{f4} | 15.24 mH | C_{f4} | 15 μ F |

reactive power droop coefficients of each DER, in p.u., are kept equal so that both active and reactive power are proportionately shared based on their kVA ratings. The test system is initially controlled using the standard droop control without any line impedance mismatch compensation (i.e. the adjustable-VOI-based scheme). The power delivered by the DER units are shown in Fig. 10 and it can be noticed that prior to $t = 3$ s although the active power is proportionately shared, the reactive power sharing is not. Then, the VOI controllers that reside in the all inverter-based DERs are activated at time $t = 3$ s. It can be noticed that the reactive power sharing is now improved, and the active power supply is practically unaffected. The above observation basically agrees with the theoretical expectation discussed in Section II-B. The VOI implementation helps to improve the standard-droop-based power sharing to the extent that the reactive power can now be shared proportionally among DERs. The simulation process is followed by a load step change at time $t = 30$ s which the total load is increased to 22.3 kW and 23.7 kVar. As seen in Fig. 10, the load active and reactive power can still be shared accurately among the inverter-based DERs despite the load change. On the other hand, the corresponding operating frequencies of the DER units, their droop output voltage magnitudes, and the PCC bus voltage magnitudes are shown in Fig. 11. It can be observed that reactive power sharing is improved at the expense of the DERs' PCC/output voltage that becomes much lower than that with only the standard droop. In the event of larger load, i.e. after time $t = 30$ s, the

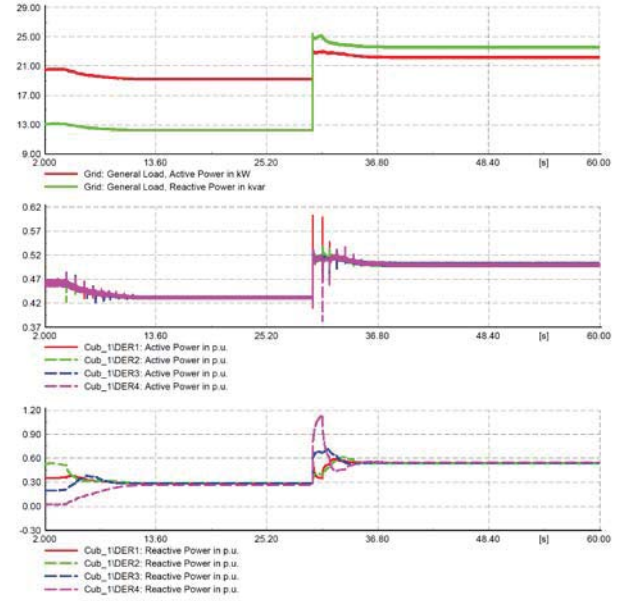


Fig. 10: Microgrid total load demand (top), inverter-based DERs active (middle) and reactive power injection (bottom) for three cases: before the activation of the VOI scheme (before 3 s); after the activation of the VOI scheme (after 3 s, before 30 s); with a load step change at 30 s.

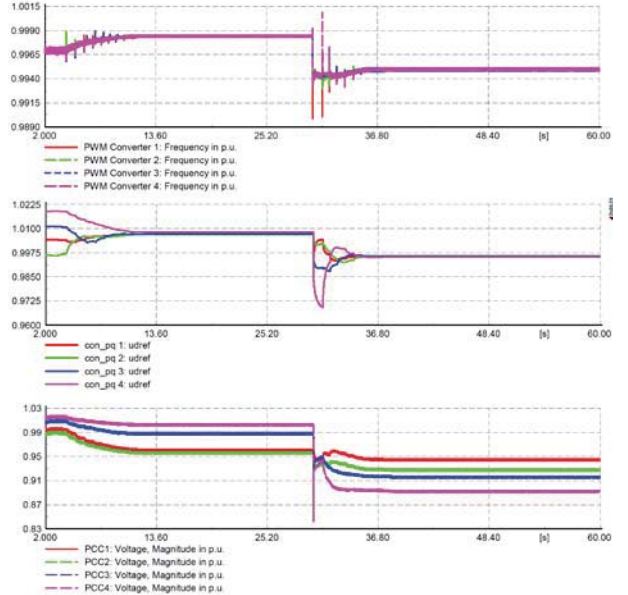


Fig. 11: The corresponding inverter-based DERs operating frequencies (top), droop output voltage readings (middle) and actual PCC voltage magnitude (bottom) for the same studies as in Fig. 10.

voltage magnitudes at PCC4 approaches 0.9 p.u. – the lower limit of grid voltage in most grid codes. This observation exemplifies that potential issues that may occur in any microgrid adopting the VOI scheme and hence the model developed here is very much relevant to enable the investigation on this aspect.

The second case study attempts to investigate the response of the controllers and the power sharing nature when plug-and-play feature of inverter-based DERs is considered. The test system is started off with a total load of 19.3 kW and 12.2 kVar. It can be again seen in Fig. 12 that prior to time $t = 30$ s, the reactive power is disproportionately shared but upon the activation of VOI scheme, the issue is again resolved. At time $t = 30$ s, DER3 is removed on-the-fly from the microgrid (e.g. by opening the circuit breaker). It is shown in Fig. 12 that the active and reactive powers from each DER are almost instantaneously re-distributed in

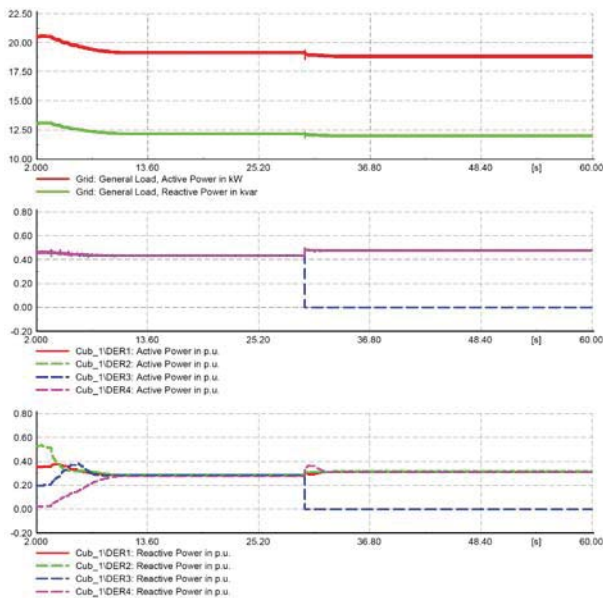


Fig. 12: Microgrid total load demand (top), inverter-based DERs active (middle) and reactive power injection (bottom) for the case of disconnecting DER3.

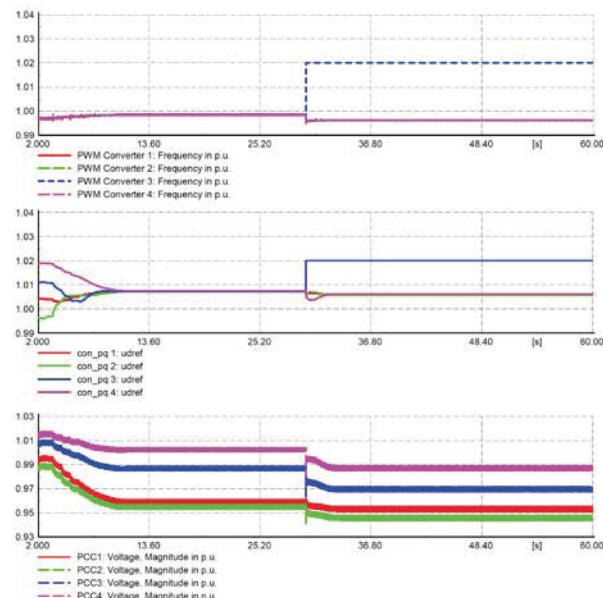


Fig. 13: The corresponding inverter-based DERs operating frequencies (top), droop output voltage readings (middle) and actual PCC voltage magnitude (bottom) for the same studies as in Fig. 12.

a proportionate manner short after the disconnection instance. The DER units operating frequencies, droop output voltages and the respective PCC bus voltage magnitudes are shown in Fig. 13 and it is noticed that even higher output voltage drops occur at PCCs, caused by the presence of VOIs. Summarily, this means, in practice, the VOI-scheme should be implemented together with some form of secondary control to restore the bus voltage levels to within the allowable limits in the grid codes.

CONCLUSION

This paper has presented a DigSILENT PowerFactory model for inverter-based DERs that is suitable for analyzing the integration of large amount of DER units into a distribution microgrid. The standard primary control of a droop-controlled DER is incorporated with adjustable virtual output impedance scheme to improve the power sharing

performance. The model can reflect the controller's dynamics onto the microgrid and this feature will be relevant when the real operating conditions such as unbalanced load, non-linear load, and intermittent weather nature are to be considered. Studies such as power sharing, voltage response, and controller interaction in microgrids can then be made possible using the developed model and platform in conjunction with the power system specialist software. This can give an early insight into the microgrid behavior during the design stage. E.g. it was shown clearly in the given study that the adjustable-VOI-droop technique improves the microgrid's reactive power sharing at the expense of large terminal voltage drops across the virtual output impedance, which leads to the needs to incorporate secondary voltage control to ensure a proper operation of the microgrid.

REFERENCES

- [1] M. P. S. Sonekar and S. B. Kudkelwar, "An advanced droop control method for proportional reactive power sharing," *Int. Research Journal of Eng. and Tech.*, vol. 5, no. 7, pp. 1736-43, 2018.
- [2] J. Khazaei, D. H. Nguyen, G. M. T. Nguyen, "Primary and secondary voltage/frequency controller design for energy storage devices using consensus theory," in *Int. Conf. on Renewable Energy Research and Applications ICRERA*, San Diego, CA, pp. 447-453, 2017.
- [3] T. V. Hoang and H.-H. Lee, "An adaptive virtual impedance control scheme to eliminate the reactive-power-sharing errors in an islanding meshed microgrid," *IEEE Journal of Emerging and Selected Topics in Power Electronics*, early access, d.o.i: 10.1109/JESTPE.2017.2760631, 2017.
- [4] L. Meng et al., "Distributed voltage unbalance compensation in islanded microgrids by using a dynamic consensus algorithm," *IEEE Transactions on Power Electronics*, vol. 31, no. 1, pp. 827-838, 2016.
- [5] M. Savaghebi, A. Jalilian, J. C. Vasquez, and J. M. Guerrero, "Secondary control scheme for voltage unbalance compensation in an islanded droop-controlled microgrid," *IEEE Trans. on Smart Grid*, vol. 3, no. 2, pp. 797-807, 2012.
- [6] M. Savaghebi, A. Jalilian, J. C. Vasquez, and J. M. Guerrero, "Secondary control for voltage quality enhancement in microgrids," *IEEE Transactions on Smart Grid*, vol. 3, no. 4, pp. 1893-1902, 2012.
- [7] M. Savaghebi, A. Jalilian, J. C. Vasquez, and J. M. Guerrero, "Autonomous voltage unbalance compensation in an islanded droop-controlled microgrid," *IEEE Trans. on Industrial Electronics*, vol. 60, no. 4, pp. 1390-1402, 2013.
- [8] M. Savaghebi, Q. Shafiee, J. C. Vasquez, and J. M. Guerrero, "Adaptive virtual impedance scheme for selective compensation of voltage unbalance and harmonics in microgrids," in *IEEE Power & Energy Society General Meeting*, Denver, USA, July, 2015.
- [9] H. Zhang, S. Kim, Q. Sun, and J. Zhou, "Distributed adaptive virtual impedance control for accurate reactive power sharing based on consensus control in microgrids," *IEEE Trans. on Smart Grid*, vol. 8, no. 4, pp. 1749-1761, 2017.
- [10] H.-J. Kim, B.-M. Han and H.-J. Cha, "Reactive-power balancing scheme for inverter-based distributed generations with different line impedances," in *Int. Conf. on Renewable Energy Research and Applications ICRERA*, Palermo, pp. 478-483, 2015.
- [11] B. Xu, F. Liu and W. Chen, "Modeling and simulation for the power sharing of micro-grid inverter," in *Int. Conf. on Renewable Energy Research and Application (ICRERA)*, Milwaukee, WI, pp. 623-627, 2014.
- [12] W. Cao, H. Su, J. Cao, J. Sun and D. Yang, "Improved droop control method in microgrid and its small signal stability analysis," in *Int. Conf. on Renewable Energy Research and Application ICRERA*, Milwaukee, WI, pp. 197-202, 2014.
- [13] X. Yang, Y. Du, J. Su, L. Chang, Y. Shi, and J. Lai, "An optimal secondary voltage control strategy for an islanded multibus microgrid," *IEEE Journal of Emerging and Selected Topics in Power Electronics*, vol. 4, no. 4, pp. 1236-1246, 2016.
- [14] A. Engler and N. Soutanis, "Droop control in LV-grids," in the *International Conference on Future Power Systems*, Amsterdam, Netherlands, November 18, 2005.
- [15] A. Bidram, V. Nasirian, A. Davoudi, and F. L. Lewis, *Cooperative Synchronization in Distributed Microgrid Control*. Cham: Springer International Publishing, 2017.

A Consensus-based Adaptive Virtual Output Impedance Control Scheme for Reactive Power Sharing in Meshed Microgrids

Yi Chyn Cassandra Wong^{1,2}, Chee Shen Lim^{1,2}, Andrew J. Cruden², Mihai D. Rotaru³, Pravat Kumar Ray⁴

¹University of Southampton Malaysia, Johor Bahru, Malaysia

²University of Southampton, Southampton, United Kingdom

³Institute of Microelectronics, A*STAR, Singapore

⁴National Institute of Technology Rourkela, India

y.c.c.wong@soton.ac.uk, c.s.lim@soton.ac.uk, mihai_dragos_rotaru@ime.a-star.edu.sg, a.j.cruden@soton.ac.uk, rayp@nitrkl.ac.in

Abstract—This paper presents a distributed secondary control scheme for accurate reactive power sharing in an islanded meshed microgrid. The scheme employs consensus control to adaptively tune the virtual output impedance (VOI) into achieving power correction. The adaptive VOI-based control structure is essentially non-linear. However, this work shows that the approximate range of stable coupling gain can be established by linearizing the problem about every probable operating point of the distributed energy resources (DERs). On the basis of islanding mode, it is shown also that only the dynamic virtual output reactance component is needed while the static component, which has been used extensively to date, can be nullified. The proposed control scheme can realize an accurate power sharing among the DERs regardless of the microgrid topology, load condition, and communication delay (within the allowable limits defined by the consensus theorem). The study is carried out in conjunction with an islanded microgrid model modified from the IEEE 34 Node Test Feeder.

Keywords — Consensus control, droop control, reactive power sharing, virtual output impedance.

I. INTRODUCTION

Microgrids have the capability to ease the problems caused by the ever-increasing penetration of distributed energy resources (DERs) into the main electricity grid. They can operate in either a grid-connected or an islanded mode. In the islanded mode, a common requirement is to share the load power among the DERs in proportion to their respective power capacities. To facilitate autonomous power sharing, standard frequency-active power (P - f) and voltage-reactive power (Q - V) droop control has been widely adopted in the early stage. However, although accurate active power is guaranteed, it is known that poor reactive power sharing is resulted, especially in a paralleled microgrid with different feeder impedances and in a meshed microgrid. This is due fundamentally to voltage discrepancies at the points of coupling of the DERs in the microgrid network [1]–[3].

Numerous control schemes focusing on accurate reactive power sharing have been reported to date. Compared to the pure-droop-based methods, virtual output impedance (VOI) control methods are relatively newer. The method essentially exploits the additional degree of freedom enabled by the inner voltage control loop. For example, the VOI concept was used to improve the power control stability and sharing accuracy in [4] and [5]. These methods, however, only consider the mismatch of DERs' output/feeder impedances but not the network impedances, which are typical in meshed microgrids. It has also been established that the static VOI value will not be able to solve the reactive power sharing problem in meshed microgrids, especially in the ones with

plug-and-play requirement.

A centralized droop control with a static virtual output reactance (X_v) and proportional-integral (PI)-tuned virtual output resistance (R_v) is proposed in [6]. Other similar centralized techniques can be found in [7] and [8] with arbitrarily chosen X_v/R_v ratio (five in [7] and one in [8]). In [9], both X_v and R_v are adaptively tuned through PI control. All these proposals share a commonality of having both static and dynamic components of the virtual impedance components. According to [10], the static component is required to maintain an inductive virtual output impedance in order to ensure a stable operation during the grid-connected mode. However, since advanced droop control is used predominantly in islanded microgrids (while the grid-connected mode uses predominantly direct power control with external commands), this setting is not considered further here. There exists also another group of VOI-based reactive power correction techniques where no communication link is required [11]–[14]. In [11]–[13], the control schemes are developed primarily for parallel-connected DERs hence their extension to meshed microgrid is conjectured to be difficult. In [14], although the control scheme can estimate the feeder impedance without knowing the network parameters, it inherently requires the voltage at the same point of common coupling for all DERs, which is not available in a typical meshed microgrid.

This work focuses on developing a consensus-based adaptive VOI control for an islanded meshed microgrid. The proposed technique is different from the previous works in several aspects: (i) instead of the common ways of utilizing both virtual impedance components, this scheme uses only the virtual output reactance to achieve the same accurate reactive power sharing performance; (ii) the control scheme does not use PI controllers which then makes the tuning of the coupling gain (for stability) significantly easier; (iii) with a simpler control structure, the approximate range of stable coupling gain is successfully established. This is achieved by analyzing the range of stable coupling gain for every probable operating point while considering some simplifying assumptions such as minimum power factor and maximum voltage drop ratio. On the basis that a microgrid operating in the islanded mode, it will be demonstrated that only the dynamic virtual reactance component is needed while the static component, which has been used extensively to date, e.g. [3], [4], [7], [9], [10], can be nullified.

The rest of the paper is organized as follows. Section II introduces the basics of adaptive virtual output impedance control for reactive power sharing. Section III presents the consensus control and the coupling gain's tuning guideline. Section IV shows the results for various test scenarios: static

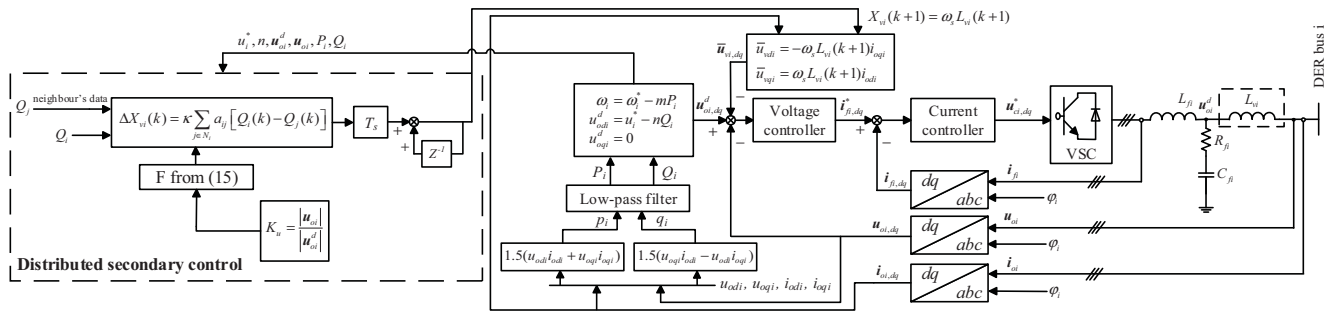


Fig. 1. Schematic diagram of the local control of a VOI-based droop-controlled DER with distributed secondary control for reactive power sharing.

load, load stepping, plug-and-play test, and communication time delay. A recently published consensus VOI control with dual-impedance control loops [9] is used as the benchmark for performance evaluation. Section V concludes the paper.

II. REACTIVE POWER SHARING ANALYSIS

A. Primary Droop Control with Virtual Output Impedance Scheme

The primary control of a VOI-controlled DER includes a power control, an output voltage control, an inverter current control and a virtual output impedance control, as shown in Fig 1. Typically, during islanded operation, DERs achieve autonomous power sharing through the P - f and Q - V droop control, expressed as

$$\begin{aligned}\omega_i &= \omega_i^* - mP_i \\ u_i &= u_i^* - nQ_i\end{aligned}\tag{1}$$

where ω_i^* and u_i^* are the per-unit no-load frequency and voltage magnitude, and m and n are the per-unit droop coefficients commonly shared among the DERs in the same microgrid. P_i and Q_i are the filtered per-unit active and reactive output power. The common base voltage is peak voltage V_B and the common base power S_i is the respective DER's kVA rating. The output voltage vector is aligned to the corresponding synchronous reference frame

$$\begin{aligned} u_{odi}^d &= u_i^* - nQ_i \\ u_{oai}^d &= 0 \end{aligned} \quad (2)$$

where u_{odi}^d and u_{oqi}^d are the synchronous d - and q -axis output voltage references for the output voltage control. The synchronous reference frame's angular position is obtainable from the respective droop frequency (1) after synchronizing with the microgrid during connection. The active and reactive output powers with low-pass filtering (with amplitude-invariant rotational transformation) are

$$\begin{aligned}\tau_c \frac{dP_i}{dt} + P_i &= \frac{3}{2} (u_{odi} i_{odi} + u_{oqi} i_{oqi}) \\ \tau_c \frac{dQ_i}{dt} + Q_i &= \frac{3}{2} (u_{oqi} i_{odi} - u_{odi} i_{oqi})\end{aligned}\quad (3)$$

where τ_c is the low pass filter's cutoff period and u_{odi} , u_{oqi} , i_{odi} , and i_{oqi} are the d - and q -axis measured output voltage and current components.

Virtual output impedance control scheme works by regulating the output voltage references from the standard droop control, i.e.

$$\begin{aligned} u'_{odi} &= u^d_{odi} - u_{vdi} \\ u'_{oai} &= -u_{vai} \end{aligned} \quad (4)$$

where u_{odi} and u_{oqi} are the output voltage references after the virtual output impedance, and u_{ydi} and u_{yqi} are the virtual

voltage magnitude. The electrical steady-state values (i.e. \bar{u}_{vdi} and \bar{u}_{vqi} , after assuming $d/dt = 0$) are calculated as

$$\begin{aligned}\bar{u}_{vdi} &= R_{vi} i_{odi} - \omega_s L_{vi} i_{oqi} \\ \bar{u}_{vqi} &= R_{vi} i_{oqi} + \omega_s L_{vi} i_{odi}\end{aligned}\quad (5)$$

where ω_s is the nominal angular frequency in rad/s and R_{vi} and L_{vi} are the virtual resistance and inductance. Primary voltage and current control through *PI* controllers are implemented. Owing space constraint, the design details are not included and interested readers are referred to [2], [3].

As mentioned, this work uses only the virtual output reactance. Typically, the virtual output impedance is comprised of two impedance components: static and dynamic, as in [3], [4], [7], [9], [10]. The static component ensures that the DER equivalent impedance is predominantly inductive, and the dynamic component is adaptively adjusted,

$$X_{vi}(k) = X_{vi,static} + X_{vi,dyn}(k) \quad (6)$$

where $X_{vi} = \omega_s L_{vi}$, and $X_{vi,static}$ and $X_{vi,dyn}$ are the static and dynamic components of virtual output reactance. However, it is anticipated that the abovementioned virtual output impedance method results in poorer (lower) voltage profile due to the presence of static component. Therefore, this work proposes a virtual output impedance method that only uses the dynamic component. It will be shown later that, as far as the reactive power sharing of a droop-controlled islanded microgrid is concerned, this is indeed sufficient and there is no need to constrain the reactance to purely inductive but a capacitive reactance is also feasible.

III. CONSENSUS-BASED ADAPTIVE VIRTUAL OUTPUT IMPEDANCE CONTROL DESIGN

A. Preliminary of Graph Theory

The communication network of a microgrid can be modeled as a graph with edges corresponding to the information flow between the DERs, denoted as the nodes in the graph. The graph is generally expressed as $\mathbf{G} = (\mathbf{V}_G, \mathbf{E}_G, \mathbf{A}_G)$ with a set of N nodes $\mathbf{V}_G = \{v_1, v_2, \dots, v_N\}$, a set of edges $\mathbf{E}_G \subset \mathbf{V}_G \times \mathbf{V}_G$ and an adjacency matrix $\mathbf{A}_G = [a_{ij}] \in \mathbb{R}^{N \times N}$. The edges \mathbf{E}_G denote the communication links between DERs and each edge $(v_j, v_i) \in \mathbf{E}_G$ represents the information flow from node j to node i . Associated with a weight a_{ij} of edge (v_j, v_i) , $a_{ij} > 0$ if $(v_j, v_i) \in \mathbf{E}_G$, otherwise $a_{ij} = 0$. Node j is called a neighbor of node i if $(v_j, v_i) \in \mathbf{E}_G$ and the set of neighbors of node i is denoted as $N_i = \{j | (v_j, v_i) \in \mathbf{E}_G\}$. The graph is termed to be undirected if $(v_j, v_i) \Rightarrow (v_i, v_j) \in \mathbf{E}_G$; otherwise directed. The in-degree matrix is defined as $\mathbf{D} = \text{diag}\{d_i\} \in \mathbb{R}^{N \times N}$ with $d_i = \sum_{j \in N_i} a_{ij}$ and hence, the Laplacian matrix of the graph is defined as $\mathbf{L}_G = \mathbf{D} - \mathbf{A}_G$.

B. Consensus-based Adaptive VOI Control

The necessary condition to achieve proportional reactive power sharing among the DERs is

$$\lim_{t \rightarrow \infty} [Q_1(t) = Q_2(t) = \dots = Q_N(t)] \quad (7)$$

We propose a linear first-order distributed control protocol for the reactive power correction problem:

$$\begin{aligned} \dot{Q}_i &= u_i \\ u_i &= -c \sum_{j \in N_i} a_{ij} [Q_i - Q_j] \end{aligned} \quad (8)$$

where $c > 0$ is the scalar coupling gain. However, the per-unit reactive output power Q_i is not directly controllable but is done through the virtual output impedance. Hence, the control input is selected as X_{vi} . Since the control of reactive power through X_{vi} is essentially non-linear, what follows attempt to linearize their relationship about an arbitrary operating point so that an approximate linear relation can be obtained for further analysis.

Fig. 2 shows the single line diagram of a DER along with the corresponding virtual output impedance Z_{vi} (being $R_{vi} + jX_{vi}$) and as seen physical equivalent impedance Z_{ei} (being $R_{ei} + jX_{ei}$). Based on Fig. 2, Z_{ei} can be given by

$$\begin{aligned} R_{ei} &= \frac{3u_{oi}^2 P_i}{P_i^2 + Q_i^2} \\ X_{ei} &= \frac{3u_{oi}^2 Q_i}{P_i^2 + Q_i^2} \end{aligned} \quad (9)$$

where u_{oi} is the output voltage magnitude. The reactive power injected by a DER before virtual output impedance and the virtual reactive power across the virtual output impedance can be expressed as (u_{oi}^d being $u_{odi} + j u_{oqi}$)

$$\begin{aligned} Q_i^d &= \frac{3u_{oi}^{d2} (X_{ei} + X_{vi})}{R_{ei}^2 + (X_{ei} + X_{vi})^2} \\ Q_i^v &= \frac{3i_o^2 X_{vi}^2}{X_{vi}} \end{aligned} \quad (10)$$

which the output current magnitude can be expressed as

$$i_o^2 = \frac{u_{oi}^{d2}}{R_{ei}^2 + (X_{ei} + X_{vi})^2} \quad (11)$$

Then, VOI-controlled DER's reactive output power can be expressed as

$$\begin{aligned} Q_i &= Q_i^d - Q_i^v \\ &= \frac{3u_{oi}^{d2} X_{ei}}{R_{ei}^2 + (X_{ei} + X_{vi})^2} \end{aligned} \quad (12)$$

With (12) and (9), the virtual output reactance is given as

$$X_{vi} = \sqrt{\frac{9u_{oi}^{d2} u_{oi}^2 Q_i}{Q_i (P_i^2 + Q_i^2)} - \left(\frac{3u_{oi}^2 P_i}{P_i^2 + Q_i^2} \right)^2} - \frac{3u_{oi}^2 Q_i}{P_i^2 + Q_i^2} \quad (13)$$

which an operating-point-dependent voltage factor K_{ui} is introduced to approximate the ratio of output voltage magnitude u_{oi} to output voltage reference magnitude u_{oi}^d . Eventually, virtual output reactance can be re-written as

$$\begin{aligned} X_{vi} &= \sqrt{\frac{9K_{ui}^2 (u_i^* - nQ_i)^4 Q_i}{Q_i (P_i^2 + Q_i^2)} - \left(\frac{3K_{ui}^2 (u_i^* - nQ_i)^2 P_i}{P_i^2 + Q_i^2} \right)^2} \\ &\quad - \frac{3K_{ui}^2 (u_i^* - nQ_i)^2 Q_i}{P_i^2 + Q_i^2} \end{aligned} \quad (14)$$

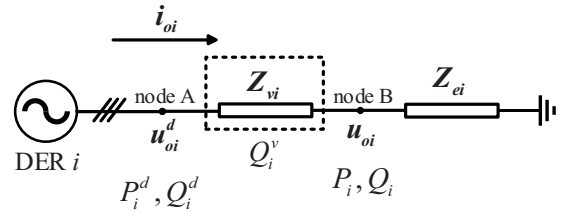


Fig. 2. Single line diagram of a three-phase DER at an arbitrary operating point and with the equivalent physical equivalent impedance (that represents the loading at that time instant) connected at the output terminal.

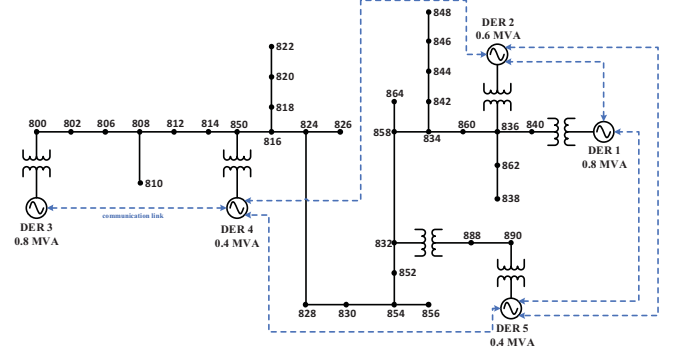


Fig. 3. Islanded microgrid test system (modified from IEEE 34 Feeder [19])

At an arbitrary operating point of K_{ui} , P_{oi} , and Q_{oi} , where that P_{oi} and K_{ui} (u_i^* and n are anyway constant) remain relatively constant with respect to the changes of X_{vi} , the dynamical relationship between X_{vi} and Q_i can be simplified as

$$\dot{X}_{vi} = F_i(K_{ui}, P_{oi}, Q_{oi}) \dot{Q}_i \quad (15)$$

where F_i depends on the operating points of K_{ui} , P_{oi} , and Q_{oi} :

$$\begin{aligned} F_i &= - \frac{9}{\sqrt{\frac{9K_{ui}^2 (u_i^* - nQ_{oi})^4}{P_{oi}^2 + Q_{oi}^2} - \frac{9K_{ui}^4 P_{oi}^2 (u_i^* - nQ_{oi})^4}{(P_{oi}^2 + Q_{oi}^2)^2}}} \\ &\quad \left[\frac{K_{ui}^2 Q_{oi} (u_i^* - nQ_{oi})^4}{(P_{oi}^2 + Q_{oi}^2)^2} - \frac{2K_{ui}^4 P_{oi}^2 Q_{oi} (u_i^* - nQ_{oi})^4}{(P_{oi}^2 + Q_{oi}^2)^3} \right. \\ &\quad \left. + \frac{2K_{ui}^2 (u_i^{*2} n - 3u_i^{*2} n^2 Q_{oi} + 3u_i^* n^3 Q_{oi}^2 - n^4 Q_{oi}^3)}{P_{oi}^2 + Q_{oi}^2} \right. \\ &\quad \left. - \frac{2K_{ui}^4 P_{oi}^2 (u_i^{*2} n - 3u_i^{*2} n^2 Q_{oi} + 3u_i^* n^3 Q_{oi}^2 - n^4 Q_{oi}^3)}{(P_{oi}^2 + Q_{oi}^2)^2} \right] \\ &\quad + \frac{6K_{ui}^2 Q_{oi}^2 (u_i^* - nQ_{oi})^2}{(P_{oi}^2 + Q_{oi}^2)^2} - \frac{3K_{ui}^2 (u_i^{*2} - 4u_i^* nQ_{oi} + 3n^2 Q_{oi}^2)}{P_{oi}^2 + Q_{oi}^2} \end{aligned}$$

Substitute (15) to (8) and applying forward-Euler discretization, the proposed consensus-based reactive power sharing control scheme is expressible as

$$\Delta X_{vi}(k) = \kappa_i \sum_{j \in N_i} a_{ij} [Q_i(k) - Q_j(k)] \quad (16)$$

where $\kappa_i = -c_i F_i(K_{ui}, P_{oi}, Q_{oi})$.

Subsequently, the virtual output reactance is obtainable from:

$$X_{vi}(k+1) = X_{vi}(k) + T_s \Delta X_{vi}(k) \quad (17)$$

C. Coupling gain Design

It is well established that consensus stability is guaranteed if the following sufficient condition is met:

$$c < \frac{1}{d_{\max}} \quad (18)$$

where $d_{\max} = \max(\mathbf{D})$ [15]. However, as revealed from (16), the effective coupling gain for a given scalar coupling gain is essentially dependent on the operating point. There are two possible ways of setting the gain κ_i value: (i) compute the local F_i value on the fly and update the local gain κ_i (in each DER); (ii) consider the smallest value F_{\min} for a given range of practical operating points and use $-cF_{\min}$ value as the global gain κ (common to all DERs). This work considers the second way as it is expected to give a more reliable consensus control but with a small penalty on the correction dynamics (to be elaborated later). The possible values of κ for a given range of operating points (i.e. of different P_o and Q_o , and with a rated power factor of 0.8) is summarized in Table I. The calculation assumes that u_{oi} is fixed at 0.9 and the load power factor is always kept equal or above 0.8 (i.e. grey-shaded column represents a power factor below 0.8). The table clearly shows that κ changes quite significant especially towards the low loading region. Therefore, it is recommended that the fixed global coupling gain κ should be chosen at high-loading operating point (e.g. $P_o = 95\%$ of P_{rated} and $Q_o = 95\%$ of Q_{rated}) to ensure stability for most operating points. It is acknowledged here that such a choice would entail a slower correction dynamic at low load region, however, since non-proportional power sharing is naturally not a concern at low-load region hence it still makes practical sense to use stability-ensuring κ suggested earlier.

D. Communication Delay

With the introduction of F in Section III-B, one can readily set the coupling gain of the first-order consensus protocol (8) based on the established consensus theorem, i.e. $c < 1/d_{\max}$. It is therefore expected that the communication time delay of this control problem can also be regarded as a standard time-delayed consensus problem ([16], [17]):

$$\Delta X_{vi}(k) = \kappa_i \sum_{j \in N_i} a_{ij} [Q_i(k-\tau) - Q_j(k-\tau)] \quad (19)$$

where τ denotes time delay. The delayed system would be asymptotically stable if and only if [9], [16]–[18]

$$0 < \tau < \frac{\pi}{2\lambda_{\max} c} \quad (20)$$

where λ_{\max} is the maximum eigenvalue of the communication graph's Laplacian matrix.

IV. SIMULATION RESULTS AND DISCUSSION

An islanded microgrid network of five VOI-controlled DERs, modified from the IEEE 34 Node Test Feeder is depicted in Fig. 3 (see [19] for detailed network parameters). The network model, together with the primary voltage, current, and droop control are constructed in the *DIGSILENT PowerFactory* for this study (see [3] for modelling details). Moreover, the performance of the proposed consensus-based reactive power sharing control scheme is benchmarked against a recently reported consensus control scheme in [9]. The scheme is known in what follows as the dual-impedance consensus control. The basic parameters of the DERs and the islanded microgrid network are tabulated in Table II. The associated

TABLE I. THE CORRESPONDING κ_i VALUES FOR DIFFERENT OPERATING POINTS WITH $c = 0.2$

| Q_o (% of Q_{rated}) | K_{κ} | P_o (% of P_{rated}) | | | | | | |
|----------------------------------|--------------|----------------------------------|-------|------|------|------|------|------|
| | | 5 | 10 | 30 | 50 | 70 | 90 | 95 |
| 5 | 0.884 | 54.52 | 32.89 | 6.86 | 2.77 | 1.48 | 0.93 | 0.84 |
| 10 | 0.887 | | 13.49 | 5.06 | 2.35 | 1.33 | 0.86 | 0.78 |
| 30 | 0.894 | | | 1.43 | 1.05 | 0.76 | 0.57 | 0.53 |
| 50 | 0.902 | | | | 0.49 | 0.41 | 0.34 | 0.33 |
| 70 | 0.915 | | | | | 0.23 | 0.21 | 0.20 |
| 90 | 0.919 | | | | | | 0.13 | 0.13 |
| 95 | 0.921 | | | | | | | 0.12 |

TABLE II. SYSTEM PARAMETERS

| Parameter | Value | Parameter | Value |
|---|--------------------------|---|--------------------------|
| System freq. | 60 Hz | P -f droop coeff. (pu) | 0.0625 |
| MV levels | 24.9/4.16 kV | No-load freq. (pu) | 1.02 |
| Inverter DC bus | 1 kV | Q -V droop coeff. (pu) | 0.075 |
| Sw. freq. F_{s1} | 10 kHz | No-load voltage (pu) | 1.02 |
| DER ratings: | | Inverter output filter impedances: | |
| Apparent power (pf) | | L-RC | |
| DER 1 | 0.8 MVA (0.8) | 0.1905 mH, 10 Ω , 132.96 μ F | |
| DER 2 | 0.6 MVA (0.8) | 0.7620 mH, 10 Ω , 88.64 μ F | |
| DER 3 | 0.8 MVA (0.8) | 0.1905 mH, 10 Ω , 132.96 μ F | |
| DER 4 | 0.4 MVA (0.8) | 0.3810 mH, 10 Ω , 66.48 μ F | |
| DER 5 | 0.4 MVA (0.8) | 0.3810 mH, 10 Ω , 66.48 μ F | |
| Feeder impedances | | | |
| Z_{of1} | 0.030 Ω , 0.35 mH | Z_{of4} | 0.043 Ω , 0.35 mH |
| Z_{of2} | 0.056 Ω , 0.35 mH | Z_{of5} | 0.043 Ω , 0.35 mH |
| Z_{of3} | 0.030 Ω , 0.35 mH | | |
| Secondary consensus control ($F_{s2} = 1$ Hz) | | Primary voltage control | |
| τ_c | 0.2 s | K_{pvi} | 1.23 |
| c | 0.2 | K_{ivi} | 4.67 |
| | | Primary current control | |
| | | K_{pci} | 0.27 |
| | | K_{ici} | 1.61 |

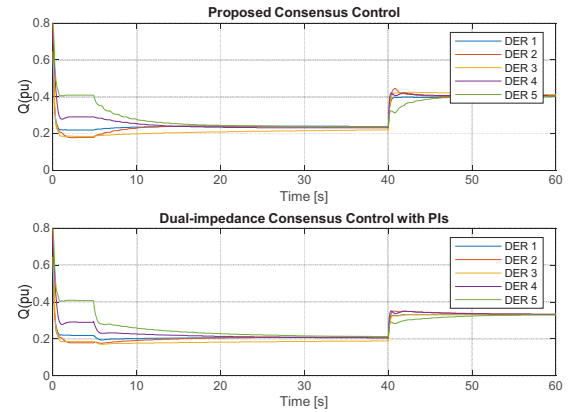


Fig. 4. (Case study 1) Steady state and load step change: reactive output power of the DERs (before 5 s) without correction, (after 5 s) with correction and (at 40 s) load step up.

communication graph's Laplacian matrix is

$$\mathbf{L}_G = \begin{bmatrix} 2 & -1 & 0 & 0 & -1 \\ -1 & 3 & 0 & -1 & -1 \\ 0 & 0 & 1 & -1 & 0 \\ 0 & -1 & -1 & 3 & -1 \\ -1 & -1 & 0 & -1 & 3 \end{bmatrix} \quad (21)$$

A. Case Study 1: Default steady-state and load change

A total load of 1.52 MW and 1.27 MVar passive load are present in the islanded microgrid network. Before $t = 5$ s, the DERs are initially controlled through standard droop scheme without any reactive power sharing correction. It can be established from Fig. 4 that prior to 5 s the reactive

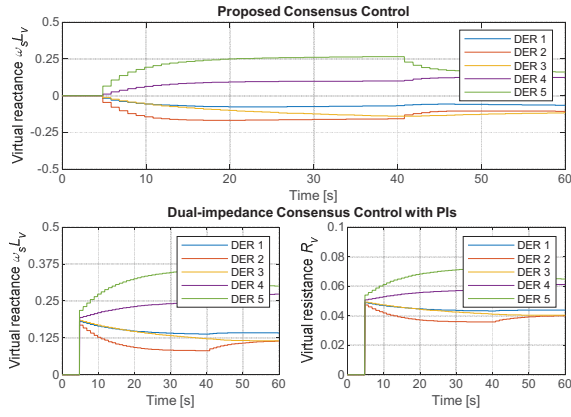


Fig. 5. (Case study 1) Default steady state and load step change: virtual output impedance values of the DERs without correction (before 5 s), with correction (after 5 s), and with load up-stepping (at 40 s).

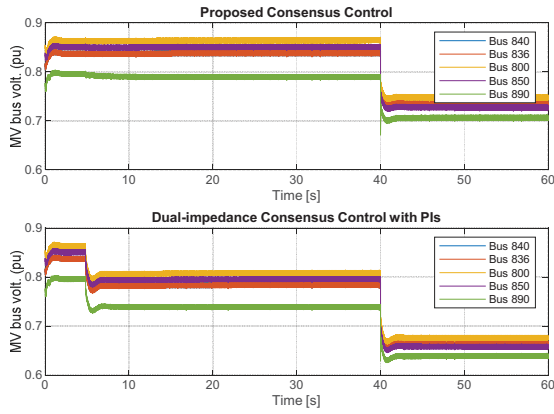


Fig. 6. (Case study 1) Default steady state and load step change: voltage magnitudes at respective MV buses of the DERs. The base voltage of bus 890 is 4.16 kV and the rest are 24.9 kV.

power is not proportionally shared among the DERs. At $t = 5$ s, the proposed control scheme is activated with the global gain κ set to 0.12. On the other hand, the controller gains of the dual-impedance consensus control are tuned in such a way that the control scheme achieves a similar settling time (see [9] for details). The controller gains are summarized here: $C_Q = 4$, $D_P = 0.03$, $D_I = 1.2$, $K_{Q_L} = 0.15$, and $K_{Q_R} = 0.02$. It is seen clearly that the load reactive power can now be shared proportionally among the DERs. The corresponding VOI values for both control schemes are shown in Fig. 5. Notice that in one case the X_v can be positive and negative while in the other case it (and R_v) has been confined to positive value only.

Next, an additional load is connected to bus 814 at $t = 40$ s. The total load demand of the islanded microgrid is therefore increased to $1.75+j1.273$ MVA. Fig. 4 shows that both control schemes continue to enable proportional power sharing regardless of load changing. However, Fig. 6 shows that the dual-impedance consensus control has larger bus voltage deviations as compared to the proposed control scheme (between 5 s to 60 s) and this is explained by the use of static impedance components.

B. Case Study 2: Plug-and-play DER

The performance of the proposed reactive power sharing control scheme considering the plug-and-play feature of a microgrid is investigated next. The islanded microgrid operates under the default loading condition as in the case of

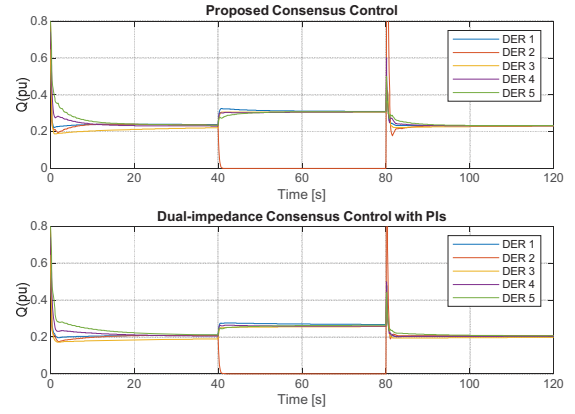


Fig. 7. (Case study 2) Plug-and-play of DER 2: reactive output power of the DERs with DER 2 disconnected at 40 s and re-connected at 80 s.

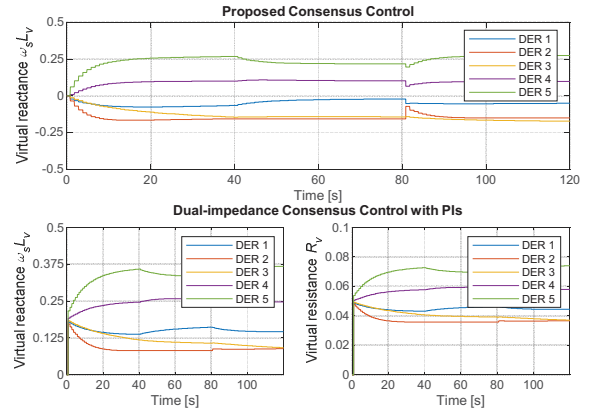


Fig. 8. (Case study 2) Plug-and-play of DER 2: virtual output impedance values with DER 2 disconnected at 40 s and re-connected at 80 s.

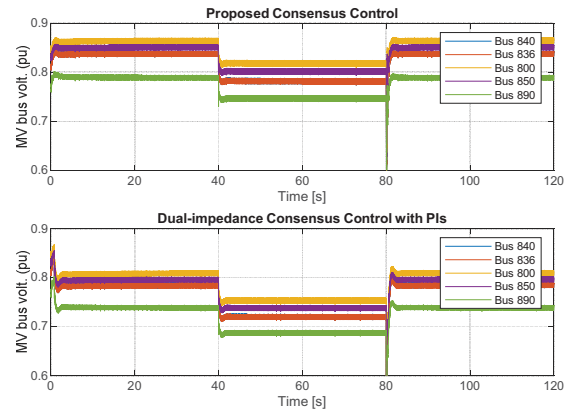


Fig. 9. (Case study 2) Plug-and-play of DER 2: voltage magnitudes at respective MV buses of all DERs.

case study 1 (after 5 s). At $t = 40$ s, DER 2 is disconnected arbitrarily, which means the communication in and out of DER 2 (to and from others) are lost. As seen in Fig. 7, proportional reactive power sharing is retained in both control schemes, as expected (since both control schemes are meant for meshed islanded microgrid with changing network topology). In Fig. 8, during disconnection, the virtual impedance values of DER 2 prior to the disconnection point is kept constant to ensure stability. Upon disconnection, it can be seen from Fig. 7 that the remaining DERs need to deliver higher reactive power to meet the load demand, which is accompanied by lowering of the MV bus voltages, as shown in Fig. 9. The spike in the DERs' reactive output power can be explained by reconnection of DER 2 without synchronization (for

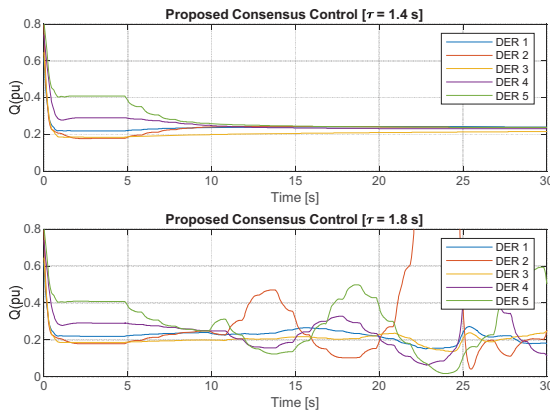


Fig. 10. (Case study 3) DERs' reactive output power with communication link delays.

simplicity). Once the system reaches steady state, the bus voltages are restored (elevated) without any noticeable compromise of the reactive power sharing accuracy with lower reactive power sharing effort. Again, Fig. 9 shows that the dual-impedance consensus control exhibits larger bus voltage deviations.

C. Case Study 3: Communication link delays

Lastly, the robustness of the proposed control scheme against communication time delays is examined here. Based on the Laplacian matrix of the communication graph and the developed consensus control protocol, the maximum allowable time delay defined in (20) is $\tau_{max} = 1.75$ s (i.e. with $\lambda_{max} = 4.48$ and $c = 0.2$). Therefore, time delays of 1.4 s and 1.8 s are tested under the default network setting (as in case study 1, after 5s). Fig. 10 shows that the proposed control scheme remains stable for $\tau = 1.4$ s but the consensus control would become unstable for $\tau = 1.8$ s.

V. CONCLUSION

This paper presents a consensus-based adaptive virtual output impedance secondary control for accurate reactive power sharing for an islanded meshed microgrid. The proposed control scheme only requires a sparse communication structure and eliminates the needs for a central control, which evict the risk of single point failure. Instead of the widely used dual-impedance (virtual resistance and reactance) consensus control, this work shows that virtual reactance alone is sufficient to ensure an accurate sharing of reactive power. In addition, instead of the usual static-dynamic impedance components, only dynamic virtual output reactance is used here. The work also proposes a systematic tuning guideline that establishes an approximate range of the consensus coupling gain to ensure system stability. It was revealed that, if the physical dynamics of the virtual output reactance and the reactive power is not considered, the consensus protocol, especially in terms of coupling gain tuning, would not be able to meet the theoretical expectation. The study is substantiated with several tests common to power sharing studies. It is proven that the proposed consensus control, with dynamic virtual reactance and without the extensive use of proportional-integral control structure, can be appropriately tuned using the developed coupling gain tuning guideline to realize accurate reactive power sharing among DERs in an islanded meshed microgrid.

REFERENCES

- [1] Y. Han, H. Li, P. Shen, E. A. A. Coelho, and J. M. Guerrero, "Review of active and reactive power sharing strategies in hierarchical controlled microgrids," *IEEE Trans. Power Electron.*, vol. 32, no. 3, pp. 2427–2451, 2017.
- [2] A. Bidram, A. Davoudi, and F. L. Lewis, "A multiobjective distributed control framework for islanded AC microgrids," *IEEE Trans. Ind. Informatics*, vol. 10, no. 3, pp. 1785–1798, 2014.
- [3] Y. C. C. Wong, C. S. Lim, M. D. Rotaru, A. Cruden, and K. Xin, "Reactive power sharing of an islanded microgrid in DigSILENT PowerFactory," in *International Conference on Renewable Energy Research and Applications*, 2018, pp. 1–6.
- [4] J. M. Guerrero, L. Gracia de Vicuna, J. Matas, M. Castilla, and J. Miret, "Output impedance design of parallel-connected UPS inverters with wireless load-sharing control," *IEEE Trans. Ind. Electron.*, vol. 52, no. 4, pp. 1126–1135, 2005.
- [5] J. M. Guerrero, J. Matas, L. Gracia de Vicuna, M. Castilla, and J. Miret, "Decentralized control for parallel operation of distributed inverters using resistive output impedance," *IEEE Trans. Ind. Electron.*, vol. 54, no. 2, pp. 994–1004, 2007.
- [6] Y. Zhu, B. Liu, F. Wang, F. Zhuo, and Y. Zhao, "A virtual resistance based reactive power sharing strategy for networked microgrid," in *International Conference on Power Electronics and ECCE Asia*, 2015, pp. 1564–1572.
- [7] T. V. Hoang and H. H. Lee, "An adaptive virtual impedance control scheme to eliminate the reactive-power-sharing errors in an islanding meshed microgrid," *IEEE J. Emerg. Sel. Top. Power Electron.*, vol. 6, no. 2, pp. 966–976, 2018.
- [8] H. Mahmood, D. Michaelson, and J. Jiang, "Accurate reactive power sharing in an islanded microgrid using adaptive virtual impedances," *IEEE Trans. Power Electron.*, vol. 30, no. 3, pp. 1605–1617, 2015.
- [9] H. Zhang, S. Kim, Q. Sun, and J. Zhou, "Distributed adaptive virtual impedance control for accurate reactive power sharing based on consensus control in microgrids," *IEEE Trans. Smart Grid*, vol. 8, no. 4, pp. 1749–1761, 2017.
- [10] J. He and Y. W. Li, "Analysis, design, and implementation of virtual impedance for power electronics interfaced distributed generation," *IEEE Trans. Ind. Appl.*, vol. 47, no. 6, pp. 2525–2538, 2011.
- [11] S. Liu and Y. Zhang, "Voltage compensation strategy using adaptive virtual impedance for reactive power sharing in an islanded microgrid," *2017 20th Int. Conf. Electr. Mach. Syst. ICEMS 2017*, pp. 1–6, 2017.
- [12] B. Wang, S. Liu, and Y. Zhang, "Reactive power sharing control based on voltage compensation strategy in microgrid," in *Chinese Control Conference*, 2017, no. July, pp. 10745–10750.
- [13] B. Liu, Z. Liu, J. Liu, R. An, and S. Song, "A novel microgrid power sharing scheme enhanced by a non-intrusive feeder impedance estimation method," in *International Power Electronics Conference*, 2018, pp. 3924–3928.
- [14] Y. Zhu, F. Zhuo, F. Wang, B. Liu, R. Gou, and Y. Zhao, "A virtual impedance optimization method for reactive power sharing in networked microgrid," *IEEE Trans. Power Electron.*, vol. 31, no. 4, pp. 2890–2904, 2016.
- [15] F. L. Lewis, H. Zhang, K. Hengster-Movric, and A. Das, "Algebraic graph theory and cooperative control consensus," in *Cooperative Control of Multi-Agent Systems*, 1st ed., London: Springer-Verlag London, 2014, pp. 23–71.
- [16] R. Olfati-Saber, J. A. Fax, and R. M. Murray, "Consensus and cooperation in networked multi-agent systems," *Proc. IEEE*, vol. 95, no. 1, pp. 215–233, 2007.
- [17] R. Olfati-Saber and R. M. Murray, "Consensus problems in networks of agents with switching topology and time-delays," *IEEE Trans. Automat. Contr.*, vol. 49, no. 9, pp. 1520–1533, 2004.
- [18] J. Zhou, S. Kim, H. Zhang, Q. Sun, and R. Han, "Consensus-based distributed control for accurate reactive, harmonic, and imbalance power sharing in microgrids," *IEEE Trans. Smart Grid*, vol. 9, no. 4, pp. 2453–2467, 2018.
- [19] IEEE Power and Energy Society, "IEEE 34 node test feeder," 2010. [Online]. Available: <http://sites.ieee.org/pes-testfeeders/resources/>.

Semi-Distributed Optimal Secondary Control Based on Decoupled Linearized Power Flow for Large-Area Droop-Controlled Microgrids

Yi Chyn Cassandra Wong
Malaysia Campus
University of Southampton
Johor Bahru, Malaysia
y.c.c.wong@soton.ac.uk

Chee Shen Lim
Malaysia Campus
University of Southampton
Johor Bahru, Malaysia
c.s.lim@soton.ac.uk

Andrew J. Cruden
School of Engineering
University of Southampton
Southampton, U. K.
a.j.cruden@soton.ac.uk

Mihai D. Rotaru
Institute of Microelectronics
Agency for Science, Technology, and
Research (A*STAR), Singapore
mihai_dragos_rotaru@ime.a-star.edu.sg

Kong Xin
Experimental Power Grid Centre
Nanyang Technological University
Singapore
xin.kong@ntu.edu.sg

Abstract—Power-flow-based optimal secondary control of microgrids has been an active research subject in recent years. However, the standard optimal control's computational burden will likely become intractable in large-area microgrids with a large number of fast-dynamic distributed energy resources (DERs). This work proposes a semi-distributed optimal control scheme to overcome the scalability issue. First, the proposed semi-distributed control strategy segregates the large-area microgrid into multiple sub-microgrids. Then, modified decoupled linearized power flow with Q - V droop is adopted to model the behavior of each sub-microgrid cluster. It is followed by forming a novel quadratic cost function that captures the interaction of both intra- and inter-cluster microgrids, in terms of load-bus voltages and DERs' reactive powers. This is achieved by exploiting the graph theory of cooperative control method. The viability and performance of the proposed semi-distributed control scheme has been verified in conjunction with three distinctive cases: reactive power sharing correction without voltage regulation, single-load bus voltage regulation without reactive power sharing correction, and optimal reactive power sharing and voltage regulation. Despite having separated instances of secondary control, it is proven that the proposed semi-distributed control adopting linear power flow algorithm can realize single-objective (i.e. optimal reactive power sharing or single bus voltage regulation) and multi-objective (e.g. load bus voltage regulation with optimal trade-offs in reactive power sharing) control in the microgrid.

Keywords—Reactive power sharing, optimal control, distributed control, voltage regulation.

I. INTRODUCTION

Microgrid is an enabling technology to integrate a large number of dispatchable and non-dispatchable distributed energy resources into the future smart grid. With advanced hierarchical control [1], [2], it can maximize the economic and technical benefits derivable from the large-number, small-scale heterogeneous power sources. In recent years, two groups of advanced control technologies, cooperative/consensus control [3]–[5] and optimal secondary control, have been actively researched in conjunction with

microgrids operating in the islanded and/or grid-connected modes. The former group of consensus/cooperative control essentially exploits the graph theory of cooperative control [3], [6]. It exhibits the advantage of algorithm simplicity and is therefore able to accommodate a large number of DERs. However, the control objectives are often of a smaller set, typically limited to the DER output voltage and power [7]–[9], sometimes include the single non-DER bus voltage [3], [10] (i.e. voltage of the bus not located at the point of coupling of any DER). On the other hand, the latter group is a natural extension from the optimal control technique commonly studied in the classical power system [11], [12]. In the secondary control context, it typically utilizes the network power flow model and exploits the multi-objective optimal control theory to strategically control or regulate the DERs into achieving a specific set of technical objectives [2], [13]. However, as the network size and the number of dispatchable DERs become larger, e.g. in future large-area heterogeneous microgrids, standard optimal control schemes will likely encounter the scalability issue due to the known computational burden, which is known to be amplified further by the small time constants of power-electronic-based DERs.

This work proposes a novel semi-distributed optimal control strategy that can optimally regulate the network's multi-bus voltages and the DERs' reactive power outputs. This is achieved by first segregating the large-area microgrid into multiple sub-microgrids, followed by adopting modified decoupled linearized power flow with Q - V droop to model the behaviour of each sub-microgrid cluster. Then, a novel quadratic cost function that captures the interaction of both intra-cluster and intercluster microgrids, in terms of load-bus voltages and DERs' reactive powers, is proposed. The intercluster interaction is captured by exploiting the graph theory of cooperative control method. The proposed semi-distributed optimal control scheme effectively reduces the supposedly large-scale optimisation control problem into multiple sub-optimisation control problems. This, together with the use of decoupled linearized power flow (instead of the established non-linear power flow), reduces the numerical

complexity of implementing optimal control for future large-area heterogeneous microgrids.

In what follows, Section II introduces the decoupled linearized power flow and the network modelling that accounts for DER droop control in place of the standard slack-bus. Section III describes the semi-distributed control structure and the cost function that considers both groups of intra- and inter-cluster DERs. The viability and performance of the proposed control scheme has been studied in Section IV in conjunction with three distinctive cases: reactive power sharing correction without voltage regulation, single-load bus voltage regulation without reactive power sharing correction, and optimal reactive power sharing and voltage regulation. Lastly, Section V concludes the paper.

II. POWER FLOW AND NETWORK MODELLING

A. Decoupled Linearized Power Flow

The matrix formulation of the *Decoupled Linearized Power Flow* (DLPF) proposed in [14] is as follows:

$$\begin{bmatrix} \mathbf{P} \\ \mathbf{Q} \end{bmatrix} = \begin{bmatrix} -\mathbf{B}' & \mathbf{G} \\ -\mathbf{G}' & -\mathbf{B} \end{bmatrix} \begin{bmatrix} \delta \\ \mathbf{V} \end{bmatrix} = \mathbf{R} \begin{bmatrix} \delta \\ \mathbf{V} \end{bmatrix} \quad (1)$$

where \mathbf{G} (\mathbf{B}) is the real (imaginary) part of the admittance matrix \mathbf{Y} , and \mathbf{G}' (\mathbf{B}') is the corresponding matrix without the shunt element. The voltage magnitude and phase angle can be determined by inverting (1), expressible as

$$\begin{bmatrix} \delta \\ \mathbf{V} \end{bmatrix} = \mathbf{R}^{-1} \begin{bmatrix} \mathbf{P} \\ \mathbf{Q} \end{bmatrix} = \begin{bmatrix} \mathbf{H} & \mathbf{M} \\ \mathbf{N} & \mathbf{K} \end{bmatrix} \begin{bmatrix} \mathbf{P} \\ \mathbf{Q} \end{bmatrix} \quad (2)$$

In an islanded microgrid, it is evident that both δ and \mathbf{V} consist of two sub-vectors, corresponding to load and droop buses. Without loss of generality, we arrange these busses in the following sequence:

$$\begin{aligned} \delta &= [\delta_L^T \quad \delta_G^T]^T \\ \mathbf{V} &= [\mathbf{V}_L^T \quad \mathbf{V}_G^T]^T \end{aligned} \quad (3)$$

Assume that the active and reactive power are sufficiently decoupled and knowing that the bus voltage phase angle in a droop-controlled islanded microgrid is a function of active power and less affected by the reactive power correction, (2) can be simplified and partitioned as

$$\begin{bmatrix} \mathbf{V}_L \\ \mathbf{V}_G \end{bmatrix} = \begin{bmatrix} \mathbf{N}_{LL} & \mathbf{N}_{LG} & \mathbf{K}_{LL} & \mathbf{K}_{LG} \\ \mathbf{N}_{GL} & \mathbf{N}_{GG} & \mathbf{K}_{GL} & \mathbf{K}_{GG} \end{bmatrix} \begin{bmatrix} \mathbf{P}_L \\ \mathbf{P}_G \\ \mathbf{Q}_L \\ \mathbf{Q}_G \end{bmatrix} \quad (4)$$

B. Modelling of a Sub-microgrid

Considering a large microgrid system having N DERs, the network is proposed to be sectionized into M sub-microgrids (sMGs) and each sub-microgrid (sMG) has N_D DERs and N_B buses that are to be controlled by the proposed sMG's secondary control layer for reactive power sharing and load bus voltage regulation. A modified droop scheme that exploits

the dispatch feature of the standard Q - V droop control is adopted here:

$$V_{Gi,m} = V_{oi,m}^* - n_{i,m} Q_{Gi,m} + n_{i,m} Q_{dis,i,m} + u_{com,m} + Q_{dcom,m} \quad (5)$$

where $V_{Gi,m}$ is the per-unit droop voltage amplitude (normalized to the network's phase peak voltage) of i^{th} DER in m^{th} sMG; $V_{oi,m}^*$ is the per-unit no-load voltage magnitude, $n_{i,m}$ is the per-unit droop coefficient; $Q_{Gi,m}$ is the filtered per-unit reactive output power, normalized to a common base power S_B ; $Q_{dis,i,m}$ is the individual reactive power dispatch command; and $u_{com,m}$ and $Q_{dcom,m}$ are the voltage and sMG reactive power correction terms commonly shared among the DERs in m^{th} sMG. For each m^{th} sMG, there is an intra-cluster and intercluster control means, i.e. \mathbf{Q}_{dis} and Q_{dcom} for accurate reactive power sharing within each sMG and among multiple sMGs.

Based on (5), voltage magnitudes at all N_D droop buses in m^{th} sMG can be expressed compactly as

$$\underbrace{\begin{bmatrix} V_{G1} \\ \vdots \\ V_{GN_D} \end{bmatrix}}_{\mathbf{V}_{G,m}} = \underbrace{\begin{bmatrix} V_{o1}^* \\ \vdots \\ V_{oN_D}^* \end{bmatrix}}_{\mathbf{V}_{o,m}^*} - \underbrace{\Phi_m}_{\mathbf{Q}_{G,m}} \underbrace{\begin{bmatrix} Q_{G1} \\ \vdots \\ Q_{GN_D} \end{bmatrix}}_{\mathbf{Q}_{G,m}} + \underbrace{\Gamma_m}_{\mathbf{u}_m} \underbrace{\begin{bmatrix} u_{com} \\ Q_{dis,1} \\ \vdots \\ Q_{dis,N_D} \\ Q_{dcom} \end{bmatrix}}_{\mathbf{u}_m} \quad (6)$$

where

$$\Phi_m = \begin{bmatrix} n_1 & \cdots & 0 & \cdots & 0 \\ \vdots & & \ddots & & \vdots \\ 0 & \cdots & 0 & \cdots & n_{N_D} \end{bmatrix} \quad \text{and} \quad \Gamma_m = \begin{bmatrix} 1 & n_1 & \cdots & 0 & 1 \\ \vdots & \vdots & \ddots & \vdots & \vdots \\ 1 & 0 & \cdots & n_{N_D} & 1 \end{bmatrix}$$

Assume that the active and reactive powers of voltage-dependent load and droop buses do not vary significantly during regulation, i.e. during reactive power correction and voltage regulation, the estimation model for secondary control can be obtained by substituting \mathbf{V}_G vector in (4) with (6) (detailed steps are given in the Appendix):

$$\mathbf{y}_m(k+1) = \mathbf{C}_m \mathbf{v}_m(k) + \mathbf{D}_m \mathbf{u}_m(k) \quad (7)$$

where sub-vectors \mathbf{P}_L , \mathbf{P}_G , \mathbf{Q}_L are the measured quantities (similar to that in [2]), and the variable vectors are

$$\begin{aligned} \mathbf{y}_m &= [\mathbf{V}_L^T \quad \mathbf{Q}_G^T]^T \\ \mathbf{v}_m &= [\mathbf{P}_L^T \quad \mathbf{P}_G^T \quad \mathbf{Q}_L^T \quad \mathbf{V}_o^{*T}]^T \\ \mathbf{u}_m &= [u_{com} \quad \mathbf{Q}_{dis}^T \quad Q_{dcom}]^T \end{aligned}$$

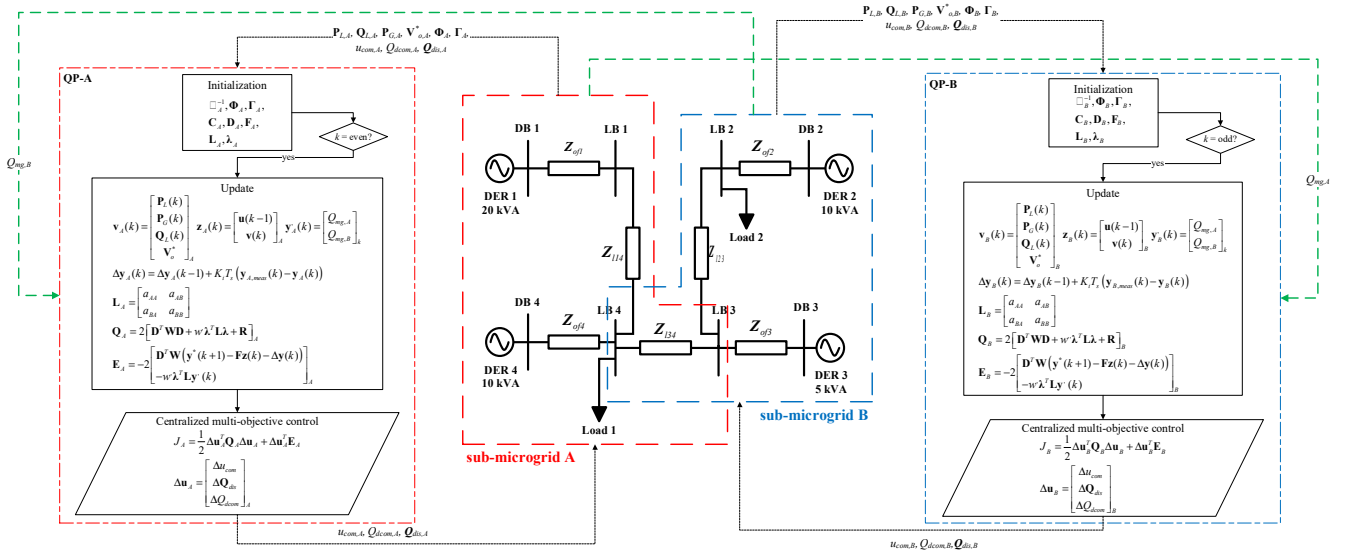


Fig. 1. Single line diagram of a two-microgrids network with detailed secondary control flowchart.

Linear power flow is known improve the computational efficiency at the slight expense of estimation accuracy. In order to eliminate this inherent error to prevent error propagation across the sMGs, an integral-based corrective term that exploits the difference between the measured and estimated quantities (akin to the standard state estimator technique) is introduced here:

$$\Delta \mathbf{y}_m(k) = \Delta \mathbf{y}_m(k-1) + K_i T_s (\mathbf{y}_m^{meas}(k) - \mathbf{y}_m(k|k-1)) \quad (8)$$

where $\Delta \mathbf{y}(k)$ is the output error at time k , $\mathbf{y}_m^{meas}(k)$ is the measured output vector; $\mathbf{y}(k|k-1)$ is estimated output vector at time $k-1$; and K_i is the integral gain with sampling time T_s . Then, (7) is modified based on (8) and the known relationship of $\mathbf{u}(k) = \mathbf{u}(k-1) + \Delta \mathbf{u}(k)$:

$$\mathbf{y}_m(k+1) = \underbrace{[\mathbf{D} \quad \mathbf{C}]_m}_{\mathbf{F}_m} \underbrace{\begin{bmatrix} \mathbf{u}(k-1) \\ \mathbf{v}(k) \end{bmatrix}}_{\mathbf{z}_m(k)} + \mathbf{D}_m \Delta \mathbf{u}_m(k) + \Delta \mathbf{y}_m(k) \quad (9)$$

III. SEMI-DISTRIBUTED OPTIMAL CONTROL FOR LARGE-AREA MICROGRIDS

Eq. (9) essentially models the effects of intra-cluster reactive power output adjustment onto the bus voltages within each sMG. Next, the inter-cluster power sharing, i.e. reactive power sharing among sMGs, is to be modelled into the semi-distributed control scheme. Adopting the consensus/cooperative control method [6], total reactive power from each sMG is regarded as first-order dynamic, given by

$$Q_{mg,m}(k+1) = Q_{mg,m}(k) + \Delta Q_{dcom,m}(k) \quad (10)$$

where ΔQ_{dcom} is the inter-cluster control input that is commonly shared among all N_D DERs in the sMG. It is important to note here that the reactive power component of each sMG has been normalized to its respective base power. This means that, for sMGs with different base power (i.e.

different size), the reactive power will be proportionately shared among the sMGs when the normalized Q_{mg} values are equal (upon correction).

The semi-distributed optimization control of load-bus voltage regulation and intra- and inter-cluster reactive power sharing is treated as a tracking problem through a modified cost function shown below:

$$J_m = (\mathbf{y}_m^*(k+1) - \mathbf{y}_m(k+1))^T \mathbf{W}_m (\mathbf{y}_m^*(k+1) - \mathbf{y}_m(k+1)) + \mathbf{w}_m^T \left(\sum_{n \in N_m} (Q_{mg,n}(k+1) - Q_{mg,m}(k+1))^2 \right) + \Delta \mathbf{u}_m^T(k) \mathbf{R}_m \Delta \mathbf{u}_m(k) \quad (11)$$

The first term in (11) weighs on the intracluster control terms to minimize the difference between the local output variables and their setpoint vector \mathbf{y}^* . The second term weighs on the inter-cluster reactive power correction control term to minimize the difference of total reactive output power between the sMGs' and their neighbours' (being $Q_{mg,n}$, where $n \in N_m$ in which N_m denotes the set of neighbours of m^{th} sMG; $Q_{mg,n}$ values are assumed constant within the control cycle such that $Q_{mg,n}(k+1) = Q_{mg,n}(k)$). The \mathbf{R} penalty factor is responsible to alter the control efforts among u_{com} , all $Q_{dis,i}$ in \mathbf{Q}_{dis} , and Q_{dcom} in m^{th} sMG. For the case of large \mathbf{R} , the control efforts among \mathbf{u} is restricted during error tracking and this leads to slower optimization rate. Notably, \mathbf{W} weighting factor enables the possibility of adjusting the priority between intracluster reactive power sharing and voltage regulation.

By substituting (10) into (11) and adopting the graph theory in consensus/cooperative control, the cost function can be formulated into a quadratic programming (QP):

$$J_m = \frac{1}{2} \Delta \mathbf{u}_m^T \mathbf{Q}_m \Delta \mathbf{u}_m + \Delta \mathbf{u}_m^T \mathbf{E}_m \quad (12)$$

where

$$\mathbf{Q}_m = 2(\mathbf{D}_m^T \mathbf{W}_m \mathbf{D}_m + w_m^* \lambda_m^T \mathbf{L}_m \lambda_m + \mathbf{R}_m)$$

$$\mathbf{E}_m = -2 \begin{bmatrix} \mathbf{D}_m^T \mathbf{W}_m (\mathbf{y}_m^*(k+1) - \mathbf{F}_m \mathbf{z}_m(k) - \Delta \mathbf{y}_m(k)) \\ -w_m^* \lambda_m^T \mathbf{L}_m \mathbf{y}_m(k) \end{bmatrix} \quad (13)$$

and \mathbf{L}_m is the Laplacian matrix of the sMG's communication graph. The \mathbf{y}_m^* term, being equal to $[Q_{mg,1} \dots Q_{mg,m} \dots Q_{mg,N_m}]^T$, is defined as

$$\mathbf{y}_m^*(k+1) = \begin{bmatrix} Q_{mg,1} \\ \vdots \\ Q_{mg,m} \\ \vdots \\ Q_{mg,N_m} \end{bmatrix}_{k+1}$$

$$= \begin{bmatrix} Q_{mg,1} \\ \vdots \\ Q_{mg,m} \\ \vdots \\ Q_{mg,N_m} \end{bmatrix}_k + \begin{bmatrix} 0 & 0 & \dots & 0 \\ \vdots & \vdots & \ddots & \vdots \\ 0 & 0 & \dots & 1 \\ \vdots & \vdots & \ddots & \vdots \\ 0 & 0 & \dots & 0 \end{bmatrix} \Delta \mathbf{u}_m(k) \quad (14)$$

$$= \mathbf{y}_m^*(k) + \lambda_m \Delta \mathbf{u}_m(k)$$

IV. SIMULATION RESULT

Fig. 1 depicts the single line diagram of a microgrid that is sectionized to two sMGs (sMG-A and sMG-B). The DER specification are tabulated in Table I together with the respective sets of secondary control parameters. In the QP optimization of each sMG, the weighting factor \mathbf{W}_m is a N_B -by- N_B diagonal matrix having the form of $\text{diag}(w_1, w_2, \dots, w_{N_B})$, and the penalty factor \mathbf{R} is a (N_D+2) -by- (N_D+2) diagonal matrix having the form of $\text{diag}(r_1, r_2, \dots, r_{N_D+2})$. For instance, in sMG-A with $N_{B,A} = 5$ and $N_{D,A} = 2$, the individual w weighting factors correspond to outputs V_{L1} , V_{L3} , V_{L4} , Q_{G1} and Q_{G4} , whereas the individual r penalty factors correspond to control inputs Δu_{com} , $\Delta Q_{1,dis}$, $\Delta Q_{4,dis}$ and ΔQ_{dcom} , respectively.

In Fig. 2, reactive output power of DER 2 and 4 are supposed to be proportional (hence equal, in pu; see relevant kVA ratings in Table I), however, a small error exists. The cause of the error was explained in Subsection II-B. Upon introducing the correction scheme with $K_i = 0.2$ (i.e. arbitrary chosen), the reactive powers are restored/corrected to the desired proportional ratio of 4:2:1:2 (as will be illustrated graphically in Subsection IV-A). In what follows, the semi-distributed secondary control scheme is investigated in conjunction with different control settings.

A. Optimal Reactive Power Sharing among DERs

The DERs are droop-controlled with the proposed secondary control deactivated. It is established from Fig. 3 that reactive power is not proportionally shared among the DERs in each sMG, and the sMGs' total powers are not proportional too. At $t = 60$ s, the intra-reactive power sharing control is initiated in both QP-A and QP-B by setting the weighting

TABLE I. SPECIFICATIONS OF THE ISLANDED MULTI-MICROGRID NETWORK AND PROPOSED CONTROL

| DER ratings: | | Q - V droop no-load voltage, V_{oi}^* | Q - V droop coefficients, n_i |
|---|---------------------------|---|-------------------------------------|
| Apparent pow. (rated pf) | | (pu) | (pu) |
| DER 1 | 20 kVA (0.8) | 1.02 | 0.075 |
| DER 2 | 10 kVA (0.8) | | 0.15 |
| DER 3 | 5 kVA (0.8) | | 0.30 |
| DER 4 | 10 kVA (0.8) | | 0.15 |
| DER output feeder impedances | | Line impedances | |
| Z_{of1} | 0.0300 Ω , 0.35 mH | Z_{14} | 0.46 Ω , 1.464 mH |
| Z_{of2} | 0.0804 Ω , 0.35 mH | Z_{23} | 0.46 Ω , 2.928 mH |
| Z_{of3} | 0.0560 Ω , 0.35 mH | Z_{34} | 0.70 Ω , 3.694 mH |
| Z_{of4} | 0.0433 Ω , 0.35 mH | | |
| Sub-microgrid's optimal secondary control | | | |
| Parameter | Value | Parameter | Value |
| Samp. freq. F_{s2} | 0.5 Hz | Integral gain K_i | 0.2 |

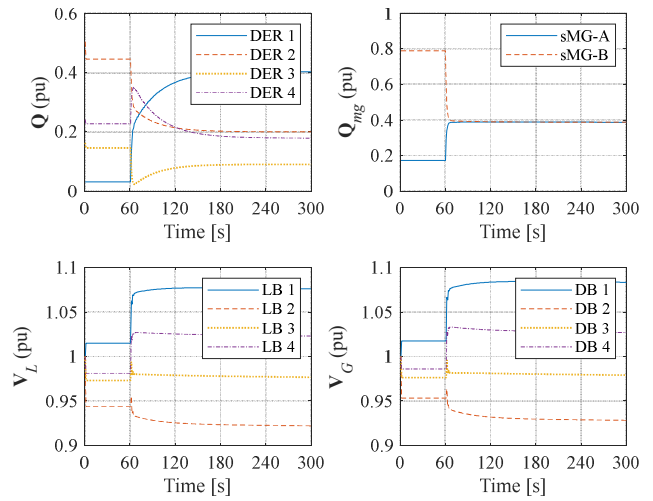


Fig. 2. Optimal intra- and inter-cluster reactive power sharing control without integral-based correction: DERs reactive output power, sMG reactive output power, load bus voltage magnitudes and DER-bus voltage magnitudes.

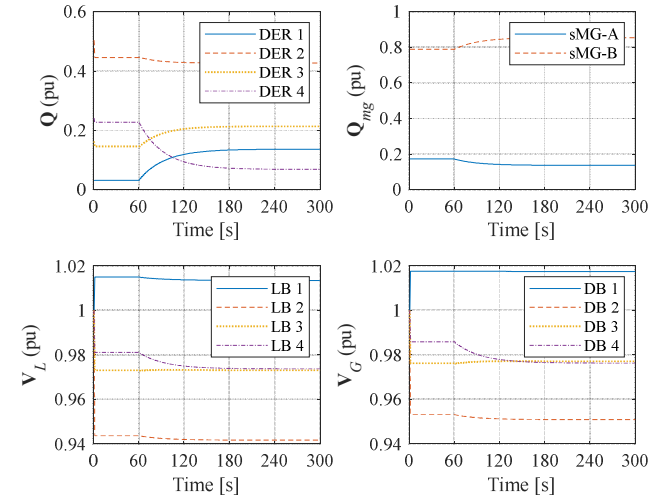


Fig. 3. Optimal intra-cluster reactive power sharing control: DERs reactive output power, sMG reactive output power, load bus voltage magnitudes and DER-bus voltage magnitudes.

element within \mathbf{R} that corresponds to Q_{dis} , to 10. Fig. 3 shows that the reactive power sharing among the DERs within each

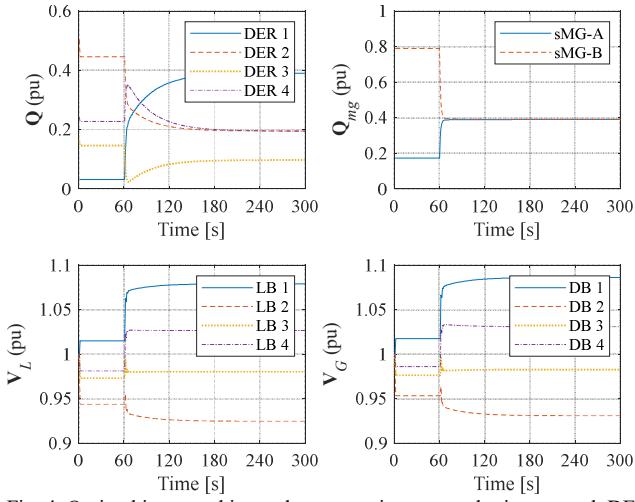


Fig. 4. Optimal intra- and inter-cluster reactive power sharing control: DERs reactive output power, sMG reactive output power, load bus voltage magnitudes and DER-bus voltage magnitudes.

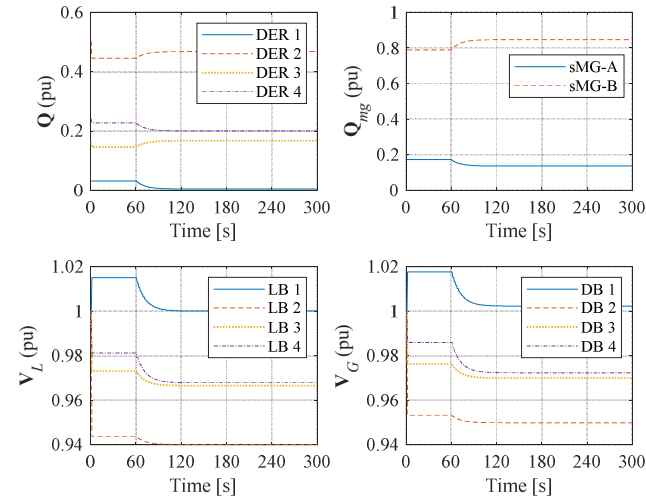


Fig. 5. Case B-I: Single load-bus voltage regulation control at sMG-A: DERs reactive output power, sMG reactive output power, load bus voltage magnitudes and DER-bus voltage magnitudes.

sMG is significantly improved (i.e. corrected), giving a steady-state ratio of 2:1, i.e., $Q_{G1}:Q_{G4}$ in sMG-A and $Q_{G2}:Q_{G3}$ in sMG-B. Fig. 3 also shows the corresponding voltages of the DER- and load-buses, which range from 0.9416 pu (i.e., LB 4) and 1.018 pu (i.e., DB 1). However, it can be noticed that reactive power is not proportionally shared between the two sMGs as the inter-cluster feature has not been activated (i.e., $w' = 0$).

Next, the performance of optimal intra- and inter-cluster reactive power sharing is examined. The inter-cluster power sharing control is activated by setting w' to 1 (with K_i remains at 0.2) at $t = 60$ s. The penalty factors within \mathbf{R} that correspond to individual DER's Q_{dis} and common Q_{dcom} , are set to 10. Fig. 4 shows that the reactive power sharing among all DERs within the microgrid is significantly improved, giving a ratio of 4:2:1:2. The bus voltages range from 0.9246 pu at LB 4 to 1.086 pu at DB 1.

B. Single Load-bus Voltage Regulation

Similarly, the islanded microgrid is initially controlled through standard droop and the voltages at LB 1 in sMG-A

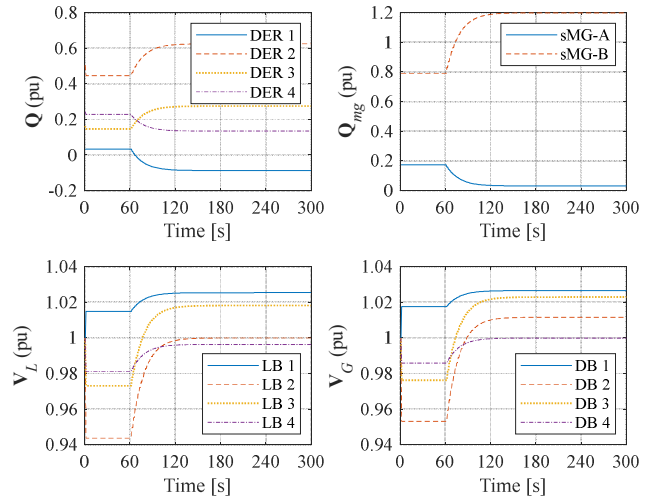


Fig. 6. Case B-II: Single load-bus voltage regulation control at sMG-B: DERs reactive output power, sMG reactive output power, load bus voltage magnitudes and DER-bus voltage magnitudes.

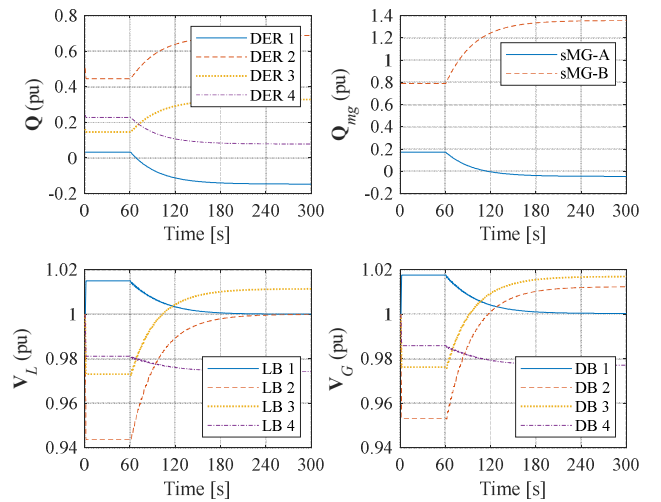


Fig. 7. Case B-III: Single load-bus voltage regulation control: DERs reactive output power, sMG reactive output power, load bus voltage magnitudes and DER-bus voltage magnitudes.

and LB 2 at sMG-B have reach the droop-steady-state of 1.015 pu and 0.9437 pu. The load-bus voltage regulation feature of the proposed optimal control is activated by setting $w_{L,A}$ (that corresponds to V_{L1} in sMG-A) to 1 in scenario B-I, and by setting $w_{L,B}$ (that corresponds to V_{L2} in sMG-B) to 1 in scenario B-II. In both scenarios the reactive power sharing feature is turned off. Penalty factor \mathbf{R} is set such that only u_{com} is activated. It is clearly seen from Figs. 5 and 6 that V_{L1} and V_{L2} are regulated to $V_{ref} = 1.0$ pu in both scenarios without noticeable improvement in reactive power sharing. The third scenario B-III is about simultaneous single-bus voltage regulation (V_{L1} in sMG-A and V_{L2} in sMG-B) in both sMGs. The semi-distributed control is activated $t = 60$ s by setting $w_{L,A} = w_{L,B} = 1$ (while keeping the rest of w values to zero). It is shown in Fig. 7 that both V_{L1} and V_{L2} are regulated to $V_{ref} = 1.0$ pu. However, it is obvious that the issue of non-proportional reactive power sharing remains, as per the theoretical expectation.

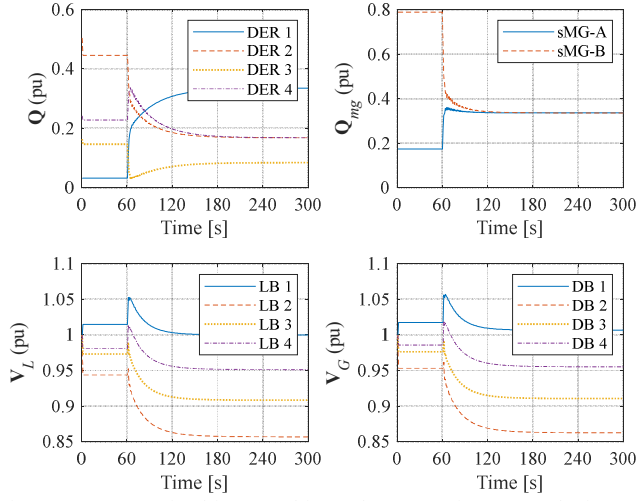


Fig. 8. Case C: Optimal intra- and inter-cluster reactive power sharing and single load-bus voltage regulation control at sMG-A: DERs reactive output power, sMG reactive output power, load bus voltage magnitudes and DER-bus voltage magnitudes.

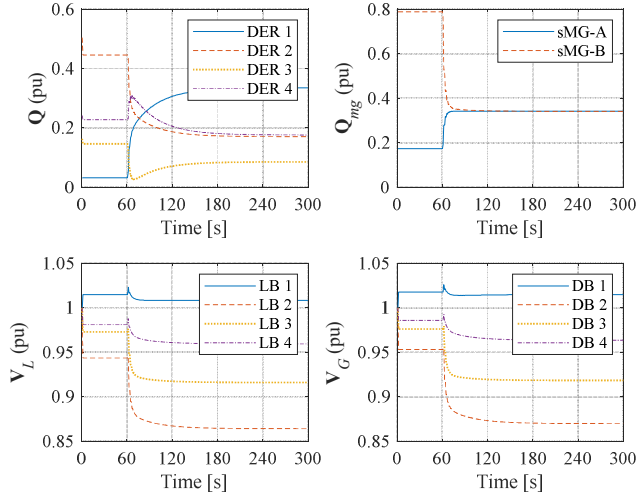


Fig. 9. Case C-I: Optimal intra- and inter reactive power sharing and multi-load bus voltage regulation control (V_L prioritized) at sMG-A: DERs reactive output power, sMG reactive output power, load bus voltage magnitudes and DER-bus voltage magnitudes.

C. Optimal Reactive Power Sharing and Voltage Regulation

The simultaneous intra- and inter-cluster reactive power sharing control and single load-bus voltage regulation is first examined. At $t = 60$ s, the semi-distributed optimal control is activated by enabling intra- and inter-reactive power sharing control (i.e., $w_{4-5,A} = w_{4-5,B} = 1$ and $w' = 1$) and setting $w_{1,A} = 1$ for V_{L1} regulation in sMG-A. The penalty factor \mathbf{R}_{A-B} is set as $\text{diag}(10,10,10,10)$ which essentially means that all control inputs are utilized. Fig. 8 shows that proportional reactive power sharing can be achieved among the DERs within the entire microgrid, despite having separated instances of secondary controllers. This demonstrates the viability of the proposed incorporation of consensus/cooperative control into the cost function in (11). In addition, V_{L1} is regulated to $V_{ref} = 1.0$ pu, as intended.

Next, the performance of the optimal control of reactive power and intra-cluster multiple load-bus voltage (more than

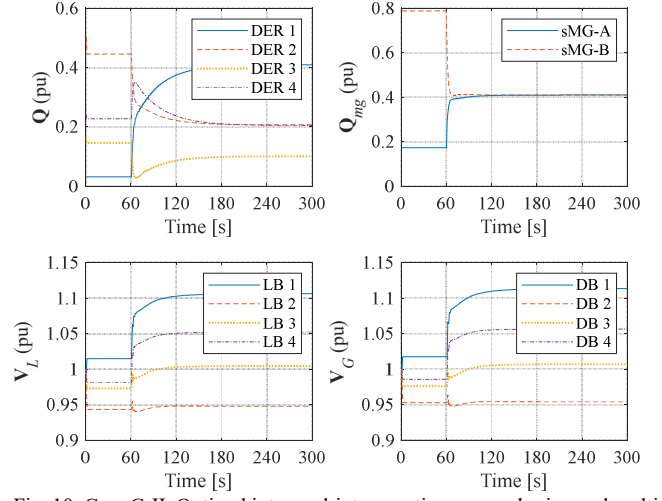


Fig. 10. Case C-II: Optimal intra- and inter reactive power sharing and multi-load bus voltage regulation control (equally weighted) at sMG-B: DERs reactive output power, sMG reactive output power, load bus voltage magnitudes and DER-bus voltage magnitudes.

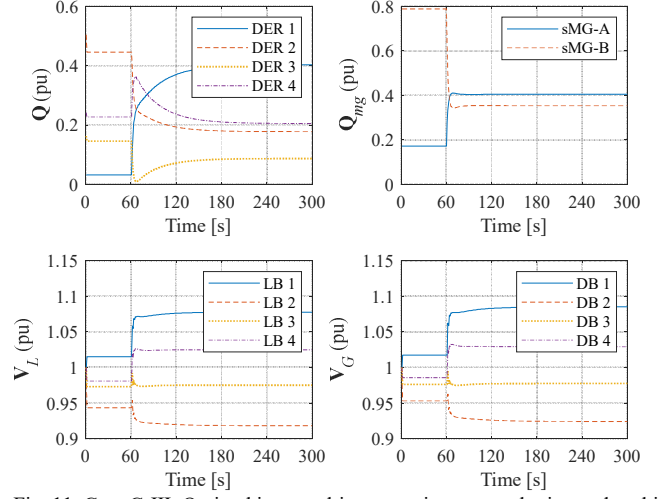


Fig. 11. Case C-III: Optimal intra- and inter reactive power sharing and multi-load bus voltage regulation control: DERs reactive output power, sMG reactive output power, load bus and DER-bus voltage magnitudes.

one bus in a sMG) is examined. In scenario C-I here, voltage regulation at LB 1 is prioritized (i.e., $w_{1,A} = 10$) along regulating the voltage at LB 3 (i.e., $w_{2,A} = 1$) in sMG-A while emphasising the intra- and inter-cluster reactive power sharing improvement. It is seen from Fig. 9 that V_{L1} (being 1.008 pu) is regulated close to $V_{ref} = 1.0$ pu and V_{L3} is regulated to 0.9162 pu, while the reactive power sharing is slightly compromised, being 0.3352:0.1705:0.0851:0.1760 (expected a 4:2:1:2 ratio if voltage regulation is not activated).

In scenario C-II, both multi-bus voltage regulation in sMG-B and reactive power sharing are weighted equally (by setting $w_{4-5,A}$, $w_{1,B}$, $w_{3-5,B}$ and w' to 1). It is shown in Fig. 10 that reactive power sharing error among all DERs is considerably improved (i.e., in a ratio of 0.4097:0.2067:0.1007:0.2051, in pu) while V_{L2} and V_{L4} are loosely regulated to 0.9479 and 1.052 pu (given $V_{ref} = 1.0$ pu).

The additional feature of inter-cluster load-bus voltage regulation (effectively, one load bus in each sMG) is examined next, through scenario C-III. At $t = 60$ s, the

proposed control scheme is activated by setting (in \mathbf{W}_A) $w_{2,A} = w_{4-5,A} = 1$, (in \mathbf{W}_B) $w_{3,B} = w_{4-5,B} = 1$, and $w' = 1$. It is seen in Fig. 11 that while V_{L3} (in sMG-A) and V_{L4} (in sMG-B) are regulated to 0.9753 pu and 1.025 pu (close to the desired 1.0 pu), both the intra-cluster and inter-cluster reactive power sharing are compromised. The overall ratio stands at 0.4028:0.1777:0.0871:0.2051, in pu, and the reactive power ratio of the two sMGs is 0.4053:0.3531 (slightly off from the 1:1, as compared to the case in Fig. 10). This result successfully demonstrates the effectiveness of the proposed semi-distributed optimal control in managing trade-offs (of reactive power sharing and load-bus voltage regulation) among all the DERs across sMGs within the microgrid, despite having separated instances of secondary controller.

V. CONCLUSION

A semi-distributed optimal control strategy that exploits the use of optimal and cooperative control techniques is proposed and studied in this work. Apart from alleviating the risk of single point of failure posed by centralised control, the complexity and scalability issue of the control problem is eased as the computational effort is distributed across the sub-microgrid secondary controllers. DLPPF is adopted in place of the classical non-linear power flow to further reduce the computational burden of the secondary control algorithm due to its non-iterative nature. The viability and the performance of the novel control scheme has been successfully verified in conjunction with three distinctive cases: reactive power sharing correction without voltage regulation, single-load bus voltage regulation without reactive power sharing correction, and optimal reactive power sharing and voltage regulation.

Beyond this proof-of-concept work, the proposed semi-distributed optimal control should be extended to a larger islanded microgrid, and the performance is to be benchmarked against recently reported techniques. Moreover, detailed primary control loops should be included to reflect a more realistic DER dynamics in the microgrid.

APPENDIX

Assume that the active/reactive load-bus power and DERs' active power (obtainable from measurement) remain relatively constant upon secondary optimal control, the voltage magnitude of DER-buses in (6) is substituted into (4) to obtain \mathbf{V}_G in terms of reactive power injection, constant droop parameters, and control inputs \mathbf{u} . This gives

$$\begin{aligned} & \begin{bmatrix} \mathbf{I} & -\mathbf{K}_{LG} \\ \mathbf{0} & -\mathbf{\Phi} - \mathbf{K}_{GG} \end{bmatrix}_m \underbrace{\begin{bmatrix} \mathbf{V}_L \\ \mathbf{Q}_G \end{bmatrix}_{m,k+1}}_{\mathbf{y}_m(k+1)} \\ &= \begin{bmatrix} \mathbf{N}_{LL} & \mathbf{N}_{LG} & \mathbf{K}_{LL} & \mathbf{0} \\ \mathbf{N}_{GL} & \mathbf{N}_{GG} & \mathbf{K}_{GL} & -\mathbf{I} \end{bmatrix}_m \underbrace{\begin{bmatrix} \mathbf{P}_L \\ \mathbf{P}_G \\ \mathbf{Q}_L \\ \mathbf{V}_o^* \end{bmatrix}_{m,k}}_{\mathbf{v}_m(k)} + \begin{bmatrix} \mathbf{0} \\ -\mathbf{\Gamma} \end{bmatrix}_m \underbrace{\begin{bmatrix} u_{com} \\ Q_{dis,1} \\ \vdots \\ Q_{dis,N_D} \\ Q_{dcom} \end{bmatrix}_{m,k}}_{\mathbf{u}_m(k)} \end{aligned} \quad (15)$$

Rearrange the known sub-vectors (i.e., \mathbf{P}_L , \mathbf{P}_G , \mathbf{Q}_L and \mathbf{V}_o^*) into a single vector \mathbf{v} to obtain (7). \mathbf{C} is a $N_B \times 2N_B$ matrix and \mathbf{D} is a $N_B \times (N_D+1)$ matrix, and they are expressed as

$$\begin{aligned} \mathbf{C}_m &= \begin{bmatrix} \mathbf{I} & -\mathbf{K}_{LG} \\ \mathbf{0} & -\mathbf{\Phi} - \mathbf{K}_{GG} \end{bmatrix}_m^{-1} \begin{bmatrix} \mathbf{N}_{LL} & \mathbf{N}_{LG} & \mathbf{K}_{LL} & \mathbf{0} \\ \mathbf{N}_{GL} & \mathbf{N}_{GG} & \mathbf{K}_{GL} & -\mathbf{I} \end{bmatrix}_m \\ \mathbf{D}_m &= \begin{bmatrix} \mathbf{I} & -\mathbf{K}_{LG} \\ \mathbf{0} & -\mathbf{\Phi} - \mathbf{K}_{GG} \end{bmatrix}_m^{-1} \begin{bmatrix} \mathbf{0} \\ -\mathbf{\Gamma} \end{bmatrix}_m \end{aligned}$$

REFERENCES

- [1] J. Schiffer, T. Seel, J. Raisch, and T. Sezi, "Voltage stability and reactive power sharing in inverter-based microgrids with consensus-based distributed voltage control," *IEEE Trans. Control Syst. Technol.*, vol. 24, no. 1, pp. 96–109, Jan. 2016.
- [2] G. Agundis-Tinajero *et al.*, "Extended-optimal-power-flow-based hierarchical control for islanded AC microgrids," *IEEE Trans. Power Electron.*, vol. 34, no. 1, pp. 840–848, Jan. 2019.
- [3] A. Bidram, A. Davoudi, and F. L. Lewis, "A multiobjective distributed control framework for islanded AC microgrids," *IEEE Trans. Ind. Informatics*, vol. 10, no. 3, pp. 1785–1798, Aug. 2014.
- [4] N. M. Dehkordi, N. Sadati, and M. Hamzeh, "Fully distributed cooperative secondary frequency and voltage control of islanded microgrids," *IEEE Trans. Energy Convers.*, vol. 32, no. 2, pp. 675–685, Jun. 2017.
- [5] Q. Shafiee, V. Nasirian, J. C. Vasquez, J. M. Guerrero, and A. Davoudi, "A multi-functional fully distributed control framework for ac microgrids," *IEEE Trans. Smart Grid*, vol. 9, no. 4, pp. 3247–3258, Jul. 2018.
- [6] F. L. Lewis, H. Zhang, K. Hengster-Movric, and A. Das, "Algebraic graph theory and cooperative control consensus," in *Cooperative Control of Multi-Agent Systems*, 1st ed., London: Springer-Verlag London, 2014, pp. 23–71.
- [7] J. W. Simpson-Porco, Q. Shafiee, F. Dorfler, J. C. Vasquez, J. M. Guerrero, and F. Bullo, "Secondary frequency and voltage control of islanded microgrids via distributed averaging," *IEEE Trans. Ind. Electron.*, vol. 62, no. 11, pp. 7025–7038, Nov. 2015.
- [8] R. Han, L. Meng, G. Ferrari-Trecate, E. A. A. Coelho, J. C. Vasquez, and J. M. Guerrero, "Containment and consensus-based distributed coordination control to achieve bounded voltage and precise reactive power sharing in islanded AC microgrids," *IEEE Trans. Ind. Appl.*, vol. 53, no. 6, pp. 5187–5199, Dec. 2017.
- [9] J. Liu, J. Li, H. Song, A. Nawaz, and Y. Qu, "Nonlinear secondary voltage control of islanded microgrid via distributed consistency," *IEEE Trans. Energy Convers.*, vol. 35, no. 4, pp. 1964–1972, Dec. 2020.
- [10] X. Wu, C. Shen, and R. Iravani, "A distributed, cooperative frequency and voltage control for microgrids," *IEEE Trans. Smart Grid*, vol. 9, no. 4, pp. 2764–2776, Jul. 2018.
- [11] F. Mumtaz, M. H. Syed, M. Al Hosani, and H. H. Zeineldin, "A novel approach to solve power flow for islanded microgrids using modified newton raphson with droop control of DG," *IEEE Trans. Sustain. Energy*, vol. 7, no. 2, pp. 493–503, Apr. 2016.
- [12] A. La Bella, S. Raimondi Cominesi, C. Sandroni, and R. Scattolini, "Hierarchical predictive control of microgrids in islanded operation," *IEEE Trans. Autom. Sci. Eng.*, vol. 14, no. 2, pp. 536–546, Apr. 2017.
- [13] X. Yang, Y. Du, J. Su, L. Chang, Y. Shi, and J. Lai, "An optimal secondary voltage control strategy for an islanded multibus microgrid," *IEEE J. Emerg. Sel. Top. Power Electron.*, vol. 4, no. 4, pp. 1236–1246, Dec. 2016.
- [14] J. Yang, N. Zhang, C. Kang, and Q. Xia, "A state-independent linear power flow model with accurate estimation of voltage magnitude," *IEEE Trans. Power Syst.*, vol. 32, no. 5, pp. 3607–3617, Sep. 2017.

Bibliography

- Abdelaziz, M. M. A. *et al.* (2013) 'A novel and generalized three-phase power flow algorithm for islanded microgrids using a newton trust region method', *IEEE Transactions on Power Systems*, 28(1), pp. 190–201.
- Afshar, Z. *et al.* (2019) 'A novel accurate power sharing method versus droop control in autonomous microgrids with critical loads', *IEEE Access*, 7, pp. 89466–89474.
- Agundis-Tinajero, G. *et al.* (2019) 'Extended-optimal-power-flow-based hierarchical control for islanded AC microgrids', *IEEE Transactions on Power Electronics*, 34(1), pp. 840–848.
- Allam, M. A., Hamad, A. A. and Kazerani, M. (2018) 'A generic modeling and power-flow analysis approach for isochronous and droop-controlled microgrids', *IEEE Transactions on Power Systems*, 33(5), pp. 5657–5670.
- Alshammari, F. and El-Refaie, A. (2020) 'Distributed averaging optimization-based technique for microgrid secondary control', *IEEE Energy Conversion Congress and Exposition*, Detroit, USA, 11–15 October. pp. 1343–1350.
- Altahir, S. Y., Yan, X. and Liu, X. (2017) 'A power sharing method for inverters in microgrid based on the virtual power and virtual impedance control', *IEEE Int. Conf. on Compatibility, Power Electron. and Power Eng.*, Cadiz, Spain, 4–6 April. pp. 151–156.
- An, R. *et al.* (2018) 'A communication-independent reactive power sharing scheme with adaptive virtual impedance for parallel connected inverters', *Int. Power Electron. Conf.*, Niigata, Japan, 20–24 May. pp. 3692–3697.
- Aprilia, E. *et al.* (2019) 'Critical bus voltage support in islanded microgrids with consensus algorithm of distributed generators', *IEEE PES Innovative Smart Grid Tech. Asia*, Chengdu, China, 21–24 May. pp. 1445–1449.
- Aslanzadeh, S. and Jamali, S. (2007) 'Study of distributed generation type and islanding impact on the operation of radial distribution systems', *Int. Universities Power Eng. Conf.*, Brighton, UK, 4–6 September. pp. 1216–1221.
- Bayat, M. *et al.* (2016) 'Coordination of distributed energy resources and demand response for voltage and frequency support of mv microgrids', *IEEE Transactions on Power Systems*, 31(2), pp. 1506–1516.
- Bidram, A. *et al.* (2013) 'Distributed cooperative secondary control of microgrids using feedback linearization', *IEEE Transactions on Power Systems*, 28(3), pp. 3462–3470.
- Bidram, A. *et al.* (2017) *Cooperative Synchronization in Distributed Microgrid Control*. Cham, Switzerland: Springer International Publishing (Advances in Industrial Control).
- Bidram, A. and Davoudi, A. (2012) 'Hierarchical structure of microgrids control system', *IEEE Transactions on Smart Grid*, 3(4), pp. 1963–1976.
- Bidram, A., Davoudi, A. and Lewis, F. L. (2014) 'A multiobjective distributed control framework for islanded AC microgrids', *IEEE Transactions on Industrial Informatics*, 10(3), pp. 1785–1798.
- Cai, H. *et al.* (2016) 'A distributed feedforward approach to cooperative control of AC microgrids', *IEEE Transactions on Power Systems*, 31(5), pp. 4057–4067.

Bibliography

- Cai, N. and Khatib, A. R. (2019) 'A universal power flow algorithm for industrial systems and microgrids - active power', *IEEE Transactions on Power Systems*, 34(6), pp. 4900–4909.
- Caron, S. (2021) *QP solvers for Python*. Available at: <https://pypi.org/project/qpsolvers/> (Accessed: 22 January 2020).
- Chen, G. and Guo, Z. (2019) 'Distributed secondary and optimal active power sharing control for islanded microgrids with communication delays', *IEEE Transactions on Smart Grid*, 10(2), pp. 2002–2014.
- Chen, Y. *et al.* (2016) 'Fast reactive power sharing, circulating current and resonance suppression for parallel inverters using resistive-capacitive output impedance', *IEEE Transactions on Power Electronics*, 31(8), pp. 5524–5537.
- Deckmyn, C. *et al.* (2018) 'A microgrid multilayer control concept for optimal power scheduling and voltage control', *IEEE Transactions on Smart Grid*, 9(5), pp. 4458–4467.
- Dehkordi, N. M., Sadati, N. and Hamzeh, M. (2017) 'Fully distributed cooperative secondary frequency and voltage control of islanded microgrids', *IEEE Transactions on Energy Conversion*, 32(2), pp. 675–685.
- Dvijotham, K. and Molzahn, D. K. (2016) 'Error bounds on the DC power flow approximation: a convex relaxation approach', *IEEE Conf. on Decision and Control*, Las Vegas, USA, 12–14 December. pp. 2411–2418.
- Elrattyah, A., Sozer, Y. and Elbuluk, M. E. (2014) 'A novel load-flow analysis for stable and optimized microgrid operation', *IEEE Transactions on Power Delivery*, 29(4), pp. 1709–1717.
- Engler, A. and Soultanis, N. (2008) 'Droop control in LV-grids', *Int. Conf. on Future Power Syst.*, Amsterdam, Netherlands, 18 November. pp. 1–6.
- Falahi, M., Butler-Purry, K. and Ehsani, M. (2013) 'Dynamic reactive power control of islanded microgrids', *IEEE Transactions on Power Systems*, 28(4), pp. 3649–3657.
- Farrar, T. (2018) *NERC addresses single points of failure in protection systems among other FERC concerns*. Available at: <https://www.trccompanies.com/insights/nerc-addresses-single-points-of-failure-in-protection-systems-among-other-ferc-concerns/> (Accessed: 16 December 2019).
- Golsorkhi, M. S. *et al.* (2019) 'Distributed control of low-voltage resistive ac microgrids', *IEEE Transactions on Energy Conversion*, 34(2), pp. 573–584.
- Golsorkhi, M. S., Hill, D. J. and Karshenas, H. R. (2018) 'Distributed voltage control and power management of networked microgrids', *IEEE Journal of Emerging and Selected Topics in Power Electronics*, 6(4), pp. 1892–1902.
- Gómez, J. S. *et al.* (2020) 'Distributed predictive control for frequency and voltage regulation in microgrids', *IEEE Transactions on Smart Grid*, 11(2), pp. 1319–1329.
- Gu, W. *et al.* (2017) 'A nonlinear state estimator-based decentralized secondary voltage control scheme for autonomous microgrids', *IEEE Transactions on Power Systems*, 32(6), pp. 4794–4804.
- Guerrero, J. M. *et al.* (2005) 'Output impedance design of parallel-connected UPS inverters with wireless load-sharing control', *IEEE Transactions on Industrial Electronics*, 52(4), pp. 1126–1135.
- Guerrero, J. M. *et al.* (2007) 'Decentralized control for parallel operation of distributed generation inverters using resistive output impedance', *IEEE Transactions on Industrial Electronics*,

- 54(2), pp. 994–1004.
- Guo, F. *et al.* (2015) ‘Distributed secondary voltage and frequency restoration control of droop-controlled inverter-based microgrids’, *IEEE Transactions on Industrial Electronics*, 62(7), pp. 4355–4364.
- Guo, Z., Li, S. and Zheng, Y. (2017) ‘Distributed model predictive control for secondary voltage of the inverter-based microgrid’, *Chinese Control Conf.*, Dalian, China, 26–28 July. pp. 4630–4634.
- Han, R. *et al.* (2017) ‘Containment and consensus-based distributed coordination control to achieve bounded voltage and precise reactive power sharing in islanded AC microgrids’, *IEEE Transactions on Industry Applications*, 53(6), pp. 5187–5199.
- Han, Y. *et al.* (2016) ‘An enhanced power sharing scheme for voltage unbalance and harmonics compensation in an islanded AC microgrid’, *IEEE Transactions on Energy Conversion*, 31(3), pp. 1037–1050.
- Han, Y., Shen, P., *et al.* (2017) ‘Control strategies for islanded microgrid using enhanced hierarchical control structure with multiple current-loop damping schemes’, *IEEE Transactions on Smart Grid*, 8(3), pp. 1139–1153.
- Han, Y., Li, H., *et al.* (2017) ‘Review of active and reactive power sharing strategies in hierarchical controlled microgrids’, *IEEE Transactions on Power Electronics*, 32(3), pp. 2427–2451.
- He, J. *et al.* (2012) ‘An islanding microgrid reactive power sharing scheme enhanced by programmed virtual impedances’, *IEEE Int. Symp. on Power Electron. for Distributed Generation Syst.*, 25–28 June. pp. 229–235.
- He, J. *et al.* (2013) ‘An islanding microgrid power sharing approach using enhanced virtual impedance control scheme’, *IEEE Transactions on Power Electronics*, 28(11), pp. 5272–5282.
- Hoang, T. V. and Lee, H. H. (2018) ‘An adaptive virtual impedance control scheme to eliminate the reactive-power-sharing errors in an islanding meshed microgrid’, *IEEE Journal of Emerging and Selected Topics in Power Electronics*, 6(2), pp. 966–976.
- Hoang, T. V. and Lee, H. H. (2019) ‘Accurate power sharing with harmonic power for islanded multibus microgrids’, *IEEE Journal of Emerging and Selected Topics in Power Electronics*, 7(2), pp. 1286–1299.
- IEEE Power and Energy Society (2010) *IEEE 34 node test feeder*. Available at: <http://sites.ieee.org/pes-testfeeders/resources/> (Accessed on 11 July 2017).
- Imran, R. M., Wang, S. and Flaih, F. M. F. (2019) ‘DQ-voltage droop control and robust secondary restoration with eligibility to operate during communication failure in autonomous microgrid’, *IEEE Access*, 7, pp. 6353–6361.
- Jamalzadeh, R. and Hong, M. (2019) ‘Microgrid optimal power flow using the generalized benders decomposition approach’, *IEEE Transactions on Sustainable Energy*, 10(4), pp. 2050–2064.
- Kersting, W. H. (2001) ‘Radial distribution test feeders’, *IEEE Power Eng. Soc. Winter Meeting*, Columbus, USA, 28 January–1 February. pp. 908–912.
- Khan, A. *et al.* (2020) ‘On the stability of power electronic-dominated grid: a new energy paradigm’, *IEEE Industrial Electronics Magazine*, (December), pp. 65–78.
- La Bella, A. *et al.* (2017) ‘Hierarchical predictive control of microgrids in islanded operation’, *IEEE Transactions on Automation Science and Engineering*, 14(2), pp. 536–546.

Bibliography

- Lai, J. *et al.* (2018) 'Distributed multiagent-oriented average control for voltage restoration and reactive power sharing of autonomous microgrids', *IEEE Access*, 6, pp. 25551–25561.
- Lai, J. *et al.* (2019) 'Cluster-oriented distributed cooperative control for multiple AC microgrids', *IEEE Transactions on Industrial Informatics*, 15(11), pp. 5906–5918.
- Lee, C. T., Chu, C. C. and Cheng, P. T. (2013) 'A new droop control method for the autonomous operation of distributed energy resource interface converters', *IEEE Transactions on Power Electronics*, 28(4), pp. 1980–1993.
- Li, Y. W. and Kao, C.-N. (2009) 'An accurate power control strategy for power-electronics-interfaced distributed generation units operating in a low-voltage multibus microgrid', *IEEE Transactions on Power Electronics*, 24(12), pp. 2977–2988.
- Liu, B. *et al.* (2018) 'A novel microgrid power sharing scheme enhanced by a non-intrusive feeder impedance estimation method', *Int. Power Electron. Conf.*, Niigata, Japan, 20–24 May. pp. 3924–3928.
- Liu, J. *et al.* (2020) 'Nonlinear secondary voltage control of islanded microgrid via distributed consistency', *IEEE Transactions on Energy Conversion*, 35(4), pp. 1964–1972.
- Liu, S. and Zhang, Y. (2017) 'Voltage compensation strategy using adaptive virtual impedance for reactive power sharing in an islanded microgrid', *Int. Conf. on Elect. Mach. and Syst.*, Sydney, Australia, 11–14 August.
- Lou, G. *et al.* (2017) 'Distributed MPC-based secondary voltage control scheme for autonomous droop-controlled microgrids', *IEEE Transactions on Sustainable Energy*, 8(2), pp. 792–804.
- Lou, G. *et al.* (2018) 'Distributed model predictive secondary voltage control of islanded microgrids with feedback linearization', *IEEE Access*, 6, pp. 50169–50178.
- Lu, L. Y. and Chu, C. C. (2018) 'Consensus-based droop control of isolated micro-grids by ADMM implementations', *IEEE Transactions on Smart Grid*, 9(5), pp. 5101–5112.
- Lu, X. *et al.* (2018) 'A novel distributed secondary coordination control approach for islanded microgrids', *IEEE Transactions on Smart Grid*, 9(4), pp. 2726–2740.
- Mahmood, H., Michaelson, D. and Jiang, J. (2015a) 'Accurate reactive power sharing in an islanded microgrid using adaptive virtual impedances', *IEEE Transactions on Power Electronics*, 30(3), pp. 1605–1617.
- Mahmood, H., Michaelson, D. and Jiang, J. (2015b) 'Reactive power sharing in islanded microgrids using adaptive voltage droop control', *IEEE Transactions on Smart Grid*, 6(6), pp. 3052–3060.
- Micallef, A. *et al.* (2012) 'Secondary control for reactive power sharing in droop-controlled islanded microgrids', *IEEE Int. Symp. on Ind. Electron.*, Hangzhou, China, 25–28 June. pp. 1627–1633.
- Mohamed, Y. A.-R. I. and El-Saadany, E. F. (2008) 'Adaptive decentralized droop controller to preserve power sharing stability of paralleled inverters in distributed generation microgrids', *IEEE Transactions on Power Electronics*, 23(6), pp. 2806–2816.
- Mueller, J. A. and Kimball, J. W. (2017) 'An efficient method of determining operating points of droop-controlled microgrids', *IEEE Transactions on Energy Conversion*, 32(4), pp. 1432–1446.
- Mumtaz, F. *et al.* (2016) 'A novel approach to solve power flow for islanded microgrids using modified newton raphson with droop control of DG', *IEEE Transactions on Sustainable Energy*, 7(2), pp. 493–503.

- Nasirian, V. *et al.* (2016) 'Droop-free distributed control for AC microgrids', *IEEE Transactions on Power Electronics*, 31(2), pp. 1600–1617.
- Olfati-Saber, R., Fax, J. A. and Murray, R. M. (2007) 'Consensus and cooperation in networked multi-agent systems', *Proc. of the IEEE*, 95(1), pp. 215–233.
- Olfati-Saber, R. and Murray, R. M. (2004) 'Consensus problems in networks of agents with switching topology and time-delays', *IEEE Transactions on Automatic Control*, 49(9), pp. 1520–1533.
- Ouyang, Y., Xia, Y. and Zou, Y. (2018) 'Active and reactive power coordinated secondary control based on control sensitivities in microgrid', *China Int. Conf. on Electricity Distribution*, 17–19 September. pp. 1053–1057.
- Owuor, J. O., Munda, J. L. and Jimoh, A. A. (2011) 'The IEEE 34 node radial test feeder as a simulation testbench for distributed generation', *IEEE Africon*. Victoria Falls, Zambia, 13–15 September.
- Peng, Z. *et al.* (2019) 'Droop control strategy incorporating coupling compensation and virtual impedance for microgrid application', *IEEE Transactions on Energy Conversion*, 34(1), pp. 277–291.
- Pham, D. M. and Lee, H.-H. (2021) 'Effective coordinated virtual impedance control for accurate power sharing in islanded microgrid', *IEEE Transactions on Industrial Electronics*, 68(3), pp. 2279–2288.
- Pogaku, N., Prodanović, M. and Green, T. C. (2007) 'Modeling, analysis and testing of autonomous operation of an inverter-based microgrid', *IEEE Transactions on Power Electronics*, 22(2), pp. 613–625.
- Pompodakis, E. E., Kryonidis, G. C. and Alexiadis, M. C. (2020) 'A comprehensive load flow approach for grid-connected and islanded ac microgrids', *IEEE Transactions on Power Systems*, 35(2), pp. 1143–1155.
- Qunais, T. and Karimi-Ghartemani, M. (2019) 'Systematic modeling of a class of microgrids and its application to impact analysis of cross-coupling droop terms', *IEEE Transactions on Energy Conversion*, 34(3), pp. 1632–1643.
- Raju P., E. S. N. and Jain, T. (2019) 'A two-level hierarchical controller to enhance stability and dynamic performance of islanded inverter-based microgrids with static and dynamic loads', *IEEE Transactions on Industrial Informatics*, 15(5), pp. 2786–2797.
- Ren, L. and Zhang, P. (2018) 'Generalized microgrid power flow', *IEEE Transactions on Smart Grid*, 9(4), pp. 3911–3913.
- Schiffer, J. *et al.* (2014) 'A consensus-based distributed voltage control for reactive power sharing in microgrids', *European Control Conf.*, Strasbourg, France, 24–27 June. pp. 1299–1305.
- Schiffer, J. *et al.* (2016) 'Voltage stability and reactive power sharing in inverter-based microgrids with consensus-based distributed voltage control', *IEEE Transactions on Control Systems Technology*, 24(1), pp. 96–109.
- Scroggins, R. (2013) *Reliability considerations in simple paralleling applications*. Available at: <https://www.csemag.com/articles/reliability-considerations-in-simple-paralleling-applications/> (Accessed: 16 December 2019).
- Shafiee, Q. *et al.* (2018) 'A multi-functional fully distributed control framework for AC microgrids', *IEEE Transactions on Smart Grid*, 9(4), pp. 3247–3258.

Bibliography

- Shafiee, Q., Guerrero, J. M. and Vasquez, J. C. (2014) 'Distributed secondary control for islanded microgrids-a novel approach', *IEEE Transactions on Power Electronics*, 29(2), pp. 1018–1031.
- Sheng, W. *et al.* (2016) 'A trust region SQP method for coordinated voltage control in smart distribution grid', *IEEE Transactions on Smart Grid*, 7(1), pp. 381–391.
- Shi, C. *et al.* (2020) 'A new secondary reactive power control strategy of microgrids based on droop control', *IEEE PES Asia-Pacific Power and Energy Eng. Conf.*, Nanjing, China, 20–23 September.
- Shi, M. *et al.* (2020) 'PI-consensus based distributed control of AC microgrids', *IEEE Transactions on Power Systems*, 35(3), pp. 2268–2278.
- Simpson-Porco, J. W. *et al.* (2015) 'Secondary frequency and voltage control of islanded microgrids via distributed averaging', *IEEE Transactions on Industrial Electronics*, 62(11), pp. 7025–7038.
- Stanoev, A. and Smilkov, D. (2013) 'Consensus theory in networked systems', in Kocarev, L. (ed.) *Consensus and Synchronization in Complex Networks*. Berlin: Springer-Verlag Berlin, pp. 1–22.
- Wang, B., Liu, S. and Zhang, Y. (2017) 'Reactive power sharing control based on voltage compensation strategy in microgrid', *Chinese Control Conf.*, Dalian, China, 26–28 July. pp. 10745–10750.
- Wang, L. (2009) *Model Predictive Control System Design and Implementation using MATLAB*. London, UK: Springer-Verlag London. Advances in Industrial Control.
- Wang, X. *et al.* (2015) 'Virtual-impedance-based control for voltage-source and current-source converters', *IEEE Transactions on Power Electronics*, 30(12), pp. 7019–7037.
- Wong, Y. C. C. *et al.* (2018) 'Reactive power sharing study of an islanded microgrid in DIgSILENT PowerFactory', *Int. Conf. on Renewable Energy Res. and Appl.*, Paris, France, 14–17 October. Paper No. 68.
- Wong, Y. C. C., Lim, C. S., Cruden, A. J., *et al.* (2020) 'A consensus-based adaptive virtual output impedance control scheme for reactive power sharing in meshed microgrids', *Int. Conf. on Power Electron., Smart Grid and Renewable Energy*, Cochin, India: 2–4 January. Paper No. 323.
- Wong, Y. C. C., Lim, C. S., Rotaru, M. D., *et al.* (2020) 'Consensus virtual output impedance control based on the novel droop equivalent impedance concept for a multi-bus radial microgrid', *IEEE Transactions on Energy Conversion*, 35(2), pp. 1078–1087.
- Wong, Y. C. C., Lim, C. S., Cruden, A., *et al.* (2021) 'A consensus-based adaptive virtual output impedance control scheme for reactive power sharing in radial microgrids', *IEEE Transactions on Industry Applications*, 57(1), pp. 784–794.
- Wong, Y. C. C., Lim, C. S., Goh, H. H., *et al.* (2021) 'An optimal secondary multi-bus voltage and reactive power sharing control based on non-iterative decoupled linearized power flow for islanded microgrids', *IEEE Access*, 9, pp. 105242–105254.
- Wong, Y. C. C., Lim, C. S., Cruden, A. J., *et al.* (2021) 'Semi-distributed optimal secondary control based on decoupled linearized power flow for large-area droop-controlled microgrids', *Int. Conf. on Green Energy, Computing and Sustainable Technol.*, Sarawak, Malaysia, 7–9 July. Paper No. 1570727021.

- Wu, X., Shen, C. and Iravani, R. (2018) 'A distributed, cooperative frequency and voltage control for microgrids', *IEEE Transactions on Smart Grid*, 9(4), pp. 2764–2776.
- Wu, Xiaoyu *et al.* (2020) 'A two-layer distributed cooperative control method for islanded networked microgrid systems', *IEEE Transactions on Smart Grid*, 11(2), pp. 942–957.
- Xu, H. *et al.* (2014) 'A reactive power sharing method based on virtual capacitor in islanding microgrid', *Int. Conf. on Power Electron. and ECCE Asia*, Hiroshima, Japan, 18–21 May. pp. 567–572.
- Xu, Y. and Sun, H. (2018) 'Distributed finite-time convergence control of an islanded low-voltage AC microgrid', *IEEE Transactions on Power Systems*, 33(3), pp. 2339–2348.
- Yang, J. *et al.* (2017) 'A state-independent linear power flow model with accurate estimation of voltage magnitude', *IEEE Transactions on Power Systems*, 32(5), pp. 3607–3617.
- Yang, X. *et al.* (2016) 'An optimal secondary voltage control strategy for an islanded multibus microgrid', *IEEE Journal of Emerging and Selected Topics in Power Electronics*, 4(4), pp. 1236–1246.
- Yao, W. *et al.* (2011) 'Design and analysis of the droop control method for parallel inverters considering the impact of the complex impedance on the power sharing', *IEEE Transactions on Industrial Electronics*, 58(2), pp. 576–588.
- Yu, D., Cao, J. and Li, X. (2018) 'Review of power system linearization methods and a decoupled linear equivalent power flow model', *Int. Conf. on Electron. Technol.*, Chengdu, China, 23–27 May. pp. 232–239.
- Zhang, B. *et al.* (2015) 'An optimal and distributed method for voltage regulation in power distribution systems', *IEEE Transactions on Power Systems*, 30(4), pp. 1714–1726.
- Zhang, H. *et al.* (2017) 'Distributed adaptive virtual impedance control for accurate reactive power sharing based on consensus control in microgrids', *IEEE Transactions on Smart Grid*, 8(4), pp. 1749–1761.
- Zhang, S. *et al.* (2019) 'An enhanced droop control strategy for accurate reactive power sharing in islanded microgrids', *IEEE PES Innovative Smart Grid Tech. Asia*, Chengdu, China, 21–24 May. pp. 2352–2356.
- Zhong, Q. C. (2013) 'Robust droop controller for accurate proportional load sharing among inverters operated in parallel', *IEEE Transactions on Industrial Electronics*, 60(4), pp. 1281–1290.
- Zhou, J. *et al.* (2018) 'Consensus-based distributed control for accurate reactive, harmonic, and imbalance power sharing in microgrids', *IEEE Transactions on Smart Grid*, 9(4), pp. 2453–2467.
- Zhou, J. and Cheng, P.-T. (2019) 'A modified Q-V droop control for accurate reactive power sharing in distributed generation microgrid', *IEEE Transactions on Industry Applications*, 55(4), pp. 4100–4109.
- Zhu, Y. *et al.* (2015) 'A virtual resistance based reactive power sharing strategy for networked microgrid', *Int. Conf. on Power Electron. and ECCE Asia*, Seoul, South Korea, 1–5 June. pp. 1564–1572.
- Zhu, Y. *et al.* (2016) 'A virtual impedance optimization method for reactive power sharing in networked microgrid', *IEEE Transactions on Power Electronics*, 31(4), pp. 2890–2904.
- Zhu, Y. *et al.* (2018) 'An enhanced virtual impedance optimization method for reactive power

Bibliography

sharing in microgrids', *IEEE Transactions on Power Electronics*, 33(12), pp. 10390–10402.